Structure-property correlations in pure copper and copper nanocomposite foils prepared by electrodeposition

A thesis

submitted by

Chokkakula Leela Pydi Pavithra

in partial fulfilment of the requirements for the award of the degree of

Doctor of Philosophy

in

Materials Engineering

School of Engineering Sciences and Technology

University of Hyderabad

June 2015

Declaration

I, Leela Pydi Pavithra Ch. **hereby declare that this thesis work entitled** *"*Structure-property correlations in pure copper and copper nanocomposite foils prepared by electrodeposition*"*, **submitted in partial fulfilment for the award of** Doctor of Philosophy **(in Materials Engineering) in the School of Engineering Sciences and Technology (SEST), University of Hyderabad is a bonafide work which was carried out by me under the supervision of** Dr. Koteswararao V. Rajulapati, Dr. Tata Narsinga Rao and Dr. Bulusu V. Sarada**. I also declare that this thesis has not been submitted previously in part or in full to this University or any other University or Institution for the award of any degree or diploma.**

Leela Pydi Pavithra Ch.
Reg. No. 09ETPM08
School of Engineering Sciences and Technology
University of Hyderabad.

Certificate

This is to certify that this thesis work entitled **"Structure-property correlations in pure copper and copper nanocomposite foils prepared by electrodeposition"**, submitted by **Leela Pydi Pavithra Ch.** bearing Reg. No. **09ETPM08** in partial fulfillment of the requirements for the award of the degree of **Doctor of Philosophy** in **Materials Engineering**, is a bonafide work that has been carried out by her under my supervision. Dr. Tata Narasinga Rao and Dr. Bulusu V. Sarada (ARCI) have also supervised the above mentioned thesis work with me. This thesis has not been submitted previously in part or in full to this or any other University or Institution for the award of any degree or diploma.

Thesis Supervisor

Dr. Koteswararao V. Rajulapati

Assistant Professor

School of Engineering Sciences and Technology

University of Hyderabad

Approved by

Prof. Rajender Singh

Dean

School of Engineering Sciences and Technology

University of Hyderabad

Certificate

This is to certify that this thesis work entitled **"Structure-property correlations in pure copper and copper nanocomposite foils prepared by electrodeposition"**, submitted by **Leela Pydi Pavithra.Ch** bearing Reg. No. **09ETPM08** in partial fulfillment of the requirements for the award of the degree of **Doctor of Philosophy** in **Materials Engineering**, is a bonafide work that has been carried out by her under our supervision. Dr. Koteswararao V. Rajulapati, University of Hyderabad has also supervised the above mentioned thesis work with us. This thesis has not been submitted previously in part or in full to this or any other University or Institution for the award of any degree or diploma.

Thesis Supervisors

Dr. Tata Narasinga Rao, Sc-'G'
Centre for Nanomaterials
ARCI, Hyderabad

Dr. Bulusu V. Sarada, Sc-'E'
Centre for Solar Energy Materials
ARCI, Hyderabad

Approved by

Dr. G. Sundararajan, Director
International Advanced Research Centre for Powder Metallurgy and New Materials (ARCI), Hyderabad

Acknowledgements

This journey would not have been possible without ARCI. My journey at ARCI has been a continuous learning process, it has been the support and guidance of the people that motivated me to register for Ph.D at University of Hyderabad.

At this juncture words fail to express my profound gratitude to Dr. G. Sundararajan (Director) ARCI, for his valuable advice in my work, spending his precious time for discussions and suggestions which helped me widen my horizon in the field of research. His insight and long-term vision have greatly influenced my research as well as thought process. I also express my thanks to Dr. S.V. Joshi (Additional Director) and Dr. G. Padmanabham (Associate Director) ARCI for providing me an excellent opportunity to carry out my research work at ARCI and for their immense support and encouragement throughout my research work during and after the reviews.

I would like to thank Prof. R. Singh (Dean), Prof. K. Bhanu Sankara Rao (Former Dean) and Prof. M. Sundararaman (Former Dean) for giving me an excellent opportunity to pursue my Ph.D at School of Engineering Sciences and Technology, University of Hyderabad.

I express my heart-felt gratitude to my supervisors Dr.Tata Narasinga Rao (ARCI), Dr. Koteswararao V. Rajulapati (SEST, Univerisity of Hyderabad) and Dr. Bulusu V.Sarada (ARCI). Each of them have dedicated a lot of time, energy and expertise throughout these years in moulding this thesis the way it is now. They are responsible for getting out the best in me as a researcher. Their constant guidance, cooperation and support has always kept me going ahead. I feel privileged to be associated with intellectuals like them during my stay at ARCI and UoH.

Words would not suffice to thank Dr. Sarada for constantly motivating me to step towards success without being dissipated by failures. This thesis would not have been possible without the help, support, patience, motivation and immense help she has provided me. I am extremely grateful to my supervisor Dr. Koteswararao who was abundantly helpful for his valuable guidance, scholarly inputs, long discussions and consistent support, encouragement I received throughout the research work.

I am grateful to Dr. Tata Narasinga Rao for providing necessary infrastructure and resources to accomplish my research work. I am extremely indebted to him for holding me to a high research standard and enforcing strict validations for each research result that helped me to sort out the technical details of my work and thus teaching me how to do research. I must also thank him for challenging my thinking by helping me question assumptions and view issues from multiple perspectives. He always set high goals for me and continuously encouraged me to achieve them.

I would like to give special thanks to my doctoral committee members Dr. V.V.S.S. Srikanth and Dr. K.A.Padmanabhan for their time and careful attention to detail and invaluable suggestions provided during the review meetings.

I would like to thank Dr. Joydip Jordar who taught me basics of research and guided me in initial stage of my research at ARCI. I am grateful to everyone in the Centre for materials characterization who has assisted me in the course of this work. I thank Dr. G.Ravichandra, Mr.M. Ramakrishna, Mr. L.Venkatesh, Mrs. Jyothirmayi and Dr. P. Suresh for making the facilities available during the research work. My Special thanks to Dr. Ravichandra and M. Ramakrishna for extended support in characterization and data analysis despite their busy schedules they have been very kind and patient and always willing to help me whenever I approached them. I am grateful to Dr. Nitin, Mr.Chandrasekhar, Dr. Neha, Dr. Saktivel, Mr. Naveen, Mrs. Nirmala and Mrs.Uma to extend their help at various phases of this research. I do hereby acknowledge all the scientists at ARCI and other faculties at SEST, UoH for their help and support. My, thanks to everyone in various centres such as Surface Engineering, Electronics, Sol-gel and Carbon materials at ARCI and Centre for Nanotechnology and Department of Physics at University of Hyderabad for their help.

I would also like to acknowledge Ramesh Reddy, G.V.R.Reddy, G.Venkatarao for their assistance with characterization, P.V.Srinivas, I.Prabhu and all the technical assistants and technicians in Centre for nanomaterials for their technical support.

A special word of thanks to A. Srinivas, (HRD), R. Prabhakara Rao, Chief admin & personnel officer and R. Vijay Kumar Chief Finance and accounts officer and other administrative staff who helped me during several administrative and financial work during my stay at ARCI.

I am indebted to all my friends at ARCI staring from project students, research fellows, Graduate trainees to Ph.D students who worked with me and helped me directly or indirectly during my research. I must thank all of the students at SEST whom I have worked with over these years, each in their own unique way. To mention a few my colleagues M.S. Archana and Sai Venkata Pramod, Sridevi, Naresh, Ramya, Harish have all extended their support in a very special way and I gained a lot from them through personal and scholarly interactions. I must thank Naga Sruti Avasarala, Puneet Chandran, Anirudh Peyyeti, Gorantla Akhila and Ram Kumar my friends who are scattered to various places now from ARCI who were there to support me at difficult times during these years.

I will never find words to tell what I owe to Sri Sri Ravishankar, AOL for helping to lead a stress free life through sudarshankriya. I am indebted to Pradip Kumar Shukla (basic and advance course teacher, AOL), Sarita Shukla and family. They are a central part of my life, my comfort cushion. Thanks for everything Sir. I would never be able repay the love and affection in any form showered by your family especially Sarita Aunty (she was my mother away from home in all my endeavours at Hyderabad), Shalki, Nani, Nanaji, Kinshuk and Shruti.

This journey would not have been possible without the support of my family. I am especially grateful to my father and mother for being very patient and supportive at critical times. I owe a lot to my parents, who had faith in me, gave liberty to pursue my studies and helped me at every stage of my personal and academic life, and longed to see this achievement come true. I would like to acknowledge my sisters Jagadamba, Varahalakshmi and brother-in- laws Ganesh and Mutyala Naidu, Kids- Bharath, Gangadhar, Samata, other family members and my best friends Suchi, Suma etc., have been continuously motivating me and for their good wishes. Special thanks to my brother-in law Ganesh who influenced me to come to Hyderabad. The work presented in this thesis would not have been possible without my close association with many people who were always there when I needed them the most. I take this opportunity to acknowledge them and extend my sincere gratitude for helping me make this Ph.D.

Above all, I owe it all to Almighty God for giving me the strength and patience to work through all these years.

Leela Pydi Pavithra Ch.

Dedicated to

The most important people in my life

My Father (Chokkakula Simhachalam) and Mother (Pyditallamma)

List of publications

Patent Filed: 1028/DEL/2009

"Novel Highly Textured Copper Foils with High Hardness & High Conductivity and a Pulse Reverse Electrodeposition Method for Their Preparation"
*B. V. Sarada, **Chokkakula. L. P. Pavithra**, M. Ramakrishna & T. N. Rao.*

Research Publication(s):

1. **Chokkakula L. P. Pavithra** , Bulusu V. Sarada , Koteswararao V. Rajulapati , Tata N. Rao , G. Sundararajan "A new electrochemical approach for the synthesis of copper-graphene nanocomposite foils with high hardness" **Scientific Reports**, 4, 4049; DOI: 10.1038/srep04049 (2014).
2. Bulusu V. Sarada, **Chokkakula L. P. Pavithra**, M. Ramakrishna and Tata N. Rao,"Nanostructured copper foils by pulse reverse electrodeposition for interconnect applications", **Nanotech Insights**, 4, 1 (2013).
3. Bulusu V. Sarada, **Chokkakula L. P. Pavithra**, M. Ramakrishna, Tata N. Rao, G. Sundararajan, "Pulse reverse electrodeposition for preparation of copper foils with high hardness and high conductivity" **Electrochemical and Solid-State Letters**, 13 (6) D40-D42 (2010)
4. **Chokkakula L. P. Pavithra**, Bulusu V. Sarada , Koteswararao V. Rajulapati , Tata N. Rao, G. Sundararajan "Process Optimization of Pulse Reverse Electrodeposition for Graphene Reinforced Copper Nanocomposites" **(**revised version under review- **Materials and Manufacturing Processes)**
5. **Chokkakula L. P. Pavithra**, Bulusu V. Sarada, Koteswararao.V Rajulapati, M. Ramakrishna, Ravi C.Gundakaram, Tata N. Rao, G. Sundararajan "Texture-property correlations in copper foils with enhanced mechanical and electrical properties prepared by pulse reverse electrodeposition" **(**under review- **Crystal Growth and Design)**
6. **Chokkakula L. P. Pavithra**, A. Naga sruti, Koteswararao.V. Rajulapati, Tata N. Rao, Bulusu V. Sarada "Preparation of high quality graphene sheets by rapid electrochemical exfoliation in an electrolyte containing HF" **(Ready for submission)**

7. **Chokkakula L. P. Pavithra**, Koteswararao V Rajulapati, Tata N. Rao, Bulusu V.Sarada "Efficient and Rapid Shortening of Carbon Nanotubes with High Quality by Ultrasonication in Ethanol" **(to be submitted)**
8. **Chokkakula L. P. Pavithra**, Bulusu V. Sarada , Koteswararao V. Rajulapati , Tata N. Rao, G. Sundararajan "Graphene reinforced copper nanocomposites : A review" **(to be submitted)**
9. **Chokkakula L. P. Pavithra**, Bulusu V. Sarada , Koteswararao V. Rajulapati , Tata N. Rao, G. Sundararajan "Approach towards enhancing the mechanical properties of electrodeposited copper and Copper-(CNT/Graphene) nanocomposites" **(Under Preparation)**

Conferences & Workshops

1. Poster Presentation on “Electrochemical Synthesis and Characterization of Copper-Graphene Nanocomposite foils” at International Conference on Nanoscience and Technology,(January 2012), Hyderabad

2. Attended a Five-day School on Surface Engineering Technologies: Research and Applications (SETRA) (August 2012)

3. Oral Presentation on “Synthesis of free standing nanostructured copper foils with high electrical conductivity and high hardness by Pulse and pulse reverse Electrodepostion” at International Symposium for Research Scholars -2010, IIT Madras, (December 2010)
4. Oral Presentation on “Copper foils with high hardness and high electrical conductivity by pulse electrodeposition” at AP Science Congress and Annual Convention of A.P. Akademi of Sciences ”Science, Technology, Education for Prosperity”(STEP) (November 2010), JNTU, Hyderabad

5. Oral Presentation on “Highly (111) textured Copper and Copper-CNT Composite foils by Pulse-Reverse electrodeposition for Electronic applications ” at Dr K.V. Rao Scientific Society, Young Scientist Awards 2010 (March 2011), Hyderabad

6. Poster Presentation on “Characterization of Electrochemically Synthesized Graphene by Electron Microscopy ” at International Conference on Electron Nanoscopy, XXXII Annual meeting of EMSI (July 2011), Hyderabad

Table of Contents

List of figures

List of tables

Abstract

The uses of copper are of prime importance in electronics industry for interconnects, PCBs etc. However, the advancement of technology is tending towards the continuous miniaturization of devices. With this, several challenges have been posed to the scientists/engineers in designing materials with enhanced performance at those smaller length scales. As these interconnects of finer dimensions have to carry larger current densities, their mechanical/structural integrity has to be maintained for a successful functioning of the respective devices. Added to that, electromigration is also a major concern. Therefore the grand challenge is to design progressively smaller components with improved mechanical and electrical properties. Copper could be strengthened using well established methods like grain refinement, alloying etc. Out of these, grain refinement offers more advantages in terms of enhancement of strength by manifold in comparison to rest of the methods. Although, decrement in grain size yields high strength materials, the electrical conductivity is often hampered. Hence, the present work focuses mainly on enhancing the mechanical properties in Cu and Cu based composites of smaller dimensions without compromising on electrical conductivity. This was achieved by controlling the grain size, type of grain boundaries and preferred crystallographic orientation (texture) simultaneously. In addition, in order to maintain the electrical conductivity, carbon in the form of carbon nanotubes (CNTs) and graphene is used as an alternative to reinforce the copper matrix.

Copper foils (of thickness less than 100 μm) with various crystallographic orientations including (111), (110) and (100) have been prepared by a rapid pulse reverse electrodeposition (PRED) technique using an 'additive-free' electrolyte. For the first time, an excellent control over (111), (100) and (101) textures in the highly textured copper foils has been achieved by optimization of the cathodic/anodic pulse parameters and current density. The grain size obtained in these foils is ranged between 300 nm to 900 nm. Hardness as high as 2.0-2.7 GPa, while maintaining the electrical conductivity in the same range as that of bulk copper was attained in these foils. The complete study of controlling the (111), (100) and (101) textures, CSL Σ3 coherent twin boundaries, grain refinement and their effect on the mechanical and electrical properties is performed in detail. PRED technique with short and high energy pulses enabled the (111) texture while increasing the forward off- time with optimized current density led to self-annealing and resulted in the formation of (100) and (101) textures. The reverse/anodic pulse applied after every forward pulse aided in the minimization of residual

stresses. Among the three textured copper foils, those with dominant (111) texture exhibited a lower electrical resistivity of ~1.65×10^{-6} Ω-cm and better mechanical strength compared to those with (100) and (101) textures.

Copper-graphene composites have been prepared by reinforcing graphene into the metal matrix. The reinforced graphene has been synthesized by an electrochemical exfoliation technique. Exfoliation of graphite electrode in a novel electrolyte containing HF under mild acidic conditions is an efficient, rapid and scalable method. The role of voltage applied for anodization has been shown to control the features of the graphene sheets. Predominantly, 1–4 or 3- 6 layered graphene sheets and larger lateral size (0.5-20 µm) were achieved with lesser defect density, higher yield (~90 %) and lower degree of oxidation. The size of the graphene sheets and the number of layers mainly depended on the voltage applied. X-ray photoelectron spectroscopy (XPS) analysis has shown the absence of fluorine in the graphene sheets at lower concentrations of HF revealing high quality sheets which can be used for various applications. The electrochemically synthesized graphene has been used for the preparation of Cu-Gr composite foils.

Cu-Gr composite foils were synthesized for the first time, by varying the graphene content and pulse parameters (PRED/DC). Application of pulse reverse current has resulted in uniform distribution of Gr in the metal matrix. Fascinating observations have been made where, hardness (~2.7 GPa) was enhanced mainly with increase in graphene content (0-0.75 g/L), while maximum elastic modulus (~137 GPa) was achieved for a graphene content of 0.5 g/L in the electrolyte. In addition to the presence of optimum amount of graphene (0.5 g/L), application of PRED technique, sheet-like structure, available surface area which is in contact with copper matrix of finer grain size, uniform distribution and spread of graphene could have influenced the mechanical and electrical properties. The major contribution in enhancement of properties was found due to the presence of graphene and its uniform dispersion and distribution as a sheet throughout the copper matrix.

CNT reinforced copper composites have been prepared using PRED with the process parameters same as that were used for the preparation of Cu-Gr composites. Agglomerates of CNTs were found at various locations in these samples. Mechanical properties are evaluated using nanoindentation. It was revealed that there was no significant improvement in the mechanical properties of Cu-CNT composites probably because of agglomeration of CNTs. To overcome this problem, CNTs are shortened using ultrasonication in an organic solvent

(ethanol). Now the length of these CNTs has been decreased to 2 μm from an initial length of ~ 10 μm. Subsequently the electrodeposition has been performed by adding these shortened CNTs to the electrolytic bath. Thus prepared Cu-CNT composite foils resulted in the less agglomeration of CNTs. This suggests that the interface between Cu and CNTs plays a crucial role in having uniform dispersion of CNTs throughout the matrix. To address this problem, CNTs are now coated with Cu and these Cu coated CNTs are added to the electrolytic bath. The Cu-CNT composites thus prepared resulted in uniform and enhanced mechanical properties. The hardness and modulus measured are about 2.4 GPa and 120 GPa respectively. However it is to be noted that these mechanical properties have decreased after subjecting these foils to annealing at 573 K. Based on our experimental observations in this study, it is suggested that, prior to using CNTs as reinforcements in Cu based composites, their agglomeration problem should be addressed in a detailed and more comprehensive manner.

In summary, this thesis reports state-of-the-art findings on control of various pulse parameters during electrodeposition in having a full control on different textures in Cu foils. Graphene was found to be highly advantageous in comparison to CNTs as a reinforcement material in Cu based composites in enhancing the mechanical properties. It is to be noted that the 2D nature (high aspect ratio and sheet-like structure) of graphene might also be playing a role in having an uniform dispersion and dictating the final properties in comparison to 1D nature of CNTs. Graphene also appears to be a better reinforment material in terms of cost, reprodcibility, industrial feasibility etc. Hence it is recommended that depending on the requirement and operating conditions, textured pure copper and Cu-Gr composites could be used for industrial applications. Highly texured and twinned copper foils could be used for room temperature applications, while copper-graphene composite foils could be used even for slightly high temperature applications as well, where grain growth is probably inhibited by the presence of graphene by preserving the initial/inherent properties.

Chapter 1. Introduction

Pure copper and copper based nanocomposites, especially copper-carbon nanotube (Cu-CNT), copper-graphene (Cu-Gr) have been the major focus since a decade for vivid applications ranging from automotive, aerospace industry to microelectronics (interconnects, micro-electromechanical systems (MEMS), printed circuit boards (PCBs)), the latter being the focal point and central application for which the current research proposes a viable solution. Advancement in technology has led to continuous decrement in dimensions of components with high performance having a variety of uses without compromising on the mechanical, electrical, thermal and physical properties. Aluminum (Al) has been used for several applications in microelectronic industry [1]. However this scenario has changed with copper and copper nanocomposites entering the fray owing to their high mechanical, electrical and thermal properties with effective electromigration resistance [1]. Use of copper in the area of microelectronics especially interconnects, PCBs has had an astounding impact in terms of achieving desirable properties [2]. Hence synthesis of copper needs to be tailor-made for these applications i.e. synthesis and strengthening of copper simultaneously via suitable methods without losing on the electrical properties while retaining its mechanical properties is essential. With this background, an earnest attempt has been made to prepare copper foils with highly preferred orientation, special grain boundaries (CSL Σ3 coherent twin boundaries) and copper nanocomposites (Cu-graphene/CNT) by pulse reverse electrodeposition in an 'additive-free' electrolyte which is a first in itself, eventually achieving high hardness while maintaining the electrical conductivity. The role of each microstructural feature towards increasing the characteristics of pure copper and influence of graphene and CNTs as reinforcements has been one of the major findings in this research. structure-property correlations were made for the very first time in pure copper, Cu-Gr and Cu-CNT based on the above studies.

1.1 Background

Copper ($Cu^{29}_{63.546}$) is an abundantly available and cost effective material with superior electrical, mechanical and thermal properties compared to the other existing materials with high electrical conductivity [1, 3]. Owing to its intrinsic characteristics, copper is chosen over

aluminum among the metals (Ag, Au etc.) which are available for electronics [1]. Table 1.1shows the contrasting properties of copper and aluminum i.e. low electromigration and less grain growth, strength being a major issue for specific applications.

Table 1.1 Properties of copper and aluminum properties of copper and aluminum

Property	Copper	Aluminum
Electrical conductivity %(IACS) at 20 ºC	101	60
Tensile strength (MPa)	200-250	40-50
Thermal conductivity at 20 ºC ($W/m^{-1}K^{-1}$)	353-401	204-249

Nanostructured copper, copper alloys (Cu- Be, Cu-Ni, Cu-Al, Cu-Cr, Cu-Ag etc.) [4] and copper nanocomposites (Cu-SiC, Cu-WC, Cu-TiO_2, Cu-TiC etc.) [4-7] have been widely used in various applications from architecture, automotive, electronics to aerospace as electrical conductors, heat exchangers and radiators, etc. Electronics industry has extensive usage of copper as electrical contacts in printed circuit boards, interconnects, radio communications etc. (Figure 1.1). The continuous miniaturization of electronic components demands for smaller and reliable materials with ever increasing performance.

Therefore strengthening of copper for specific applications at smaller dimensions in electronic circuits is of prime importance. Copper can be prepared by several methods depending on the applications. Although traditional strengthening methods increase the mechanical properties of copper but they affect thermal and electrical properties.

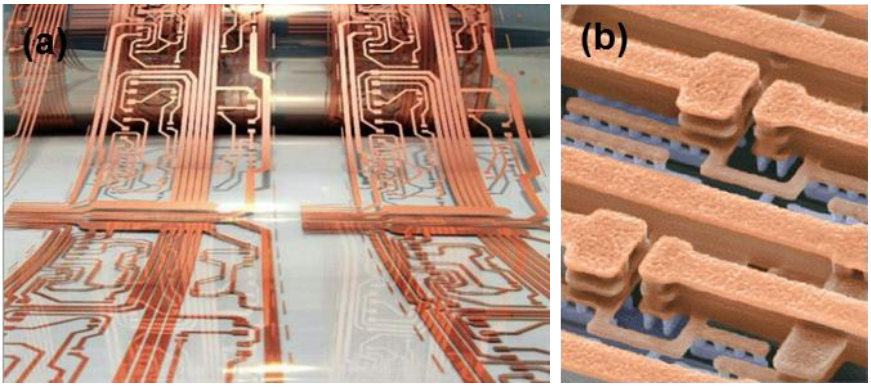

Figure 1.1 Copper as a material for electronics industry (a) flexible printed circuit board [8] and (b) interconnects (adopted from [9])

Physical vapour deposition, chemical vapour deposition, thermal spraying, electrodeposition, electroless deposition, diffusion coatings, and laser based techniques (laser cladding, etc.) are some of the techniques available for synthesis of copper foils. Several attempts have been made to strengthen copper by various approaches including alloying (substitutional/ interstitial) and precipitation hardening (coherent/semi-coherent phase) [10] or dispersion by reinforcement of micron, submicron, or nano-sized metal oxide (Al_2O_3, TiO_2, SiO_2) [5] or carbide (WC, SiC, TiC etc.) particles [6, 7] as the second phase and/or deformation by cold rolling etc. Although the mentioned strengthening methods increase the mechanical properties in copper, they result in decrement of thermal and electrical properties. Hence, it is utmost necessity to strengthen copper, with simultaneous retention of electrical conductivity.

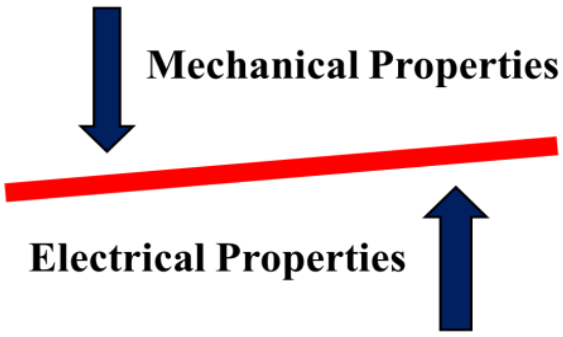

Figure 1.2 Balance between mechanical and electrical properties of copper.

In order to attain this balance between the electrical and mechanical properties in copper, among the vivid techniques available to synthesize copper, electrodeposition has been

chosen for the preparation of copper and copper nanocomposites. It is a simple, economical and environmental friendly room temperature method where deposition can be made on complex shapes with uniform thickness. In addition, the microstructure of pure copper was modified by either controlling the texture/grain refinement/introduction of special grain boundaries. Selective reinforcements such 1D MWCNTs and 2D graphene are introduced into the copper matrix in order to achieve both mechanical and electrical properties simultaneously [11, 12].

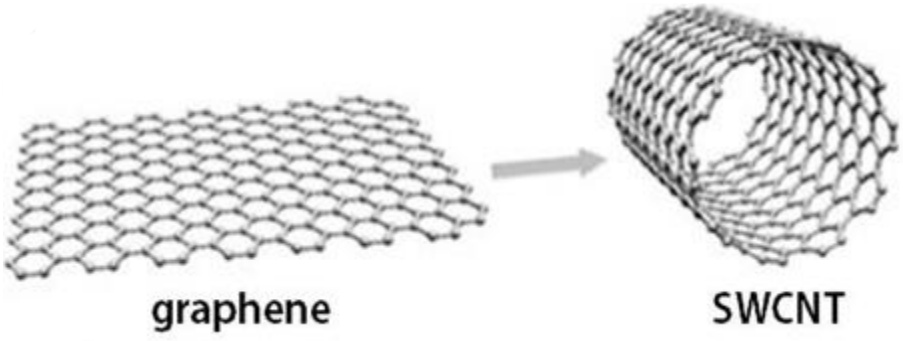

Figure 1.3 Graphene and carbon nanotube (adopted from [13]).

1.2 Problem statement

Copper has been used for several electronic applications such as PCBs, interconnects, etc. Because of the miniaturization of the technologies and associated components, fabricating smaller components with simultaneous possession of enhanced mechanical and electrical properties has been a grand challenge. For example, copper for PCBs requires high strength in order to carry large currents at room temperature or slightly higher temperatures due to electromigration. However, retaining the electrical properties while strengthening the copper by traditional methods has been an uphill task. Therefore in an effort to find a suitable material (in this case it is Cu and Cu based nanocomposites) in addressing some of the above challenges, the current study has been performed. It involves preparation of highly textured and twinned copper foils, Cu-Gr composite foils and Cu-CNT composite foils by a novel PRED technique, without adding any additives in the electrolyte. The preferred crystallographic orientation increases the electromigration resistance [2, 14-16] whereas twinning increases the electrical conductivity [17]. Adoption of graphene/CNTs as reinforcements in copper could improve

mechanical and electrical properties and could inhibit the coarsening of microstructural features of Cu matrix as the operating temperatures sometimes are slightly higher than ambient temperatures. Further the processing technique, PRED governs the grain size, texture, type of grain boundaries in pure copper and uniform distribution and dispersion of reinforcement in composites without the use of additives. Hence the electrical conductivity can be retained in the copper foils with high stability of texture and mechanical properties with negligible residual stresses.

1.3 Pure copper and copper nanocomposite foils with enhanced mechanical and electrical properties

1.3.1 Pure copper

Controlling the mechanical properties and electrical properties in pure copper is possible by controlling the grain size, texture (preferred crystallographic orientation) and twinning (special grain boundaries) [18-20]. Each microstructural feature has its role in enhancing the material properties such as mechanical, electrical and thermal properties. Majority of material properties are mainly influenced by the grain size, type of grain boundaries and texture in any metal. Among the microstructural features, grain refinement plays a major role in enhancing the mechanical properties of a material according to the Hall-Petch relation [21-23],where the mechanical properties such as hardness and tensile strength are inversely proportional to the grain size, while, preferred crystallographic orientations (texture) influence the electromigration resistance [16], oxidation resistance, thermal stresses and voids etc., [24, 25] of the material depending on their atomic density of that particular crystal plane. In addition, special grain boundaries such as low energy high angle grain boundaries, also called as coherent twin boundaries (CSL Σ3 boundaries) [26] are the key strengthening candidates in attaining hardness as well as electrical conductivity by hindering the dislocation motions. At the same time, the electrical conductivity can be maintained by reducing the scattering of electrons at the twin boundaries in the material [20, 27-29]. These special boundaries also help in delaying the atomic diffusion through the twin boundary region [14, 30]. Several efforts have been devoted towards the preparation of copper foils with preferred orientation and twinning in order to achieve both electrical and mechanical properties by electrodeposition

technique [19, 31-37]. Majority of them are by DC and PED with limited reports by PRED [35]. Most of these studies have used organic additives in the electrolyte in order to control the microstructural features such as grain size, or introduction of twin boundaries or texture [32, 38-43]. PED and PRED play a significant role in influencing the change in texture, grain size and type of grain boundaries without the use of additives. There are very limited studies where PRED technique was used to control the texture, twin density in an effort to increase the high hardness of copper [35, 38]. To the best of our knowledge, no reports have appeared on controlling the three textures and twin density in copper by varying the pulse parameters in PRED technique and no correlation has been made so far between processing parameters/properties. In the present work, impetus is on preparing the copper foils by a rapid approach in electrodeposition to succeed in achieving the required properties in copper by controlling three essential microstructural characteristics such as (111), (100), and (110) textures, CSLΣ3 coherent twin boundaries and grain size without additives in the electrolyte during the PRED process and correlate the mechanical properties and electrical properties with these microstructural features.

1.3.2 Copper nanocomposites

Copper (Cu) matrix nanocomposites have witnessed an enormous growth during the past decade, due to their enhanced mechanical and thermal properties leading to numerous industrial applications [44]. However, reinforcement of small oxide/carbide particles into copper matrix [4-7] leads to large decrement in electrical conductivity while enhancing the mechanical properties. Hence they are not desirable for electronic applications. Carbon, in the form of fibres, fullerenes, CNTs and graphene as reinforcement material can be a better option where the mechanical properties are enhanced and the electrical properties of copper are maintained. Since its discovery, a number of investigations have been carried out using CNTs as reinforcement in polymers, ceramics and metals by different techniques which have proved to be an alternate to fibres [45, 46]. Enormous research has been carried out to make use of CNTs as reinforcement for composite materials for several applications such as structural applications for their high specific strength as well as functional materials for their exciting thermal and electrical characteristics. Among the various processes, powder metallurgy and electrodeposition are the most commonly used techniques for preparing CNT reinforced

composites [44]. However, CNT-metal matrix composites have been received less attention in recent times due to the processing cost of CNTs, entanglement due to the van der waal interactions leading to the agglomeration, improper dispersion and distribution, weak interfacial bonding due to tubular structure. In contrast, recently emerged graphene with two dimensional sheet-like structure having high aspect ratio and large surface area compared to CNTs, has been attracted a great deal of interest by the scientific community as a viable replacement for CNTs in overcoming the aforementioned challenges. Therefore by graphene reinforcement is expected to have a positive influence on the various properties of the composites [47].

Graphene is a proven candidate as a reinforcement material in improving the strength of polymers as well as metal matrix composites due to its excellent mechanical properties [47]. In addition, graphene is also shown to block dislocation motion in well-designed nano layered metal-graphene composites resulting in ultra-high strength [48]. The extremely superior properties of graphene (Gr), consisting of a single to few layers of covalently bonded sp^2 carbon atoms, hexagonally packed in a honeycomb crystal lattice, allow it to surpass CNTs as an ideal reinforcement into the composites [47, 49]. Graphene, unlike CNTs, can be prepared by inexpensive methods in large quantities by chemical and electrochemical exfoliation of graphite [50, 51]. Several researchers have also reported an enhancement in mechanical [52], thermal [53] and electrical properties [54] of polymer based composites with small amounts of Gr introduced into the matrix. However, in case of Cu-Gr nanocomposites, only few studies have been reported either on mechanical or electrical and thermal properties by different approaches. Preparation methods include powder metallurgy, molecular level mixing, electrodeposition etc. Electrodeposition technique, especially with application of pulsed currents is an easy, cost effective and scalable method to incorporate filler materials with nano-sized dimensions homogeneously throughout the matrix [55]. Since the electrodeposition is a room temperature process, the inherent properties of graphene (Gr) and graphene oxide (GO) could be preserved during the preparation of the composites unlike in the conventional sintering processes where high temperature is involved. High temperatures (>600 °C) could destroy the graphene [12]. Therefore the primary focus of the current research work has been preparation of Cu-Gr nanocomposites by DC, PED and PRED techniques with optimized graphene content to be incorporated into the copper matrix by an appropriate technique for

enhanced mechanical and electrical properties simultaneously. The graphene, in the current study, has been prepared by an electrochemical exfoliation route. Copper-CNT composite foils were also prepared by the pulse reverse electrodeposition and few attempts have been made to overcome the challenges in improving the properties by shortening of CNTs, electroless deposition of Ni, Cu on CNTs etc.

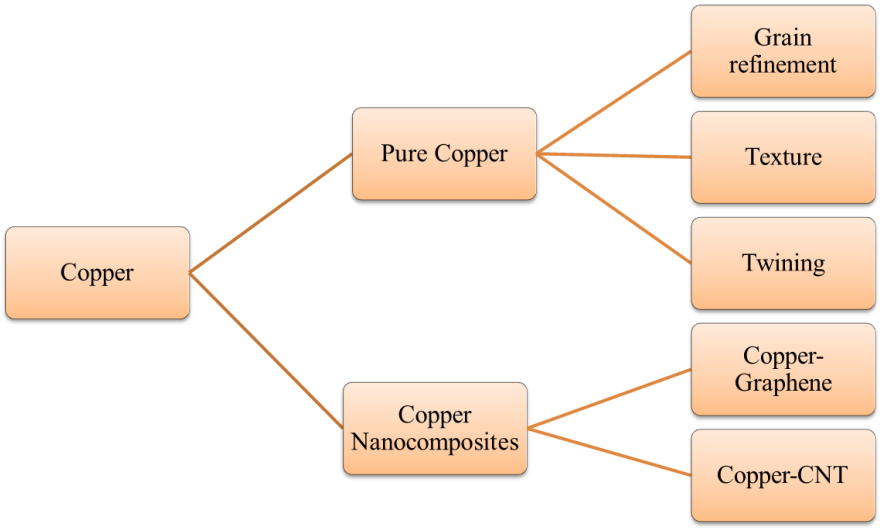

Figure 1.4 Approach towards enhancing mechanical properties while maintaining the electrical properties.

1.4 Thesis objectives

- Preparation of pure copper foils using pulse reverse electrodeposition technique in an 'additive-free' electrolyte.
- To control various process parameters during electrodeposition to achieve maximum control on (111), (101) and (100) textures and the twin density in copper foils.
- Preparation of graphene in bulk quantities using electrochemical exfoliation using an electrolyte containing HNO_3 and HF.
- Preparation of Cu-Gr composite using various electrodeposition techniques in an effort to achieve enhanced mechanical and electrical properties.

- Preparation of Cu-CNT composites.
- Detailed microstructural/structural characterization of above synthesized materials using XRD, SEM, TEM, Raman spectroscopy, XPS, FTIR etc.
- Evaluation of mechanical properties of these novel materials using depth sensing nanoindentation at room temperature.
- Measurement of electrical resistivity using four-probe method at room temperature.
- Evaluation of structure-property correlations and to make recommendations for a better copper based material with enhanced mechanical and electrical properties too address some of the challenges being faced by the electronics industry.

1.5 Thesis organization

Chapter 1 discusses the scope and approach towards achieving the mechanical and electrical properties in pure copper and copper nanocomposites.

Chapter 2 discusses the importance of copper and copper nanocomposites for industrial applications and strengthening mechanisms of copper by different approaches. In addition, brief description about electrodeposition process, different techniques in electrodeposition process such as DC, pulse current and pulse reverse electrodeposition with advantages and disadvantages are mentioned. Further literature on synthesis of highly textured copper, recent studies on copper, Cu-Gr and Cu-CNT composites which are relevant to our approach in achieving the mechanical properties by strengthening are being discussed.

Chapter 3 discusses experimental details for the preparation of individual systems such as pure copper, synthesis of graphene, Cu-Gr, copper-CNTs and methods/techniques used for characterization of copper and copper nanocomposite foils.

Chapter 4 discusses texture evolution, control over twin density and their texture-property correlations in pure copper foils synthesized by PRED in 'additive-free' electrolyte. This part of the work has been published in **"Electrochemical and Solid-State Letters"**, 13 (6) D40-

D42 (2010) as a short communication and full length article is under review in **"Crystal Growth and Design".**

Chapter 5 discusses the graphene synthesis by electrochemical anodization being a part of preparation of Cu-Gr composites. This part of the work is ready for submission.

Chapter 6 discusses the influence of pulse parameters and graphene concentration in the electrolyte on the mechanical and electrical properties of Cu-Gr nanocomposite foils prepared by electrodeposition. Part of this work has been published in **"Scientific Reports"**, 4, 4049; DOI: 10.1038/srep04049 (2014) and the remaining part is a revised version which is under review in **"Materials and Manufacturing Processes".**

Chapter 7 discusses the studies carried on the influence of geometry of 1D CNTs with 2D graphene and attempts made to achieve the mentioned properties. Part of the work is ready for submission.

Chapter 7 discusses the studies carried on the influence of geometry of 1D CNTs with 2D graphene and attempts made to achieve the mentioned properties.

Chapter 8 discusses structure-property correlations including summary of main findings in copper, Cu-Gr and Cu-CNT composites and the conclusions.

Chapter 9 is on the suggestions made and the scope for the future studies on improving the properties of pure copper and copper composites

Chapter 2. Literature review

2.1 Electrodeposition

Electrodeposition is a well-established, inexpensive and scalable processing method for coating metals as thin layers [56-58]. It is a surface phenomenon which involves the reduction of metal ions on the cathode and forms a solid metal coating from liquid state by using electric current [59]. It has several advantages over other coating processes like physical vapour deposition, chemical vapour deposition, thermal spray coatings, electroless plating etc. A simple experimental setup can be used to deposit metal coatings of uniform thicknesses on complex shapes and surfaces can be achieved at room temperature. The drawback of this technique is that, only conducting material can be coated on a conducting substrate with the application of current/voltage. Copper in particular, is the material of interest in the current research study.

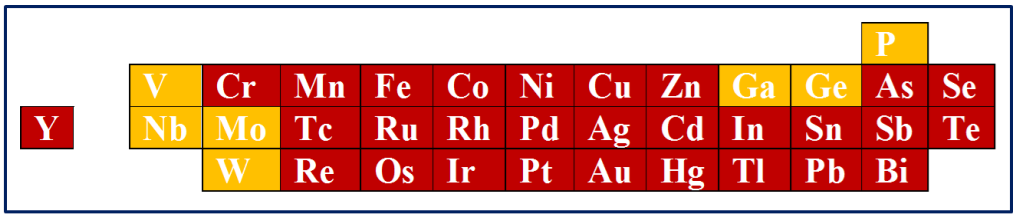

Figure 2.1 Metals platable from aqueous solutions (red) and platable in combination with one of the others (alloy plating) (Yellow) redrawn from [60]).

All the elements which are in the periodic table cannot be deposited by this route. Figure 2.1 depicts the elements in the periodic table which can be electrodeposited. In addition, along with these elements micron to nano sized particles such as oxides, nitrides, carbides, carbon in the form of fibres, tubes etc. can also be co-deposited along with the metal ions by dispersing them in the electrolyte with the addition of a surfactant/additive. In this technique, the metal/substrate on which plating is done is the cathode and the metal to be plated is the anode. Both anode and cathode are immersed in the electrolyte, which contains one or more dissolved metal salts with other ions to allow the flow of electricity acting like a medium. A power source with a rectifier supplies the current to the electrochemical cell. The anode is connected to the positive terminal of the supply, and the cathode is connected to the negative terminal.

Schematic of electrodeposition is shown in Figure 2.2. Initially when current is supplied to the anode comprising the metal atoms it oxidizes and dissolves in the solution (also ions are formed from the electrolyte). These dissolved metal ions are attracted towards the cathode and are reduced at the interface between the solution and the cathode, and are finally coated as a metal. This can be elaborated as, during the reduction process, initially the cations get stripped off from the hydrated complex as shown in Figure 2.2 and adsorbed as bare metal ions on the cathode. These bare metal ions then get reduced by combining with electrons on the cathode surface hence becoming neutral atoms. This process continues with the migration of atoms over the substrate until they get adsorbed at active sites which are kinks and steps present on the surface also called as nucleation sites. Continuous adsorption of atoms results in constant spreading of the single atomic layer over the cathode/substrate surface. These adsorbed atoms move over the substrate surface interacting with each other forming bigger clusters in order to become stable. Many such clusters collide with other and grow in size and ultimately deposits as a thin coating. During deposition, larger islands grow and sometimes they leave certain portions of the substrate uncoated in the form of channels and holes which are later on filled up forming a continuous film.

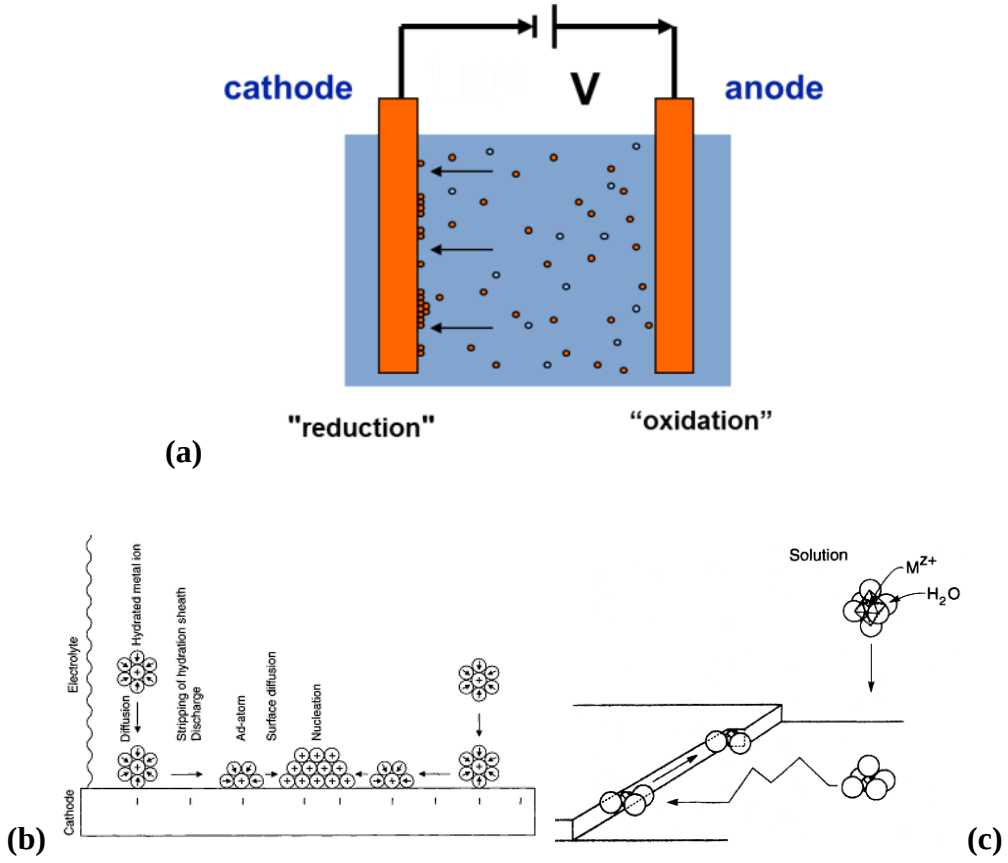

Figure 2.2 Schematic showing (a) a typical electrolytic cell and (b-c) the deposition process (adopted) [61].

Reactions at the anode:

$$Cu^0 \rightleftharpoons Cu^{2+} + 2e^- \qquad (2.1)$$

$$H_2O \rightleftharpoons \frac{1}{2}O_{2(g)} + 2H^+_{(aq)} + 2e^- \qquad (2.2)$$

Reactions at the cathode:

$$Cu^{2+}_{(aq)} + 2e^- \rightleftharpoons Cu^0_{(s)} \qquad (2.3)$$

$$2H^+_{(aq)} + 2e^- \rightleftharpoons H_{2(g)} \qquad (2.4)$$

2.2 Faraday's law

Faraday's law states that the amount of electrochemical reaction that occurs at an electrode is proportional to the quantity of electric charge 'Q' passed through an electrochemical cell. Thus, if the weight of a product of electrolysis is 'w', then Faraday's law [61] states that

$$w = ZQ \qquad (2.5)$$

Where, 'Z' is the electrochemical equivalent, the constant of proportionality. Since Q is the product of the current I in amperes and the elapsed time t in seconds,

$$Q = I \times t \qquad (2.6)$$

Therefore,

$$w = ZIt \qquad (2.7)$$

In electrodeposition, rate of reaction such as oxidation and reduction at the anode and cathode respectively, are controlled by the electrical current (amps), supplied to the electrochemical cell and the duration. Therefore, depending on the type of current and time for which it is supplied, mainly two types of electrodeposition are in practice: DC and pulse current deposition techniques. In DC, current is supplied continuously until the required thickness is achieved irrespective of the time. In PED, current is given in pulses with a definite time called forward pulse/cathodic pulse. Each pulse follows an off-time (no current is supplied during off-time). This again follows the next pulse and so on. Sometimes, these pulses are given in negative direction called anodic pulse in addition to the cathodic pulse (forward pulse). Wave forms of DC, pulse and pulse reverse electrodeposition are shown in Figure 2.3.

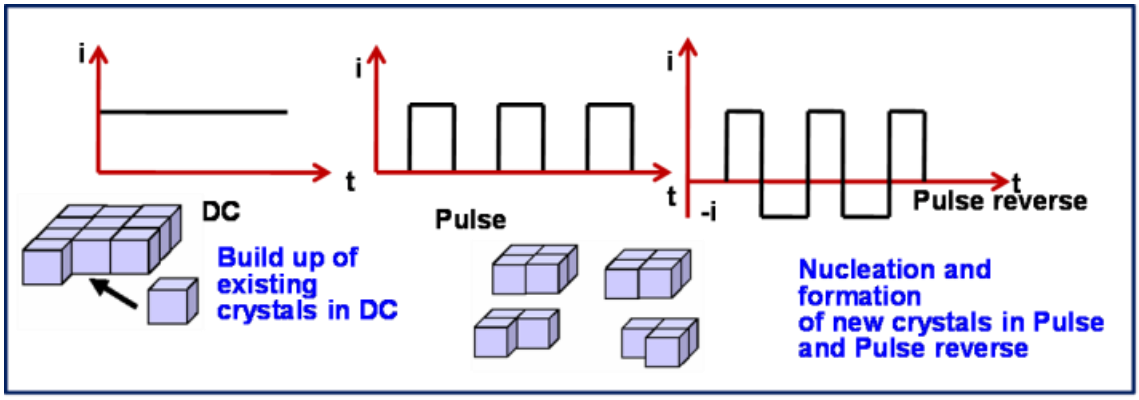

Figure 2.3 Current waveforms for DC, pulse and pulse reverse electrodeposition.

These pulses are usually in square form because square waves have an advantage of controlling wide range of duty cycle. In addition, Faradays law given in section 2.1.1 can quantify the amount of deposited material.

2.3 Direct current electrodeposition

In this process, direct current (DC) is supplied to the plating bath as shown in Figure 2.3; constant current/voltage is applied for deposition using a power source in the form of a battery or a rectifier [61]. Due to the constant and continuous supply of current, there is a continuous reactions takes place at the surface of anode and cathode. This results in the continues reduction of metal ions on the cathode leading to the uninterrupted growth of crystals instead of new nucleation sites. Therefore, the as deposited coating ends up with high porosity and roughness and with larger residual stresses. Figure 2.3 indicates the current flow in the DC deposition

2.4 Pulse electrodeposition (PED)

Pulse plating was performed for the first time in the 1970s by Western Electric for depositing gold for crossover circuits in electronic switching [62]. In this plating, time was reduced by 50% with the application of pulse compared to DC. In PED, the current supply is made in a series of short pulses as shown in Figure 2.4.

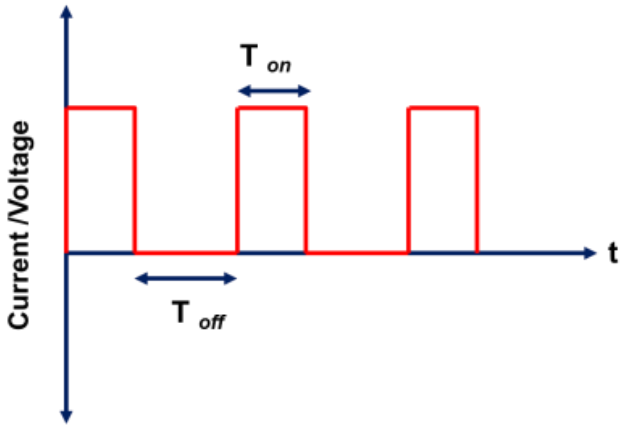

Figure 2.4 Square wave shapes for pulse electrodeposition.

These pulse cycles can be controlled with pulse timings at required rates. Defined changes in these cycles offer vivid results to the deposited material in terms of microstructure, physical, mechanical, thermal and electrical properties [63]. Modulated current in the form of waves is used in the form of pulses with $T_{F\,on}$ and $T_{F\,off}$ times. For a pulse, during the on-time, due to the application high current, deposition takes place and during the off-time, no current flows in the system hence no deposition. The off-time is a relaxation time in which deposited grains rearrange to more stable positions and also adsorbed impurities are removed from the coating. The 'on' and 'off'-time completes the first cycle. During the second cycle, deposition takes place at new nucleation sites that might be formed during off-time. In addition, PED allows application of high current densities during deposition. Most of the impurities and gases entrapped during the deposition will diffuse out during the off-time. Hence, the pulse parameters have great influence on the properties of the as deposited coating free from porosity, dendritic growth, pinholes, with smooth, dense and fine nanocrystalline structures and better current efficiency compared to DC. Deposit properties can be expressed with duty cycle and average current density as given below

$$Duty\ cycle\ \% = \frac{t_{on} \times 100}{t_{on} + t_{off}} \qquad (2.8)$$

$$Average\ current\ density\ i_{avg} = \frac{\boldsymbol{i_{fwd} \cdot t_{on}}}{(\boldsymbol{t_{on} + t_{off}})} \qquad (2.9)$$

PED coatings are characterized by high hardness, high wear resistance and low coefficient of friction. PED has several other advantages over DC in terms of throwing power, distribution, porosity and metal usage.

2.5 Pulse reverse electrodeposition (PRED)

PRED is also categorized under PED, the difference being the application of anodic pulse in addition to the cathodic pulse. PED has deposition (on-time) with a relaxation (off-time) in the iterations on the cathodic side. For the same iteration if an anodic step (reverse) is added after every cathodic pulse that is called pulse reverse technique. If an anodic/reverse pulse is applied after every cathodic pulse, which is referred as pulse-reverse electrodeposition. PRED exhibits several advantages over both DC and PED electrodeposition [63, 64]. During PRED, current is given in the form of modulated wave like in PED. Different types of waveforms for PRED are given in Figure 2.5. Similar to pulse, in PRED as well, during forward pulse deposition takes place and for the duration of forward off-time, no deposition occurs at the cathode. In PRED, during the reverse pulse anode acts as cathode and vice versa resulting in removal of some of the deposited material. Along with the removal of the deposited layer, removal of entrapped impurities and hydrogen also takes place due to the oxidative reaction. In PRED four parameters are required for the application of cathodic and anodic pulses, which influence the properties of the final deposit. The duty cycle and average current density for the PRED is given as

$$Duty\ cycle\ \% = \frac{t_{fwdon}}{t_{revon}+t_{fwdon}} \qquad (2.10)$$

$$Average\ current\ density\ i_{avg} = \frac{(i_{fwd}.t_{fwdon})+(i_{rev}.t_{revon})}{(t_{fwdon}+t_{revon})} \qquad (2.11)$$

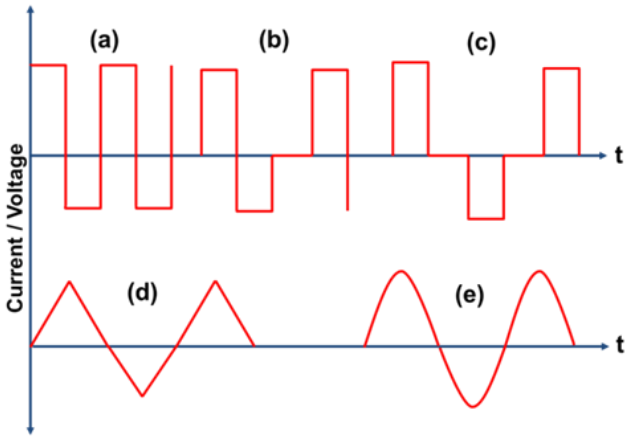

Figure 2.5 Types of waveforms for PRED.

The main difference from the DC and PED is PRED makes deposit very smooth, highly dense, porosity free and retards the grain growth. PRED reduces the amount of impurities on the foil resulting in improved mechanical and electrical properties. PRED allows independent variation of pulse waveform, cathodic /anodic pulses, duty cycle and applied potential which controls the properties such as microstructure, adhesion, composition, crystallinity and electrical properties [63, 65] Currently, pulse reverse (PR) plating is widely used in printed circuit board (PCB) manufacturing, but long before this became relevant and industrially important, for several applications such as coatings, decorative applications [66]. Though, pulse plating technique results in smooth, compact and fine grained structures, macro throwing power is worse than that for DC plating. Best throwing power can be obtained by pulse reverse plating. In addition, use of additives involves high cost and limits ductility and conductivity of the deposited copper [67]. In addition, during the deposition process the anodic current results in electro crystallization on the cathode surface with preferred orientation (smaller crystal grains) with smoother, brighter deposits with lower internal stresses [68]. However, in case of composites, pulse reverse plating method has been developed in order to enhance the particle concentration in electrodeposited metal matrix composite coatings [69, 70]. It was also previously shown that the particle concentration deposited in pulse reverse plated coatings can be increased up to six times over that with unmodulated, DC electrodeposition [71].

Generally, deposition processes using DC method require the use of additives to control deposit structure, properties and current distribution. By selecting the appropriate process parameters the properties of deposits made by pulse current (PC) and pulse reverse current (PRC) techniques can be improved with addition of minimum or no additives in electrolytes. The present research evaluates the influence of cathodic time ($T_{F\ on}$), anodic time ($T_{R\ on}$), relaxation time ($T_{\ F/R\ off}$), and applied current used in the PC and PRC techniques [72]. PED and PRED have numerous advantages over existing DC electrodeposition which are mentioned in Table 2.1.

Table 2.1 Advantages of Pulse/PRED [64]

Metallurgical	Physical	Electrical	General
• Improved density • Lower porosity and roughness • Finer grain size • Better mechanical properties • Reduced residual stresses • Reduced hydrogen embrittlement	• Improved adhesion • Increased throwing power • Uniform thickness • Better control of alloy composition • Better colour and brightness	• Higher conductivity • Lower contact resistance • Better bondability	• Reduced process limitations • More flexibility of metal content in bath • Reduction/elimination of additives • Reduced process (plating) time

2.6 Deposition mechanism for pure metals and composites during electrodeposition

In electrodeposition process, when current/voltage is applied across an electrolytic cell, the deposition [61, 73] follows the described manner. Initially, electron flow will be moving from the anode to the cathode.

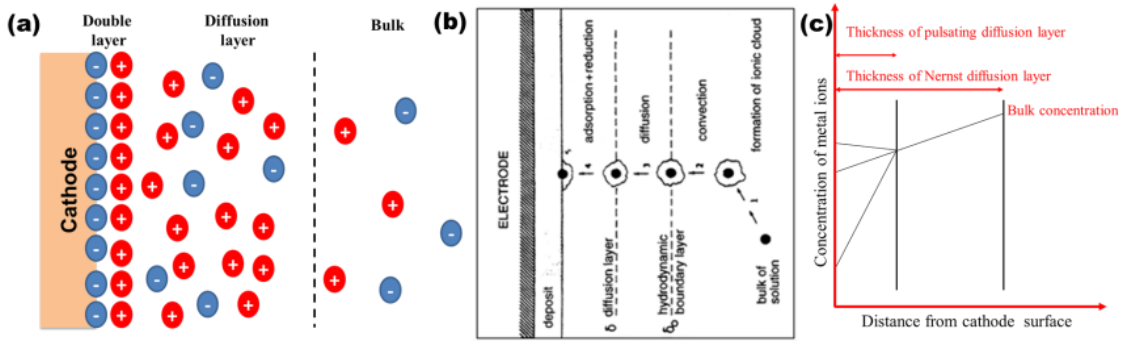

Figure 2.6 Deposition mechanism in copper and composites and diffusion layer in pulse electrdeposition (adopted from [61]).

During this process, ions pass through a diffusion layer and a double layer (Figure 2.6). Mechanism of electrodeposition is the migration of metal cations towards the cathode and the deposition on the cathode. There are three main mechanisms involved in deposition of ions on the electrode surface that include migration (due to the potential gradient the ions move through electrolyte), convection (which involve the movement of ions through an electrolyte from the bulk solution by stirring etc.) and diffusion. Diffusion has a major role in deposition where concentration gradient is the driving force. However, during the current flow, the deposition or reduction of cations on the cathode takes place; thereby concentration gradient is established in the electrolytic cell. Therefore the ions tend to move from high concentration region to lower concentration region that is towards the cathode. The thickness of this diffusion layer is called as the Nernst or Nernstian layer (Figure 2.6). Under static condition, this diffusion layer thickness would be ~0.2 mm. Under conditions of convection such as stirring etc., this thickness will decrease up to ~0.001 mm. This diffusion layer thickness varies with the pulse parameters in case of PED and PRED. During PED and PRED both on-time and off-times influence the diffusion process. Unlike in DC method, during the off-time, reduced/consumed ions at the cathode surface are replenished from the bulk electrolyte. Therefore the diffusion layer breaks down and builds again during on-time. Thus, building and breaking down of diffusion layer occurs in pulse and PRED leading to a quasi-steady state. The two sides of the Nernst diffusion layer are called as pulse diffusion layer and stationary diffusion layer. Pulse diffusion layer is also called as inner layer which is located at the immediate area of the cathode surface. Stationary diffusion layer also known as the outer layer, extends up to the bulk from the other end of the inner layer. The thickness of the pulse diffusion

layer (δp), determines the distance for the ions to travel across to reach the electrode surface which is considerably smaller than Nernst diffusion layer (δN) [74].

2.6.1 Nernst equation

Nernst equation [61] can be used to relate the reduction potential of a half-cell (or the total voltage (electromotive force) of the full cell) at any point in time to the standard electrode potential, temperature, activity, and reaction quotient of the underlying reactions and species used.

$$E = E^0 - \frac{RT}{nF} \ln Q_c \qquad (2.12)$$

'E' is cell potential (V) under specific conditions, 'E^0'is cell potential under standard-state conditions, 'R' is ideal gas constant which is 8.314 J/mol-K, 'T' is temperature (kelvin), which is generally 25 °C (298 K), 'n' is number of moles of electrons transferred in the balanced equation, 'F' is Faraday's constant, the charge on a mole of electrons which is 95,484.56 C/mol and $\ln Q_c$ is the natural log of the reaction quotient at the moment in time.

The pulsating diffusion layer thickness for single pulse [75] is given as

$$\delta_p = (2Dt_{on})^{1/2} \qquad (2.13)$$

Where, D is the diffusion coefficient and for PED and PRED, the diffusion layer thickness varies with the pulse parameters such as cathodic /anodic "on" and "off" times. The diffusion models for PED and PRED are described by Chang [76] and Ibl [75]. This enables the ion transport and facilitates metal ion consumptions at a higher rate at the electrode surface and implies higher limiting current densities. Higher limiting current densities in PED and PRED compared to DC deposition results in good nucleation rate and finer deposit crystallites.

Guglielmi [77] in 1972 (Figure 2.6b) has proposed a mechanism for composites in which the adsorption and electrophoretic attraction has a combined effect for the electrodeposition of the composites. This model has been used for several copper based composites including the co-deposition of alumina particles as reinforcement in the metal matrix etc. However, influence of several parameters has not been explained in this model. In 1987 Celis [78] developed a

mathematical model for the prediction of amount of particles incorporated during co-deposition. As shown in Figure 2.6(b), initially an adsorbed layer forms around the particles by the ionic species immediately after the addition of these particles to the electrolyte before the deposition process starts. Subsequently convection transfer of these particles towards the cathode takes place. Thereby diffusion through double layer and adsorption of particles with ionic species on the cathode occurs, leading to final reduction of ions and incorporation of particles into the metal matrix.

Hence, with this brief understanding of the electrodeposition and its advantages over other techniques, PRED technique is chosen as a suitable technique for synthesizing copper and copper nanocomposite foils.

2.7 Strengthening mechanisms in copper based materials

Strength of a material is very sensitive to its microstructure. Strength/hardness of a material is related to how easily a dislocation moves in a crystal lattice and this in turn governs the associated plasticity. Traditionally, there are four strengthening mechanisms [79] for increasing the mechanical properties of a metal, (i) Grain refinement (ii) solid solution hardening, (iii) precipitation/particle reinforcement hardening and (iv) work hardening. Each method has its own significance in controlling the properties. By grain size refinement, the number of grain boundaries increases which help to block dislocation motion. In solid solution strengthening, solute atoms disturb the periodicity of the lattice and induce stresses. In strain hardening, the deformation in the metal increases dislocation number and thereby these dislocations interfere with the movement of neighbouring mobile dislocations.

Certain methods for instance grain refinement, alloying and particle reinforcement though increase the hardness/strength of the materials, also lead to adverse effects on toughness, elongation and electrical properties depending upon the element used for alloying/reinforcing [4]. Work hardening increases strength yet leads to reduction in the electrical conductivity of materials. For example, electrical conductivity of work hardened copper decreases by 2 to 3% IACS. Figure 2.7 indicates the mechanical and electrical properties of copper strengthened by different methods.

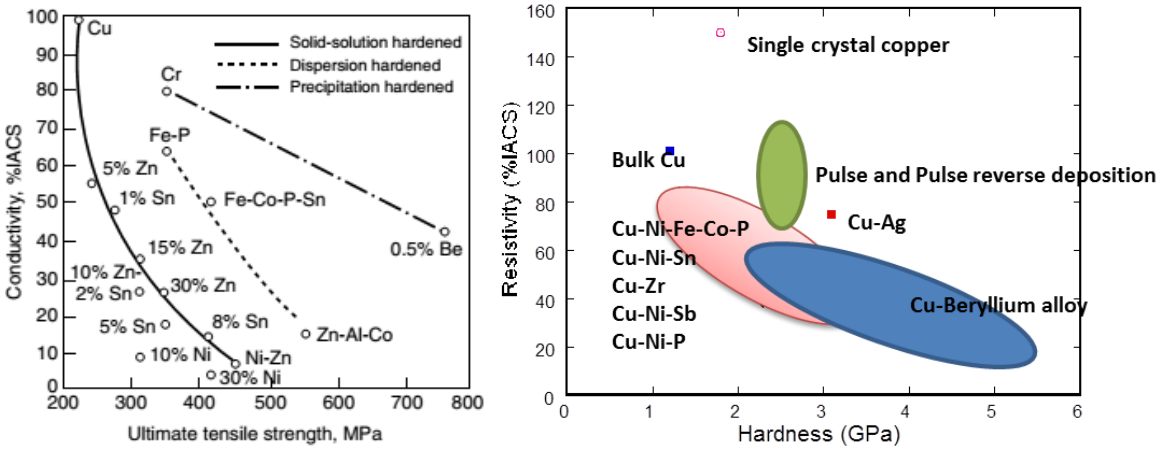

Figure 2.7 Mechanical and electrical properties of strengthened copper by different methods (adopted from [4]).

Figure 2.7 elucidates that strengthening of copper leads to decrease in the electrical properties [4, 17]. This is the main reason for avoiding second phase materials unless they are very advantageous, for example, carbon as reinforcement filler in enhancing the required properties in conjunction with mechanical properties.

2.7.1 Grain refinement

Grain refinement is one of the most common and effective methods adopted to control the properties of a material by reducing the grain size. In the early stages of deformation, grain boundaries act as trapping locations to hinder the dislocation motion and also barriers to slip. By reducing the grain size the number of grains and grain boundaries increases. Therefore, the distance moved by the dislocation becomes small before facing a grain boundary. This leads to the increase in mechanical strength or hardness. Figure 2.8 represents the polycrystalline material composed of grains and grain boundaries with the arrangement of atoms.

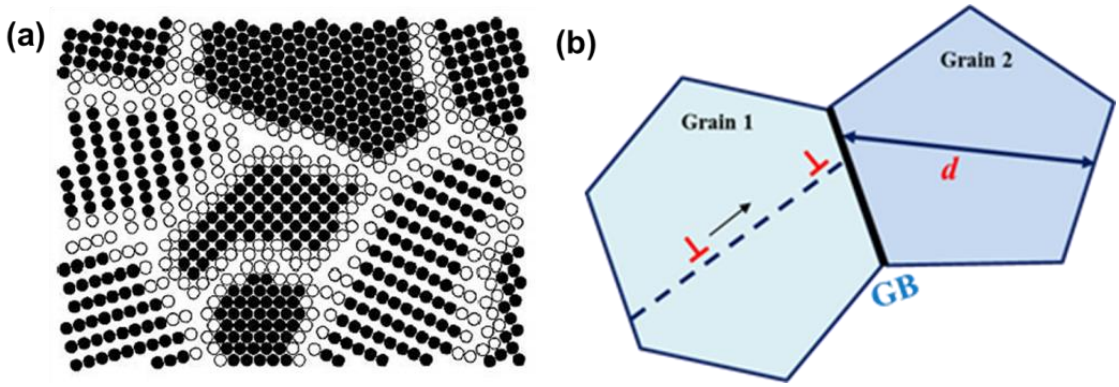

Figure 2.8 Grain boundary strengthening (a) example for a polycrystalline material [80], and (b) are graphical representation of grain boundary between the two grains and atomic arrangement at the grain boundary (adopted from [29]).

The dependence of mechanical properties on grain size is explained by Hall-Petch relationship [21, 23, 81]. The Hall-Petch equation relates the grain size to the yield strength and hardness as

$$\sigma_y = \sigma_0 + K\, d^{-1/2} \qquad (2.14)$$

$$H = H_0 + K' d^{-1/2} \qquad (2.15)$$

Where σ_y and H are yield strength and hardness of the material respectively, d is the grain diameter and σ_0, H_0 and K, K' are material constants.

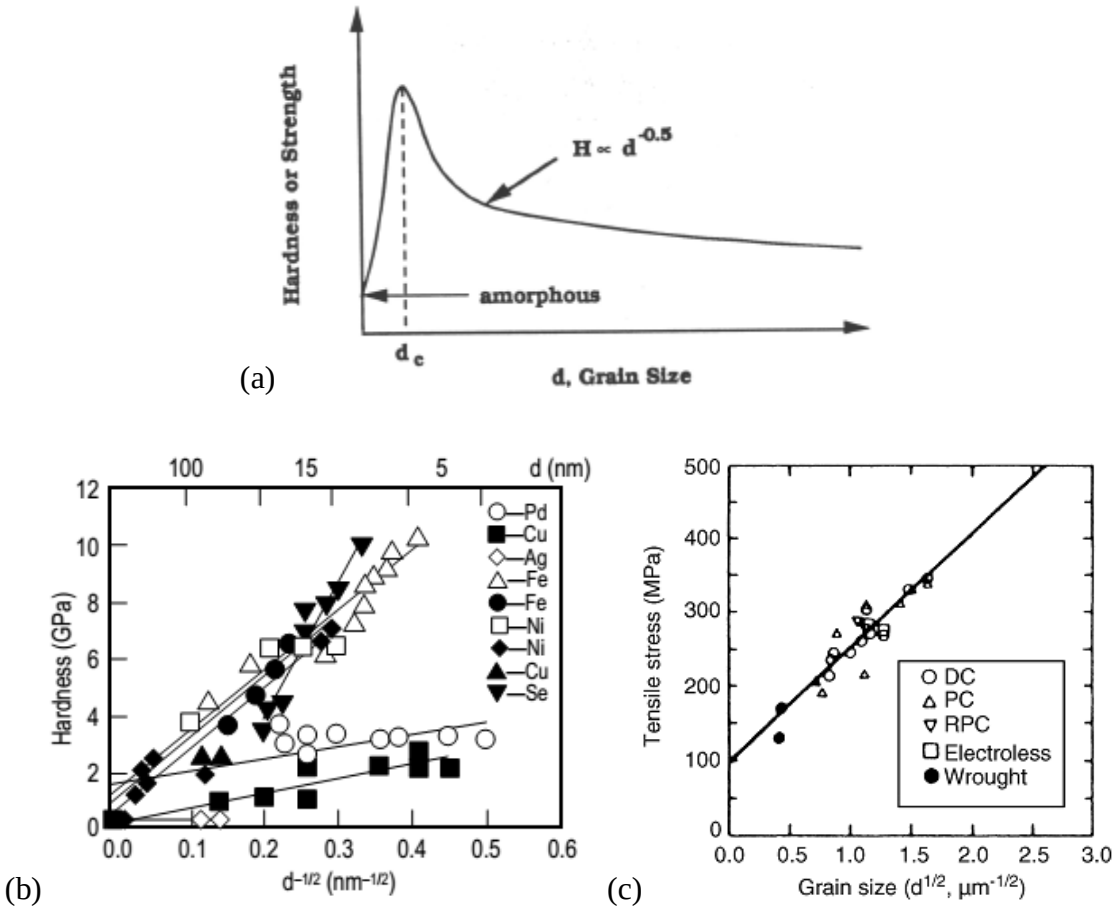

Figure 2.9 (a) Hall-Petch relation grain size vs. hardness or strength (adopted from [81]) (b) hardness vs. grain size for pure phase materials (adopted from [82]) (c) tensile properties of copper vs. grain size (adopted from [82]).

According to Hall-Petch equation, hardness can be increased by decreasing the grain size. As the grain size decrease, dislocations pile up at each grain boundary, this leads to the increase in stress concentration in the grain across the grain boundary. Therefore stresses applied to move these dislocations must be higher. However, there is a limit up to which the hardness and grain size are inversely proportional beyond which the material tends to follow inverse Hall-Petch relation [21, 23, 81, 83] where, the grain size and hardness are proportional. The Figure 2.9 shows the relationship between the grain size and mechanical properties obtained from measurements for pure phase materials and copper. This indicates that the enhancement of mechanical properties was observed while decreasing the grain size.

2.7.2 Solid solution hardening

Solid solution alloying is the addition of atoms of one element (alloying element/solute element) into the crystal lattice of base metal which causes lattice distortions in the base metal [84]. This in turn results in lattice strains in the host lattice surrounding the alloying atom which restricts the movement of dislocations.

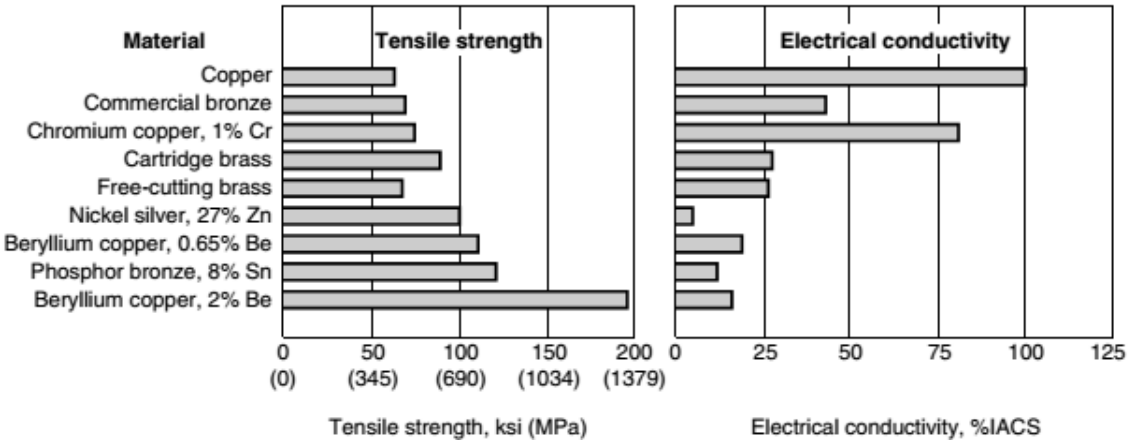

Figure 2.10 Strength and electrical conductivity of copper and copper alloys (adopted from [4]).

Elements used in solid solution strengthening are usually increase the strength, depending on the proportion of solute elements. In case of copper, alloying is done in order to improve strength without reducing the ductility. However, alloying often degrades the electrical and thermal properties (Figure 2.10).

2.7.3 Work hardening

Strain hardening/work hardening [84] is one of the most important methods of strengthening where strength is improved by plastically deforming the metal by rolling, drawing etc. Plastic deformation results in distortion of atoms in the metal from their equilibrium positions and subsequently hardening takes place. The deformation can be carried out at low, moderate and high temperatures. If the working temperature is above recrystallization temperature it is called hot working while below the recrystallization temperature it is cold working. However, certain metals e.g., copper which is very ductile can be hardened by cold working. Therefore, it is difficult to deform a metal/alloy plastically further after work hardening as it requires high

stresses for additional deformation. During work hardening, dislocation density increases and these dislocations interact with other dislocations and impede the motion of dislocations in the metal. An annealed metal will have dislocations about 10^6-10^8/cm^2, while a cold-worked metal may contain dislocations ~10^{12}/cm^2.

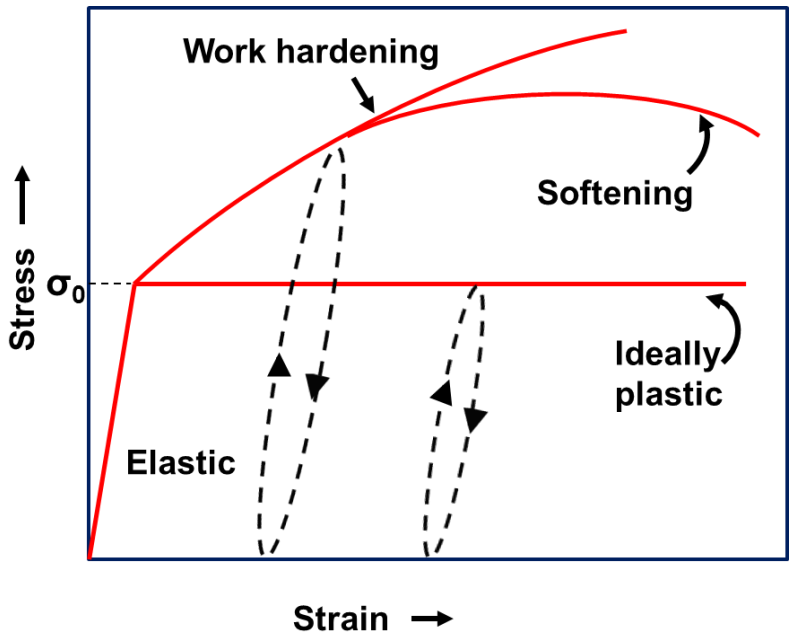

Figure 2.11 Typical stress-strain curve redrawn for a strain hardened materials (adopted from [84]).

2.7.4 Texture

In polycrystalline materials, the word 'texture' is used to describe any feature of the microstructure that lends to the anisotropic behaviour of the polycrystalline body. Anisotropy refers to the directional dependence of properties. The value of a given property of an anisotropic material will differ for any randomly chosen direction [85]. Mechanical, magnetic and electronic properties vary widely as a function of crystallographic direction in a single crystal. In polycrystalline materials, this directionality of properties can be a consequence of crystallite size, particle morphology and/or preferred orientation. Each preferred orientation has its own significance in numerous applications.

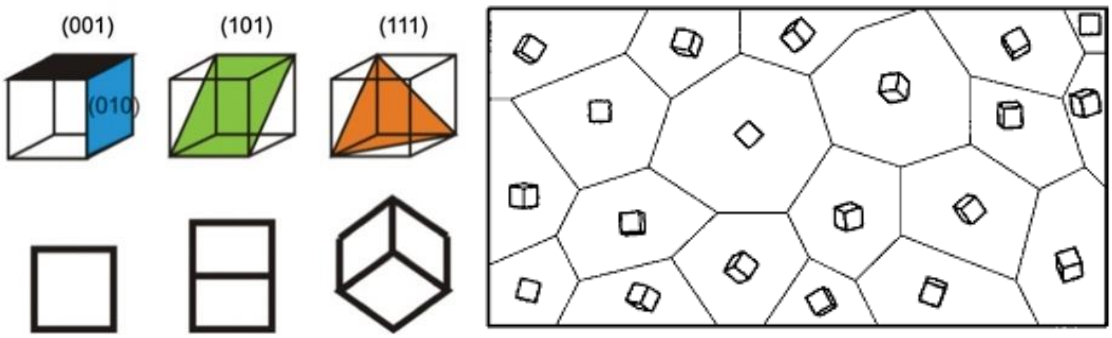

Figure 2.12 FCC crystal and cystallographic planes (adopted from [86]) and randomly oriented polycrytalline material respectively (adopted from [85]).

Therefore it is necessary to control the texture in order to obtain desired properties. In the present discussion, texture refers only to preferred orientation of the crystalline lattice, or crystallographic texture. Although the properties of single crystals can be strongly anisotropic, if all possible crystalline lattice orientations occur in similar manner, then the properties of a polycrystalline material can be isotropic, on an average. When preferred orientation exists, the structure is said to be textured or it has a strong texture. When the lattices are randomly oriented, the structure has no texture or is termed randomly textured [85]. A very strong texture is useful for optimizing the properties of an engineering component in a given direction. The fact that many structural and electronic properties are anisotropic, such applications demand the design of components with properties significantly better in a direction of interest than those that could be obtained from a randomly textured material (Figure 2.12). Hence it is important to have a preferred orientation. The basic difference in the crystallographic orientation is the atomic arrangement in a given crystallographic lattice plane which can be (111), (100) and (101) preferable for fcc materials. Figure 2.13 (a) shows the (111) plane of an fcc metal (b) shows the atomic arrangement and atomic density of (111) plane for a fcc metal. (c) Highly textured polycrystalline material. (111) is known to be densely packed plane compared to (100) and (101) planes in fcc metals, however obtaining a preferred orientation in (111), (100) and (101) depends on the processing parameters during the synthesis.

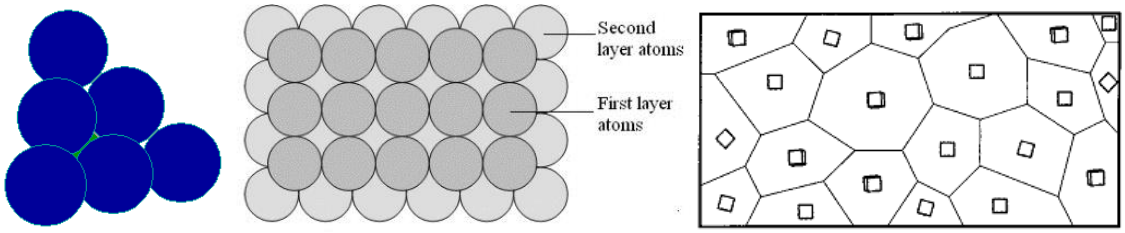

Figure 2.13 Arrangement of atoms in (111) plane and highly textured polycrystalline material respectively (adopted) [85].

2.7.5 Twinning

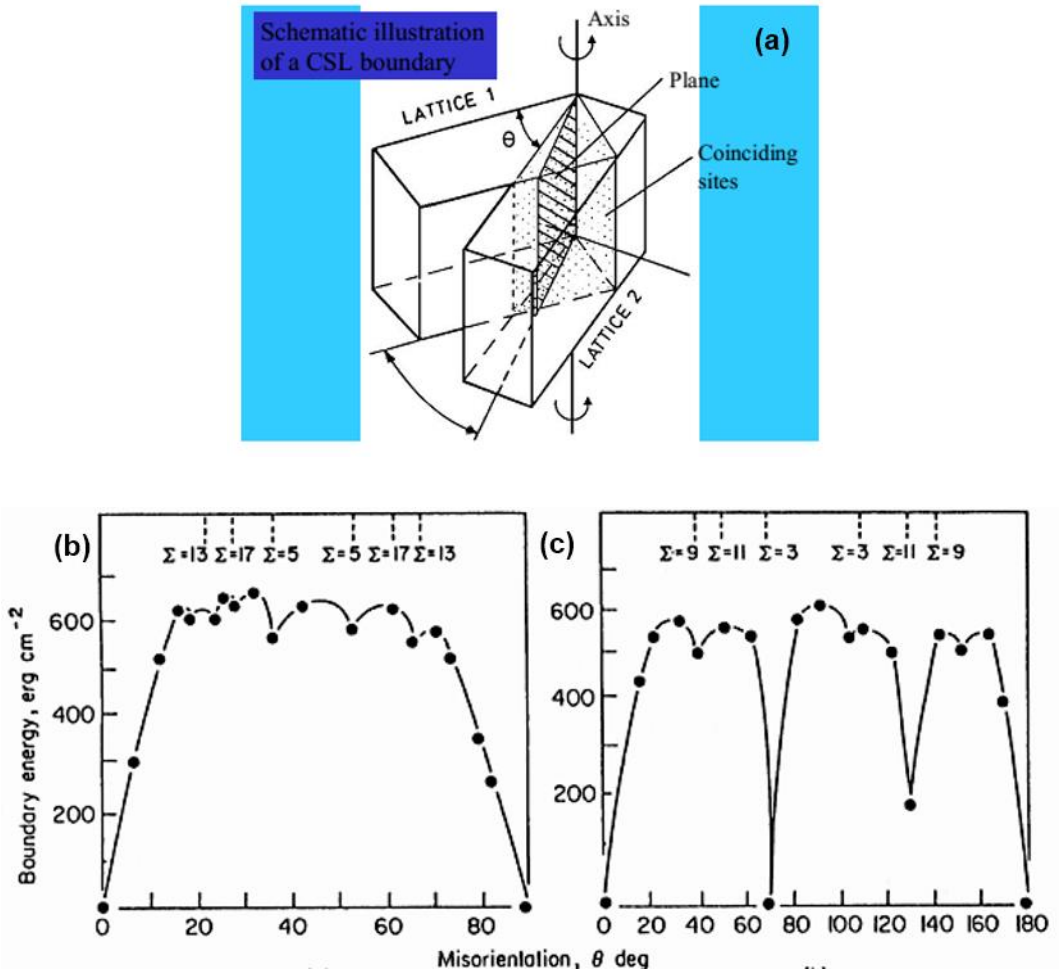

Figure 2.14 (a) Representation of rotation of two lattices about an axis (b-c) energies of various Σ boundaries (adopted from [87]).

As mentioned earlier, grain boundaries play a major role in controlling the mechanical and electrical properties depending on the atomic arrangement and fit between two grains at the grain boundaries. Depending on the misfit/misorientation angle between the two grains, these grain boundaries are of two types, small/low angle and high angle grain boundaries. A small angle grain boundary is an array of dislocations that produces a small misorientation (5-15°) between the adjoining grains. High angle grain boundaries have a larger misfit with the adjoining grains /at grain boundary with misorientation (>15°). Due to the small misfit at the grain boundary, the energy of low angle grain boundaries is lesser than the regular grain boundaries. However, these small angle grain boundaries are not very effective in blocking slip. Apart from the low angle grain boundaries, there are special grain boundaries among high angle grain boundaries with misorientation (>15°). These special grain boundaries are called coincidence site lattice (CSL) boundaries. Contrary to the majority of low-energy boundaries, CSL boundaries have greater mobility than that of random boundaries. CSL boundaries occur when one grain rotates at certain angle about an axis (Figure 2.14) relative to another grain that results in a three-dimensional atomic pattern and in which a certain fraction of lattice points coincide in the two grains as shown in Figure 2.15(a). CSL boundary is characterized by a parameter Σ, the reciprocal of the fraction of lattice sites that coincide in both the lattices [26, 88]. This Σ value changes from Σ1- Σ29 and so on depending on the lattice sites coinciding. Each Σ has significant energy associated to it depending on the number of CSLs. It has been observed that CSL grain boundaries with relatively low values of Σ can have a significant influence on the mechanical behaviour of a polycrystalline material as the small values of Σ result in short-period ordered structures in the grain boundary. CSL boundaries with Σ less than 29 show several advantages over random grain boundaries or boundaries with higher Σ values have many advantages such as lower grain boundary energy in pure metals, lower diffusivity, lower electrical resistivity, greater resistance to grain boundary sliding, fracture, cavitation and greater resistance to corrosion etc. Among the Σ boundaries, Σ3 boundaries have lowest energy associated with them among the high angle grain boundaries and called CSL Σ3 twin boundaries. A twin boundary is a plane across which lattice structure is similar to special mirror image as shown in Figure 2.14. CSL Σ3 twin boundaries again have two subsets called as coherent and incoherent twin boundaries. Σ3 indicates that one lattice site is coinciding in every 3 lattices coinciding at the grain boundary which can be clearly seen in Figure 2.15(a). Here,

black coloured circles indicate the CSL Σ3 lattices where, in every red/blue colour lattice points, one black coloured circle is coinciding. These boundaries have lower energies than those of random high-angle boundaries and other Σ boundaries (Figure 2.14(b)).

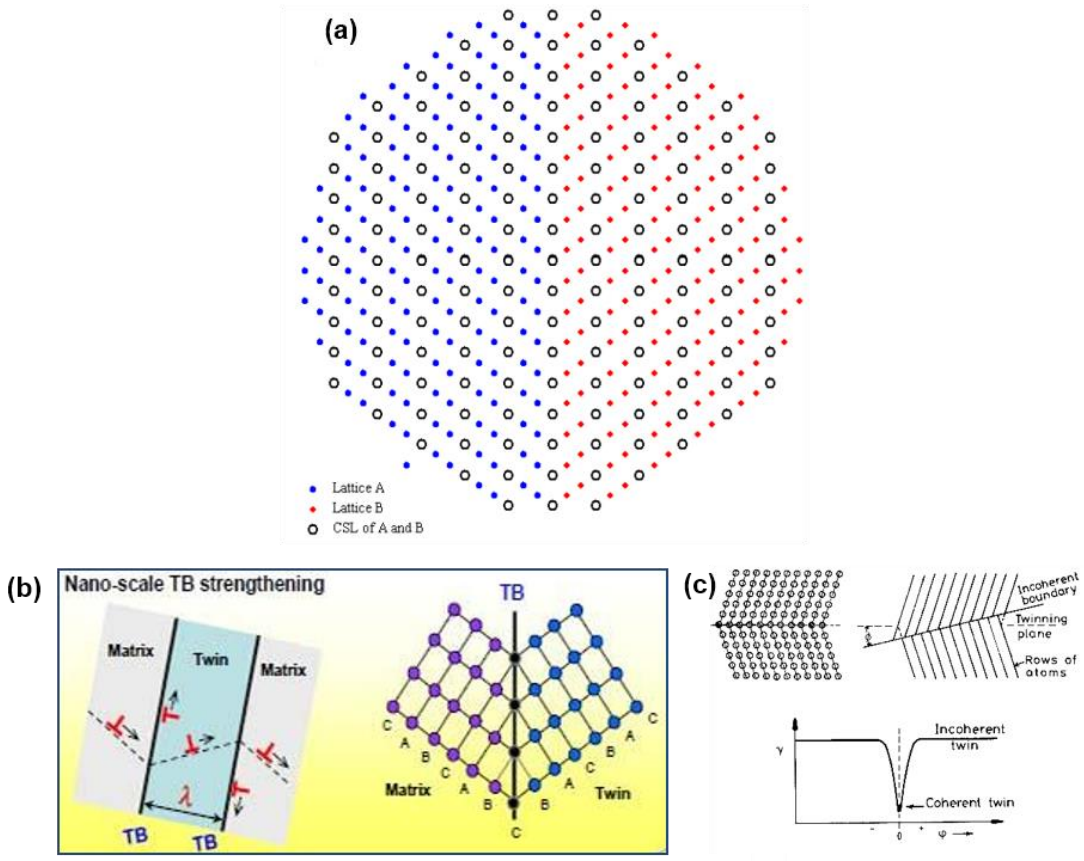

Figure 2.15 (a) representation of CSL for Σ3 boundary (adopted from [87]) (b) Coherent twin boundary and arrangement of atoms (adopted from [29]) (c) scheme represent the atomic arrangement at coherent and incoherent twin boundary (adopted from[89]).

Twin boundaries can be produced by several means such as, during deformation or heat treatment of certain metals. The control of the density of low Σ boundaries can be a means of producing a superior polycrystalline material [84]. The two most common twin orientations are (1) rotation twins (coincidence), produced by a rotation about a direction <hkl> called the twinning axis, and (2) reflection twins, where the two lattices maintain a mirror symmetry with respect to a plane [90] called the twinning plane. However, all the twin boundaries cannot be effective in blocking the dislocation motion while reducing the electron scattering. CSL Σ3 coherent twin boundaries are very important in maintaining electrical conductivity while

enhancing the strength of the material. Coherent twin boundary, which lies on a {111} plane common to both adjoined grains, possesses the lowest energy of ~0.01 J/m^2 compared to any other boundary (~1.0 J/m^2) [91, 92]. Usually CSL Σ3 boundaries have a misorientation of 60° <111> and the maximum allowable deviation for CSL Σ3 boundaries according to Brandon criteria [93, 94].

$$v_m = v_0 \, \Sigma^{-1/2} \qquad (2.16)$$

Where, the proportionality constant, v_0, is generally taken to be 15°, and accordingly the permeable deviation can be known for twin boundaries. For increasing the strength while maintaining the electrical conductivity. According to the Randle the twin boundaries need to be coherent where the maximum permeable deviation is up to 3° [26, 88, 95].

2.8 Composite materials

Composite material is a material with two or more chemically/physically distinct phases. First phase is a continuous phase called matrix which is large in volume fraction and the second phase is called reinforcement [90, 96]. The second phase can be randomly distributed or arranged, the later influencing matrix properties. Hence, in most of the cases, the second phase materials are harder than the matrix material in order to achieve intermediate properties of both the matrix and reinforced element. Reinforcement materials are in the form of continuous fibres, particles, short fibres, whiskers, etc. The size, shape,distribution and volume fraction of reinforced material influence the properties like strength, toughness, stiffness, thermal conductivity, electrical conductivity, coefficient of thermal expansion etc., of the composite [84, 96, 97]. However in tailor-made composites focussed on the mechanical and electrical properties, type of reinforcement and interfacial bonding plays an important role. In the current research, carbon in the form of nanotubes and graphene is used as reinforcement. Several models were proposed for strengthening mechanisms depending on the geometry and physical properties of reinforced element specially for CNTs. Orowan looping, thermal mismatch and shear lag are the reported strengthening mechanisms for CNT reinforced aluminum composites [98]. Among the three mechanisms, Orowan looping [99] is most probable mechanism where, the second phase particles inhibit the dislocation motion in two distinct ways; one is reinforced

element may get cut by the dislocations and in the second case the reinforced elements may allow the dislocations to bypass, leaving a dislocation loop around them as shown in Figure 2.16.

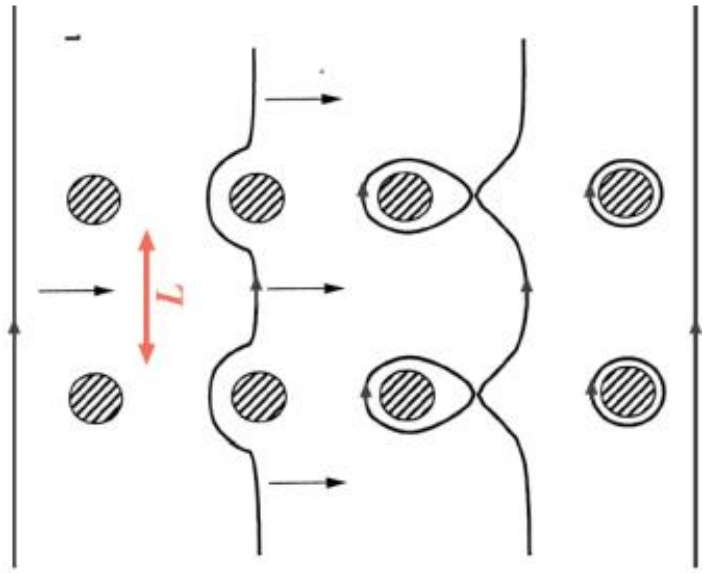

Figure 2.16 Orowan looping mechanism for particle reinforced composites (adopted from [99]).

Shear lag model is proposed for short fibre composites where the load is transferred from the matrix to fibres through an interfacial shear stress [96, 100]. The load transfer depends on the length of the fibre; longer fibre implies more strength that can be transmitted from matrix to fibre. In thermal mismatch, the strength increases due to the stresses developed with different coefficients of thermal expansion of dissimilar phases [90]. Finally the strength of the composite is taken care by the shear strength of the interfacial phase. Interface helps in the easy transfer of stress from the matrix to the CNTs. In addition to these mechanisms, strengthening may also occur due to grain refinement and increase in number of dislocations induced due to the second phase material and clustering of CNTs.

Strengthening mechanisms were not reported in case of graphene/CNTs copper matrix composites. However the above mentioned mechanisms may or may not hold true for copper matrix. It is expected that since CNTs/graphene are very strong, strengthening occurs by transmission of load from the matrix to graphene/CNTs. In addition, they possess high modulus that allows the matrix to carry high loads. During loading, CNTs/graphene and matrix both

undergo elastic deformation. Then as the load increases, the matrix deforms plastically while CNTs undergo elastic deformation. After reaching the maximum load both reinforced material and matrix deform plastically. During this deformation, load transfer occurs from matrix to reinforced element then breakage or pull out of reinforced element occurs. Hence it is expected that the achieved strength will be intermediate to both the matrix and reinforced element and other properties are also a combination of both the phases in case of composites [101]. Further, processing techniques may vary the microstructure and distributions of CNTs/graphene leading to different degrees of strengthening.

In the present study, grain refinement, grain boundary engineering, texture and carbon as reinforcement filler for strengthening copper have been adopted, without compromising the electrical properties. Therefore, based on the selection of these strengthening methods, next section discusses in detail about the relevant studies on synthesis of copper with improved mechanical and electrical properties.

2.9 Recent studies on copper and copper nanocomposites

Pure copper can be strengthened by several methods, while maintaining electrical conductivity as that of bulk copper, such as accumulative roll bonding (ARB) process [102] , equal channel angular pressing process [103], friction stir process [104] and both equal-channel angular pressing and high-pressure torsion [105] in addition to the electrodeposition. In ARB process using cold roll-bonding mechanisms, pure copper was severely deformed in order to achieve the required properties. Highly deformed pure copper has ultrafine grains with high angle grain boundaries and the strength increased up to 723 MPa, attributed from grain refinement and strain hardening while the electrical conductivity is retained. In Equal channel angular pressing, ultrafine grained pure copper of grain size about 70–200 nm was obtained. Tensile tests showed that the yield strength slightly increased and micro hardness increased by a factor of 1.7 with an electrical conductivity of 81% IACS. Friction stir processing is a surface modification process to improve the surface strength of pure copper where grain size was refined from 19 μm to 3 μm with an increase in hardness from 0.85 GPa to 1.14 GPa while maintaining the electrical properties. Combination of both equal-channel angular pressing and high-pressure torsion resulted in increase in both hardness and electrical conductivity with an

increase in the strain during processing. Noticeable increase in the hardness of (~270%) and the electrical conductivity of 97% was reported. For copper nanocomposites, Al_2O_3, SiC, TiB_2 etc. are the major elements incorporated by different techniques. By dispersion of SiC the hardness increased up to 229HV, yet the electrical conductivity decreased to 54-69% IACS [106]. With Al_2O_3 [5] and TiB_2 [107] also same trend has been followed.

Among the reports available on achieving mechanical and electrical properties, majority of them have shown only a slight/moderate improvement in the mechanical properties while retaining the electrical properties. In addition, the processing methods are also expensive and take several hours for synthesis. Therefore electrodeposition has been chosen since it is an economical and scalable method in attaining the mechanical and electrical properties simulatanously.

2.9.1 Studies on optimization of both mechanical and electrical properties by electrodeposition

Electrodeposition is a well-favoured method for the synthesis of copper and composite coatings as it has several advantages over other existing methods. Open issues include the weight of each parameter in the process, mechanisms of additive influence, kinetics of the process etc. suggesting the fact that it is not fully understood. Depending on the required properties such as mechanical, electrical etc., deposition technique can be chosen [108].

Improving the hardness by controlling the microstructure, grain size etc. independently by the addition of additives is studied by several researchers [32, 33, 41, 109]. Among the available methods, electrodeposition with the application of pulse and pulse reverse current are promising and one of the most economical methods to synthesize highly dense nanostructured copper films. In this method, nature of grain boundaries, grain size and texture can be precisely controlled by controlling various pulse parameters. The variables that control this process are electrolyte composition, pH, concentration, current density, temperature, agitation, etc. A detailed discussion of the literature regarding electrodeposition and its usage to synthesize nanostructured copper is presented in the further sections. Very few studies are available on achieving the said hardness while maintaining the electrical conductivity by controlling texture, high angle grain boundaries etc.

Cui et al., [31] reported the synthesis of (111), (200) and (220) textured Cu with a high density of {1 1 1} twins by PED. Mechanical and electrical properties of these Cu films were controlled mostly by the textures and twin densities and to a smaller extent by grain size. UTS and the ductility are equally improved. Formation of texture in the Cu films resulted from both texture of the substrates and pulse parameters such as pulse current density. The increase in current density leads to reduced twin spacing with the crystallographic orientation of {1 1 1}, with increased electrical resistivity and mechanical strength also revealing the nearly linear relationship between them [31] (Figure 2.17).

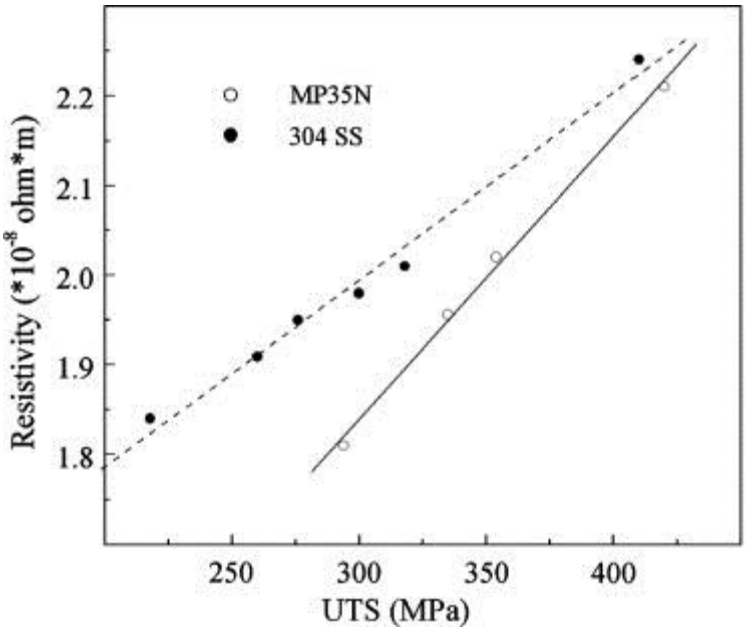

Figure 2.17 Relationship between ultimate tensile strength and electrical resistivity for pulse electrodeposited copper (adopted from [31]).

From the Figure 2.17, it is evident that though attempts have been made to increase the strength by introducing twins while controlling texture and avoiding additives, ultimately the resistivity also increased linearly in the PED copper foils claiming that higher density of twins results in an increase in the electrical resistivity of Cu films due to the electron scattering effect at TBs [110].

In contrast, Lu et al. [17, 20, 29] reported an ultrahigh strength in electrodeposited copper with the presence of twin boundaries. They argued that these twin boundaries act as obstacles for strain propagation as well as slip propagation. These twin boundaries may also impart high

electrical conductivity unlike the conventional grain boundaries. The authors also have observed that as the twin boundary density increases, they possess the capacity to store the dislocations. This results in increasing rate of strain hardening with high yield strength at high flow stresses at 77 K. It has also been shown that copper with high density twins increase the tensile strength up to 1 GPa with an elongation to failure of 30% [111]. Recently they also reported maximum strength by varying the twin lamellar thickness and found that as the twin thickness decreases to 15 nm the strength increases, reaching a maximum strength of about 1100 MPa. .

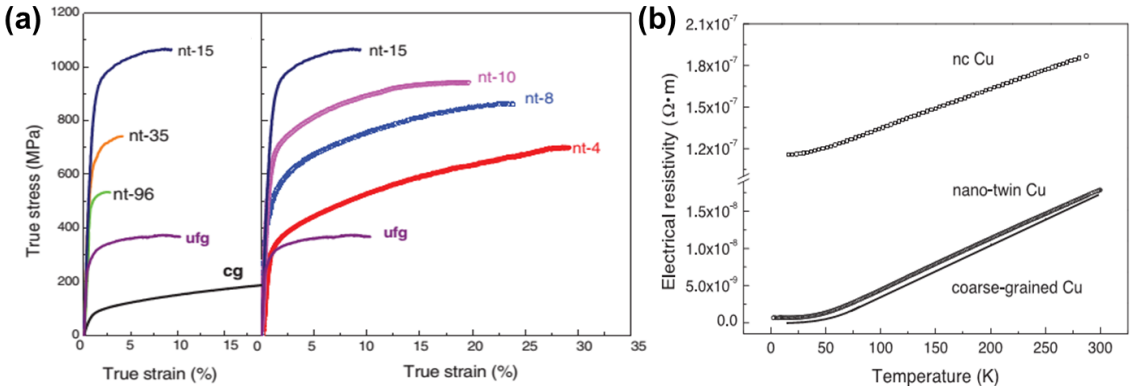

Figure 2.18 (a) True stress-strain and (b) electrical resistivity for nanotwinned copper (adopted from [20]).

As twin boundaries influence electrical conductivity, nanotwinned copper shows increased resistivity with decrease in twin spacing to 15 nm (1.75 μΩ-cm), slightly higher than that of bulk copper. With increase in twin spacing from 15 to 90 nm, the resistivity has been increased (1.75 to 2.12 μΩ-cm) which is attributed to the grain boundary scattering. In the above reports, twinning was controlled in order to achieve the mechanical and electrical properties simultaneously.

Later Lui et al. [112] have studied the influence of pulse parameters on controlling the texture, grain size and fraction of twins boundaries. The authors have suggested that with increasing the current density high-density of twin boundaries with 60°<1 1 1> with a plane of {1 1 1} were observed with the preferred orientation of <011> in copper films as shown in Figure 2.19.

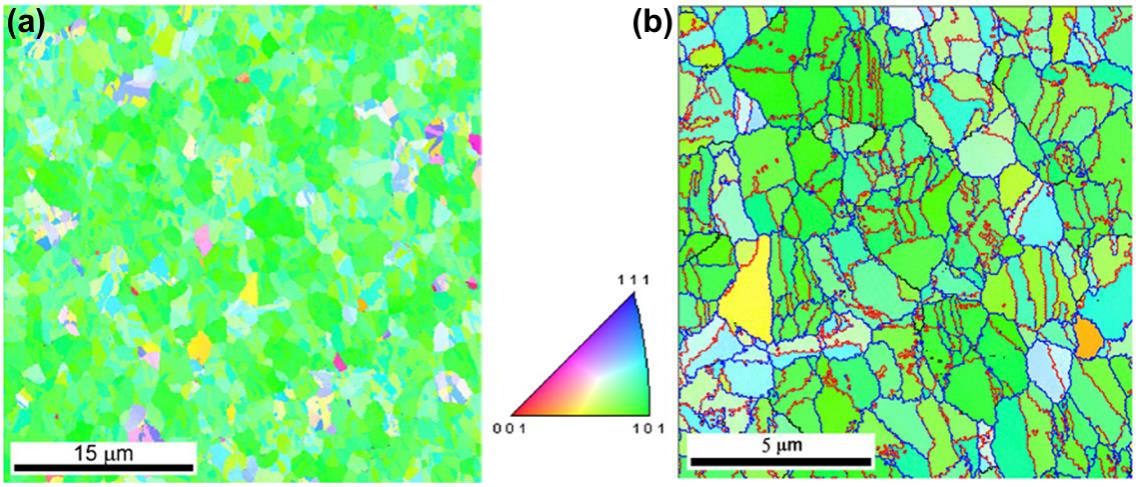

Figure 2.19 Inverse pole figure map of copper foils deposited with a current density of 0.5 a/cm^2 showing a preferred orientation of (101) and large fraction of twins indicated in red color respectively (adopted from [112]).

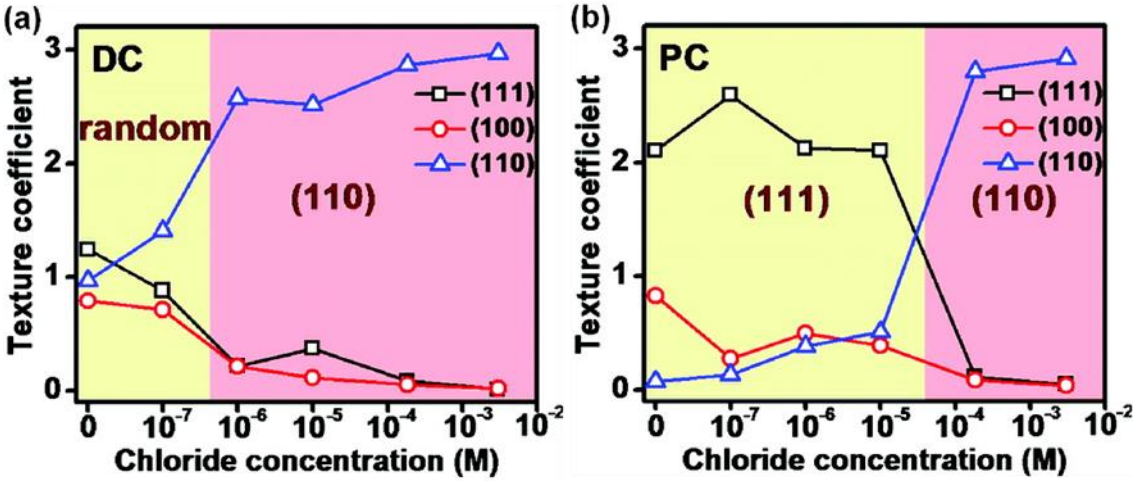

Figure 2.20 Crystallographic texture of Cu films deposited by varying chloride concentration in electrolyte (a) DC-deposited and (b) PC-deposited Cu films (adopted from [32]).

Chan et al., [32] reported that with the variation of chloride concentration as an additive in the electrolyte and with an optimum electrodeposition method, it is possible to control the crystallographic orientation, twinning and mechanical properties of Cu films. Texture was manipulated using DC and PED techniques. DC deposited copper films have shown orientation of (110) with increase in the chloride concentration whereas the pulse current deposited copper showed (111) orientation and changes to (110) as the chloride concentration varied from 10^{-4}-10^{-5} M (Figure 2.20). In addition, pulse current deposited Cu films have 30-50% enhanced

hardness compared to DC and (111) textured films have shown a high hardness of 2.7 GPa compared to (110) textured films (2.4 GPa) with the chloride addition as an additive. Very recently Lu et al. [113] have studied the anisotropic growth of highly (111) textured copper synthesized by PED with large fraction of twin boundaries and the transformation of <111> to <100> crystals has been observed during the heat treatment at 450°C (Figure 2.21).

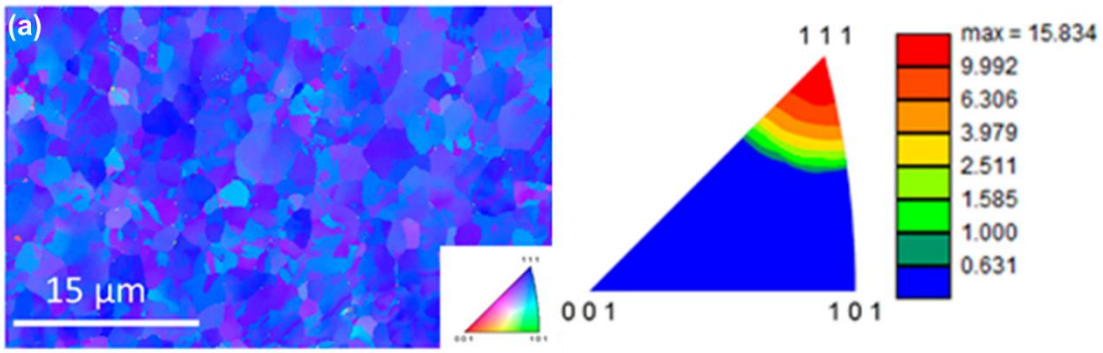

Figure 2.21 EBSD map of copper film preferentially orientated toward <111> with inverse pole figure and pole figure with the pole density (adopted from [113]).

From the above studies, it can be noted that structure- property correlations in pure copper, such as mechanical and electrical properties were studied only by few researchers, either by introducing twin boundaries with the application of DC, PED or by controlling texture and twin boundaries. The correlation is limited either to the mechanical properties with texture or the electrical properties alone. No correlation has been made so far on the texture-property correlations for mechanical and electrical properties simultaneously using PRED. Therefore our main focus is on controlling and simultaneously increasing the mechanical and electrical properties of the (111), (100) and (101) textures using PRED.

2.9.2 Graphene

Graphene, a newly isolated form of carbon, with sp^2 -bonded carbon atoms densely packed in a honeycomb crystal lattice, has garnered appreciable attention as a potential candidate for next generation applications. The applications could be in electronics, memory, biotechnology, sensor, energy storage devices etc. due to its exceptional mechanical, electrical, thermal properties, high current carrying capacity, chemical inertness and optical transmittance [114,

115]. Graphene was first synthesized by micromechanical cleavage from graphite [116]. This approach facilitates the production of high quality graphene for several applications [117]. Graphene can be of either single-layer, two, three or few layers. A single layer graphene is defined as a single two-dimensional hexagonal sheet of carbon atoms. Graphene is harder than diamond and about 100 times stronger than steel [118]. The tensile strength of graphene exceeds 1 TPa [119]. The robust graphene is stretchable and can be elongated up to 20% of its initial length.

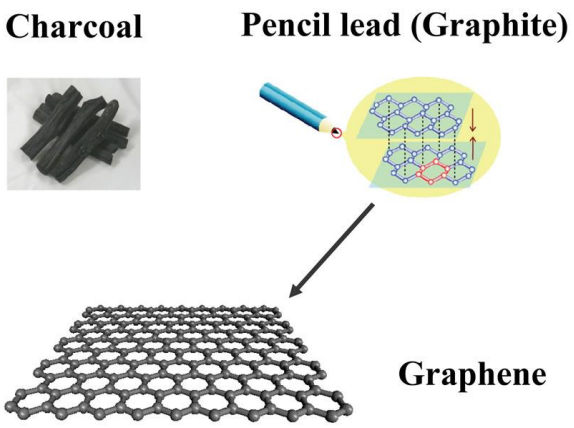

Figure 2.22: Allotrope of in the form of charcoal, graphite and graphene (adopted from [120]).

Electrons flow through graphene (at one hundredth the speed of light) more easily than through copper making graphene a better conductor compared to copper. The properties of graphene are tabulated below.

Table 2.2 Properties of graphene

Property (Unit of measure)	**Typical value parallel to Surface**	**Typical value Perpendicular to surface**
Density (g/cc)	2.2	2.2
Thermal conductivity (W/m-K)	3000	6
Thermal expansion (CTE) (deg-K)	$4\text{-}6\times10^{-6}$	$0.5\text{-}1.0\times10^{-6}$
Modulus (GPa)	1,000	-
Tensile strength (GPa)	5	-
Electrical conductivity (S/m)	10^{7}	10^{7}

Graphene has a lot of potential applications, especially in terms of industrial applications for optical and electronic devices such as ballistic transistors, field emitters, and components of integrated circuits, transparent conducting electrodes, sensors, touch-screens, liquid crystal displays, organic photovoltaic cells and organic light-emitting diodes (OLEDs) etc. [49]. Graphene can be used to create ultra-light components for aviation industry, to improve fuel efficiency. Therefore to control the structure and properties of graphene a variety of processing techniques were used by researchers to garner specific applications which require graphene production in large scale [121-124]. The subsequent sections will discuss different synthesis techniques of graphene and its main applications.

2.9.2.1 Graphene synthesis

Synthesis of graphene started as early as 1975 [125] by depositing carbon on platinum. However, due to lack of consistency in the properties of graphene and the number of layers, the process was not studied extensively. After several attempts since 1999 [126, 127], in 2004 Novoselov et al. have synthesized graphene through exfoliation [116, 128]. Since then this technique has been used to efficiently synthesize graphene in large scale.

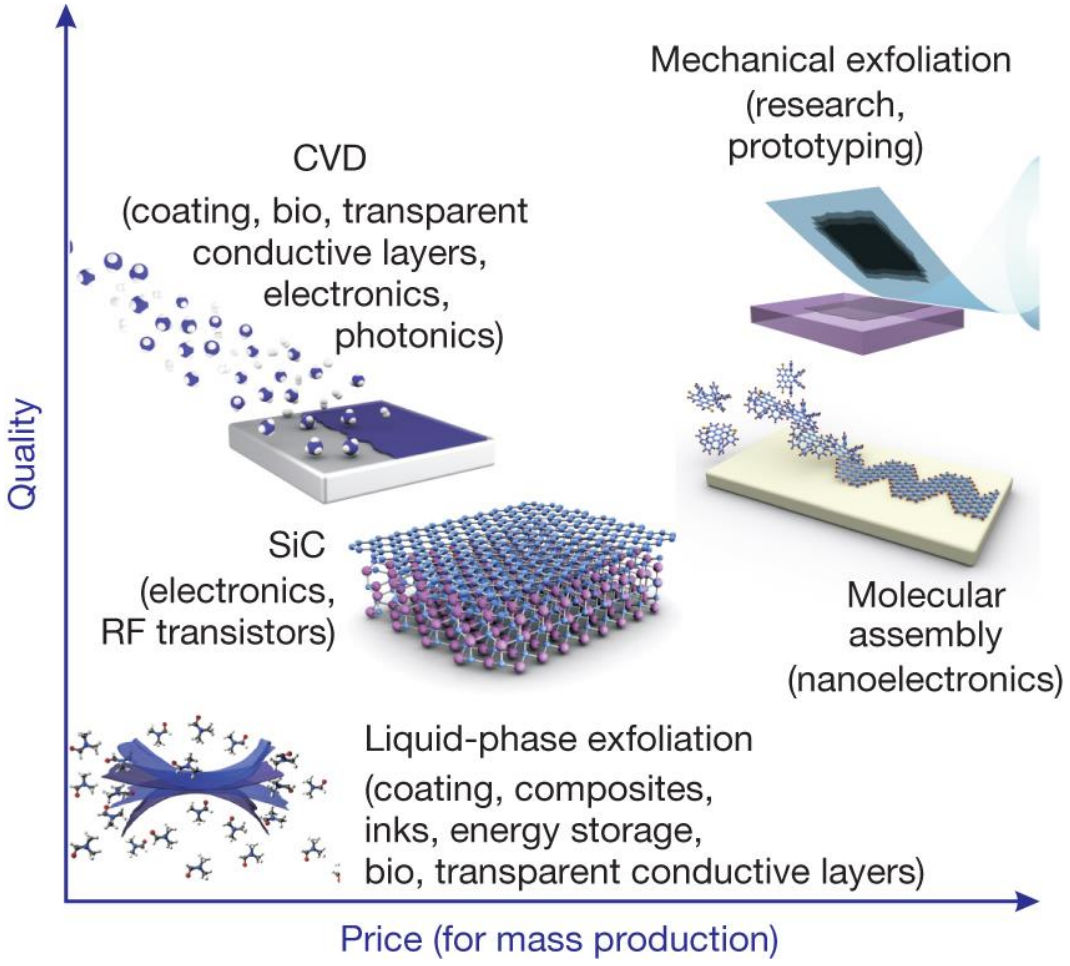

Figure 2.23 Several methods of mass-production of graphene (adopted from [129]).

Chemical vapour deposition, thermal decomposition of SiC, un-zipping of CNTs etc. have been used for synthesis of graphene [129, 130] shown as in Figure 2.23. Exfoliation methods have been discussed in detail owing to their popularity in scalability etc.

2.9.2.2 Exfoliation methods

Graphite is a stack of a number of graphene sheets bonded together by weak van der waals forces. Hence graphene can be produced from graphite if these van der waal bonds can be broken. Fundamentally there are two different methods for graphene preparation. One method is separating graphene from graphite called exfoliation and the other is growing single layer graphene on any substrate. Exfoliation is a repeated peeling process which uses mechanical or chemical energy to break weak van der waals bonds. Exfoliation can be mechanical

exfoliation, microwave exfoliation, thermal exfoliation, chemical exfoliation or electrochemical exfoliation etc. [131-137]. Most of the reports are based on mechanical and thermal exfoliation [49, 138-141] as these result in large quantities of yield. In mechanical exfoliation, graphene is separated by peeling it off from graphite using adhesive tape/ scotch tape. After peeling off, multiple-layer graphene remains on the tape. By repeated peeling, the multiple-layer graphene is cleaved into few-layers of graphene. The glue is dissolved in acetone and graphene is collected [142-144]. The obtained graphene considerably differs in size and number of layers, where the sizes range from nanometers to several micrometers with single to few layer graphene with almost no defects. This process is very easy to produce and scalable, yet the main drawback remains in the lack of control over the size and number of layers. Chemical/liquid phase exfoliation was first used by Horiuchi et al. to produce graphene from natural graphite [145]. In this method, graphene is synthesized by oxidizing graphite in an organic solvent or acids by reducing its energy barrier or directly with the use of chemicals. The exfoliated graphite solution is then sonicated for several hours and centrifuged until the thinnest graphene from different sizes is obtained. In liquid phase exfoliation also, the size and number of layers of graphene cannot be controlled. Though the complexity in producing large quantities of graphene by liquid phase exfoliation route is low, it takes several hours to few days to obtain the final product. In addition, toxicity is a major concern due to the chemicals used in the liquid phase exfoliation as it produces graphite oxide as a by-product. However, this requires thermal/chemical reduction. After severe oxidation under acidic conditions during the process, the graphene oxide is of extremely bad quality compared to pristine graphene [51].

2.9.2.3 Electrochemical exfoliation

Electrochemical exfoliation [50, 146, 147] is similar to liquid phase/ chemical exfoliation technique. Major difference being, the use of current/voltage for electrochemical exfoliation for the graphite to be exfoliated under mild acidic conditions, instead of very strong acids used in chemical exfoliation. In liquid phase exfoliation, though the method of reduction from graphene oxide is potentially of low cost, the initial oxidation process often damages the honeycomb lattices of graphene. The minimum time or rapid process of exfoliation results in defect- free graphene and usage of optimized voltage results in controlled number and size of layers of graphene in bulk. This method is very simple, single-step, economical, environment

-friendly and is conducted in ambient temperature. When the electrolysis starts, the oxidation occurs at the anode (graphite) and reduction occurs at cathode. As time proceeds, the mild acidic molecules intercalate through the graphite layers. This further results in oxidation along the edges of graphite layers leading to exfoliation of graphene. The extent of oxidation depends on the product of electrolytic current/voltage applied and time, which is equal to the number of electrons for oxidation. However, the oxidation rate is very low compared to other liquid exfoliation methods.

Electrochemical exfoliation in a mild aqueous electrolyte is used to synthesize graphene in bulk quantities in the current research which in turn is used for the preparation of copper based nanocomposites.

2.10 Copper- graphene composites

Carbon nanomaterials, including carbon nanotubes (CNTs) [148], graphene [149] etc., have received tremendous scientific interest as potential reinforcements. Though CNTs have exceptional properties, the tubular structure and high aspect ratio of CNTs led to entanglement resulting in rough and porous nanocomposites [44, 150]. It is envisaged that the recently discovered graphene can be an ideal alternative to replace CNTs. In addition to the expensive production cost of CNTs, the major drawback in preparing the metal-CNT composites is the poor dispersibility of CNTs, which tend to entangle and form agglomerates in the matrix, hindering the development of these composites. For nanocomposites, dispersion, size, shape and interfacial bonding between the matrix and the reinforcement play an important role in enhancing the mechanical and electrical properties [151].

Graphene (Gr), as mentioned in the earlier section, the most recently discovered allotrope of carbon exhibits excellent mechanical [152], electrical [116] and thermal properties [153]. Several studies have shown that graphene can be a better replacement for CNTs in nanocomposites and reported a significant improvement in mechanical properties even at lower graphene content [154]. Economical and scalable methods are reported for the synthesis of graphene [121], as compared to CNTs, facilitating the large scale development of graphene reinforced nanocomposites effectively [155]. Considerable work has been explored for synthesizing graphene reinforced polymer-based [154] and ceramic-based [156] composites,

while metal-graphene composites with aluminum [157, 158], nickel [159], magnesium [160] and Cu [12, 48] as metal matrices have also been synthesized. Al-Gr composites have shown only a slight enhancement in mechanical properties, the reason being the formation of carbide during processing [158]. Recently, magnesium nanocomposites reinforced with copper–graphene nanoplatelet hybrid particles prepared through semi powder metallurgy method have exhibited higher tensile and compressive strength compared to the monolithic Mg, Mg–1Cu–xGNPs nanocomposites [161]. The influence of graphene in enhancing the properties compared to CNTs as reinforcement material, due to its sheet like structure has been discussed. Notable literature related to the synthesis of Cu-Gr composites through powder metallurgy route reported an 80% improvement in the yield strength [162], young's modulus [162] and thermal properties [163, 164] whereas no improvement was observed in electrical properties [165]. These insignificant changes are probably due to inhomogeneous dispersion/distribution of graphene, insufficient densification and issues related to interfacial bonding [165]. Very recently few-layer graphene (FLG) and copper powder mixed by ball milling followed by spark plasma sintering (SPS) shown 2.5 times higher strength than copper and 70.4% of IACS of copper [166]. Cu matrix composites reinforced with graphene nanosheets decorated with Ni nanoparticles (GNS–Ni) hybrids have shown 61% increase in Young's modulus (132 GPa) and 94% improvement in yield strength (268 MPa) [167] and similar study on Ni nanoparticles decorated graphene nanoplatelets (Ni-GPLs) as a reinforcing component in Cu matrix (Ni-GPL/Cu) have shown 42 % higher than that of monolithic Cu [168]. Gr/Cu composites by an electroless plating process and followed by a spark plasma sintering technique have resulted 107% and 21% increase in tensile strength and Young's modulus respectively, for 1.3 wt.% Gr/Cu composites [169]. The combination of ball milling and high-ratio differential speed rolling (HRDSR) technique was utilized to fabricate 0.5 and 1 vol.% MLG/Cu composites [170]. In addition, the radiation damage resistance and interface stability of copper–graphene nanolayered composite has also been studied by atomistic simulations [171]. On the other hand, an anomalous change in elastic modulus, yield strength and ultimate tensile strength was observed in Cu-Gr composites synthesized through molecular level mixing and nano-layered composites [12, 48]. Although electrodeposition has been reported as an effective method for synthesis of composites in the case of CNT reinforced composites, especially for copper [172],

research on electrodeposited Cu-Gr composites was limited to the usage of DC technique with major focus on the electrical and thermal properties [173-175].

Koltsova et al. [176] have shown improvement in hardness of 39% compared to pure copper by compacting graphene and copper powder followed by annealing and rolling.

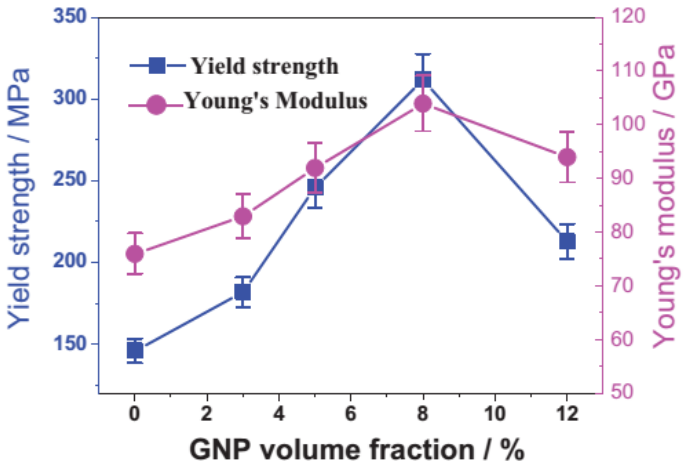

Figure 2.24 Young's modulus and yield strength of Cu-Gr composites (adopted from [162]).

Recently Chu et al. [162] reported synthesis of graphene nano platelets (GNP) reinforced copper matrix composites by powder metallurgy route with a combination of ball milling and hot-pressing. The graphene volume percentage was varied between 0-8% and dispersed in copper matrix by ball milling. Mechanical and microstructural studies showed a significant increase in yield strength and young's modulus up to 114 and 37% respectively as the graphene volume increased. The homogeneous dispersion of graphene resulted in grain refinement and enhancement of properties.

From Figure 2.24, it can be clearly observed that with increase in the volume% of graphene, the properties are enhanced up to 8% volume. Beyond, 8 vol. % yield strength and young's modulus significantly reduced by 46 and 24% respectively, due to the probable aggregation of graphene. Dong et al., [165] have studied the thermal and electrical properties of graphene nanosheets (GNS)/copper composite prepared by spark plasma sintering (SPS). Due to the interfacial thermal resistance and poor wettability, the composites have not shown any improvement in thermal and electrical resistivity [165]. An anomalous change in elastic

modulus, yield strength and ultimate tensile strength was observed in synthesis of copper-graphene through new approaches like molecular level mixing and nanolayerd Cu-Gr composites, respectively [12, 48]. Kim et al. [48], demonstrated an ultra- high strength of 1.5 GPa for Cu-Gr composite nano pillars by designing alternating layers of Cu and mono layered Gr with 70 nm repeat layer spacings, indicating the possibility of achieving high strength even in practical processes.

Electrodeposition has often been reported as an effective method for the synthesis of composites, in the case of CNT reinforced composites, especially for Cu [172]. Research on electrodeposited Cu-Gr composites was mainly limited to the usage of DC technique with major focus on the electrical and thermal properties [173, 174]. Jagannadham [174] has recently reported the synthesis of graphene composites with copper as the matrix. Cu-Gr composites were prepared by electrochemical co-deposition from copper sulphate electrolyte containing graphene oxide suspension. Thermal conductivity of the composite samples with different thickness was measured. Composite foils with thickness greater than 200 µm showed an improvement in thermal conductivity of 460 W/m-K at 300 K (27°C) compared to that of electrolytic copper (380 W/m-K). And thermal conductivity decreased from 510 W/m-K to 440 W/m-K as the temperature increased from –23 °C to 77 °C.

Compared to the conventional techniques of electrodeposition, PRED is expected to increase the content of reinforcement and ensure uniform dispersion in composite films [172]. In addition, PRED controls grain size, incorporation of reinforced filler, roughness, porosity and stresses in the composite and reduces hydrogen evolution during deposition thus influencing the performance of the composite foil in terms of mechanical and electrical properties [177].

2.11 Copper-CNT composites

The demand for a superior material with enhanced mechanical and electrical properties for the electronics industry has led to the development of Cu-CNT composites by different methods [101, 178, 179]. Excellent mechanical properties, high thermal and electrical conductivity of CNTs has led to the research on CNTs into practical applications like resin-CNT, ceramic-CNT, and metal-CNT composites [46, 180-182]. Several metal matrix composites (Al, Ni, Cu etc.,) [44] have been reinforced with CNTs. In addition, much work has been devoted to

develop copper-CNT composites for thermal, electronic applications etc. In 2006 for the first time, Chen et al. [178] demonstrated CNT reinforced metal matrix composites by DC electrodeposition having aligned SWNTs in the composites. CNT reinforced metal nanocomposites provide thermal conductivity and electrical conductivity 2 to 3 times higher than pure copper deposited by DC electrodeposition.

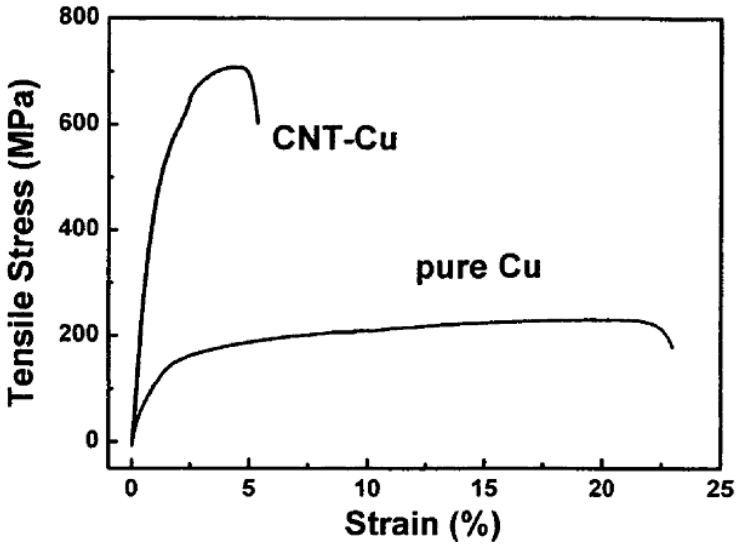

Figure 2.25 Tensile properties of Cu-CNT composite prepared by electrodeposition (adopted from [178]).

Fabricated copper has a standard electrical conductivity (resistivity of 1.72×10^{-6} Ω -cm), while the copper coated SWNT composite was reportedly found to have much higher electrical conductivity as compared to copper (>40%), with an electrical resistivity of $1.22\text{x}10^{-6}$ Ω-cm.

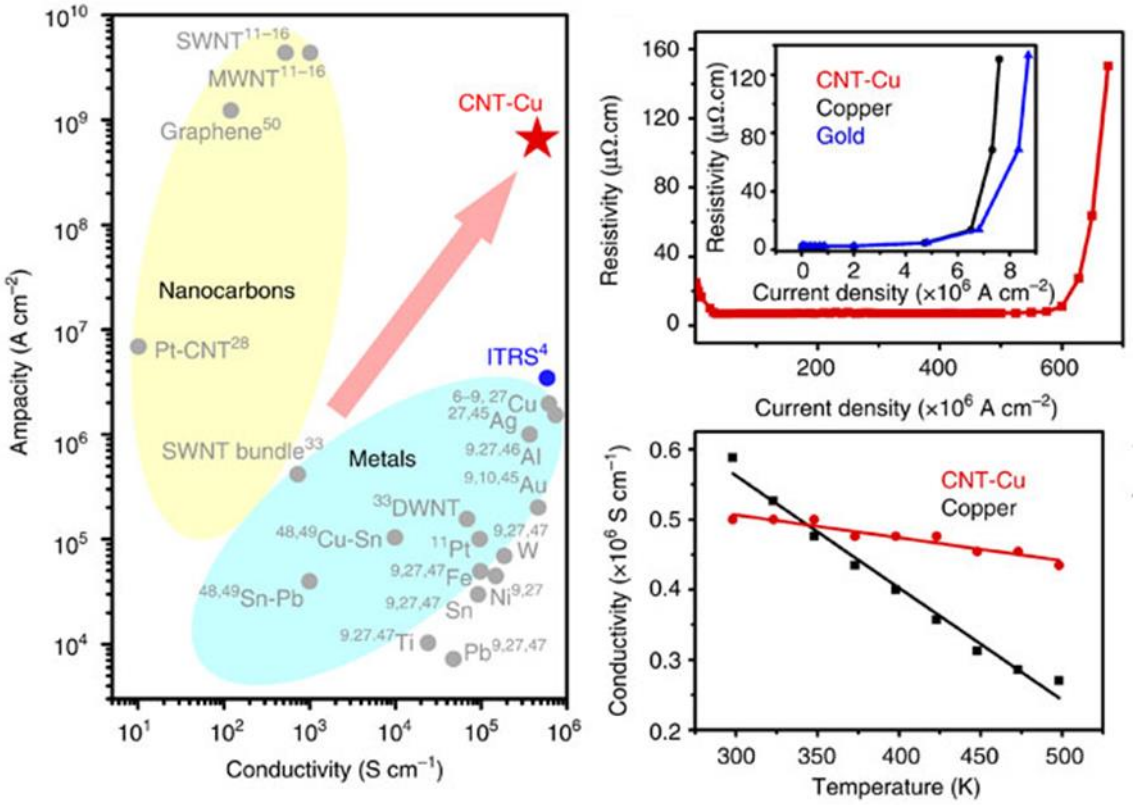

Figure 2.26 Electrical properties of Cu-CNT composite (adopted from [183]).

Several attempts have been made to achieve higher strength and electrical conductivity. However reproducibility could not be achieved by this method due to lack of aligned CNTs. Majority of the research was concentrated on increasing the CNTs content for increasing the strength, which resulted in a compromising electrical conductivity due to the agglomeration of CNTs. Instead, ampacity and electromigration resistance have been improved (Figure 2.26) by reinforcing CNTs into the copper matrix [183].

Only few reports are available on PRED of Copper-CNT composites. It has been reported that PRED method is used to smoothen the surface morphology of plated nanocomposite films [172]. PRED method during the composite plating with granular or spherically shaped nanoparticles results in separation of most of the nanoparticles from the composite film during the anodic pulse. Hence incorporation of particles content in to the matrix is reduced while employing granular or spherically shaped nanoparticles [172]. CNTs having a fibrous shape; are expected to be attached to the matrix even during the anodic pulse. Therefore PRED of a

metal/CNT composite is expected to increase the CNT content of the composite film over conventional methods [172]. Coming to MWCNTs, the number of MWCNTs in the composite film fabricated by PRED is higher than that fabricated by DC electrodeposition. There were no significant defects such as voids in the Cu/MWCNT composite film produced by PRED, as in the case of DC electrodeposited Cu/MWCNTs [172]. In addition, since electrodeposition is a low temperature process it does not lead to any chemical reaction between the CNT and metallic matrix. Thus, the inherent properties of both the CNT and the matrix can be preserved. Secondly, during the electroplating co-deposition of metallic ions and CNTs are driven towards the cathode and deposit onto the cathode simultaneously. Metallic deposition on CNTs is an atomic-level process that involves electron transport from cathode to metallic ions via CNTs; resulting in good interfacial bonding between the CNT and the metallic matrix achieved. Also, the simultaneous co-deposition of CNTs and metallic ions ensures the homogeneous dispersion of CNTs within the metal matrix [184].

2.12 Scope of the current work

Electrodeposition is a rapid, economical and environmentally suitable technique that has been adopted to synthesize copper foils with enhanced mechanical and electrical properties. In this process, by controlling the current density, pulse parameters, microstructural changes could be brought out in the synthesized foils. This has been realized in the current investigation in copper, copper nanocomposites such as Cu-Gr and Cu-CNTs. These changes depend upon the application of the current and the time for which it is supplied. There are three types of electrodeposition depending on the current/voltage supplied during the deposition process such as direct current deposition (DC), pulse current deposition (PED) and pulse reverse/anodic electrodeposition (PRED).

Among the three methods, PRED facilitates several advantages both over DC and PED. Major difference is the application of a reverse/anodic pulse making the deposit very smooth, highly dense, better surface quality and minimized grain growth compared to DC and PED. Generally, deposition processes using DC require the usage of additives to control deposit structure and properties as well as current distribution [33, 63]. The use of additives results in high costs and limits ductility and conductivity of the deposited copper [67]. PRED reduces the usage of

additives during deposition, thus minimizes the amount of impurities in the foil, resulting in brighter deposits with lower internal stresses [68], improved mechanical and electrical properties. However, when it comes to composites, PRED method has been developed in order to enhance the particle concentration in electrodeposited metal matrix composite coatings [69, 70]. It was also previously shown that the particle concentration deposited in pulse reverse plated coatings can be increased up to six times compared to unmodulated, DC electrodeposition [71]. In summary in the current study efforts have been made to strengthen copper without compromising on its electrical conductivity by an appropriate electrodeposition method (PRED). Further, for the first time, the effect of preferred crystallographic orientation, reinforcing elements such as CNTs, graphene has been studied in order to evolve a comprehensive understanding in establishing structure-property correlations.

Chapter 3. Experimental details

This chapter introduces the materials and methods used for the synthesis of copper and copper nanocomposite foils. Synthesis of copper includes the highly (111), (100) and (101) textured foils with high hardness while maintaining electrical conductivity as that of conventional copper. For copper nanocomposites, CNT/Gr was used as a reinforcement and were synthesized by PRED technique.

3.1 Base electrolyte

Composition of base electrolyte used for electrodeposition of copper and copper nanocomposites *

Table 3.1 Composition of base electrolyte and details of the experimental set-up.

Electrodeposition unit	DPR series pulse power supply (Dynatronix, USA)
Regulation mode	Current/Voltage
Anode	Electrolytic copper (99.99%)
Cathode	Titanium alloy
Composition of electrolyte	Copper sulphate ($CuSO_4.5H_2O$) – 250 g/L De-ionized water and sulphuric acid (H_2SO_4)
Temperature during deposition	15-20 °C, pH- 1-0.5 (maintained by adding H_2SO_4)
Additives	None used

***** Composition of the base electrolyte is same for pure copper and copper nanocomposite depositions.

3.2 Pre-treatment for cathode and anode

Titanium cathode was given “mirror-like” surface finish. Subsequently it was subjected to ultrasonication in acetone medium followed by dipping in boiling water. This procedure was employed mainly to remove impurities from surface and to relieve the substrate from residual

stresses. Electrolytic copper was polished to remove the oxide layer and cleaned with 10% HCl in DI water followed by ultrasonication.

3.3 Electrodeposition of pure copper

Copper foils were synthesized by pulse reverse electrodeposition technique under constant current density mode in an 'additive-free' electrolyte using DPR series pulse power supply (Dynatronix, USA). The electrolytic bath contained 250 g/L of copper sulphate in deionized water with pH maintained between ~1-0.5. The pH was controlled with the addition of sulphuric acid to the electrolyte. Temperature was maintained between 15-20 °C during the deposition. After the deposition for required durations, the deposited copper was peeled off from the titanium substrate as a foil.

3.4 Copper-graphene composite foils

For the synthesis of copper nanocomposite foils, graphene has been considered as reinforcement. The graphene used in this study has been developed by an electrochemical method in our own laboratory. Details of this method are given in Section 3.4.1

3.4.1 Electrochemical synthesis of graphene

Graphene can be synthesized by various approaches such as mechanical, chemical, thermal and electrochemical exfoliation methods. However, the present study focuses on the electrochemical approach due to its several advantages.

Table 3.2 Electrolyte and experimental details

Electrochemical set up	DPR series pulse power supply (Dynatronix, USA)
Anode & cathode	Graphite rods
Regulation mode	Constant voltage (varied between 4-18 V)
Electrolyte*	Aqueous mild electrolyte (HNO_3) and HF, De-ionized water (3:0.5)

*Electrolyte composition is varied and optimized.

Since graphene was prepared by electrochemical exfoliation involving an anodization process, the surface of graphene contained oxygen functional groups. These functional groups that are attached to graphene during the electrochemical synthesis aid in homogeneous dispersion in the electrolyte due to their hydrophilic nature. In addition, these oxygen functional groups strongly improve the interfacial bonding between the metal and the reinforcement [151]. Therefore the extra step of functionalization required for the mechanical and thermal synthesis methods has been avoided.

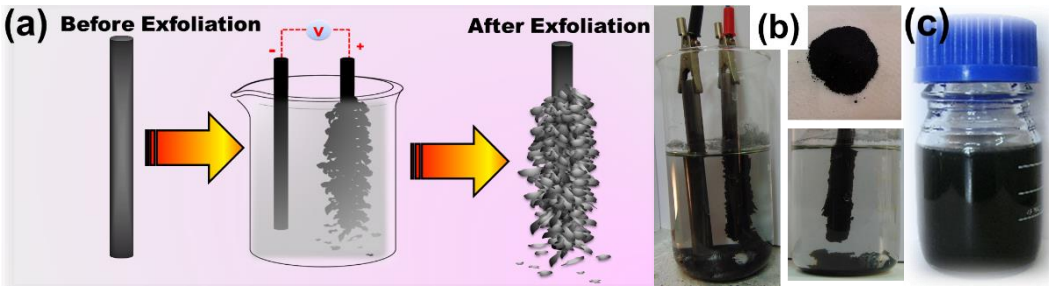

Figure 3.1 (a) Schematic Representation of the experimental set up for electrochemical exfoliation of graphite, (b) Exfoliated graphite rod and dried graphene powder (c) dispersed graphene sheets in ethanol and dried powder.

HF and HNO_3 of analytical reagent grade were purchased from Fisher Scientifics. High purity Graphite rods were used both as anode and cathode. Both the electrodes were placed at a distance of 2-3 cm to each other in the electrolyte during the exfoliation process. Figure 3.1(a) schematically represents the exfoliation of the graphite rod. HF (0.5-2%) and HNO_3 (3%) were

mixed in water at different concentrations, which was used as the electrolyte under mild acidic conditions. Static potentials varying from 4V–18V were applied for about 3h by using a DC power supply (Dynatronix). At the initial stage of exfoliation, the surface of the graphite rod is expected be wetted and the interaction between the graphite surface and the F^- and NO^{3-} ions produced due to the application of the bias voltage might be taking place. Within a few minutes, the rapid exfoliation of the graphite rod progresses and causing a bulge in the electrolyte. Due to the continuous application of the voltage, the exfoliation into few layered graphene takes place as long as the flakes are attached to the rod. Slowly, the graphene sheets start to dissociate from the rod and fall into the electrolyte. The size and the no. layers also depend on the bias voltage. The exfoliated graphene sheets were then ultrasonicated for few minutes for further dissociation and washed thoroughly several times in water until the pH of the solution was close to neutral, followed by washing in ethanol. The exfoliation products were then separated by centrifugation and/or filtration and dried. Basic experimental set up shown in Figure 3.1(a-c), illustrates the exfoliation process used for the synthesis of graphene from graphite in the current study. Exfoliated graphene was collected after the anodization process by thorough centrifugation, washing, filtering etc., with deionised water. This collection was then dried. The collected graphene powder was used for the co-deposition along with copper in Cu-Gr co-deposition.

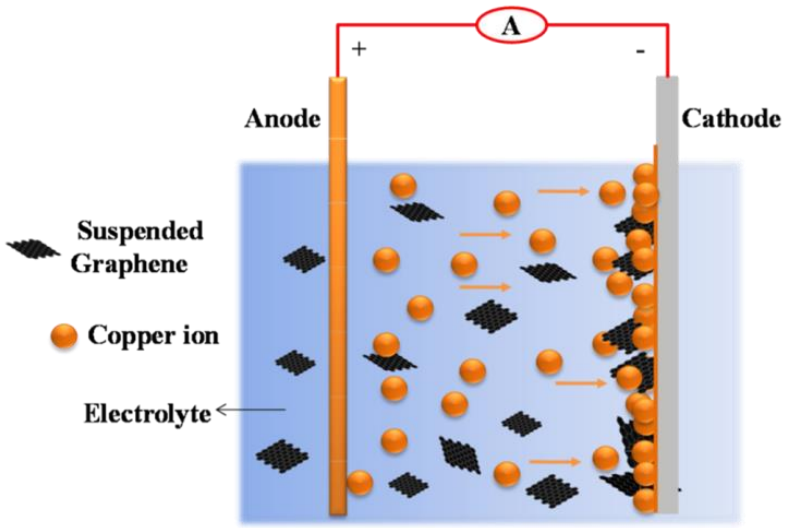

Figure 3.2 Schematic of experimental set up used for electrodeposition of Cu-Gr composite foils in the current study.

Basic electrodeposition set up for the composite foils is shown in Figure 3.2 and details of the electrolyte for composite deposition are given below

Table 3.3 Experimental details for Cu-Gr deposition

Electrodeposition unit	DPR series pulse power supply (Dynatronix, USA)
Deposition technique	Direct, pulse and pulse reverse techniques
Regulation mode	Current
Anode	Electrolytic copper
Cathode	Titanium alloy
Graphene	0.1-0.75 g/L
Surfactant	Poly acrylic acid (PAA)5000
Composition of electrolyte	Copper sulphate ($CuSO_4.5H_2O$) De-ionized water and sulphuric acid (H_2SO_4)
PAA 5000	15-25ppm/0.1g of graphene
Ultrasonication	Prior to the deposition 2-4 hr (0.1-1 g/L of graphene)
Temperature during deposition	15-20 °C, pH- 1-0.5 (maintained by adding H_2SO_4)
Additives	None used

Cu-Gr composite foils were deposited on titanium plates using PRED technique by optimizing the current density. Following this, pulse parameters as well as graphene content were also optimized separately. A polymeric surfactant PAA5000 of ~15 ppm for 0.1 g/L of graphene was added to the electrolyte to disperse graphene in the copper sulphate electrolyte and to avoid agglomeration. Graphene content in the electrolyte was varied between 0.1-0.75 g/L and the foils prepared are designated as P1 (0.1 g/L), P25 (0.25 g/L), P35 (0.35 g/L), P5 (0.5 g/L) and P75 (0.75 g/L) respectively, which is the nomenclature adopted for the entire dissertation. The applied pulse parameters for PRED technique were ~0.1 A/cm^2 and ~0.01 A/cm^2, for the forward and reverse pulses respectively. For the forward pulse, $T_{F\,on}$ was in the range of 15–50 ms and $T_{F\,off}$ was in the range of 50–100 ms, for reverse pulse, $T_{R\,on}$ and $T_{R\,off}$ were in the range of 1–10 ms. Cu-Gr composite foils were synthesized by DC using the optimized graphene content in the electrolyte in order to compare with PRED. DC electrodeposition was done by

applying a current density of 0.025 A/cm^2. Initially, pure copper was deposited in blank electrolyte (without graphene) as a seed layer for few minutes to enable easy separation of the deposited composite foil from the titanium substrate. This step was followed by composite deposition in the respective electrolytes containing varied concentrations of graphene. All depositions were performed under magnetic stirring with the bath temperature between 15-20 °C. Compact and highly dense composite foils with a thickness of ~30 µm were deposited by DC and PRED technique using Dynatronix pulse power supply (DuPR10-3-6). The electrodeposited Cu and Cu-Gr foils were annealed at 300 °C for 30 min under argon atmosphere in a tubular furnace in order to evaluate the microstructural stability.

3.5 Copper-CNT composites

In order to study the influence of tubular structure of CNTs in enhancing the strength as well as electrical conductivity, CNT reinforced Cu composite coatings are prepared using an electrochemical deposition technique with the optimized pulse parameters. Initially, CNTs were functionalized by acid treatment using the procedure given in section 3.5.1, followed by washing with de-ionised water until the pH becomes neutral in order to make the surface of the CNTs hydrophilic due to the presence of oxygen functional groups. The chemical interaction analysis revealed that the oxygen present in the surface functional groups can enhance the interaction between carbon and Cu. The oxygen present in the functional groups could promote electron exchange between Cu and carbon atoms, or directly interact with Cu thus playing a key role in the formation of Cu-CNT surfaces [151]. The functionalization process for the CNTs is discussed in the next section.

3.5.1 Functionalization of CNTs

Carbon nanotubes were functionalized by the well-established chemical method. As received multi walled carbon nanotubes (MWCNTs) were suspended in acidic medium of H_2SO_4 (98%) and HNO_3 (70%) (1:3) and stirred for 2 hr at a temperature of 120°C. The oxidized CNTs were then washed several times until the pH of functionalized CNTs solution becomes neutral. Carbon nanotubes were filtered using a polymer filter membrane and later dried at 60-80 °C.

3.5.2 Deposition of Cu-CNTs

Functionalization was followed by deposition of Copper-CNT composites which includes different steps such as dispersion of CNTs with the addition of surfactant to make the CNTs homogeneously disperse in the electrolyte.

Table 3.4 Experimental details for Cu-CNT composites

Electrodeposition unit	DPR series pulse power supply (Dynatronix, USA)
Deposition technique	Pulse reverse electrodeposition (PRED)
Regulation mode	Current
Anode	Electrolytic copper
Cathode	Titanium alloy
Composition of base electrolyte	Copper Sulphate ($CuSO_4 .5H_2O$) De-ionized water and sulphuric acid (H_2SO_4)
Surfactant	Poly acrylic acid (PAA)5000
PAA 5000	15-25 ppm/0.1 g of CNTs
Ultrasonication	Prior to the deposition for 2-4 hr (0.1-1 g/L of CNTs)
Temperature during deposition	15-20 °C, pH- 1-0.5 (maintained by adding H_2SO_4)
Additives	None used

Initially content of the CNTs used for the deposition was 0.1 g/L and deposition, follows the same procedure as in section 3.4. However, due to the length of CNTs, which is in the order of 5-20 µm, Copper-CNT composite films were not formed. Instead powdered composite has formed. Therefore, shortening of CNTs was attempted in order to deposit a highly dense composite foil. The CNTs were shortened by ultrasonication method without damaging the CNTs walls.

3.5.3 Shortening of CNTs

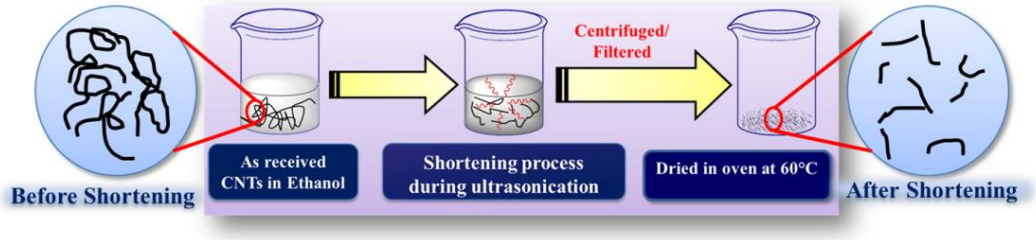

Figure 3.3 Scheme representing the process of shortening SWCNTs and MWCNTs.

SWCNTs and MWCNTs were procured from NANOSHEL, USA. As-received CNTs were ultra-pure without any metal catalysts (purity >98%). Analytical grade ethyl alcohol (Alfa-Aesar) was used as the organic solvent. SWCNTs and MWCNTs of 0.05 gm. each were taken separately in 50 ml of ethyl alcohol and were dispersed using an ultrasonicator (Telsonic-Ultrasonics, 33 kHz) for about 30-120 min. Ultrasonicated CNTs were separated by centrifugation/filtration and dried in an oven. Figure 3.3 illustrates schematic of the shortening process.

3.5.4 Electroless deposition of copper on MWCNTs

In order to enhance the interfacial bonding and dispersion of CNTs, in this case, CNTs are shortened and then functionalized. These shortened and functionalized CNTs are decorated with copper. Electroless deposition has several steps viz, sensitization, activation and coating of copper. Sensitization includes addition of 2.26 gm. of $SnCl_2$ –$2H_2O$ to 1ml of HCl (38%) and the volume was made up to 100 ml with de-ionized water and stirred. This sensitized mixture was aged for 72 hr at room temperature (25°C). An activating solution was made containing 0.025 g. of $PdCl_2$ in 1.3 ml of HCl (38%) and the volume was made up to 50 ml with deionized water. 0.05 g of the oxidized tubes was then sensitized by sonicating in 50 ml of $SnCl_2$– HCl solution (of a specified age) for 3 min and the mixture was subsequently stirred for 7 min. The sensitized tubes were separated from the sensitizing medium by centrifugation and washed with deionized water. The sensitized nanotubes were then stirred in 50 ml of $PdCl_2$–HCl activating solution for 0.5 hr. The activated CNTs were separated from the

activation medium by centrifugation and were washed with de-ionized water. The composition of the electrolyte for the electroless deposition of copper is give as Table 3.5

Table 3.5 Electrolyte composition for electroless deposition of Cu on CNTs

$CuSO_4$-$5H_2O$	3.1 g/L
Disodium salt of EDTA	20 g/L
HCHO (added later)	20 g/L
Na_2SO_4-$10H_2O$	40 g/L
HCOONa	20 g/L
Polyethylene glycol	6.6 g/L (pH=7, adjusted with NaOH at 25 °C)

Decoration with copper was achieved by stirring the activated and sensitized tubes in 50 ml of Cu bath (composition as shown above, pH 7) for 15 min, followed by the addition of 1 g. of HCHO. After 5 min the suspension was filtered and washed with deionized water. The pH was varied using NaOH solution to study its effect on metal decoration.

3.6 Characterization techniques utilized

Copper and copper nanocomposite foils were characterized by various techniques for microstructural details, mechanical and electrical properties. Microstructural/structural details are obtained using Field Emission Scanning Electron Microscopy, Electron Back scattered diffraction, X-ray diffraction, Transmission electron microscopy, focused ion beam milling, Raman spectroscopy, Fourier-transform Infrared spectroscopy, X-ray photo electron spectroscopy and simultaneous thermal analyzer. Mechanical and electrical properties were evaluated using depth sensing nanoindentation, four-probe electrical resistivity method respectively. Since the majority of the characterization was done at ARCI, the relevant details about respective equipment are adopted from ARCI web page.

3.6.1 Field emission scanning electron microscopy (FESEM) and electron backscatter diffraction (EBSD)

Scanning electron microscope with field emission (FESEM HITACHI S4300) is used for microstructural evaluation of the copper and copper composite surfaces at high magnifications (> 200000X). This system is attached with an energy dispersion spectroscopy (EDS) unit and an electron backscatter diffraction (EBSD) unit [185]. When an incident electron beam falls on a sample, the interactions of the electrons with the material produces various types of electrons from the sample depending on the energy after interaction, namely secondary electrons, backscattered electrons, x-rays etc. The secondary electrons are important to study the microstructure of the sample. Backscattered electrons are elastic in nature and are the source for the EBSD technique, using which crystallographic information (texture), microstructural information, orientation of individual grains, grain shape and size, type of grain boundaries including grain boundary statistics can be obtained. The copper sample is held inclined at an angle of 70° from the ground in order to enhance the backscattered electrons and these emergent backscattered electrons undergo diffraction. The electron beam moves on the copper sample surface in a systematic manner based on a step size, which is 20-40 nm, which was used, in the present research. The diffracted backscattered electrons are collected on a phosphor screen where they form bands called Kikuchi bands that are analyzed and indexed based on known crystallographic inputs. The electron beam passes on the surface and electron diffraction occurs at each point on the entire area of interest and mapped in EBSD. FESEM is used to study the morphology of electrodeposited copper and to observe the reinforced elements such as graphene, CNTs etc., in the copper matrix and their distribution.

3.6.2 X-ray diffractometry

X-ray diffraction (XRD) (D8 ADVANCE, BRUKER), was used to study the structural (crystalline, amorphous) information of the material can be retrieved [186]. Materials can range from bulk, thin films/coatings and powders of metals, alloys, ceramics, organic and inorganic compounds. In XRD, Cu is used generally as x-ray source and a high speed 1D

LYNXEYE detector is mounted on a vertical goniometer in order to carry out angular scans from 5 to 160° with an angular resolution of 0.002°. XRD was used to confirm the preferred crystallographic orientations of the electrodeposited copper foils and copper nanocomposites. Information of the reinforcements was also obtained. In the present study XRD analysis using Cu K-α radiation of wavelength 1.54056 Å with a step size being 0.05° and a scan speed of 3 sec/step.

3.6.3 Raman spectroscopy

Raman Spectrometer (LabRAM HR800- Horiba JOBINYUON Micro Raman spectrometer) is an exceptional instrument to study the organic compounds present in the composites [187, 188]. Intrinsic nano probing combined with micro Raman spectroscopy makes it very sensitive to short range structure in the nanomaterials. Raman spectroscopy can be used to analyse almost all the variety of materials including aqueous solutions since it is not affected by the large water absorption effects found in FTIR. No sample preparation is required, hence making it an easy characterization technique. Raman spectroscopy actually instigates from the bond vibrations. Having a spot size of 500 nm, Raman has a resolution of 0.36 cm^{-1} and micro Raman provides phase identification where, even traces of secondary phases can be detected as the polarisibility changes with the nature of the bonding.

Raman spectroscopy was used to determine the number of layers and crystallinity in graphene, to study the crystallinity and defects in the as-received, functionalized and shortened SWCNT and MWCNTs by observing the variation in D- band, G- band, 2D band and I_D/I_G ratio. In addition, presence of graphene and copper oxide was also observed in the Copper – graphene composites by Raman studies. The measurements were carried out by using Argon-ion laser with power and wavelength of 16 mW, 514 nm respectively.

3.6.4 Fourier transform infrared spectroscopy (FTIR)

Fourier transform infrared spectroscopy (Spectrum GX Optica, Perkin Elmer, USA) with wave number region: 7000-370 cm^{-1} has been used. FTIR measures the infrared radiation frequencies, which were absorbed by a material at the frequencies of vibration of the

interatomic (chemical) bonds within that material. This gives us the details about interatomic (chemical) bonds, which are present in a material. The frequencies of bond vibrations fall within the frequency range of the infrared part of the electromagnetic spectrum. A single bond may vibrate in more than one mode and only those modes, which involve a change in dipole moment, will absorb infrared radiation. When a molecule is irradiated with all the infrared frequencies, it will absorb those frequencies which match bond vibrations with a change in dipole moment, and will not absorb those frequencies which do not match bond vibrations with a change in dipole moment [189]. FTIR has been used to study the functional groups present on the surface of graphene and CNTs.

3.6.5 Transmission electron microscopy (TEM)

Transmission electron microscopy is used to study the microstructural features of the samples at very high magnifications (> 500000X) in transmission where, FESEM cannot provide enough resolution [190]. Samples of 3 mm diameter are prepared such that the thickness of the thin region is about 50-60 nm or less. The preparation of this electron-transparent sample involves several steps including dimpling, precision-ion milling or twin-jet polishing and electropolishing. The incident electron beam can be accelerated to 200 kV and on passing through the sample, several interactions take place. The transmitted beam is then used for imaging and electron diffraction studies. The system is equipped with a LaB_6 filament, EDS and electron energy loss spectroscopy attachments both of which are techniques for elemental analysis. In the later technique the energy lost by the incident beam on passing through the sample is measured and thus elemental information is obtained.

TEM has been used to study the microstructural features of graphene synthesized electrochemically and to confirm the presence of graphene and CNTs in the copper matrix. Although graphene and CNTs in the copper matrix can be distinguished in FESEM, the features including distribution, number of layers in graphene/length and number of walls in CNTs cannot be observed, TEM has been used to serve this purpose. TEM has also been used to observe the length reduction in CNTs after the cutting process. For the composite foils TEM samples have been prepared using electropolishing (lectroPol5) for about 12 seconds with a

flow rate of 19-23 and applied voltage of 12-13 respectively until the required thickness is achieved this followed by Twin-jet polishing to get the thin region using an electrolyte contains HNO_3 and methanol mixture at an applied voltage of 8-12V at -10°C.

3.6.5.1 Focussed ion beam milling/microscopy (FIB)

Focussed ion beam milling (Carl Zeiss Neon 40) system is equipped with an electron beam and a focused ion beam (FIB). The Ga-ion beam is used to remove material from the sample surface in a controlled fashion and the electron beam is used to carry out the imaging. As in-situ FE-SEM is present in the FIB unit, live imaging is possible. Applications include study of coatings, cross-sections, growth mechanisms, corrosion etc. If an EBSD unit is attached to the dual beam microscope, the three-dimensional extent of grains in the sample can be mapped out. FIB was used to study the grain size distribution of Cu-Gr composites with different concentration of graphene and to study the DC and PRED deposited Cu-Gr samples. In case of pure copper FIB was used to confirm the equi-axed grain growth throughout the cross-section of the textured copper foils.

3.6.6 X-ray photoelectron spectroscopy (XPS)

X-ray photoelectron spectroscopy is an effective and quantitative tool for determining the elements and elemental composition on the surface of the material [191]. In addition, XPS also provides the surface structure, hybridization, bonding and functionalities with binding energy present in graphene. In the present study, to determine the elemental composition of graphene x-ray photoelectron spectroscopy (XPS) (Omicron Nano Technology, UK) has been used.

3.6.7 Nanoindentation

Nanoindentation is a standard and well-known method to investigate mechanical properties like hardness, elastic modulus, fracture toughness, strain- rate sensitivity, scratch resistance [192] etc. Hardness of engineering materials has been widely studied using various indentation techniques including nanoindentation. Hardness is proportional to the applied load P divided by the contact/projected area of the material [193]. Therefore nanoindentation is mainly

concerned with the depth of penetration in nm and the applied load in µN. During nanoindentation, the indenter tip (Berkovich) of known geometry is projected onto the selected area of the testing material surface by applying load either until it reaches the chosen maximum load or it reaches the designated depth. Once it reaches the required load/depth, holding segment is introduced for material to relax then unloading takes place. The same loading and unloading process is repeated for several times at different positions on the surface to have meaningful statistical analysis of the data.

In simple terms the load applied over area of the impression left gives the hardness value. This area is calculated as a function of contact depth whereas in other traditional indentation techniques, projected area is taken into consideration. The hardness is extracted from the load-displacement plots obtained during nanoindentation using the method described by Oliver and Pharr [194, 195].

$$H = P_{max}/A\ (h_c) \qquad (3.1)$$

Where, P_{max} is the peak load applied, A is the contact area, h_c is the vertical distance along which contact is made (contact depth) and A (h_c) is area function defined as

$$A(h_c) = 24.5h_c^2 + C_1h_c^1 + C_2h_c^{1/2} + C_3h_c^{1/4} + \ldots\ldots + C_5h_c^{1/16} \qquad (3.2)$$

C_1, ….C_5 are the constants of area function given as $C_1 = 1.6991E^{+4}$, $C_2 = -1.1537E^{+6}$, $C_3 = 1.1977E^{+7}$, $C_4 = -3.0602E^{+7}$, $C_5 = 1.9918E^{+7}$

The reduced modulus (E_r) is calculated using

$$E_r = \frac{\sqrt{\pi}}{2}\frac{S}{\sqrt{A}} \qquad (3.3)$$

Where, S is the measured stiffness, defined as $S = \partial p/\partial h$, taken as slope of initial linear portion of the unloading curve

The elastic modulus E is calculated from reduced modulus E_r using the equation given below:

$$\frac{1}{E_r} = \frac{(1-\vartheta_i^2)}{E_i} + \frac{(1-\vartheta^2)}{E} \qquad (3.4)$$

Where, E_r is the reduced modulus, E and ν are the Elastic modulus and Poisson's ratio (0.33 for Cu) of the sample. E_i and ν_i are the elastic modulus and poisson's ratio of the indenter (for diamond, E_i is 1140 GPa and ν_i is 0.07 respectively). May be it is better to give equation numbers

Hardness and elastic modulus were determined for (111), (100) and (110) textured and twinned pure copper foils by MTS Nanoindenter XP in CSM (continuous stiffness measurement) mode. For the copper nanocomposites (Graphene and MWCNTs), Hysitron Triboindenter TI950 was used in a quasi-static mode.

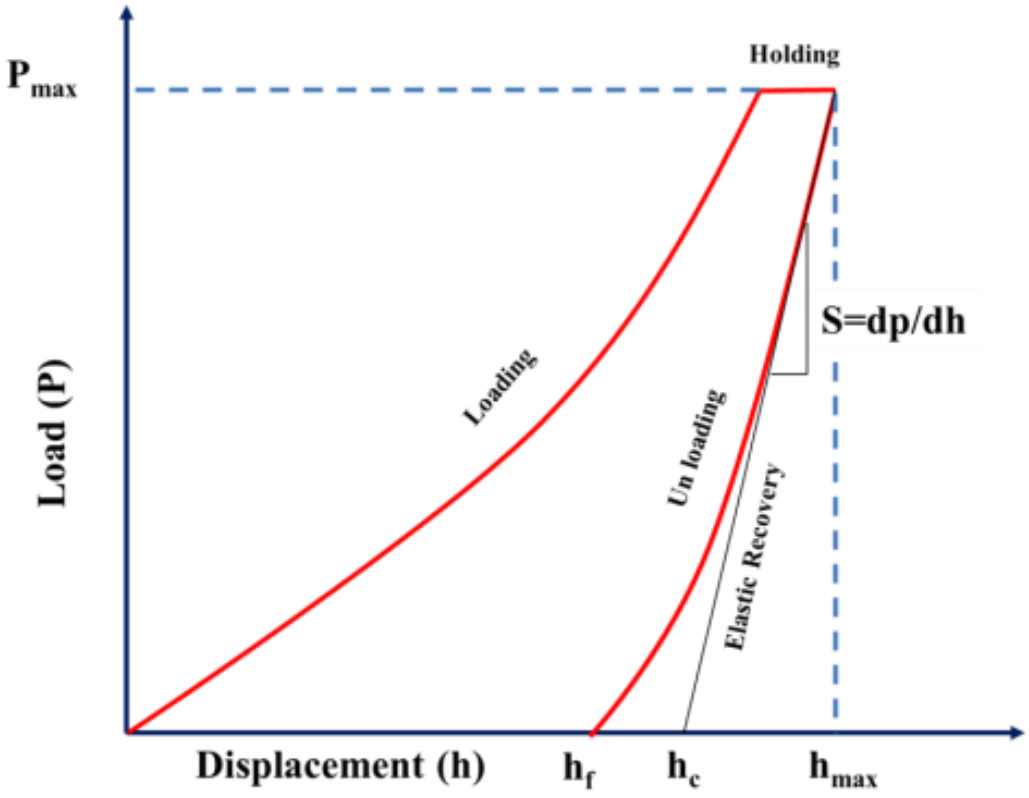

Figure 3.4 Load-displacement curve in nanoindentation (redrawn from [193]).

For the copper foils, the indentation was done at constant depth mode where the maximum depth of penetration was 2000 µm. Similarly composite foils were tested at a maximum constant load; applied peak load was in the range of 2000 µN at constant loading rate of 500 µN/sec.

3.6.8 Four-probe electrical resistivity

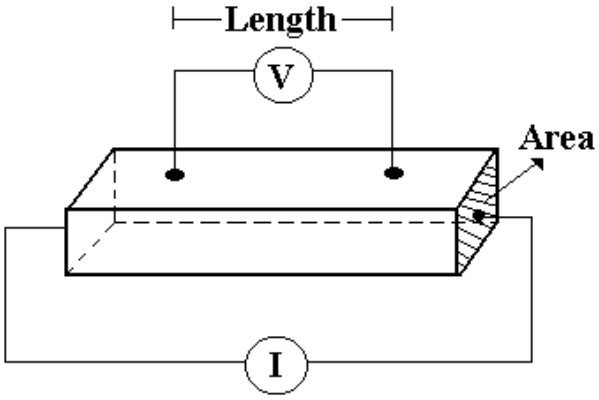

Figure 3.5 Schematic represents the Four-probe electrical resistivity set-up.

Four-probe resistivity consists of four equally spaced probes connected to the sample as shown in the Figure 3.5. Current (I) is supplied to the foils through the outer probes and simultaneously the voltage (V) drop is measured between the inner probes. The resistivity of the sample is given by

$$\text{Resistivity, } \rho = \frac{RA}{l} \qquad (3.5)$$

Where 'R' is resistance, 'A' is area of cross section, and 'l' is length between voltage probes.

This method was used for pure copper foils with sample of 4 cm length, width of 1.5 cm and thickness of 100-200 µm. Four probe resistivity measurements were done using Loresta GP; Mitsubishi chemical analytech Co., Ltd, Japan. By using this method, resistivity can be measured in the range 10^{-6} to 10^{7} Ω with 4-digit accuracy of (± 0.5%).

The resistivity was measured as volume resistivity (ρ_v), which is similar to the above method, the only variation being the thickness of the sample.

$$\rho_v = R[\Omega] \times RCF \times t[cm] \quad (3.6)$$

Where, 'R' is resistance,'t' is thickness of the sample and 'RCF' is resistivity correction factor.

The resistivity correction factor (RCF) changes with change in sample shape, size as well as measuring positions. In the 4-pin probe method, if the sample size or measuring position are not fixed, the electric energy distributed in the sample is changed. The resistivity correction factor (RCF) is used to obtain the correct values for the volume or surface resistivity. In addition to the four probe electrical resistivity, electrical conductivity can be measured by eddy current electrical conductivity gauge, (Sigmatest 2.069, FOERSTER, USA) ranging from 0.5 to 65 MS/m. It is a single probe portable device to measure electrical conductivity of non-ferrous metals and coatings (as thin as 180 nm) at different testing frequencies with external and internal heating compensations. It is also used for thin and irregular shaped nano to micron sized films and bulk materials (smooth or rough) with minimum and maximum size of diameter being 5 mm and 300 mm respectively.

For textured copper foils and composite foils in addition to these techniques, resistivity values were also confirmed by I-V characteristics obtained using keithley ammeter and volt meter.

The characterization of the pure copper, Cu-Gr and Cu-CNT samples is discussed in detail in the individual chapters.

Chapter 4. Electrodeposition of pure copper with various crystallographic orientations and evaluation of its mechanical and electrical properties

This chapter discusses in detail about the texture evolution and control over the twin density in copper foils prepared by a rapid pulse reverse electrodeposition (PRED) technique in an additive-free electrolyte. Subsequently, correlation to its mechanical and electrical properties with the obtained microstructure has been made. For the first time, a novel approach has been demonstrated involving a rapid PRED technique in order to manipulate the (111), (100) and (110) textures, CSL Σ3 coherent twin boundaries (special grain boundaries) and grain size.

Electrodeposition was performed in constant current density mode. A detailed experimental procedure has already been discussed in chapter 3. Range of optimized pulse parameters in order to control the texture in copper foils is mentioned in Table 4.1.

Table 4.1 Pulse parameters used in PRED

Texture	Pulse duration (ms)				Forward current density (A/cm^2)	Reverse current density (A/cm^2)
	$T_{F\,on}$	$T_{F\,off}$	$T_{R\,on}$	$T_{R\,off}$		
(111)	5-15	20-50	2	2	0.5	0.1
(100)	10-20	100-200	2	2	0.25-0.5	0.1
(101)	15-20	1000-2000	2	2	0.4-1	0.1

Pulse parameters and current densities for the forward pulse were varied while the reverse pulse parameters were kept constant. Electrolyte composition, pH and temperature of the electrolytic bath during the deposition were maintained constant for all depositions. PRED technique facilitated rapid deposition and a coating of about 50-100 µm thick was feasible in about 1h of deposition. The as-deposited foils were peeled off from the substrate to make them free standing prior to characterization. The surface of the copper foils was electropolished to determine the texture by electron backscatter diffraction (EBSD). The step size during the EBSD scanning was about 40 nm. The diffraction patterns from EBSD data were analysed

using orientation imaging microscopy (OIM™ V6.1) analysis software from EDAX-TSL to determine the crystal orientations in each grain, grain boundary misorientations such as low angle grain boundaries (LAGBs), high angle grain boundaries (HAGBs) and other grain boundary statistics. Confirmation of the texture in large areas of the copper foils was also done conventionally by x-ray diffraction (BRUKER D8 ADVANCE) with Cu K_α radiation (λ=1.5406 Å). Hardness and elastic modulus of copper foils were measured using an MTS XP Nanoindenter; the indentations were performed in the continuous stiffness measurement (CSM) mode using a Berkovich indenter at a constant maximum indentation depth of 2 μm. The electrical resistivity measurements were carried out by four point probe technique and electrical conductivity was measured by eddy current electrical conductivity gauge (Sigma test 2.069, FOERSTER, USA).

4.1 Texture validation by EBSD and XRD

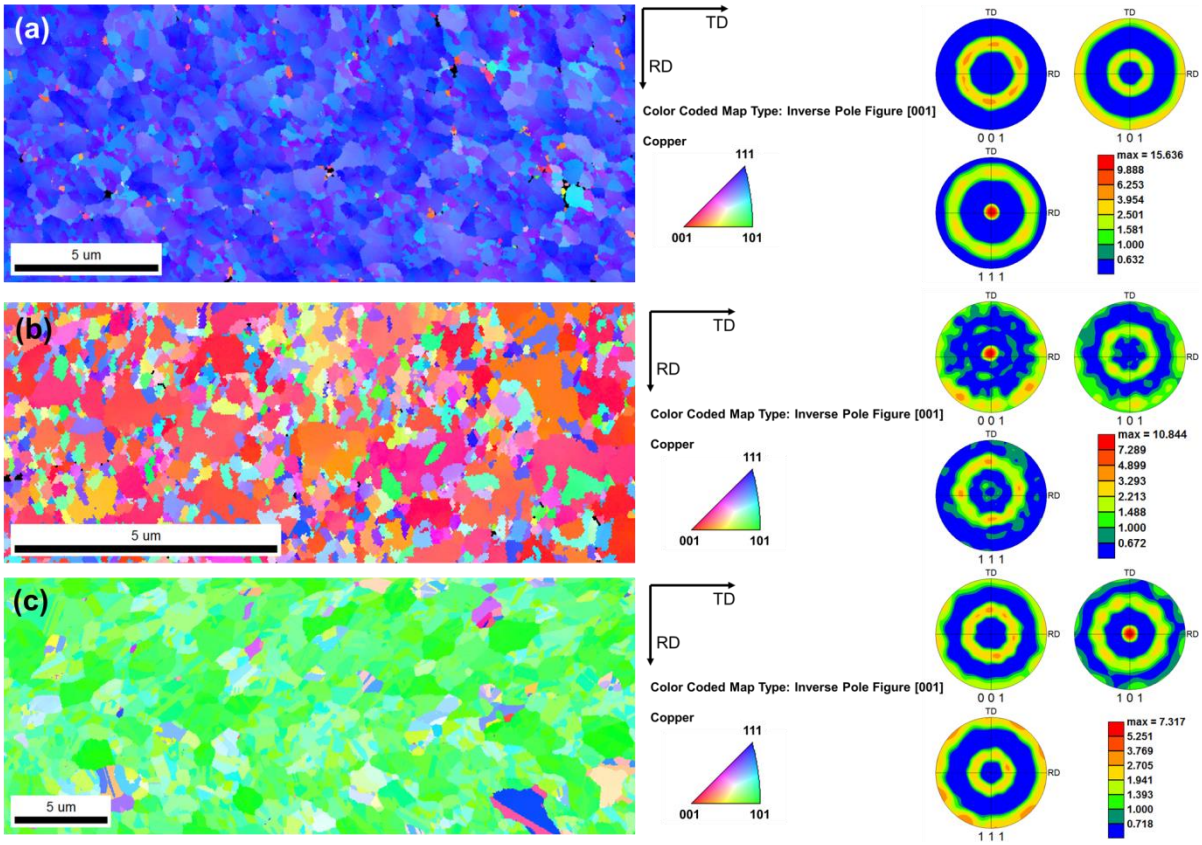

Figure 4.1 (a), (b) and (c) indicate the crystallographic orientation maps for copper foils highly oriented towards (111), (100) and (101) textures respectively as indicated by the color codes allocated in the inverse pole figure (crystal direction with respect to the sample normal) and pole figures with pole densities given to the right of the respective image.

The crystallographic orientations of the highly (111), (101) and (100) textured foils in the present study have been obtained by adjusting the pulse parameters as well as the current density. The various parameters that have been used during the deposition process are given earlier. Figure 4.1(a-c) shows the representative crystallographic orientation maps/OIM maps of the copper foils and corresponding colour coded inverse pole figures (IPF). Pole figures with colour scale indicate the crystallographic orientations of each grain and their pole densities respectively from the pole figures for a selected area of the foils at the microscopic level. In the present study, the orientation maps were processed from the normal direction (ND) of the sample, indicated as crystallographic plane normal, which is parallel to the normal direction. It can be seen from Figure 4.1(b) that the pole in pole figure of the sample with (100) texture

is shifted by 8° with respect to [-1, 3, 23]. A similar shift has been reported where, authors have further mentioned that a shift of 12° is acceptable [196].

From the EBSD orientation maps, it is evident that the copper foils are highly textured with a pole density of 15.63, 10.84 and 7.31 calculated from the orientation distribution function (ODF) indicating the preferred orientation for <111>∥ ND, <100>∥ND and<101>∥ ND textured foils, respectively. EBSD data shown in this study have been cleaned up using OIM^{TM} data analysis software. After grain confidence index (CI) standardization and neighbour CI correlation, a partition was created for each scan consisting of only those data points with CI ≥ 0.1. Thus it was ensured that the data used for the analysis is of high quality.

In order to confirm the texture of the copper foils at the macroscopic level, XRD patterns were obtained and the texture coefficients were calculated to confirm the preferred orientations. From XRD patterns (Figure 4.2), it is clear that these three foils are preferentially oriented along (111), (220) and (200) respectively. The reflections from the crystallographic planes of (111), (220) and (200) from XRD correspond to (111), (101) and (100) from EBSD [197].

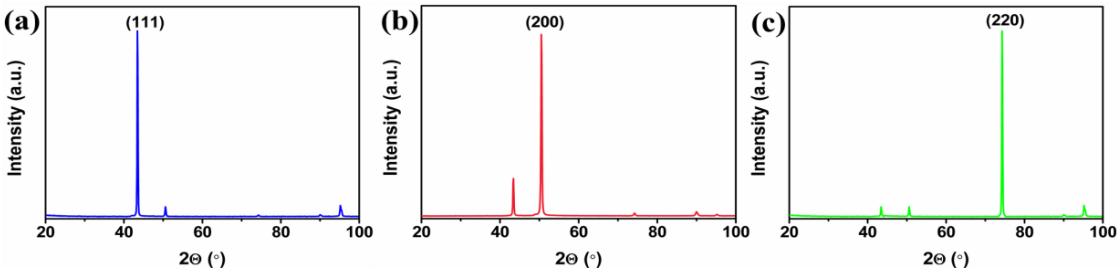

Figure 4.2 X-ray diffractograms of (a) (111) (b) (100) and (c) (110) textured copper foils.

The texture coefficient (T_c) [198] was calculated from the XRD patterns by using equation 4.1.

$$T_{c(hkl)} = \frac{I_{(hkl)}/I_{0(hkl)}}{1/n \sum I_{(hkl)}/I_{0(hkl)}} \qquad (4.1)$$

Where T_c is the texture coefficient of (hkl) plane, $I_{(hkl)}$ and $I_{0\,(hkl)}$ are measured and relative intensities of the corresponding planes respectively and 'n' is the number of reflections. It has been reported that Tc>1 indicates a preferred crystallographic orientation [199] and T_c~1 indicates a random orientation [198].

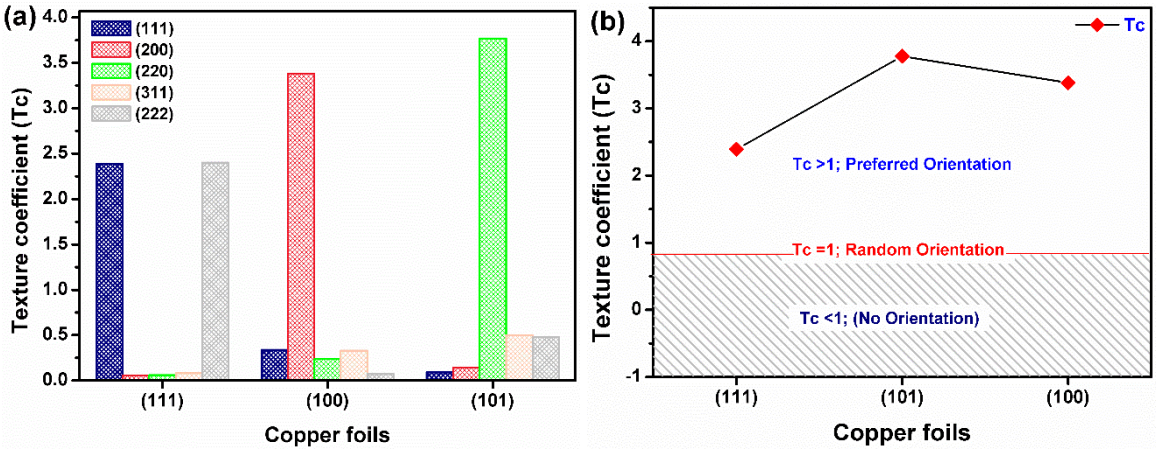

Figure 4.3 Texture coefficients of (a) each plane and (b) total T_c of the copper foils with (111), (100) and (101) textures.

From the XRD patterns (Figure 4.2), for the (111), (100) and (101) textured copper foils, the texture coefficients (T_c) were calculated as 2.39, 3.38 and 3.78 respectively. These larger values of T_c show a strong texture in these foils (Figure 4.3). The texture coefficients calculated for various crystallographic directions in all these foils are shown in Figure 4.3(a&b). According to the texture formation studies in fcc metals, at initial stages of the deposition, the crystallographic orientation is dominated by substrate texture at the interface due to its large interfacial energy in conventional DC and PED processes [97]. During the electrodeposition process, surface energy, strain energy or a combination of both and the energy arising out of various interfaces may control the texture formation [85]. However, texture of the films is also influenced by several aspects such as pH of the electrolyte, applied current densities, pulse parameters, additives, impurities, thickness of deposit, stress/strain formation in the deposit [200] and their relaxation etc. In most of the cases the crystallographic orientation changes from (111) to (100) and to (101), respectively depending on the changes that occur during the deposition process [201, 202]. Apart from these, the stability of the surface plane of the metal also has a significant role [203, 204]. However, the stability of the individual surface plane of fcc metals during the texture formation follows the order as (111) > (100) > (101) [19] as minimization of surface energies in these metals follow the order of $\gamma_{(101)} > \gamma_{(100)} > \gamma_{(111)}$ [205]. Therefore initially copper growth is generally is expected to be inclined towards the (111) direction irrespective of the deposition technique used. It is mainly driven by several reasons like low surface energy of the (111) plane which in turn depends on the coordination

number [206] and atomic density when compared to other (100) and (101) planes [201, 207-209]. During the deposition, development of (111) texture is favoured at large current densities applied at low temperatures due to minimization of surface/interfacial energy during growth process. Our previous study has also revealed that (111) texture is favourable at high current densities with short forward pulses and short reverse pulses [35]. In addition, low deposition temperatures are suggested in order to minimize the surface and interfacial energies, for twin boundary formation, good surface properties and to reduce the usage of additives [61]. Although (100) and (101) textures are known to be dominated by the strain energies [210] due to the anisotropy in elastic constants of copper [197], (100) and (101) grains nucleate at (111) boundaries dutring initial stages of electrodeposition [211] and gradually change to either (101) or (100) depending on the stresses. This usually occurs at higher current densities and low temperatures during conventional deposition process [197]. Specially for thicker and free standing films, lowest strain energy density in the elastic regime favours (100) direction and is considered as free growth mode formed due to H_2 co-deposition during DC and PED [212, 213]. However, during deposition, (100) growth is favoured slightly at larger off-times [214] and (101) is known to be favoured at very large off-times [17]. This happens by consuming (111) grains resulting from the stress driven recrystallization during PED due to lower strain energies favoured at high current densities [215]. High current densities results in high initial stresses, causing defects within the grains which are associated to the strains leading to the formation of texture. Increase in (101) with the extent of self-annealing and at very low deposition rates was reported to be because of higher off-times [32]. Further due to lesser atomic density in the plane and high broken bonds, (101) is known to be dissolved more easily compared to (111) and (100) textures. Therefore, (101) growth appears to be highly favourable during PED technique with longer off-times [216].

Accordingly, moderate changes in the pulse parameters have been made in our PRED conditions to deposit films with various orientations namely (111), (100) and (101) textures during deposition of the copper foils. In PRED, several processes occur at the cathode [35] as well as the anode during each cycle [217]. During the cathodic pulse or forward pulse, copper ions get reduced at the cathode and deposit as copper metal, while forward off-time aids in relieving of stresses and rearrangement of crystals, leading to texture development [218, 219]. In addition, uniform diffusion of Cu ions occurs from the bulk of the electrolyte towards the

cathode, improving the deposition process [109]. Short anodic pulse, during which current is applied in the negative direction, removes the deposited copper partially, resulting in the availability of fresh active nucleation sites during each cycle. This will lead to grain refinement and equi-axed grain formation throughout the thickness (~100microns).

Anodic pulse also aids in the formation of twin boundaries due to strains formed during the anodic pulses [219, 220]. In addition to the dissolution of loosely bonded atoms, removal of entrapped hydrogen and impurities, etc. will also happen during the anodic pulse. Hence, with the applied cathodic and anodic pulses with optimum on and off-times, a number of microstructural changes take place that could influence the texture. However, the stabilization of texture is taken care by the applied anodic pulse immediately after forward pulse in every cycle by relieving all the induced stresses which can change the texture during room temperature annealing after the deposition. In the present case, for (111) textured foils, high forward current densities with shorter forward and reverse pulses with low reverse current densities were applied at low temperatures. High current densities are employed in order to increase the nucleation sites which aid in grain refinement and also to have low impurity levels [61]. For (100) and (101), slightly large forward off-times were employed in comparison to (111) with same anodic pulse. Pulse parameters were employed to control the textures, avoiding use of additives in the electrolyte since additives stay as impurities in the deposited foils and disturb the texture during room temperature annealing. The mechanism for formation of texture during each cycle in process is not understood as of today. However in the current study the formation of highly stable (111) texture is probably due to rapid pulses which are leading to preferred orientation [19]. The formation of (100) texture is possibly by self-annealing during the forward off-time due to high induced stresses leading to high strain energies at high current densities [218, 221]. Very long forward off durations might allow the formation and growth of (101) because (101) growth occurs at grain boundaries of (111). In addition, the PRED foils have also exhibited high compactness, high surface smoothness and less porosity [61, 63]. Here the deposition rates are quite fast compared to PED due to high current densities with application of a reverse pulse. In case of PED, longer pulse off-times are required for the rearrangement of the deposited grains for minimization of energy, removal of the residual stresses and adsorbed hydrogen along with impurities from the surface. In case of PRED, the applied reverse pulse takes care of the processes happening during off-time of PED,

wherein reverse pulse removes impurities quickly and also acts as an internal stress reliever after each cycle and porosity reducer by having new nucleation sites. This leads to grain refinement [222] and twin formation due to stress/ strain development during the deposition while reducing the deposition times. In addition, anodic pulse increases the stability of texture with equi-axed grain growth throughout the thickness of the foils, which can be observed from field ion beam (FIB) milled micrograph (Figure 4.4) with the usage of moderate current densities, which is not the case in DC and PED.

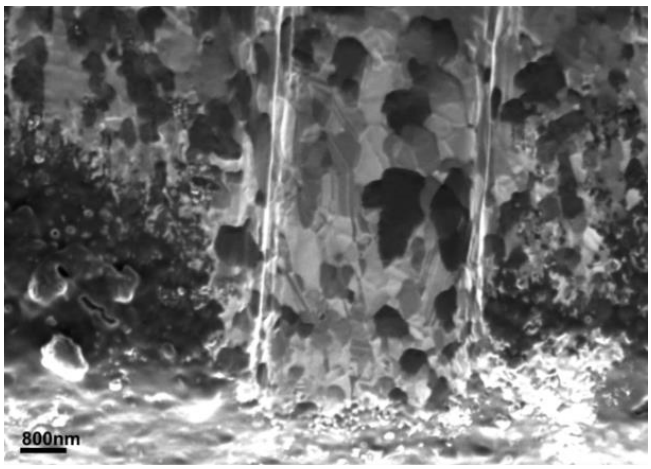

Figure 4.4 FIB micrograph showing the equi-axed grains throughout the cross-section of PRED deposited copper foil.

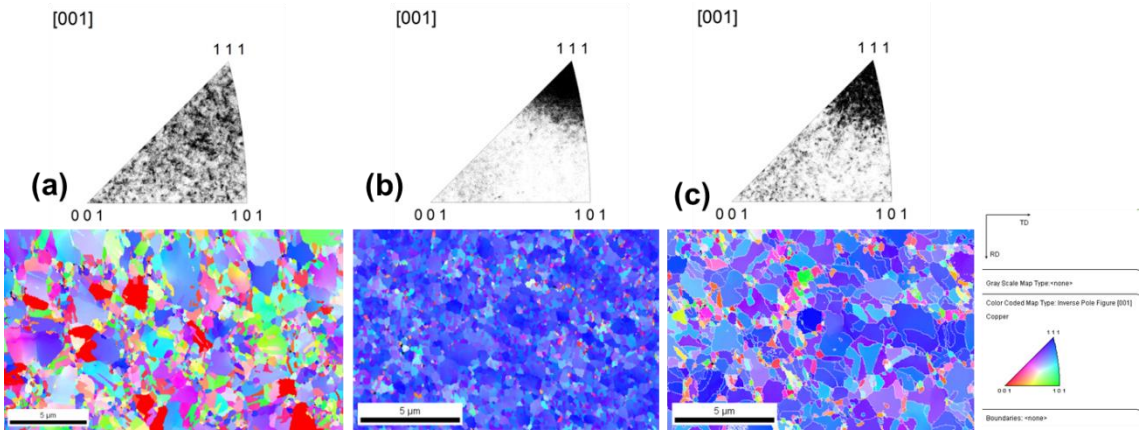

Figure 4.5 Representative EBSD orientation maps and respective inverse pole figures of copper foils prepared by electrodeposition (a) randomly oriented DC/PED synthesized copper foil without reverse pulse, (b) PRED copper foil highly oriented towards (111) and (c) slight deviation from (111) to random orientation of PRED copper foils after 6months.

The EBSD orientation maps with IPF figures in Figure 4.5 is an observation that confirms the influence of reverse pulse in controlling the texture formation, stability of texture and equi-axed grain growth. Further, the additive-free electrolyte results in the absence of impurities contributing to high electrical conductivity.

In addition to texture evolution, the copper foils have been further characterized to study the grain size, type of grain boundaries etc. It is known that grain size and grain boundaries play a significant role in controlling the mechanical and electrical properties besides texture [17]. Analysis of copper foils by EBSD yields the information regarding grain misorientations, grain boundary distributions including sub-grain boundaries, LAGBs (5-15°), HAGBs (>15°) and special grain boundaries [99]. The special grain boundaries including low-energy coincident site lattice boundaries (CSL) and coherent twin boundaries in all the textured foils are distinguished by different coloured plots. In addition to all these, the grain size distribution and grain boundary fractions are also estimated from EBSD.

4.2 Grain size distribution and grain boundary statistics

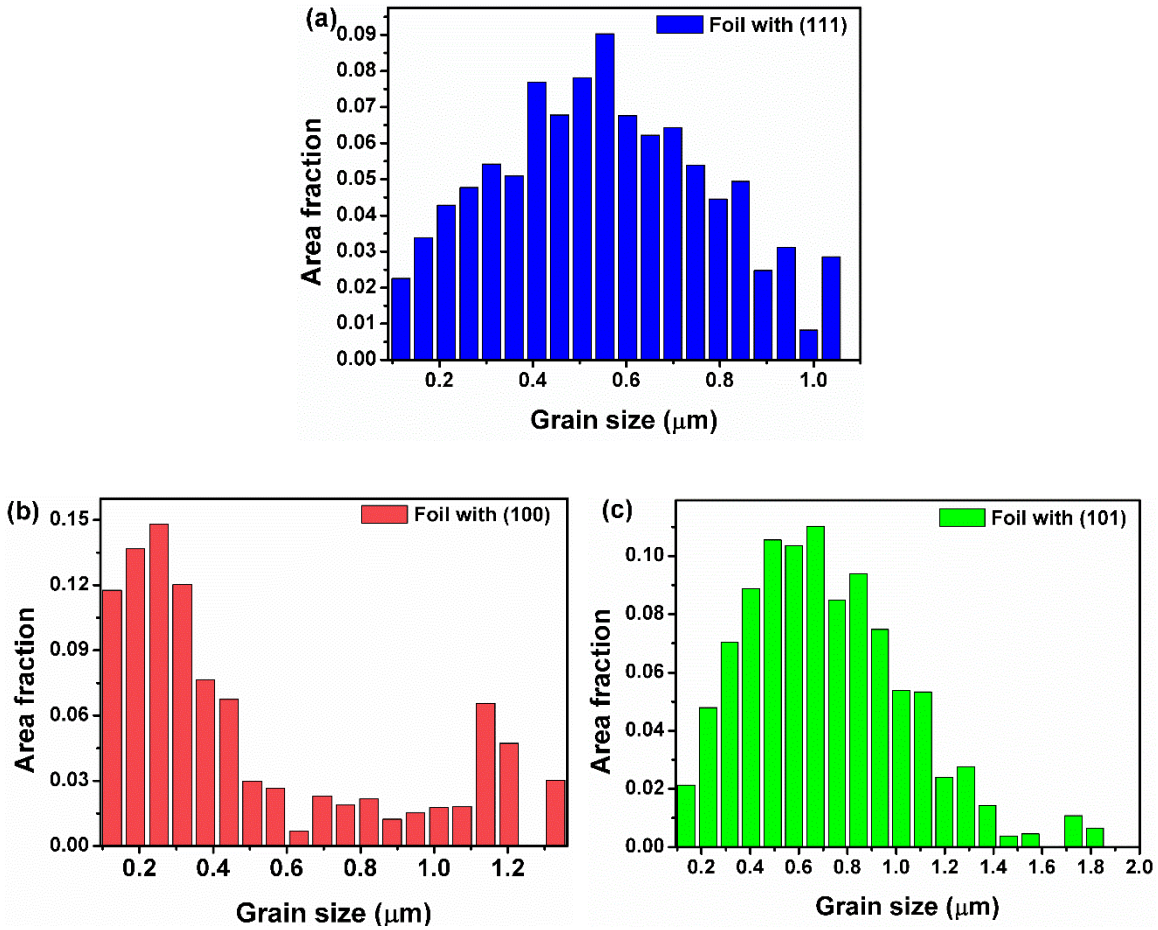

Figure 4.6 Grain size distribution of (a) highly (111) textured, (b) (100) textured, (c) (110) textured copper foils.

Figure 4.6 shows the grain size distribution in copper foils with (a) (111), (b) (100) and (c) (101) textures respectively. The corresponding statistics and grain size distribution histograms are also shown. It is seen that the foil with (111) texture had an average grain size of 0.57±0.2 μm with majority of the grains in the submicron range. The (100) and (101) foils had an average grain size of 0.72±0.3 μm and 0.97±0.5 μm respectively.

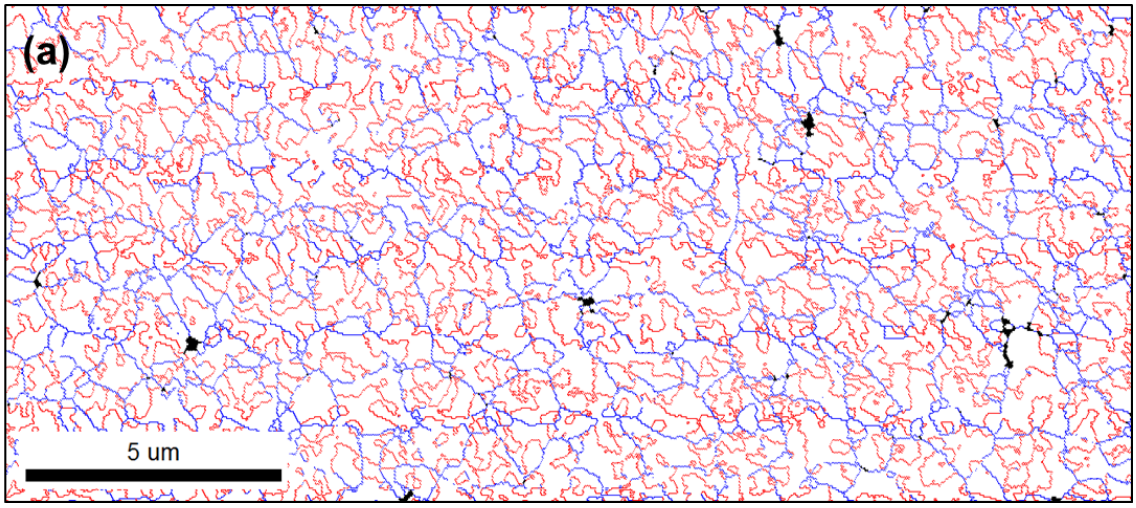

TD
RD

Boundaries : Rotation Angle

Min	Max	Fraction	Number	Length
15°	180°	0.666	71580	1.65mm

Boundaries : CSL

Sigma	Tolerance	Fraction	Volume	MDF Value	Number	Length
3	8.66	0.404	0.0176	23.01	43455	1.00355mm
Summary	-	0.404	0.0176	23.01		

* For statistics – any point pair with misorientation
Exceeding 1* is considered a boundary
Total number = 107500, total length = 2.48mm

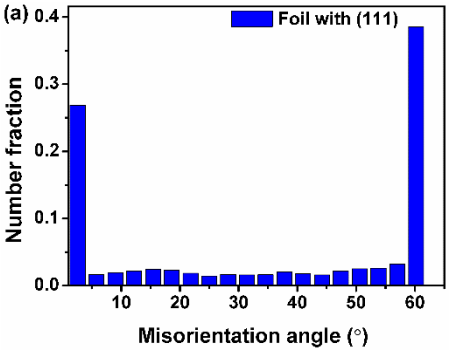

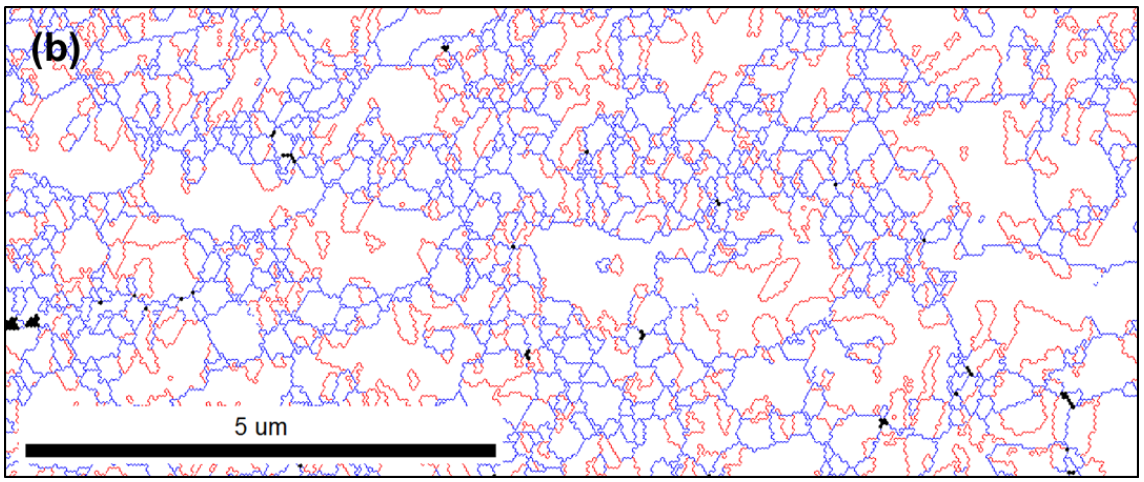

TD
RD

Boundaries : Rotation Angle

Min	Max	Fraction	Number	Length
15°	180°	0.788	27210	628.39 microns

Boundaries : CSL

Sigma	Tolerance	Fraction	Volume	MDF Value	Number	Length
3	8.66	0.306	0.0176	17.41	10557	243.803 mm
Summary	-	0.306	0.0176	17.41		

* For statistics – any point pair with misorientation
Exceeding 1* is considered a boundary
Total number = 34513, total length = 797.04 microns

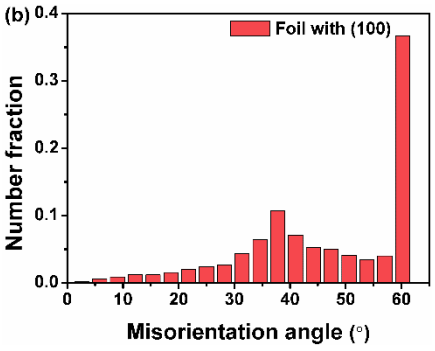

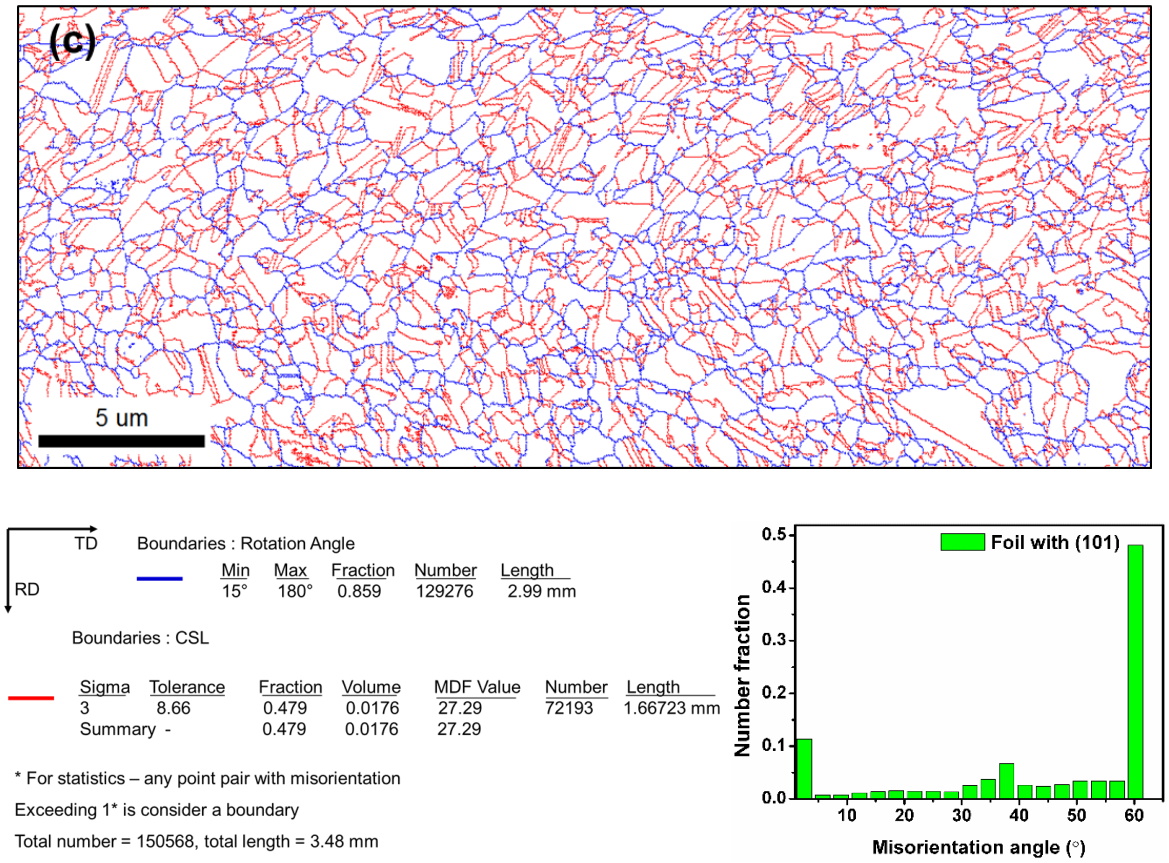

Figure 4.7 Grain boundary misorientation for copper foils highly oriented towards (a) (111), (b) (100) and (c) (101) respectively.

From the EBSD data, the fractions of LAGBs and HAGBs are calculated. The low angle boundaries are 6.2%, 2.8% and 2.9% among the total number of grain boundaries respectively (Figure 4.7) whereas HAGBs are 66.6%, 78.8% and 85.5% for foils with (111), (100) and (101) textures, respectively. HAGBs were indicated in blue color and Σ3 boundaries were indicated in red color (Figure 4.7). It can be observed that a large fraction of HAGBs are with a misorientation angle of ~60°. LAGBs generally have very less energy due to the minimum misfit at GBs between the adjacent grains which leads to increase in the hardness [218]. These LAGBs were found in larger fraction in foils with (111) texture as compared to other textured foils. HAGBs have high energy with large misfit at the GBs that may have no significant influence on the mechanical and electrical properties. According to Randle [95], special grain boundaries called CSL Σ3 coherent twin boundaries, categorized under the HAGBs, lead to increase in the mechanical strength as well as electrical conductivity. These are essential for improving the properties due to mirror-like arrangement of atoms at the GBs with the

misorientation of 60° <111>. Consequently, in order to measure the fraction of coherent twin boundaries (CSL Σ3) among the HAGBs, the analysis was carried out. From the grain boundary statistics, the most important feature of all the textured copper foils is that among the total length of grain boundaries, the large fraction of grain boundaries is accounted for CSL Σ3 (60° to <111>) boundaries (Figure 4.7). It was observed that highly (111) textured copper has 40.4%, (100) has 30.6% and (101) has 47.8% Σ3 boundaries among total boundaries. However, among the fraction of HAGBs (111) has 60.6%, (100) has 38.8% and (101) has 55.9% Σ3 boundaries. From the analysis, though (100) and (101) textures have large fraction of HAGBs, fraction of Σ3 boundaries is higher in (111) and (101) compared to that of (100). This is because, Σ3 boundaries are more common in (101) texture and boundaries with Σ < 27 and LAGBs are more common in (100) texture compared to (111) texture [223, 224]. This could be the probable reason that (100) has less fraction of LAGBs and slightly large fraction of Σ < 27 boundaries such as Σ9 etc., in addition to the Σ3 boundaries (Figure 4.7). These boundaries lead to a decrease in the fraction of Σ3 boundaries among HAGBs (30.6% of total length of GBs and 38.8% among HAGBs). Here the length of HAGBs accounts to 78.8% of total length of GBs. Also, Σ boundaries < 27 are resistant to intergranular corrosion. As a result, in the (111) and (101) textured foils, the fraction of CSL Σ3 boundaries were 40.4% and 47.8% among the total length of GBs and 60.6% and 55.9% among HAGBs respectively. This is in agreement with literature that (100) and (101) favours the Σ boundaries other than Σ3 boundaries compared to (111) [224]. Though all the textured foils have significant fraction of CSL Σ3 boundaries, coherent twin boundaries contribute better for the enhancement of electrical conductivity. The boundaries with a deviation of only a few degrees from the ideal Σ3 boundary condition (60°<111>) can be considered as coherent twin boundaries which are essential for enhancing the electrical conductivity and ductility along with other mechanical properties [26]. According to the Brandon criterion [93, 94], for CSL Σ3 boundaries including coherent and incoherent twin boundaries, the allowable deviation can be up to 8°. Also Randle [26] has reported that the deviation must be in between 1-3° for coherent twin boundaries, with low energy compared to conventional CSL and HAGBs. Coherent twin boundaries are the only boundaries which can reduce the scattering of electrons at GBs leading to enhancement in the electrical conductivity which is not the case with incoherent twin boundaries [89].

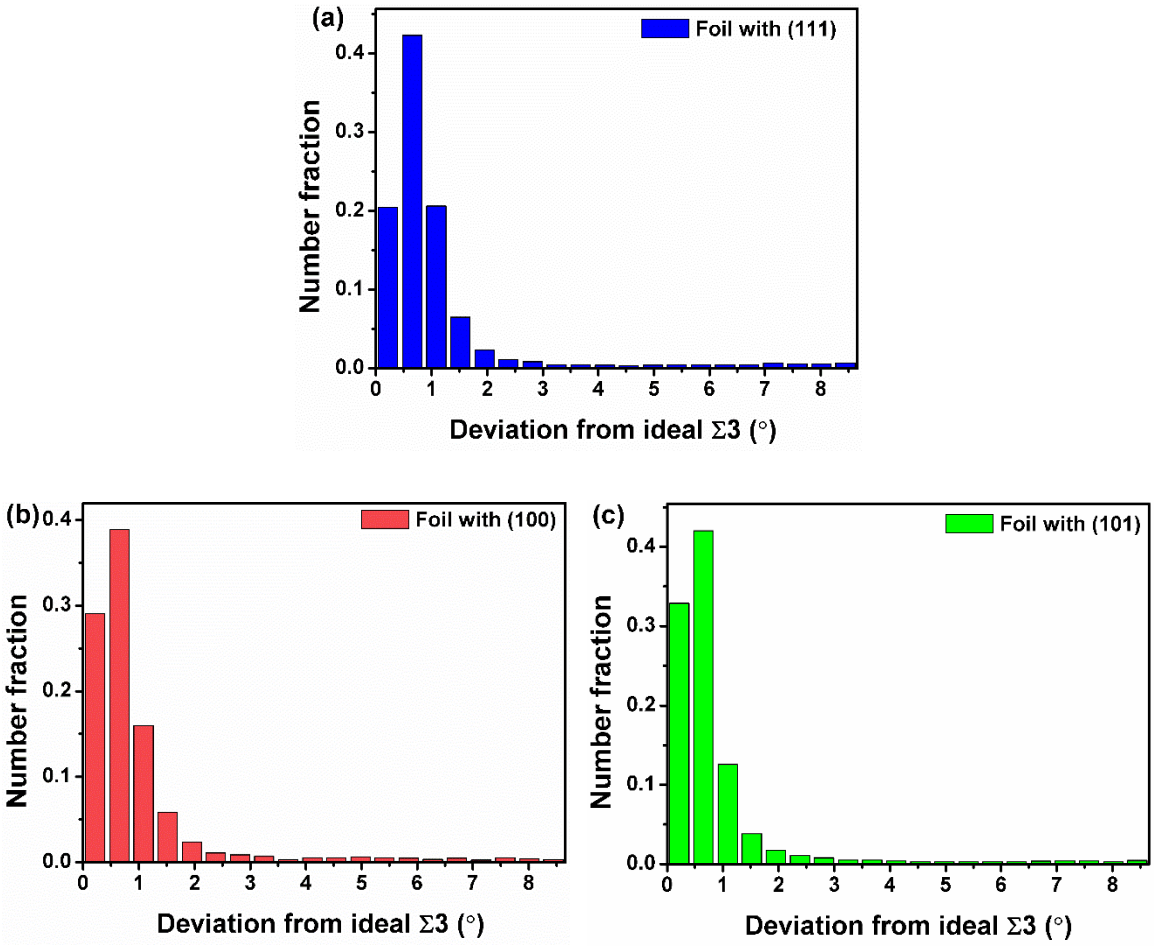

Figure 4.8 Deviation from the CSL boundary in copper foils with (a) (111) (b) (100) and (c) (101) textures.

In the present study, it is found that in (111), (100) and (101) textured copper foils, majority of these CSL Σ3 boundaries are very close to the ideal Σ3 condition from the GB statistics (Figure 4.8). An angular deviation of 1° from the reference condition is considered to calculate the percentage of coherent twin boundaries (CSL Σ3) which is found to be ~80% (Figure 4.8). The twins formed in the present deposition process are growth-in twins and the formation of these twins reduces the total interfacial energy of the system. As mentioned earlier, these twins are formed due to the induced stresses and strains during the PRED. In all the textured foils, the presence of twin boundaries is confirmed after a detailed analysis of EBSD data. Mechanical and electrical properties were measured for the copper foils prepared by PRED with good control over the texture.

4.3 Mechanical and electrical properties of highly textured copper foils

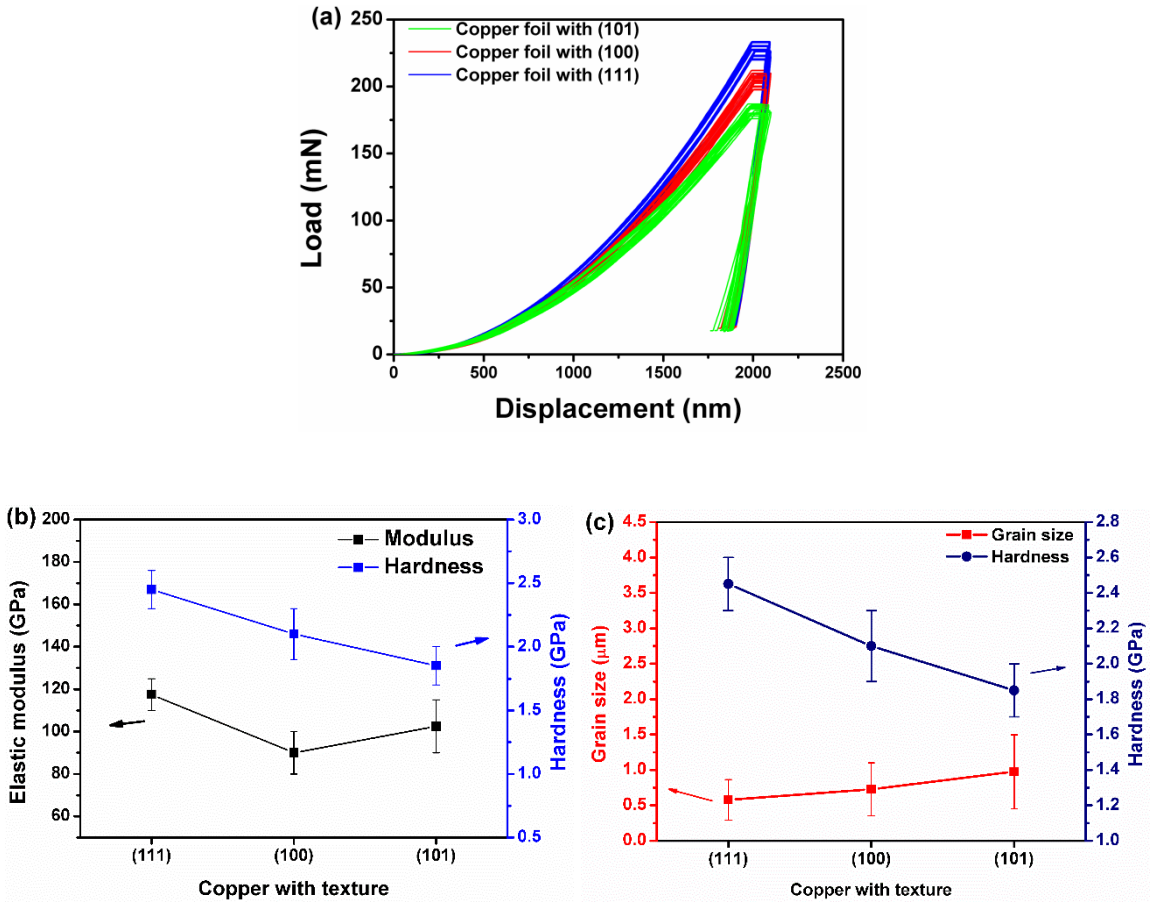

Figure 4.9 (a) Load-displacement curves for copper foils highly textured towards (111), (100) and (101) (b) hardness and modulus vs. texture (c) grain size, hardness vs. texture.

Nanoindentation has been used to evaluate the mechanical properties of these foils. Hardness and modulus are measured performing indentation at different locations in the foils of 1 cm^2 area, which shows overlapping curves indicating high structural homogeneity of the foils (Figure 4.9). Figure 4.9(b) shows the representative load-displacement curves indicating the variation of hardness and modulus with variation in the copper foils with varied textures. Copper foils with dominant (111) texture have shown excellent hardness in the range of ~2.2-2.7 GPa and elastic modulus in the range of ~110-130 GPa. The hardness value of these copper foils is superior to that of bulk copper and modulus is comparable to that of bulk copper. Since there is a slight difference in the average grain size obtained for various foils in this study, Figure 4.9(c) was made by incorporating both hardness and grain size values of various

textured foils. It is clear from Figure 4.9(b) that the hardness is high for the (111) textured foils (2.45±0.15 GPa) while slightly lower values are observed for (101) (1.85±0.15 GPa) and (100) (2.1±0.20 GPa). Similarly, (111) textured foils exhibited highest modulus (117 ± 7.5 GPa), in comparison to (101) (102 ± 12.5 GPa) and (100) (90 ± 10 GPa) foils. It has already been shown experimentally that the Young's modulus for Cu (111) is 193 GPa, which is 2.9 times higher than Cu (100) with 69 GPa [85]. Generally for all fcc metals, elastic modulus follows a trend with $E_{(111)} > E_{(101)} > E_{(100)}$ [85, 225]. A similar trend has been observed for the elastic modulus of the highly textured foils in this study. High energy due to low atomic density and coordination number of (100) and (101) planes leads to slightly lower modulus. In order to correlate the texture dependent mechanical properties, the critical resolved shear stress (CRSS) values for Cu single crystal have been taken into consideration for comparison, as CRSS is an indirect measure of hardness [226]. The present study deals with the highly textured copper foils, which are expected to exhibit mechanical properties similar to those of single crystal copper. The trend observed in the hardness values for different crystallographic orientations of the highly textured copper foils is in line with that reported CRSS values [227, 228]. Dub et al. [228] have reported a CRSS of 4.56 GPa and 3.8 GPa for (111) and (100) planes, respectively for copper single crystal. The ratio (1.2) in the CRSS for (111) and (100) is in agreement with the observed ratio (1.19) of the average hardness value in the present study for these two textures.

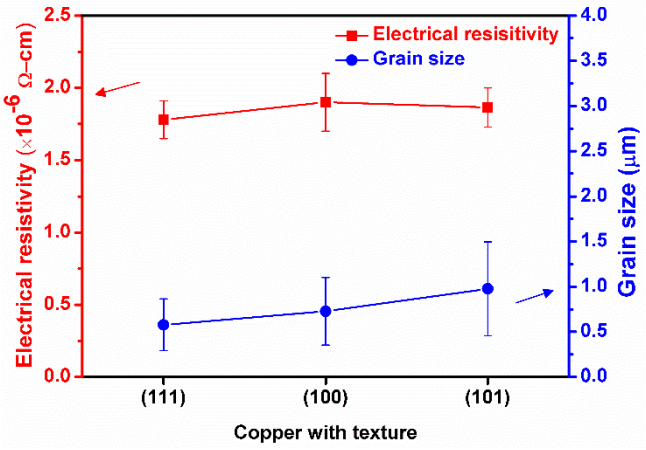

Figure 4.10 Variation of electrical resistivity and grain size with respect to different textures in copper foils.

Electrical conductivity was found to be 56-66 MS/m for all the foils in this study (electrical conductivity for bulk copper the value is 58-62 MS/m). In addition, resistivity measurement made using 4-probes have shown that all the copper foils including (111), (100) and (101) exhibited a low electrical resistivity in the range from ~1.65-2.0×10^{-6} Ω-cm, which is 85-104 % of that of bulk copper. Usually, when the grain size is reduced, the volume fraction of grain boundaries increases, leading to the scattering of electrons at the grain boundaries resulting in reduced electrical conductivity. In contrast to that, the electrical conductivity of the copper foils in the present study has not deteriorated with the grain refinement as well as texture development (Figure 4.10). This could be attributed to several aspects such as preferred crystallographic orientations (texture), low impurities and the presence of CSL Σ3 coherent twin boundaries, which reduce the scattering leading to enhancement in the electrical conductivity.

In addition to the mechanical and electrical properties, the structural stability is also important while adapting these copper foils for various electronic applications. In order to evaluate this, the copper foils are stored at room temperature for six months. Subsequently hardness of these foils was measured and it was found that the hardness has decreased by only 5% in comparison to its as-deposited value [35]. This constancy of hardness at room temperature is probably due to the absence of grain growth [210]. Further the very slight deviation from the preferred orientation (texture) to random orientation was observed in the representative orientation map and IPF are shown in Figure 4.5(b-c). An additional feature observed is that density of all the textured foils was found to be 8.92 ± 0.05 g/cm^3 i.e., about 99.6% of that of the bulk copper, using Archimedes principle method.

Hence, it has been mainly observed during the present study that in PRED the usage of ‘additive-free’ electrolyte reduces the impurities in the deposited material, resulting in minimal stresses giving stability to mechanical and electrical properties with texture in addition to the hydrogen embrittlement. Among the copper foils which were deposited using different pulse parameters in order to control the texture, high hardness in (111) is probably due to the high atomic density in (111) resulting in compact structure with low energy [229]. The enhancement of properties (mechanical, electrical) also results from low residual stresses and large number of coherent twin boundaries, which behave similar to conventional grain boundaries in

blocking the dislocation motion while reducing the scattering of electrons. Similarly, in spite of large number of grain boundaries, the electrical conductivity of the foils is high due to LAGBs in (111), about 6.2% among the total number of grain boundaries with low energy and low mobility contributing to lower resistivity of the foils. The highly uniform orientation of the grains in (111) textured foils (texture coefficient) results in the reduction in scattering of electrons leading to lower values of electrical resistivity [221]. (111) is harder compared to the other planes because of the difficulty in activating the {111} <01$\bar{1}$> slip systems [230]. Further, predominant advantage with highly (111) textured copper is, it improves the electromigration resistance compared to all other textures [16]. In the present study, among all textured copper foils, the highly (111) textured foil has prominent properties compared to the rest due to its standalone features. Thus, the enhancement of hardness in (111) is probably due to the grain refinement, texture and presence of CSL Σ3 coherent twin boundaries compared to other (100) and (101) textured foils.

4.4 Control over twinning

It has already been mentioned in the above section that CSL Σ3 coherent twin boundaries can enhance the strength as well as electrical conductivity by minimizing the scattering at GBs, the pulse parameters are optimized to synthesize the highly twinned copper foils. The properties of copper foils with different twin densities synthesized by pulse reverse electrodeposition were studied. At this point, two copper foils with different twin densities with dissimilar twin lamellae were prepared by PRED and characterized by EBSD. The variation in pulse parameters to control the texture of the coper foils, can also control the twin density at the same time by increasing the reverse anodic pulse current density. These pulse parameters aid in obtaining the twinning and they inturn influence the properties.

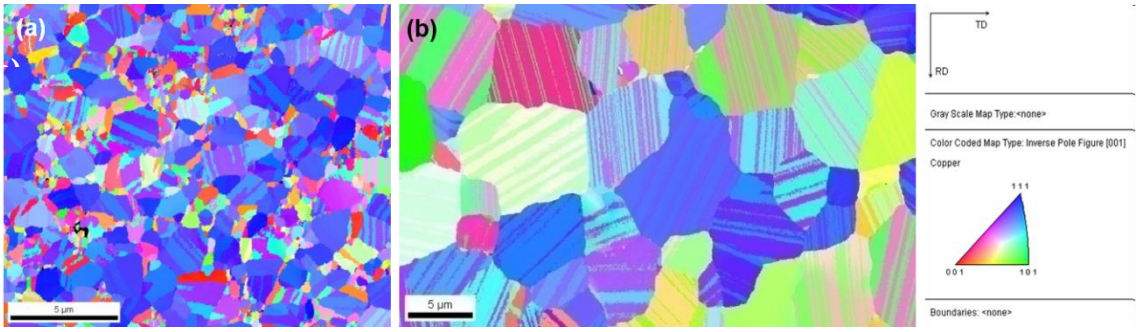

Figure 4.11 EBSD orientation maps of two different copper foils with (a) smaller grains and (b) larger grains with different twin lamellae thicknesses.

Copper foils with various twin densities were synthesized by optimizing the pulse parameters in PRED. Figure 4.11 shows (a) with twin lamellae of ~300 nm and (b) with the twin lamellae ~100 nm for copper foils characterized by EBSD. From the grain size distribution of copper foils from Figure 4.12 with variation in twin densities, these copper foils have shown a large variation in the grain size. However from the EBSD data, it can be observed that the fraction of twin boundaries in both the foils have variation in the number of twin boundaries and their twin lamellae. The grain boundary statistics were calculated from EBSD shown in Figure 4.13. The misorientation angles for both twinned copper foils have large fraction of Σ3 coherent twin boundaries, which are 40.4% and 76% respectively with a fraction of HAGBs of 75.5% and 85.5% of total length of GBs. However, considering the Σ3s among the HAGBs the moderately and highly twinned copper foils have fractions of 53.7% and 89.8% of CSL Σ3s (Figure 4.13). In addition, moderately twinned copper foil has other Σ< 27 boundaries (Σ9) etc., which are included among the HAGBs and resulted in smaller fraction of Σ3s among the HAGBs. However, in highly twinned copper foils the fraction of Σ3s is higher among the HAGBs.

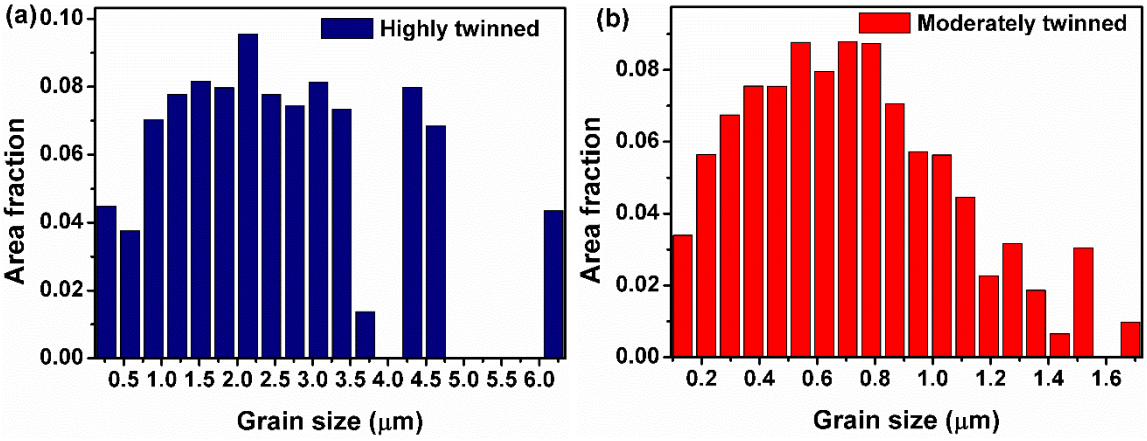

Figure 4.12 Grain size distributions for twinned copper foils.

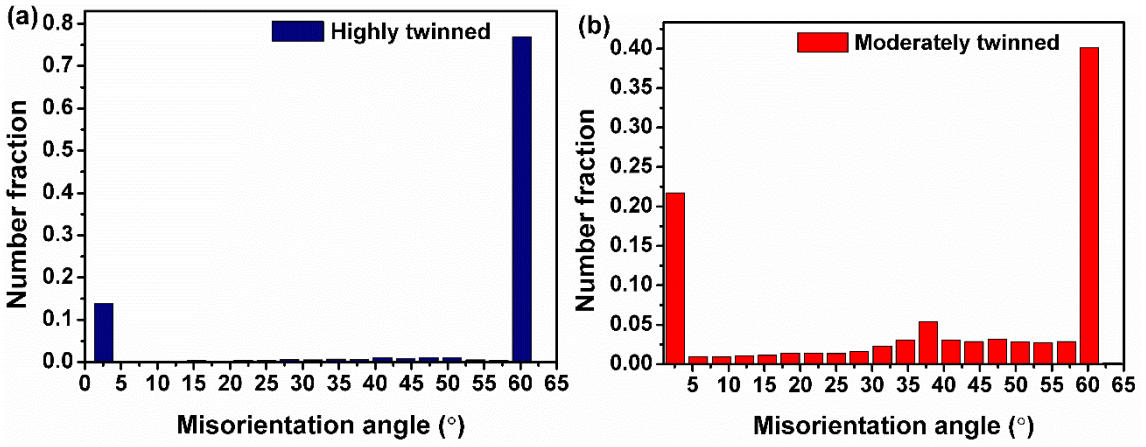

Figure 4.13 Grain boundary statistics in (a) highly twinned and (b) moderately twinned copper foils.

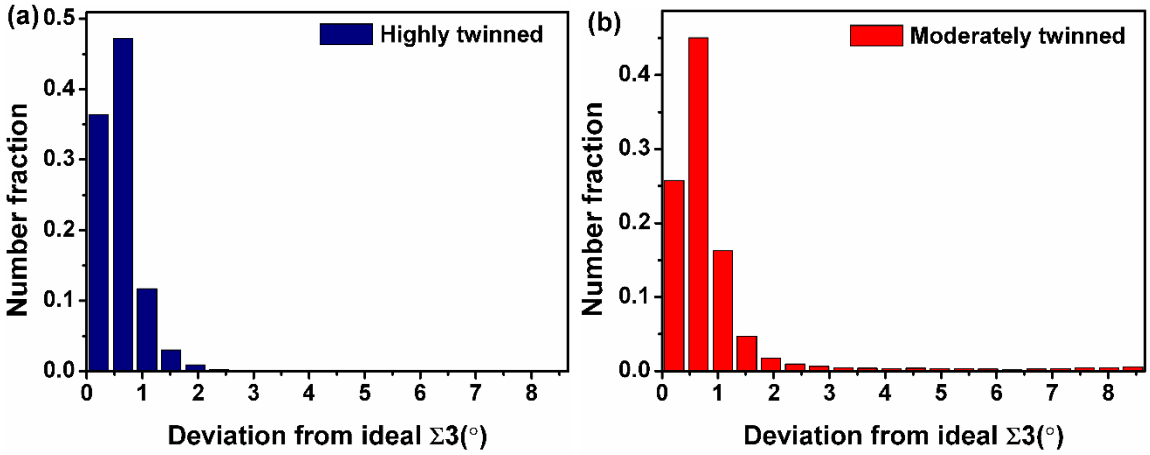

Figure 4.14 Deviation from the CSL boundary in (a) highly twinned and (b) moderately twinned copper foils.

Further, these foils were characterized for the mechanical and electrical properties. The foils with smaller grain size of 1-2 µm with twin lamellae thickness of ~300 nm exhibited a hardness of ~2.0 GPa showing an electrical resistivity of 1.76×10^{-6} Ω-cm. The copper foil with larger grain size of 5-7 µm with twin lamellae thickness of ~100 nm has exhibited a similar hardness of ~2.0 GPa and an electrical resisistivty of 1.73×10^{-6} Ω-cm. Therefore, from the grain boundary statistics and properties, it can be concluded that the enhancement of hardness and electrical conductivity could be due to the presence of CSL Σ3 coherent twin boundaries.

From Figure 4.13 both the copper foils have sufficient fraction of CSL Σ3 coherent twin boundaries. Twinned copper foils with smaller grains have lesser fraction of CSL Σ3 coherent twin boundaries compared to the highly twinned copper foils with larger grain size. This can be easily seen in the EBSD map (Figure 4.13). However, fraction of these grain boundaries can be obtained only after detailed analysis on grain boundary statistics. In moderately twinned copper foil, the fraction of CSL Σ3 boundaries were about 50%. CSL Σ9 boundaries which have misorientation angle between 35°-40° were also present and these boundaries may not be contributing to the observed properties.

In case of highly twinned copper, the fraction of CSL Σ3 coherent twin boundaries were very high (>90%) and there are negligible fraction of other Σ boundaries including low angle grain boundaries (< 5%). Due to more fraction of coherent twin boundaries and also because of twin lamellae (thickness is ~100 nm) contributing in increasing the hardness along with the

electrical conductivity. However the hardness is comparable to that as moderately twinned copper. It is to be noted that although the grain size is 5-7 μm, because of the presence of twin lamallae with finer thicknesses (~100 nm) high hardness has been achieved. It appears that these twins with varied twin lamellae thickenesses might act as barriers for dislication motion and also helps in reducing the scattering of electrons leading to improve the electrical conductivity.

4.5 Summary

To summarise this chapter, the control over texture and twin density has been achieved by optimizing the pulse parameters with the use of PRED in an 'additive-free electrolyte. Highly (111), (100) and (110) textured copper foils with the alignment of <111>||ND, <100>||ND, <101>||ND were prepared successfully. Current densities between 0.4-1.0 amp/cm^2 enable the texture formation due to rapid pulses. Increment in forward off ($T_{F\,off}$) duration controlling the textures at shorter forward pulses (111) forms, at slightly higher off-times (100) formation occurs and at very large off-times, (110) formation occurs due to the self-annealing process. The increase in anodic current density leads to the formation of special grain boundaries. Further, reverse pulse results in equi-axed grain structure with high stability in maintaining texture with negligible stresses. Here the deposition rates are quite rapid compared to PED [31] due to high current densities with application of reverse pulse. PED requires longer pulse off-times for the rearrangement of deposited grains that results in minimization of energy, removal of the residual stresses and adsorbed hydrogen along with other impurities from the surface. In PRED, the applied reverse pulse takes care of the processes that happen during the off-time of PED. The reverse pulse during PRED removes impurities quickly, and also acts as stress reliever after each cycle. It also aids in reducing the porosity by generating new nucleation sites leading to grain refinement [222]. It also favours the twin formation due to the stress / strain developed during the deposition and also results in reduced deposition times. In addition the usage of 'additive-free' electrolyte in PRED results in foils with no unwanted impurities leading to high electrical conductivity. Among all the textured copper as well as twinned copper foils, the highly (111) textured copper foil has the enhanced properties. In spite of the presence of large number of grain boundaries, the electrical conductivity of the foils is

maintained due to presence of small angle grain boundaries and twin boundaries. Small angle and special boundaries (twins) exhibit one order of magnitude lower electrical resistivity compared to that of conventional/ high angle grain boundaries. The highly preferred orientation of these grains results in reduced scattering of electrons. Optimization of pulse parmeters also resulted in control over the twin density.

Chapter 5. Electrochemical synthesis of graphene

This chapter deals with the electrochemical synthesis of graphene for the preparation of copper-graphene nanocomposite foils. The electrochemically synthesized graphene in the present study has been used to reinforce into copper matrix by electrodeposition.

The existing methods for preparation of graphene include chemical vapour deposition, mechanical exfoliation, chemical and electrochemical exfoliation techniques [116, 231, 232]. Although graphene with high quality with required number of layers can be produced from the chemical vapour deposition technique, large scale preparation is the need of the hour. Massive production at very large scale by use of a simple, environment-friendly and economically feasible technique with good reproducibility to produce high quality graphene is essential for several of the above mentioned applications. Liquid phase chemical exfoliation methods, although can produce graphene at large quantities, the quality of graphene is still a challenge. Chemical exfoliation such as Hummers method involves severe acidic environment causing damage to the graphene sheets produced [233, 234]. In addition, control over the size and number of sheets is not possible by using this method. Due to the violent interactions from the gaseous species produced from the acids used at high concentrations, the resultant product after the process still contains several thicker flakes, reducing the yield [51]. The chemical structure of graphene with the hexagonal lattice is also severely damaged, limiting its use in several applications [235].

Very recently, electrochemical exfoliation, a better controllable method by the variation of the type of electrolyte, its concentration and the potential used for anodization has been intensively explored by several researchers both for fundamental studies and technical applications [147, 235]. Electrochemical exfoliation technique shows several advantages over the chemical methods since it is a single step process requiring ambient temperature [236]. Furthermore, the duration is much lesser, in contrast to the chemical approaches. Yet another advantage of this process is the feasibility to upscale, where milligrams to several grams of graphene can be produced with a control over the size and number of layers, with simple variation in the parameters and electrolyte concentration [237]. Mainly electrochemical exfoliation has been done using two types of electrolytes, namely ionic liquids containing imidazolium compounds

[147, 238] and aqueous electrolytes containing HNO_3, H_2SO_4, H_3PO_4 etc. [50, 239, 240]. Use of ionic liquids result in low yield of the graphene produced by exfoliation, which may also be attached or modified with nitrogen or ionic liquids several times, bringing an inferiority to its properties. Aqueous acidic electrolytes on the other hand, play an active role in the electrochemical exfoliation of graphite into graphene, larger amount of oxygen functional groups get attached to graphene, depending on the concentration of the electrolyte, applied potential etc. Su et al. have demonstrated a fast electrochemical method to obtain thin graphene sheets, with a large lateral size, exhibiting electrical properties that are superior to the reduced graphene oxide prepared by the regular chemical exfoliation methods by using electrolytes containing H_2SO_4 [50]. An electrochemical exfoliation method was reported for large scale production of few layer graphene of high quality from graphite using oxalic acid as the electrolyte. The graphene sheets produced by this method were stable up to 800 °C, thus have shown a capability for their potential application in solid oxide fuel cells as gas diffusion layer [241]. Khanra et al. have prepared graphene by an electrochemical exfoliation of graphite in an aqueous medium, using 9-Anthracene carboxylic (9-ACA) acid as the surface functionalizing material to improve the dispersion capacity and specific capacitance of graphene at a constant DC power supply [242]. Parvez et al. have reported use of aqueous solutions containing different inorganic salts such as $(NH_4)2SO_4$, Na_2SO_4, K_2SO_4 etc. in order to prepare highly conductive few layered graphene films at large quantities containing low oxidative degree [133]. Zhou et al have prepared few-layer graphene by electrochemical intercalation of graphite using Na+/ dimethyl sulfoxide complexes as the intercalation agent in an electrolyte containing NaCl, dimethyl sulfoxide and thionin acetate, demonstrated that a lower content of defects were observed compared to graphene prepared by chemical methods [243].

However, an alternative technique is highly essential for the production of few layered graphene exhibiting superior features, at large quantities for its use in battery and supercapacitor applications and as a better reinforcement in metal, polymer and ceramic nanocomposites. Choice of electrolyte and voltage play a critical role in achieving high quality graphene with better yield and lesser number of functional groups attached. In the present work, we report for the first time, a highly efficient electrochemical exfoliation method to prepare few-layered graphene with large lateral size, by using a novel acidic electrolyte containing HF

and HNO_3 at very low concentrations. The process is scalable to achieve graphene at remarkably large quantities, up to gram-scale, while maintaining the quality. Electrochemical exfoliation in a mixture of HF and HNO_3 has also formed graphene containing lesser oxygen functional groups, with a mechanism similar to that of ionic liquids (ILs). However, post-treatment of the sheets was much easier compared to that of ILs, where no residual impurities were found in the final product.

The morphology of the few layered graphene sheets have been characterized by FESEM (HITACHI S4300), and TEM (FEI Tecnai G^2 200 KV). The chemical composition was characterized by XPS (Omicron Nano Technology, UK). Raman spectroscopy (LabRAM HR800- Horiba JOBINYUON), XRD (D8 ADVANCE, BRUKER) and FTIR (Spectrum GX Optica, Perkin Elmer, USA) to study their features including number of layers, quality of the graphene prepared, the functional groups present and the lateral size.

5.1 Results and discussion

A mixed solution containing HF and HNO_3 in water was used as the electrolyte in the present work. The effect of the concentration of HF was studied by varying it from 0.5% to 3%, while maintaining the concentration of HNO_3 at 3% in the electrolyte. The experimental set-up for the exfoliation of high purity graphite is demonstrated in Chapter 3 Figure 3.1, where a graphite rod was used as anode for exfoliation and another graphite rod was used as cathode. Graphite was exfoliated using different voltages from +4V to +18 V and the features of the graphene sheets obtained were compared. During the first few minutes, rapid exfoliation was not observed. It is expected that the initial reactions where interaction of the F^- and NO^{3-} with the surface of graphite may be taking place in addition to the wetting of the surface [241]. Within a few minutes, complete expansion of the graphite is started and the graphene sheets dissociated from the rod partially during the exfoliation and completely during ultrasonication which was performed after the ultrasonication. Figure 3.1(b) shows the photo of the exfoliated graphite, dried graphene powder and the graphene suspension in poly ethylene glycol after ultrasonication and washing. About 10 g of graphene was obtained with an anodization time of 6 hr. The amount of graphene depended on the voltage applied and the duration of the process.

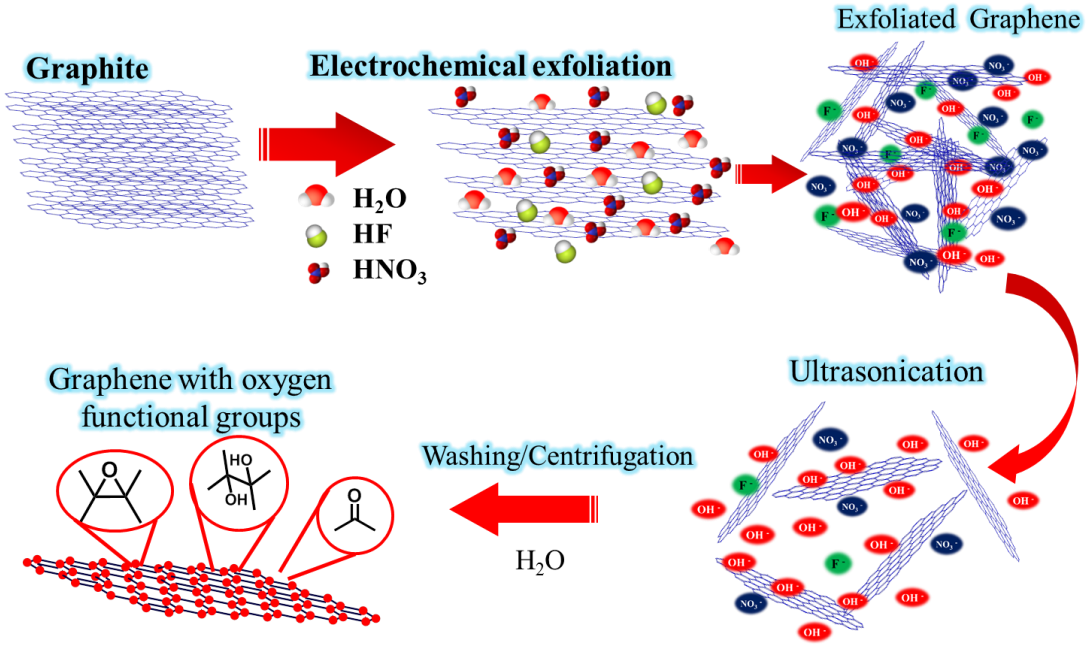

Figure 5.1 Schematic representation of the mechanism of electrochemical exfoliation of graphite in electrolyte containing HF.

Mechanism of the exfoliation of graphite into graphene sheets, in the electrolyte containing HF and HNO_3 is illustrated in Figure 5.1. The mechanism can be deduced both from the concentration of the electrolyte and the voltage applied. Anodic oxidation of water produced both hydroxyl and oxygen radicals depending on the voltage applied, while formation of F^- and NO^{3-} ions mainly depend on the concentration of the acid in the electrolyte. Oxidation and the hydroxylation of water initiates the corrosion of graphite at the edges, grain boundaries and defect sites. This process then facilitates the intercalation of the anionic F^- and NO^{3-} ions and aids the expansion of the graphite into graphene sheets. Due to the higher oxidation potential of F^- and NO^{3-}, they act only as intercalators aiding the expansion, while water sacrificially oxidizes to form the radicals and oxidize graphite anode, which also aid in the cutting of the sheets [244].

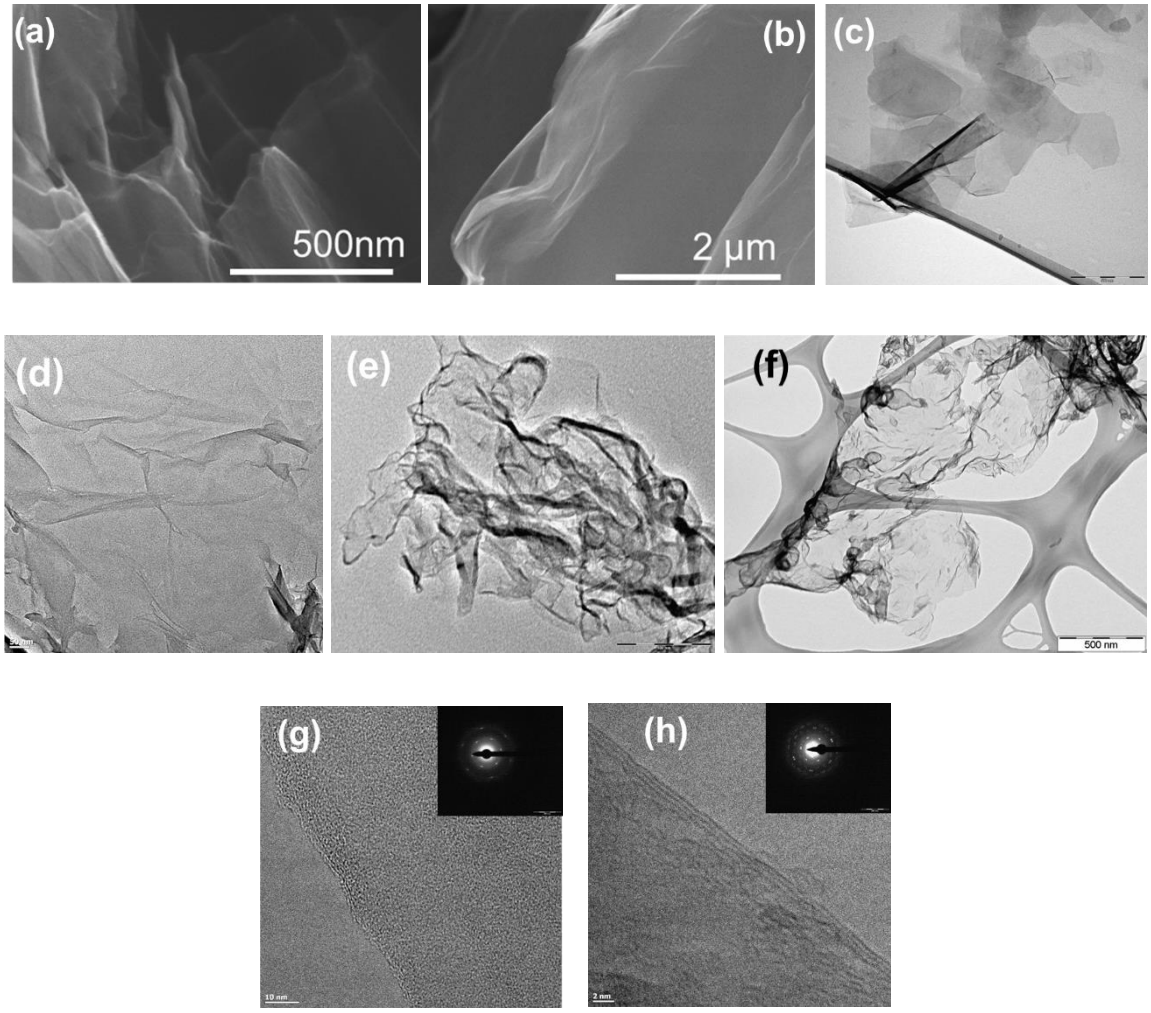

Figure 5.2 (a, b) FESEM micrographs of graphene (c, d, e, f) low magnification TEM micrographs and (g, h) high magnification TEM micrographs of graphene sheets prepared by electrochemical exfoliation. (diffraction patterns indicate (g) single layer, (h) double/multi layered graphene.

The morphology of the graphene sheets was demonstrated by FESEM and TEM. FESEM micrographs of the graphene sheets obtained from the exfoliation of the graphite rod, in Figure 5.2(a-b) clearly demonstrate their large lateral size and random orientation. The lateral size of the graphene sheets is further investigated from the TEM micrographs (Figure 5.2 c-f). Graphene sheets were dispersed into ethanol and then spread onto a holy carbon grid prior to the observation in TEM. It can be noticed clearly from the typical TEM micrographs that the lateral size of the graphene sheets extends from few hundreds of nanometers to several microns. The size of the sheets varied mainly depending on the voltage applied. At a lower voltage of 4 V, 500 nm to 2 µm sheets were typically obtained (Figure 5.2 c-d) while application of a higher

voltage of 18 V resulted in graphene sheets above 5 µm and up to ~ 20 µm (Figure 5.2 e-f). Very small amount of sheets were also sized ~ 40 µm. Another interesting feature is the control over number of layers of graphene with application of voltage. Lower voltage resulted in 3-6 layers, while application of higher voltages have demonstrated 1- 4 layers (Figure 5.2 g-h). The insets of Figure 5.2(g-h) reveal the selected area diffraction patterns (SAED) of the few layered graphene obtained at different voltages. These diffraction patterns exhibit a typical 6-fold symmetry, which is consistent with the crystalline hexagonal structure of the graphene sheets. These results indicate a violent exfoliation of the graphite into the graphene sheets. The results also clearly demonstrate that the voltage plays a major role in controlling the number of layers in addition to the electrolyte used, which will be discussed later in this work.

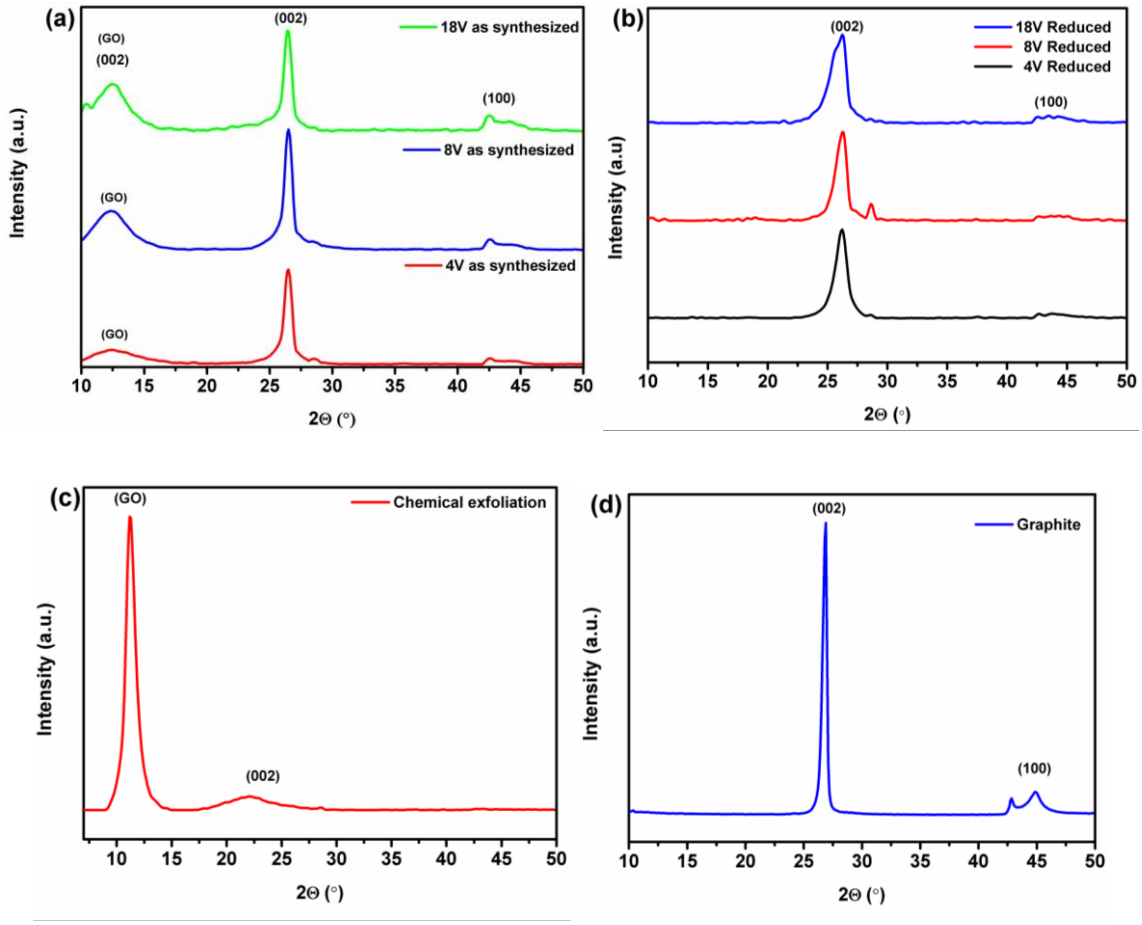

Figure 5.3 X-ray diffractograms of (a&b) electrochemically exfoliated graphene sheets at different voltages before and after annealing (c) chemically exfoliated graphene (d) graphite.

The X-ray diffractograms (Figure 5.3) of the exfoliated graphene displayed a peak at ~26.5° (d-spacing ~3.37Å) for the graphene sheets exfoliated at all the voltages, which can be attributed to the (002) diffraction of the graphitic structure. The presence of a small amount of the functional groups in graphene sheets acts as spacers between layers and result in a lower 2θ value with large d-spacing compared to that of graphite (26.77°, d-spacing ~3.33Å). The 2θ value further decreased to ~26.2 after annealing under argon atmosphere at 600 °C for 3 hr, indicating a similar d-spacing of ~3.36 Å. In addition, the spectra observed for the graphene sheets after annealing were broader than those for the as-anodized sheets. The (002) peak of the oxide was found to be broad and increased with increase in the exfoliation voltage.

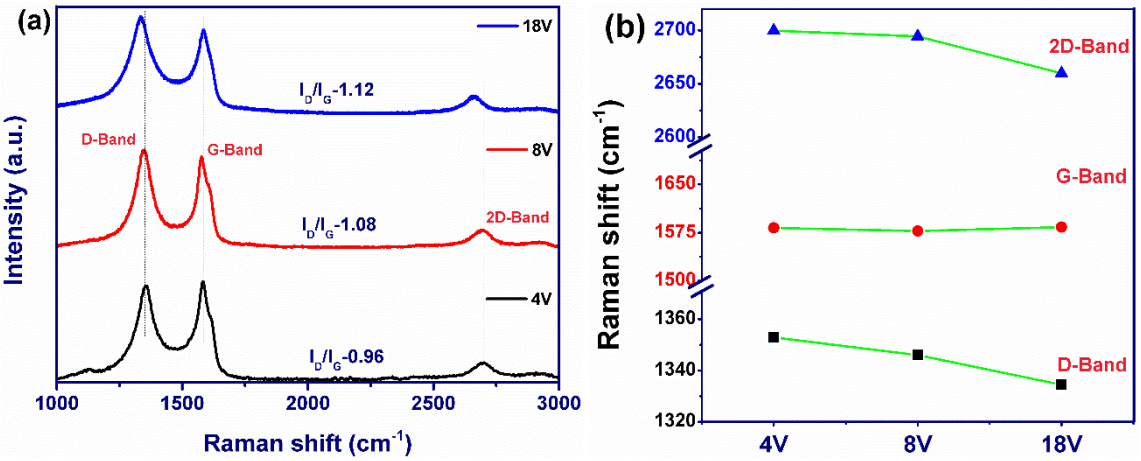

Figure 5.4 Raman spectra of the graphene sheets prepared by exfoliation at different potentials.

Raman spectroscopy was then used for studying the quality of the graphene sheets as well as the number of layers. Figure 5.4 (a) shows the Raman spectra of the graphene sheets obtained at different voltages, using a 514 nm laser. The peak positions are shown in Figure 5.4 (b). D band observed at ~ 1350 cm^{-1} can be attributed to the defects, functional groups and the edges causing structural disorder to graphene. The G-band observed at ~1580 cm^{-1} represents a graphitic nature of the material. The most interesting observation from the Raman spectrum is the position of 2D band which clearly indicates the number of layers of graphene [188, 245]. A clear shift in the 2D band clearly towards the lower wave number (~2669 cm^{-1}) clearly indicates that at higher voltages, few layered graphene sheets are formed compared to those formed by the application of lower potentials. The ratio of I_D/I_G varied from 0.96 to 1.12 showing that the disorder did not change significantly with increase in exfoliation voltage. An

important observation from the Raman spectra is that there was no distortion in the peaks showing that no flourographene was formed. It has been reported by Karlicky et al. that the G-band slowly disappears as the content of fluorine increased [246]. Graphene sheets prepared using an exfoliation voltage of 8V have been found to give 1-4 layers. Therefore further characterization has been done using sheets formed at 8V, while varying the concentration of HF in order to study the influence of F^- concentration on the exfoliation process.

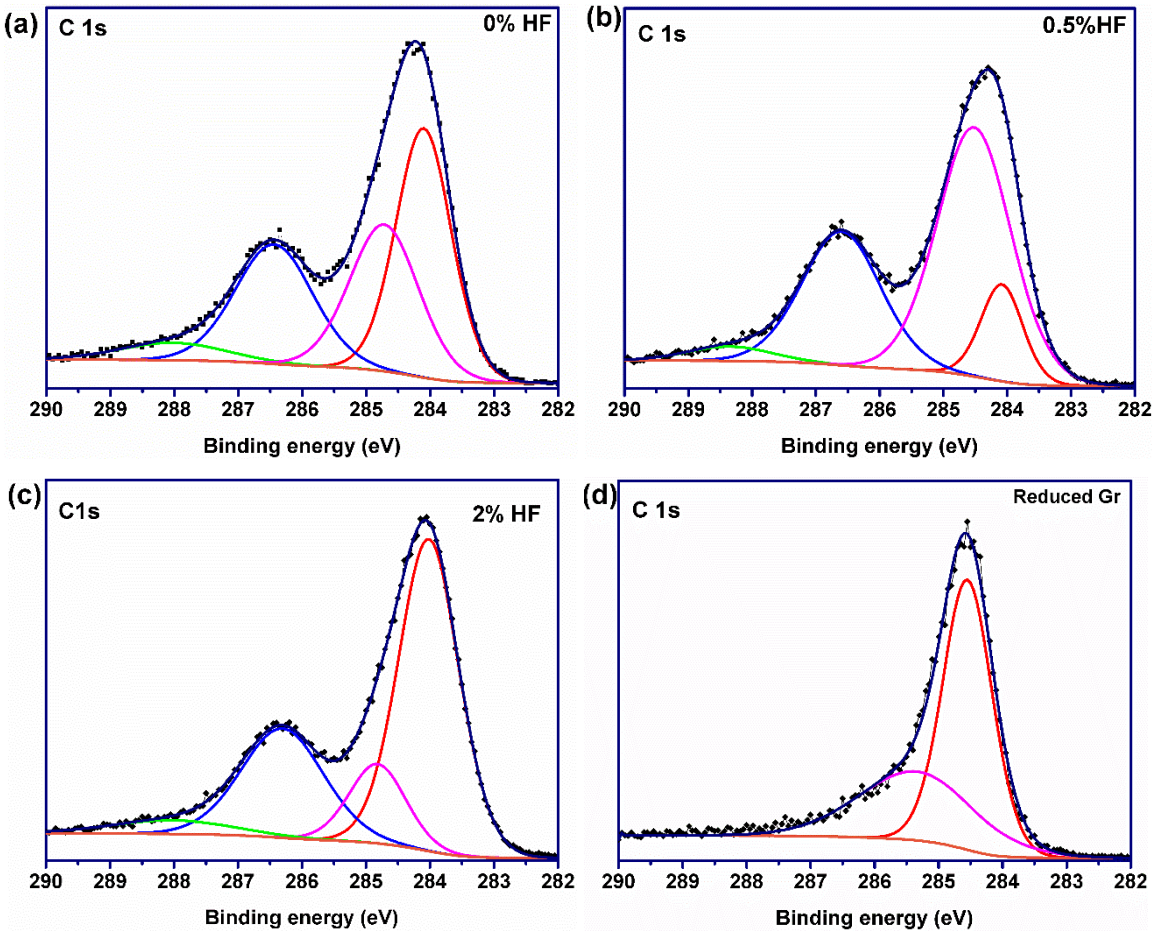

Figure 5.5 Effect of concentration of HF in the electrolyte: XPS spectra and deconvoluted peaks of (a) 0% HF, (b) 0.5% HF,(c)2% HF and (d) 0.5% HF reduced graphene.

X-ray photoelectron spectroscopy (XPS) was used to study the chemical composition of the graphene prepared at different voltages (Figure 5.5). Different concentrations of HF ranging from 0.5% to 2% were used in the electrolyte while maintaining the concentration of HNO_3 at 3%. Graphene prepared with 0.5% HF have shown no traces of fluorine and only 7.5% oxygen.

The C/O ratio was ~12.33. However, with increase in HF concentration, the ratio of C/O decreased, while small fraction of fluorine was also found (Table 5.1).

Table 5.1 XPS data for electrochemically synthesized graphene

C 1s	1 (C-C)	2 (C-O)	3 (C=O)	4 (C-C)/(C=C)
0%HF	~284.1	~286.44	288.025	284.718
0.5% HF	284.083	286.599	288.353	284.517
2%HF	284.017	286.305	288.037	284.819
Reduced graphene	284.549	285.349	-	-

The possibility of formation of fluorographene is being performed as a separate study and is out of scope of the present work, due to its increasing application in batteries and supercapacitors. The deconvoluted spectra of the C1s peak reveal the C-C peak at 284.5 eV, C-O and C=O at 286.5 eV. Absence of C-F peak at 288.1 eV indicates pure graphene sheets indicating the absence of graphene fluoride [247]. Further, from the XPS spectra, fluorine is shown to be absent in the graphene sheets prepared by using 0.5% HF while increase in in the HF concentration has shown traces of Fluorine which increased further with increase in concentration.

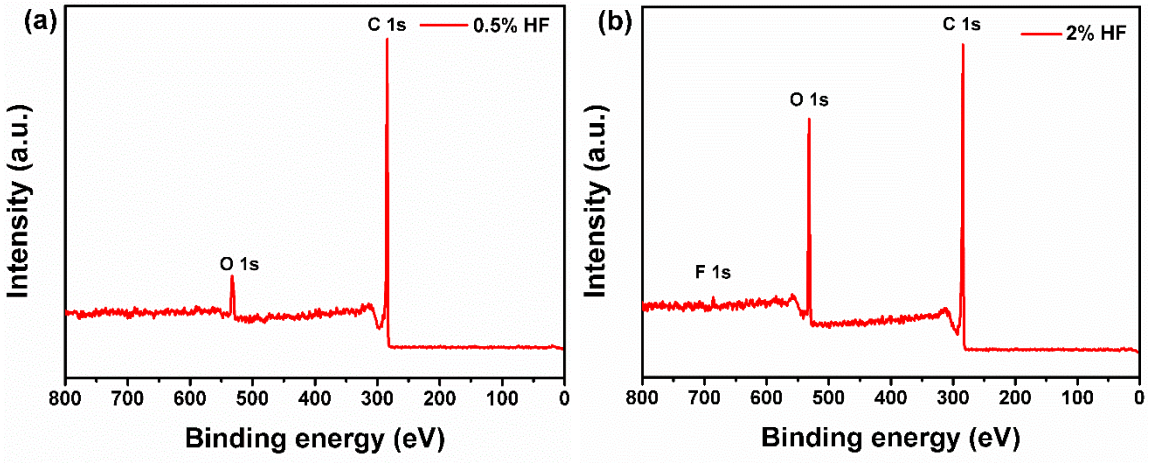

Figure 5.6 XPS spectra of graphene synthesized with (a) 0.5% HF (b) 2% HF in electrolyte compositions (Atom %) of C, O and F.

Table 5.2 Atom % of C, O and F obtained from XPS

	C 1s (at%)	O 1s	F 1s
0.5% HF	92.49	7.51	-
1% HF	80.15	17.83	2.02
2% HF	79.45	17.78	2.77

Figure 5.6 and Table 5.2 gives the complete information on the XPS data for different concentrations of HF used in the electrolyte. An important observation from these studies is that the content of oxygen was much lesser amounting to only 7.5%, compared to the graphene sheets prepared using H_2SO_4 or by chemical exfoliation methods [50, 239]. This could be anticipated due to the faster intercalation and expansion of graphene in the presence of F^-. Chemical exfoliation methods result in large quantities of atomic % of oxygen. Smaller amount of oxygen functional groups in the graphene sheets are advantageous for different applications, especially in case of preparation of nanocomposites by electrochemical deposition, where, these groups is essential for the dispersion of graphene as reinforcement material. However, larger concentrations of the oxygen functional groups influence the resistivity, limiting their use in electronic applications in their pristine form or in nanocomposites.

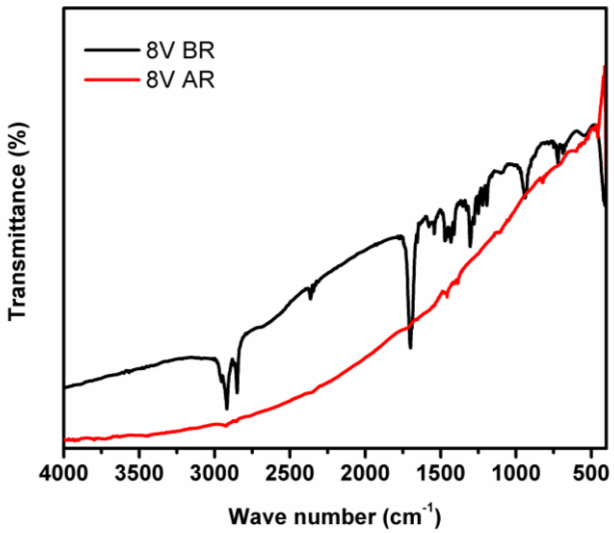

Figure 5.7 FTIR spectra for as prepared (BR) and reduced graphene (AR).

FTIR spectra (Figure 5.7) were further used to study the functional groups present in the graphene sheets prepared at 8V with 0.5% HF and for the sheets after annealing at 600°C under argon atmosphere. The spectra clearly indicate the presence of different oxygen functional groups for the as-prepared sheets, while the functional groups disappeared after annealing indicating a reduction in the number of oxygen functional groups. Absence of C-F peak at 1260 cm^{-1} indicates that the graphene sheets were free of fluorine [246].

5.2 Summary

To conclude, our present electrochemical exfoliation method using an alternative electrolyte containing HF and HNO_3, effectively exfoliated graphite to form a single to few layered graphene (1~6) sheets with lesser oxygen functional groups, thereby significantly improving the features for their application in nanocomposites, electronics and energy applications. Graphene sheets of larger size could be prepared at large quantities, measuring up to several grams demonstrating the feasibility of the present method to prepare graphene in industrial scale. Absence of fluorine/graphene fluoride could be observed from Raman spectra, XPS, FTIR and XRD analysis at lower concentrations of HF in the electrolyte.

Chapter 6. Preparation of copper-graphene composite foils and their mechanical and electrical properties

This chapter forms the basis to correlate the properties of pure copper with that of copper-graphene (Cu-Gr) nanocomposites. The influence of graphene reinforcement in controlling the electrical and mechanical properties has been studied. The electrodeposition technique, especially with application of pulsed currents is an easy, cost-effective and scalable method to incorporate filler materials with nano-sized dimensions homogeneously throughout the matrix [55]. In addition, electrodeposition being a low temperature process, the properties of graphene (Gr) and Graphene Oxide (GO) can be preserved during the preparation of the composites unlike the conventional sintering processes which could destruct Gr/GO since they involve temperatures higher than the decomposition temperature of Gr/GO (>600 °C) [12]. To the best of our knowledge, there are no reports on Cu-Gr composites prepared either by pulse reverse electrodeposition (PRED) or by optimization of graphene content with enhanced mechanical properties while retaining the electrical properties similar to that of pure Cu. Hence as part of the research, influence of graphene content and pulse parameters has been studied simultaneously, all of which have been discussed sequentially in this chapter.

6.1 Optimization of graphene content

In this study we mainly focus on synthesizing the Cu-Gr composite foils with enhanced hardness without compromising the electrical conductivity simultaneously using PRED technique. PRED technique has been chosen initially as it is superior over application of DC current technique for the preparation of composites in order to achieve homogeneous microstructure with well-dispersed reinforcement throughout the matrix. In addition, PRED has better control over DC in reducing the grain size, incorporation of reinforced filler, roughness, porosity and stresses in the composite and reduces hydrogen evolution during deposition, thus influencing the performance of the composite foil in terms of mechanical and electrical properties [177].

In order to disperse the graphene in the copper sulphate electrolyte and to avoid the agglomeration, it was dispersed by adding a polymeric surfactant PAA5000, ~15 ppm for 0.1

g/L of graphene in the electrolyte. Graphene content in the electrolyte was varied between 0.1-0.75 g/L and the foils prepared are designated as P1, P25, P35, P5 and P75 for corresponding graphene content dispersed in the electrolyte respectively. Composition of base electrolyte and pulse parameters for deposition of the Cu-Gr foils have been optimized and are same for all the depositions, except for the quantity of graphene added to the electrolyte. The applied current densities for the forward and reverse pulses were ~0.1 A/cm^2 and ~0.01 A/cm^2, respectively. While for the forward pulse, $T_{F\ on}$ is in the range of 15–50 ms and $T_{F\ off}$ is in the range of 50–100 ms, for reverse pulse, $T_{R\ on}$ and $T_{R\ off}$ are in the range of 1–10 ms. Electrochemically synthesized graphene ~0.5 µm–2 µm diameter consisting of 1-4 layers is used for co-deposition. Since graphene was prepared by electrochemical exfoliation as mentioned in the chapter 5 which is an anodization process, the surface of graphene contained oxygen functional groups. Compact and highly dense composite foils with a thickness of ~30 µm were deposited by PRED technique using Dynatronix pulse power supply (DuPR10-3-6). Initially, pure copper was deposited in blank electrolyte (without graphene) as a seed layer for few seconds to enable easy separation of the deposited composite foil from the titanium substrate. This step is followed by composite deposition in the respective electrolytes containing varied concentrations of graphene.

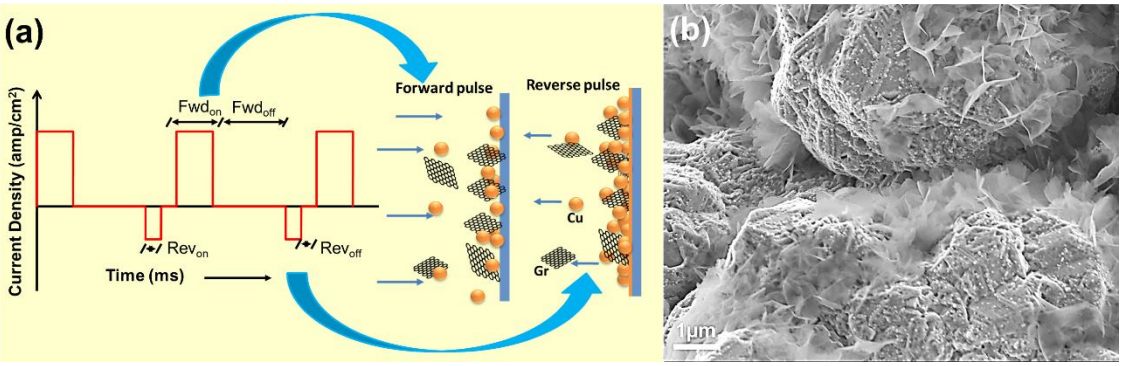

Figure 6.1 (a) Scheme of the PRED process for deposition of Cu-Gr composite foils and (b) FESEM of Cu-Gr composite representing the alignment/co-deposition of graphene and copper.

Deposition cycle and process for the preparation of Cu-Gr composite foils by PRED are schematically shown in Figure 6.1. During $T_{F\ on,}$ copper ions and graphene containing oxygen functional groups were reduced and co-deposited on the cathode with respect to its given current amplitude. During the $T_{F\ off,}$ rearrangement of existing crystals along with removal of

the stresses formed during deposition takes place [63] and removal/dissolution of the loosely bonded graphene and copper takes place during $T_{R\ on}$. In addition, the impurities or gases that are entrapped during the $T_{F\ on}$ where rapid deposition takes place are also removed from the surface of the deposit. Added to it, roughness and porosity are reduced due the controlled diffusion layer. Grain refinement occurs due to the incorporation of filler material leading to high performance materials with enhanced and controlled properties [101].

The foils are characterized by field emission scanning electron microscopy (FESEM) (HITACHI S4300), focused ion beam milling imaging (Carl Zeiss Neon 40), transmission electron microscopy (TEM) (FEI TECNAI G^2 S-Twin operated at 200 kV) and Raman spectroscopy (LabRAM HR800-JOBINYUON) for microstructural/structural studies to confirm the presence of graphene and its distribution. Hysitron Triboindenter TI950 and Four-probe resistivity setup (Mitsubishi-Loresta Series) have been used to evaluate mechanical and electrical properties respectively. The significant findings of this study are mentioned below.

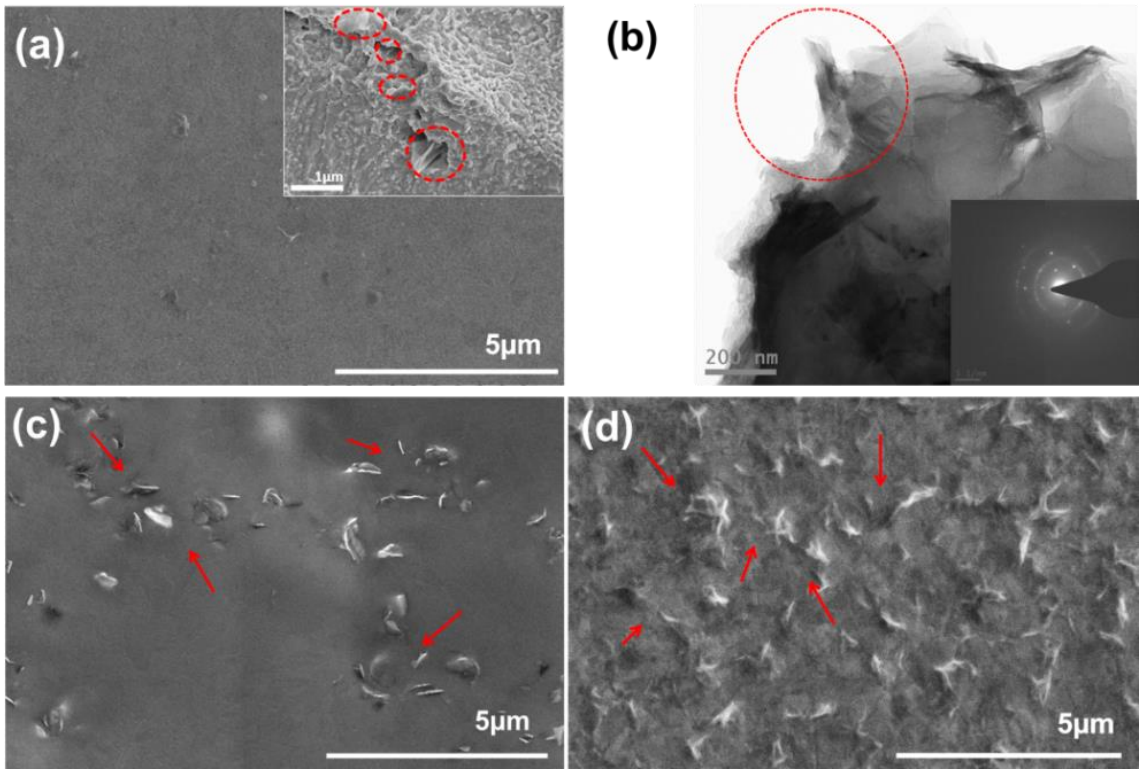

Figure 6.2 Confirmation of presence of graphene and distribution in composite foils illustrated by (a) FESEM micrograph for electropolished and etched (inset) P1 (b) TEM micrograph for P1 (inset) shows the diffraction pattern, (c)&(d) FESEM micrographs of electropolished P25 and P5 shows the presence of graphene and distribution in the composite foils respectively.

Figure 6.2 (a) shows the FESEM micrograph of the Cu-Gr composite foil (P1) prepared by PRED and inset shows the presence of graphene in etched surface of copper. Due to small concentration and transparent nature of graphene used for preparing these Cu-Gr composites, obtaining good contrast in FESEM for the Copper matrix and graphene was difficult. At smaller concentrations, i.e., for P1 and P25, graphene was even more difficult to be distinguished from copper; therefore, presence of graphene was confirmed from TEM (Figure 6.2b) Inset of Figure 6.2(b) shows the diffraction pattern obtained for Cu-Gr composite (P1) foil. Figure 6.2(c-d) shows the FESEM micrograph of P25 and P5, arrows indicating the presence of graphene. The FESEM micrograph for P25 (Figure 6.2c) has clearly indicated the presence of graphene. However, graphene distribution in P25 is found to be random due to lesser incorporation although better than that of P1. Figure 6.2d shows the uniform distribution of graphene throughout the copper matrix which was observed in the composite foil P5 (Figure

6.2d). In addition to the good dispersion of graphene in the Cu-Gr composites, very few agglomerates of the graphene were found in all the composites.

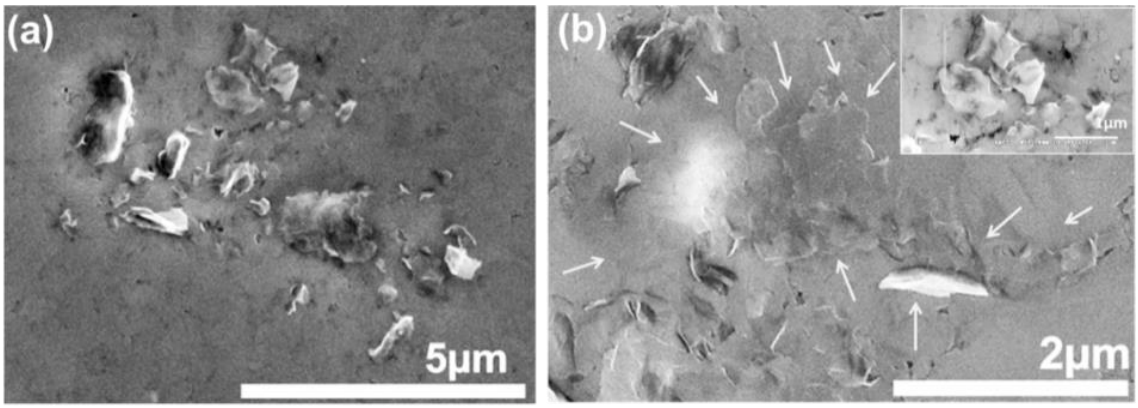

Figure 6.3 (a) and (b) Agglomerated graphene in the copper matrix observed by FESEM for P75. Inset of Fig. b shows the magnified micrograph

Whereas, the microstructure of electropolished surface of P75 showed agglomeration of graphene throughout the surface of the matrix (Figure 6.3 a, b& inset), compared to all the Cu-Gr composite foils (P1-P5) due to the saturation in dispersion of graphene in the electrolyte resulting in non-uniform dispersion of graphene in the copper matrix. Therefore from FESEM observations, P5 with 0.5 g/L graphene is the best possible concentration which gives best distribution of the reinforcing material in the Cu-Gr composite foils.

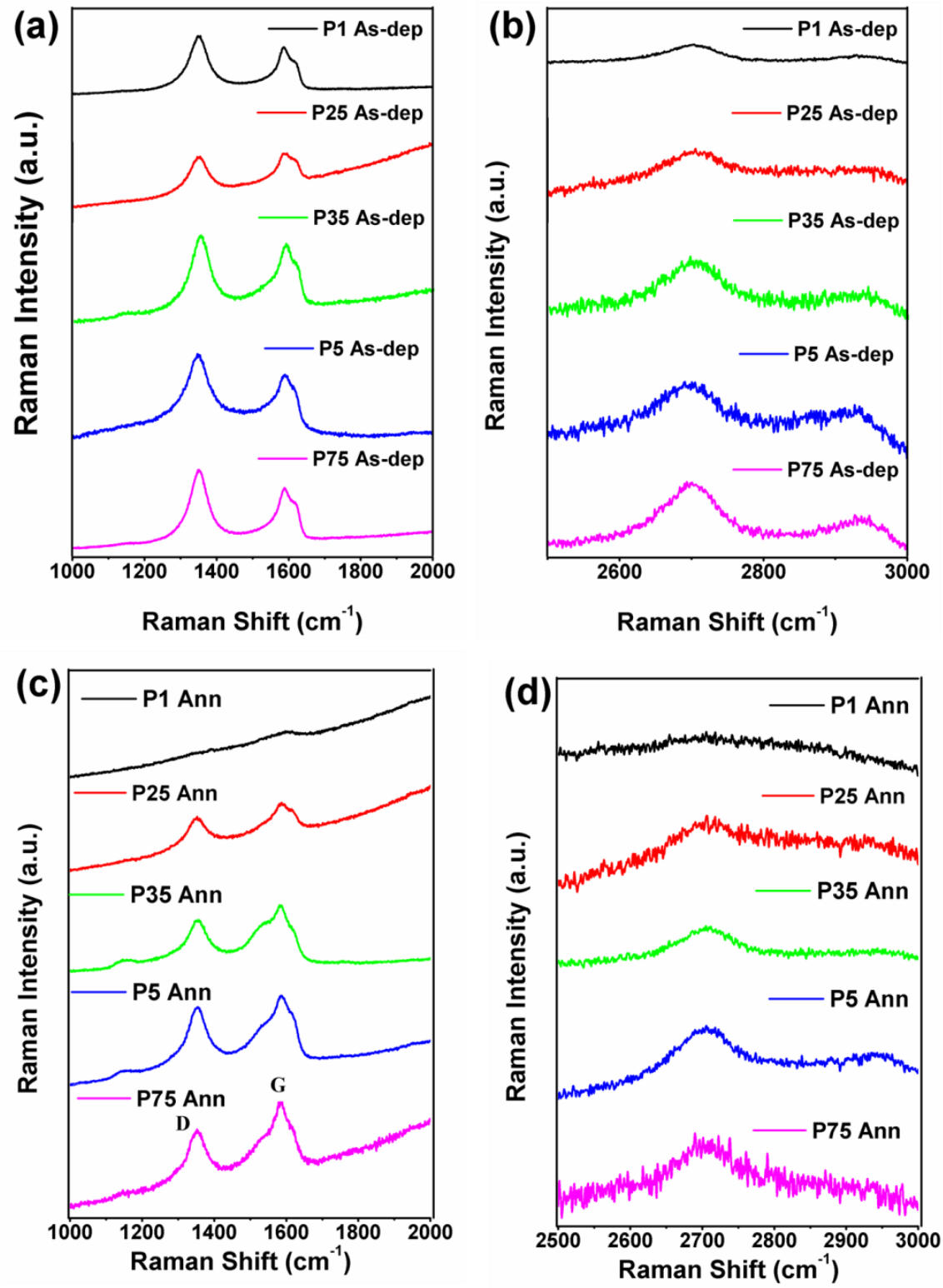

Figure 6.4 Raman spectra for Cu-Gr composite foils prepared by PRED with varied graphene content in the electrolyte. (a) &(b) for as deposited Cu-Gr composite foils and (c)&(d) for annealed composite foils indicating the D-band and G-band in (a&c) and 2D-band in (b&d) respectively.

The presence of graphene in the composite foils was also confirmed by Raman spectroscopy using Ar ion laser source (514nm). Raman spectroscopy, a powerful tool to determine the presence of Gr, the number of layers, crystallinity, defects etc., in Cu-Gr foils macroscopically. Spectra were found similar to those of pure graphene which has D-band(~1350 cm^{-1}), G-band (~1580 cm^{-1}) and 2D-band (~2700 cm^{-1}) as main characteristic peaks corresponding to typical disordered, graphitic and G' bands of graphene respectively known for graphene, for all the samples P1-P75 (Figure 6.4). Figure 6.4 shows the Raman spectra for as-deposited (Figure 6.4 a&b) and annealed (Figure 6.4 c&d) Cu-Gr composite foils G-band, D-band (Figure 6.4a&c) and 2D band (Figure 6.4b&d). It is also observed that with increase in the content of graphene in the composite, the intensity of the bands increased for both as-deposited and annealed composites. The intensity of D-band was slightly higher compared to G-band in the as deposited composite (Figure 6.4a), which may be due to the crumpling/folding of graphene in addition to the presence of oxygen functional groups. It has been reported that in case of CNT reinforced composites, Raman bands change their positions and intensities due to stresses and strains induced at the interface [248]. Further, after heat treatment, a small increment in the G-band for the composites was observed upon annealing (Figure 6.4c) which resulted in decrement of I_D/I_G ratio indicating graphitization due to the reduction of functional groups attached [101]. Further, no significant difference was observed in the peak positions of the composite foils upon annealing. The I_D/I_G ratios for different as-deposited and annealed Cu-Gr composite foils are given in Table 1, indicating a lower decrement of D/G ratio after annealing. For all the composite foils I_D/I_G is <1 indicating the less density of defects in the graphene [101, 170].

Table 6.1 I_D/I_G ratios for Cu-Gr composite foils

Copper-Graphene	**Raman Intensity Ratios (I_D/I_G)**				
	P1	**P25**	**P35**	**P5**	**P75**
As-Deposited	1.1867	0.951	1.07	1.1039	1.244
Annealed	0.789	0.88	0.8266	0.9049	0.8058

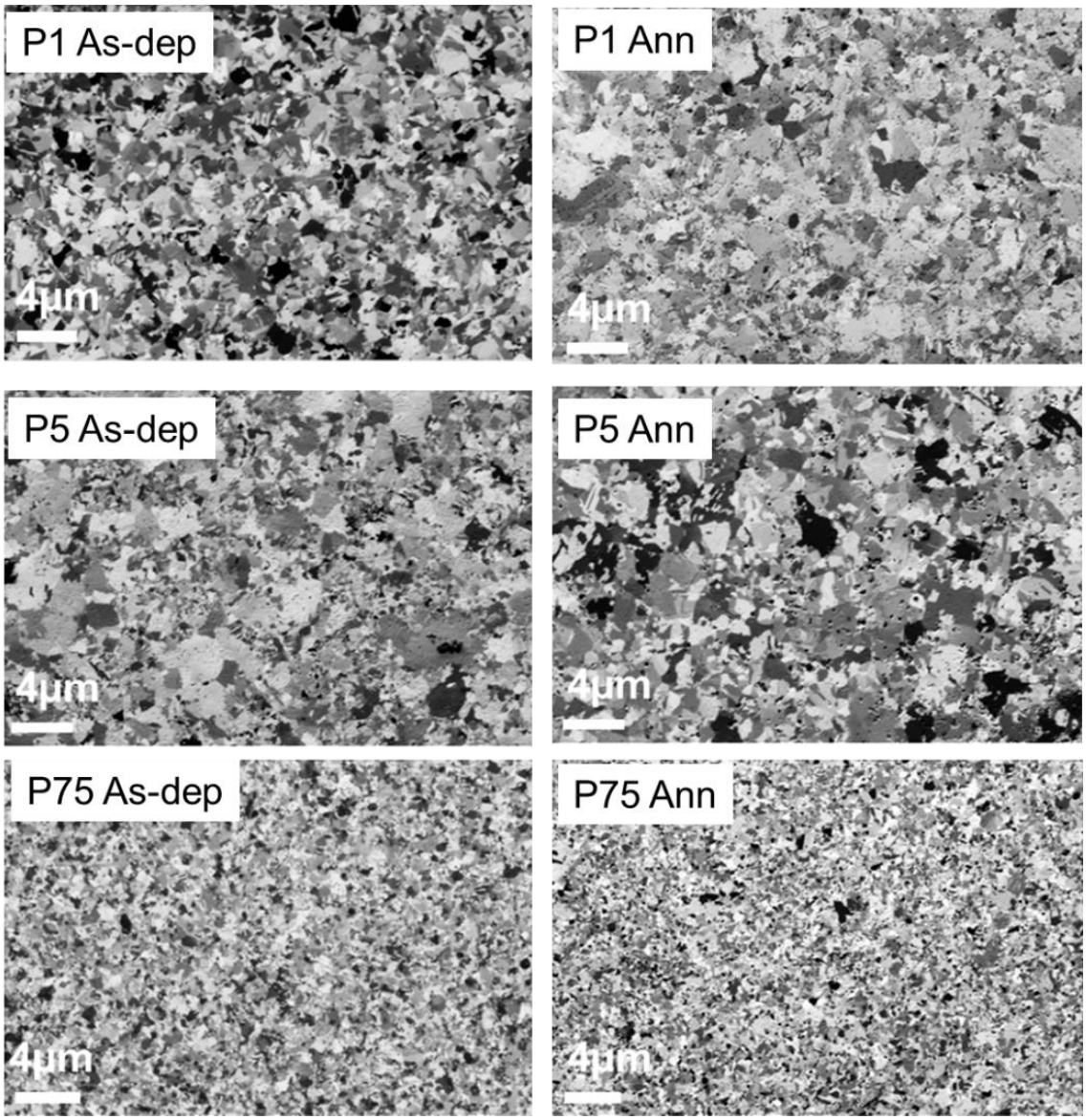

Figure 6.5 Micrographs showing grain size distribution of P1, P5 and P75 as-deposited and annealed Cu-Gr composite foils respectively.

Cu-Gr composite foils were also annealed at 573 K in Ar atm for 30 min in order to study the effect of annealing on grain size and mechanical properties of Cu-Gr composites. As-deposited and annealed Cu-Gr composite foils were electropolished and etched by Focussed Ion Beam (FIB). The etched surface was observed for the grain size distribution. The electropolished and FIB etched samples were shown in Figure 6.5. The grain sizes of the foils were estimated from the micrographs of electropolished surface of Cu-Gr composite foils etched by FIB (Focused Ion Beam) (Figure 6.5) to study the influence of graphene in controlling the grain size. Figure

6.6(a-f) shows the plots indicating grain size distribution in the as-deposited and annealed Cu-Gr composite foils for, P1, P5 and P75, which cover the whole range of graphene concentration used in the present study.

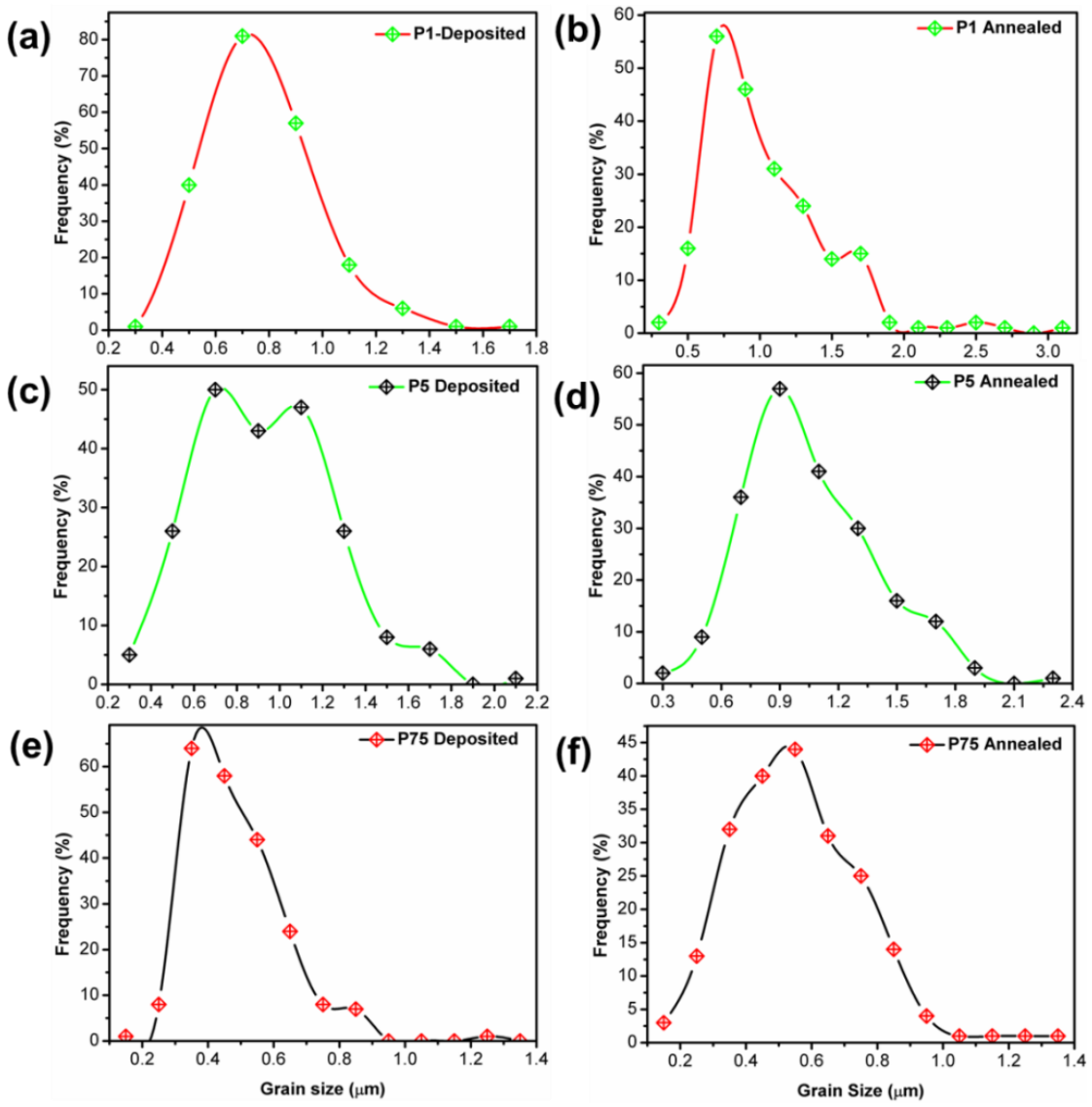

Figure 6.6 Variations in grain size distributions of (a), (c) (e) as-deposited and (b), (d), (f) annealed Cu-Gr (P1, P5 and P75) composite foils respectively.

From the grain size distribution plots, it is observed that the rain size is decreased significantly with the graphene content at P75 compared to P1 and P5.

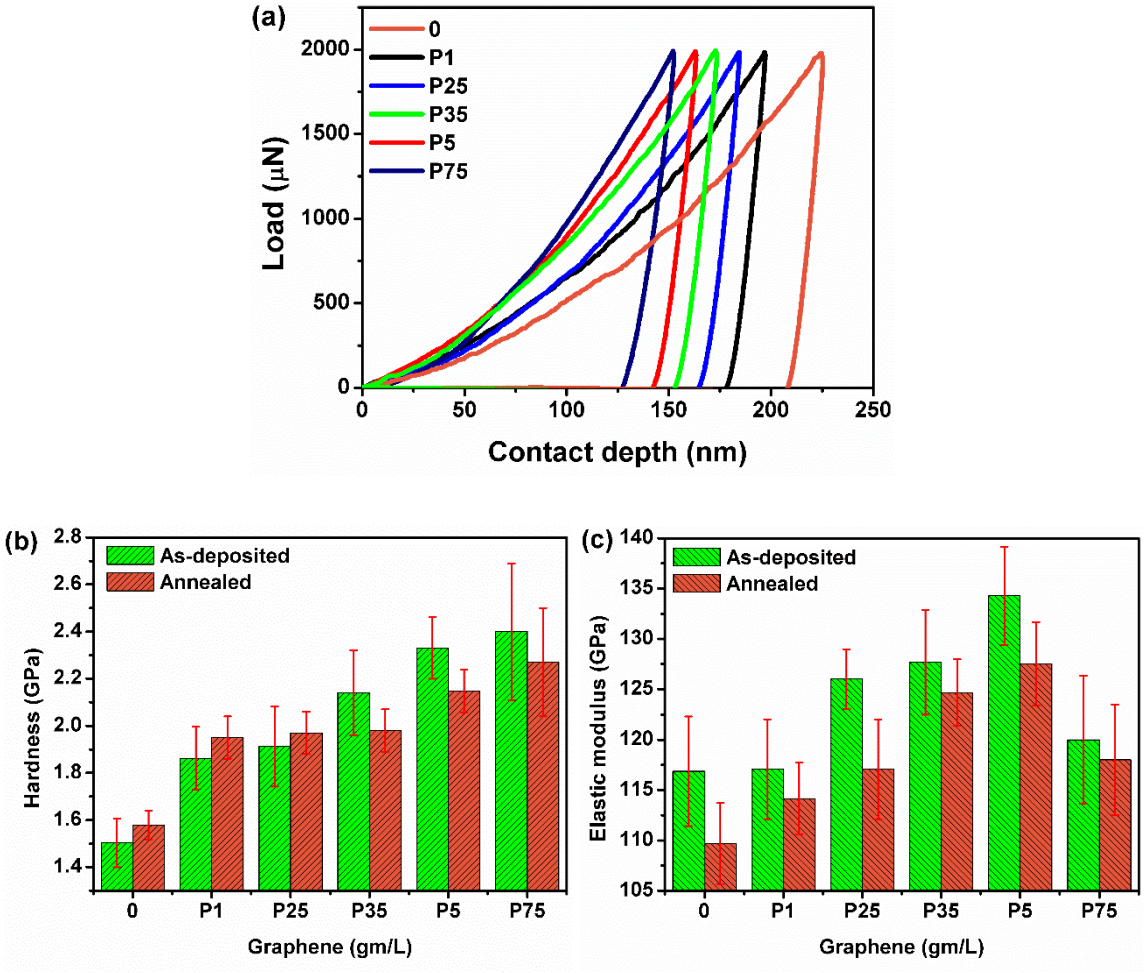

Figure 6.7 Plots indicating (a) representation of load vs. displacement curves, (b) hardness and (c) elastic modulus of the composite foils with variation in graphene content in the electrolyte for samples 0-P75.

Cu-Gr samples were characterized by nanoindentation to determine the hardness and modulus of the electrodeposited composite foils. Berkovich indenter was used for indentation with an applied peak load of 2000 μN, at a loading rate of 500 μN/Sec. Figure 6.7 (a-c) shows the representative load-displacement curves and harness and Modulus plots. Hardness and modulus were calculated using the method suggested by Oliver and Pharr [194, 195] from the load-displacement curves. It is clear from Figure 6.7 (a) that as the graphene content in the electrolyte is increased (P1-P75), the load-displacement curves have shifted to the left with lower contact depths, suggests that as the graphene content in the composite is increased, hardness increases and reached a maximum value of ~2.7 GPa for the as deposited P75 sample. This enhancement of hardness is attributed to the presence of graphene as well as the decrease

in the grain-size, also observed from (Figure 6.6). On subjecting the Cu-Gr nanocomposites to heat treatment, a slight increment in the hardness of the annealed Cu-Gr foils with lower content of graphene (0-P25) was observed, which could be mainly due to the formation of twins during the annealing process [249].

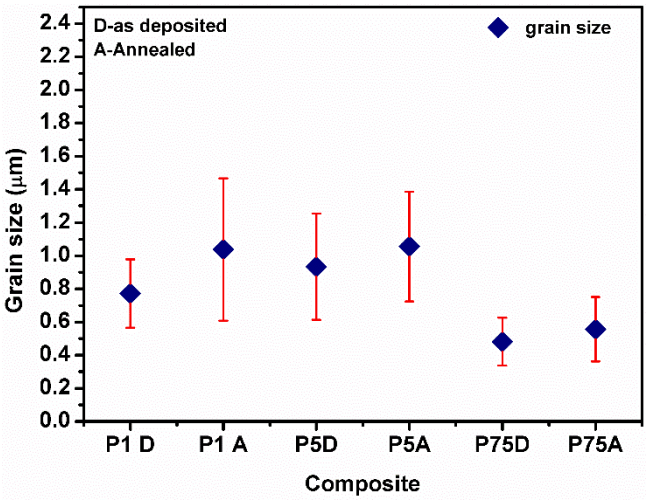

Figure 6.8 Variation of grain size in as deposited and annealed P1, P5 and P75 copper–graphene composite foils.

The influence of graphene in controlling the grain size in as-deposited and annealed composite foils is given in a consolidated plot which shows deviation in the grain size for the same composite foils given in Figure 6.8. The influence of graphene in P1 was minimal due to the lower graphene content present in the foils, observed from the grain size of P1. The grain size of sample P1 before annealing was ~0.89±0.43 μm and upon annealing increased to ~1.18±0.66 μm with large deviation. This deviation is due to the very small amount of graphene incorporated into the foils (Figure 6.8). However, the scatter in the hardness values is small probably due the formation of twins during annealing.

All the graphene reinforced copper matrix composite foils in the as-deposited condition have followed a trend in increasing hardness gradually from 1.5 GPa to a maximum of ~2.7 GPa (~125% enhancement compared to that of bulk copper (1.2 GPa)) with the addition of graphene in the electrolyte from 0-P75. It is expected that for the samples P35-P75, the decrease in hardness after annealing is probably because of the reduction in internal stresses. The elastic modulus for the composite foils was calculated from the unloading portion of the load vs.

displacement curves. Figure 6.7(c) shows a gradual increment from ~117 GPa to ~139 GPa in as deposited foils as the graphene concentration is increased from 0-P5. However, for P75, elastic modulus significantly decreased to ~119 GPa (±6.36 GPa) though the grain size is finer (P75 before annealing- 0.48±0.14 µm and after annealing 0.55±0.19 µm). The substantial decrease in the modulus with larger deviation could be due to the agglomeration and non-uniform distribution of graphene. Similar behaviour was already observed in CNT reinforced composites [250]. In addition, stresses introduced during the electrodeposition process due to the agglomerated graphene in the composite lead to the large variation of ±0.3 GPa in hardness values of P75 at different areas in the composite. Because of possible annihilation of deposition-induced internal residual stresses, during annealing the modulus might be decreasing in all the samples after annealing. Though the modulus is independent of the microstructure, in case of composites it depends on the reinforced element in the matrix, its distribution and interfacial bonding between the reinforced element and the matrix [251]. According to the rule of mixtures, the modulus can be estimated by Halpin-Tsai model [252], provided the volume fraction of graphene in the Cu-Gr composite foils is known. However, graphene which is added into the electrolyte does not incorporate completely during the deposition as the incorporation and distribution of graphene depends on the pulse parameters and mass transport limitations. Also, quantification of such extremely small quantities of graphene incorporated into matrix is very difficult and efforts are being made for these quantitative estimations.

Nanoindentation studies indicated that, irrespective of the grain size, optimum quantity of graphene to be dispersed in the electrolyte is observed to be 0.5 g/L (P5). Beyond 0.5 g/L, though the properties can be enhanced by increasing the dispersion time by ultrasonication, graphene appear to agglomerate during deposition as the graphene content is large. In addition, ultrasonication/dispersion takes several hours to disperse the graphene when the graphene concentration is increased; this further results in extra-long time for the deposition. Moreover, beyond the optimum concentration of 0.5 g/L graphene, the deposit becomes brittle as observed during our experimental studies. Hence, the ideal amount of graphene that can be added to the electrolyte to incorporate into matrix by PRED in order to improve the properties is found to be 0.5 g/L.

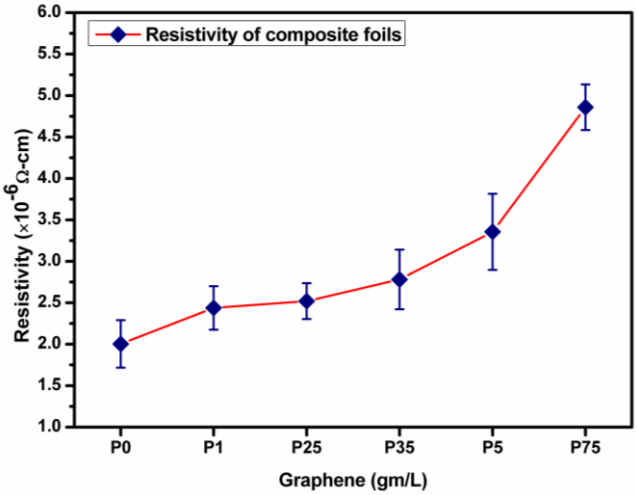

Figure 6.9 Variation of electrical resistivity of as-deposited Cu-Gr composite foils with graphene content in the electrolyte.

As copper is of interest in electronic applications, to study the influence of graphene, electrical resistivity is of great importance. Electrical resistivity was measured by Four-probe resistivity for as-deposited Cu-Gr composite foils deposited with different concentrations of graphene. From Figure 6.9, it was observed that, the composite foils have shown a slight increment in resistivity compared to that of pure Copper prepared with same pulse parameters. The resistivity of the composite foils also increased with increase in the content of graphene in the foils from 2.0×10^{-6} Ω-cm to 5.2×10^{-6} Ω-cm. The presence of traces of oxygen functional groups remained in graphene even after reduction during deposition could be the contributing factors for enhancing the resistivity of the composite foils. Since, P5 is found to be the sample with optimum concentration of graphene from nanoindentation studies to achieve enhanced mechanical properties; PRED deposited Cu-GR-P5 composite foil was annealed at 573K in Ar atm and characterized for electrical resistivity. The resistivity was found to decrease from ~3×10^{-6} Ω-cm to ~ 2.3×10^{-6} Ω-cm after annealing, comparable to pure Copper. Though the presence of oxygen functional groups in graphene increased the resistivity of the composite slightly as the amount of graphene added in the electrolyte was increased, this can be overcome by annealing due to the removal of some of the oxygen functional groups attached to graphene.

Using a simple and economical PRED technique by systematically varying the graphene concentration from 0-0.75 g/L in the electrolyte have shown a remarkable enhancement in the hardness from 1.5 GPa to ~2.7 GPa (~125% higher than bulk copper) with increase in

graphene. Similarly the elastic modulus is also increased from ~117 GPa to ~139 GPa (~30% higher than bulk copper) for 0-P5 with a slight decrement in modulus after annealing, whereas a substantial decrement in the modulus to ~119 GPa, was observed for as deposited P75with further decrement after annealing , clearly indicating the importance of dispersibility of graphene. The electrical resistivity of Cu-Gr composites increased gradually as the graphene content is varied from 0-0.75 g/L. From the hardness and modulus data, it appears that the optimum amount of graphene to be added in the electrolyte in order to enhance the mechanical properties was 0.5 g/L (P5) for which, annealing at 573K reduced the resistivity to ~2.3×10^{-6} μΩ-cm which is comparable to that of bulk Copper.

6.2 Influence of deposition technique

In the earlier section it is observed that the mechanical properties of the composite foils were evaluated and found to improve with the optimum graphene content. Therefore this section dedicated on evaluation of effect of pulse parameters for synthesis of Cu-Gr composite foils with optimum Gr content. Hence, this study reports the main findings of the composite foils prepared by PRED and DC, in order to correlate the properties and show the superiority of PRED with electrodeposition technique while keeping the graphene concentration constant at 0.5 g/L in the electrolyte. In addition to study the influence of graphene, pure copper foils were also synthesized by DC and PRED.

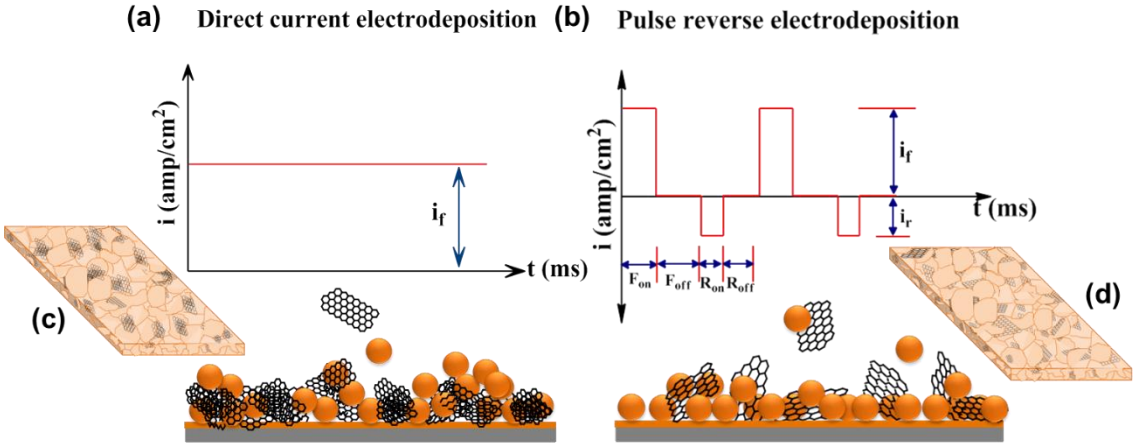

Figure 6.10 (a)&(b) Schematic represents the current waveforms and the co-deposition of Cu and Gr, (c) & (d) Cu-Gr nanocomposite foils, by DC and PRED respectively.

Figure 6.10 (a-d) represents the schematic of the electrodeposition process employed in the current investigation. Figure 6.10(b &c) shows the schematic representation explaining the pulse pattern and the deposition process during DC and PRED. DC electrodeposition was done by applying a current density of 0.025 A/cm^2. In case of PRED, the current densities for the forward and reverse pulses are optimized by performing the depositions in the range of 0.05-0.2 A/cm^2 and 0.005-0.015 A/ cm^2 respectively. The forward pulse on ($T_{F\,on}$) time is in the rage of 15-50 ms, $T_{F\,off}$ is in the range of 50-100 ms and $T_{R\,on}$ and $T_{R\,off}$ are in the range of 1-10 ms. Subsequently, these foils were annealed under argon atmosphere at 300°C for 30 minutes in order to reduce GO to Gr. It is also plausible that GO in the Cu matrix could partially reduce to Gr during the electrodeposition because of application of large cathodic pulses during the deposition process. It has been reported that Gr and GO exhibit hardness and modulus in the same range where GO shows a slightly lower hardness [253].

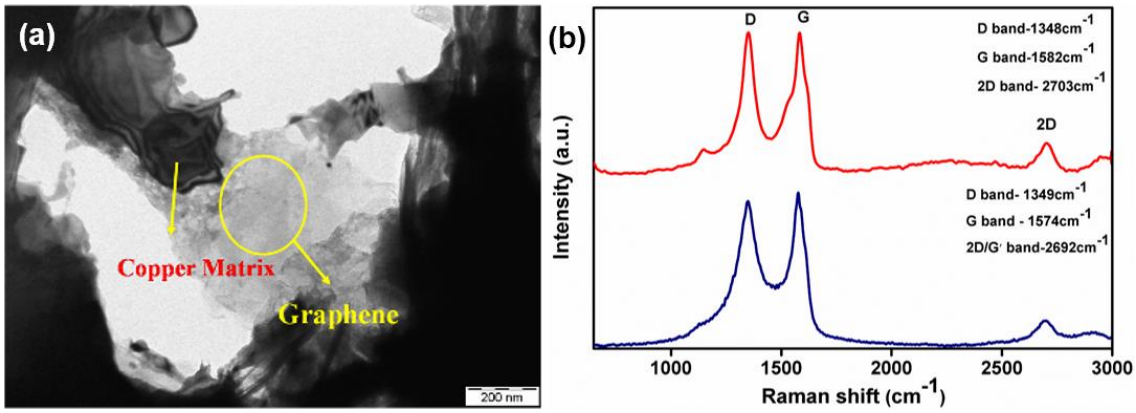

Figure 6.11 (a) Transmission electron micrograph of copper-graphene composite foil and (b) Raman spectra of graphene and composite.

DC and PRED Cu-Gr composite foils were examined by TEM and Raman spectroscopy to confirm the presence of graphene. Figure 6.11a shows the TEM micrograph of the Cu-Gr composite confirming the presence of Gr in the Cu matrix, (b) Raman spectra of graphene and Cu-Gr composite. In the Raman spectra (Figure 6.11b), composite foils with Gr as reinforcement have shown a D-band at a wave number of 1348 cm^{-1}, and slight shifts in the G-band (from 1574 to 1582 cm^{-1}) and 2D bands (from 2692 to 2703 cm^{-1}) from those observed for Gr. As mentioned in the earlier section similar spectra were observed with a slight increment in the intensity of the D- band compared to the G-band.

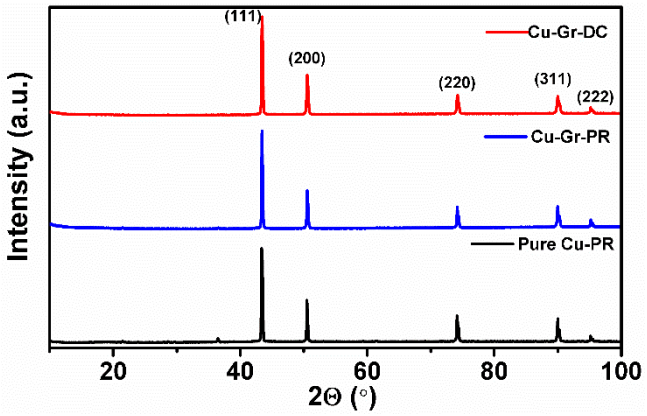

Figure 6.12 X-ray diffractograms of PRED Cu, DC-Cu-Gr and PRED Cu-Gr before annealing.

Crystallographic orientation of the composite was characterized by XRD (D8 BRUKER D8 ADVANCE X-ray diffractometer). X-ray diffraction (XRD) patterns for pure Cu foils and Cu-Gr foils prepared by DC & PRED are shown in Figure 6.12. Similar patterns were observed for all the composite foils. Peaks corresponding to Gr/GO were not observed since the amount of GO incorporated into the composite is too small to be detected by XRD.

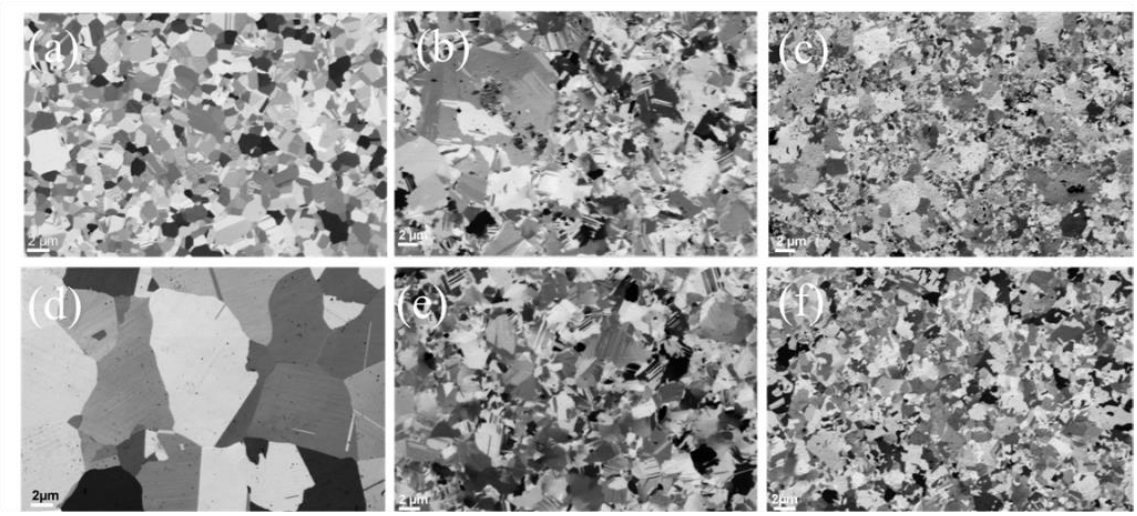

Figure 6.13 Grain size distributions of (a) (b) &(c) PRED Pure Cu, DC Cu-Gr , PRED Cu-Gr before annealing and (d) (e) &(f) PRED Pure Cu, DC Cu-Gr, PRED Cu-Gr after annealing respectively.

Figure 6.13(a-c) show the micrographs of focussed ion beam (FIB) etched surface of the electropolished pure Cu foils prepared by PRED, Cu-Gr foils prepared by DC and PRED respectively. PRED pure Cu has nearly uniform grain size (Fig. 3a). While Cu-Gr composite foils electrodeposited by DC resulted in grains with broader size distribution (Figure 6.13b) compared to those prepared by PRED (Figure 6.13c). Growth twins are also present in as-deposited pure Cu as well as composite foils. PRED is advantageous over DC electrodeposition because it offers to vary several key processing parameters including current applied, pulse duration and duty cycle that enables a smooth, highly dense, uniform deposit while minimizing hydrogen embrittlement. This in turn improves the properties of the deposited material. The forward pulse restricts the mass transfer process and controls the grain size; whereas the reverse pulse minimizes the dendritic morphology and helps in removal of extended Gr and loosely adsorbed Cu or Gr, in addition to entrapped hydrogen during each pulse [63]. Furthermore, the incorporation of Gr into the matrix is expected to be higher in PRED. In case of DC deposition, due to the continuous application of current, the deposition is rapid at the most active nucleation sites and continuous incorporation of Gr along with the Cu deposition results in roughness of the surface as well as formation of Gr clusters in the matrix. We have already shown in the chapter 4 that use of PRED with controlled pulse parameters enables highly dense, smooth, highly textured (111) Cu foils with high hardness and with good electrical conductivity [35].

The most interesting results have been achieved for the annealed Cu-Gr composite foils. Figure 6.13(d-f) shows the micrographs of the annealed PRED-Cu, DC-Cu-Gr and PRED-Cu-Gr foils respectively after etching the surface with FIB. Grain size in the pure Cu foil increased maximum up to 10 microns upon annealing (Figure 6.13d), whereas Cu-Gr foils have not shown any significant increase in the grain size (Figure 6.13e& f) due to the presence of Gr as the second phase material at the grain boundary. Where graphene obstructs the motion of grain boundaries and thus retards grain growth. It is well established that the morphology of the second phase plays a significant role in the grain growth kinetics. Needle-like structures as well as flake-like structures of the reinforcement material are found to be more effective in controlling the overall microstructural features of the composite [254, 255]. In addition to being a good reinforcement material, Gr with its sheet-like structure is expected to be a better grain growth inhibitor.

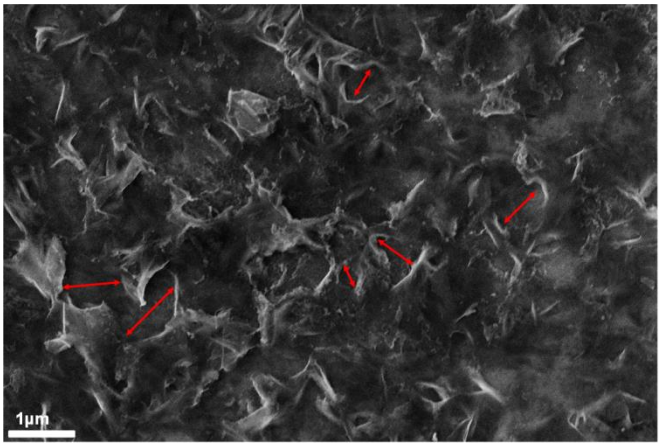

Figure 6.14 FESEM micrograph of Cu-Gr composite foil prepared by PRED.

The FESEM micrographs show the presence of graphene sheets at the grain boundaries of copper and the distance between the graphene sheets is found to be comparable to that of the grain size of the matrix.

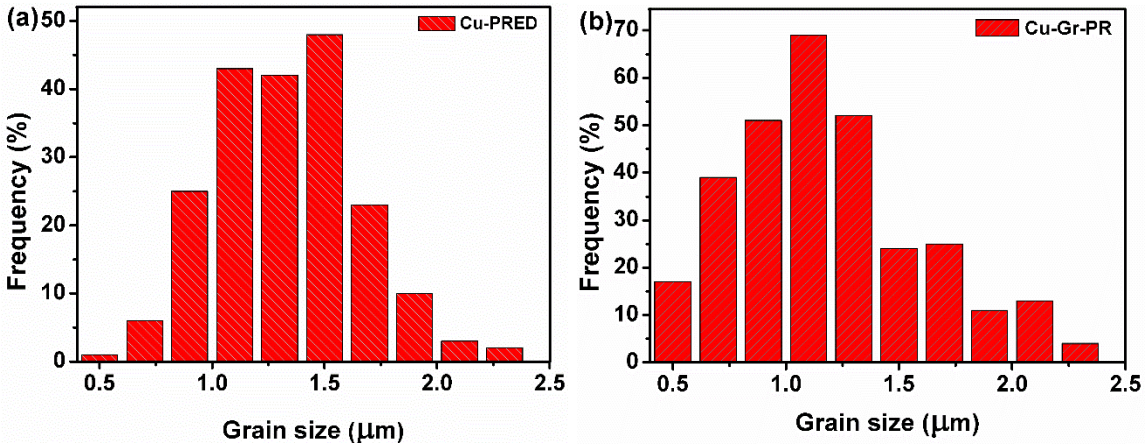

Figure 6.15 Grain size distribution for pure copper and copper-graphene composite foils prepared by PRED.

The grain size distribution in as-deposited pure Cu and Cu-Gr composite foils is shown in the Figure 6.15. The average grain size measured from about 250 grains using linear intercept method is found to be maximum up to ~1.3±0.3 μm and ~1.2±0.4 μm for the as-deposited pure copper and Cu-Gr composite foils, respectively, prepared by PRED as shown in the Figure 6.15. The corresponding micrographs are shown, where the average distance between the graphene sheets in the copper matrix is ~800 nm – 1.2 μm. The separation distance between two graphene sheets located at the grain boundaries is indicated by arrows in red colour in

Figure 6.14. Hence it is clearly evident from the FESEM micrograph of the surface of the electropolished Cu-Gr foil (Figure 6.14) that the Gr is distributed along the grain boundaries.

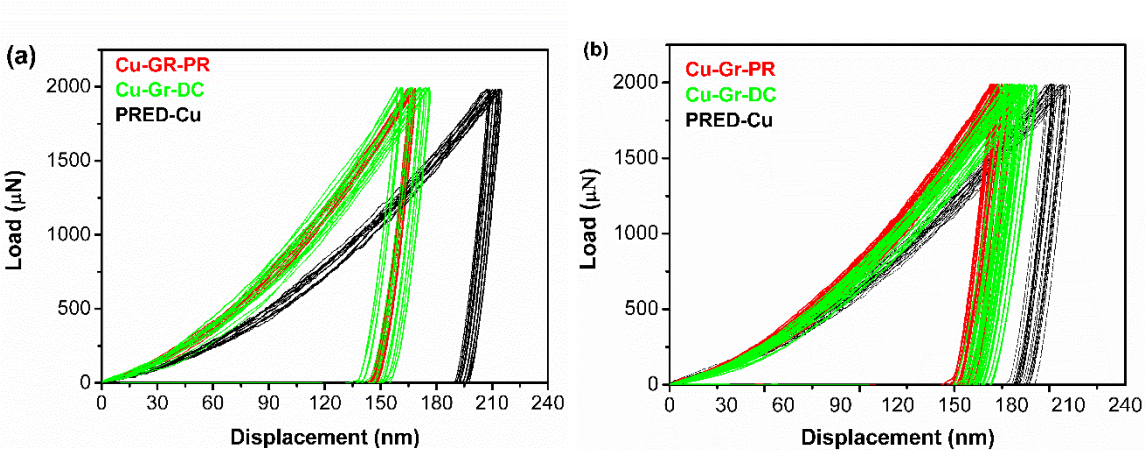

Figure 6.16 Load-displacement curves of (a) as deposited and (b) annealed PRED pure Cu, Cu-Gr composite foils.

Hardness and elastic modulus of the Cu-Gr foils prepared by PRED and DC are evaluated by nanoindentation technique with a Hysitron Triboindenter. The applied peak load was 2000 μN with a loading rate of 500 μN/sec, a Berkovich tip was used for the indentation. The load displacement-curves obtained during nanoindentation are shown in Figure 6.16 (a-b).

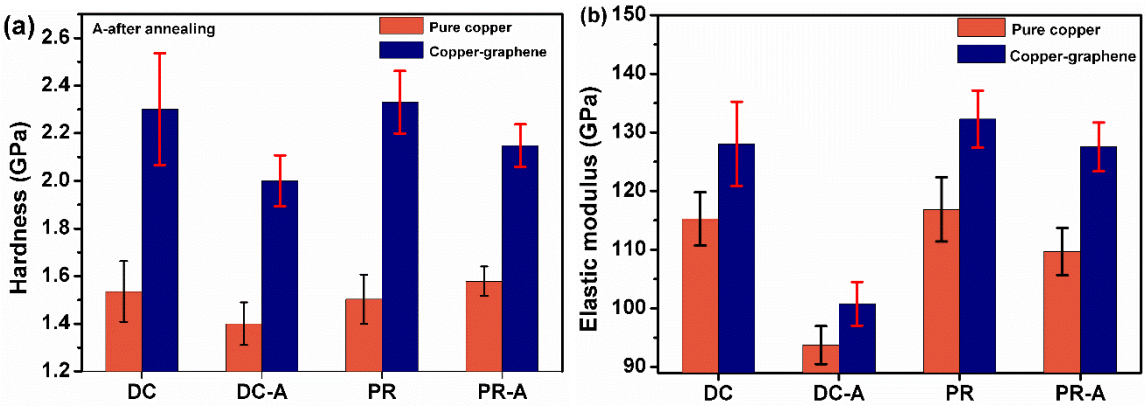

Figure 6.17 (a) Hardness and (b) elastic modulus of as deposited and annealed pure Cu and Cu-Gr composite foils prepared by DC and PRED.

The corresponding hardness and modulus calculated from the unloading curve from the load-displacement curves are shown in Figure 6.17(a-b). Each hardness or elastic modulus datum point is an average of 25 indents performed under similar conditions. The hardness and the

elastic modulus obtained for pure Cu synthesized by PRED and DC electrodeposition are also shown for comparison. The pure Cu foils exhibited hardness in the range of 1.4 – 1.6 GPa, whereas the composite foils have shown a hardness in the range of 2.1-2.5 GPa. This suggests that the inclusion of Gr substantially increases the hardness by 96% in these novel composites. In comparison to DC conditions, PR conditions yielded higher hardness values for the composites because of the absence of agglomeration and thereby uniform distribution of Gr throughout the composite. The overall hardness of these composites will have contributions from three factors, 1) finer grain size of the matrix, 2) presence of twins and 3) presence of Gr as a reinforcement. Since the grain size of the matrix is comparable in both the composites prepared by different processing parameters (DC and PRED), it is clear that Gr makes the difference in increment of the hardness values. The -COOH and –OH groups attached to the Gr improve the covalent bonding between the metal matrix and the filler material enabling the efficient load transfer [12, 256]. Uniform dispersion and spread of Gr throughout the matrix arrests the grain growth during deposition and subsequently blocks the dislocation motion during deformation process. The decrement in the hardness of Cu-Gr composite films upon annealing is not significant, because of the retention of same microstructural features. Even though GO present near the surface of the film is possible to undergo reduction during annealing, residual functional groups present in bulk of the Cu retain the interfacial bonding between Cu and GO. In contrast, as-deposited pure Cu foils contain larger grains due to absence of Gr resulted in much lower hardness values compared to Cu-Gr foils and showed drastic grain growth during annealing. However, against the expectations, the hardness for these foils did not decrease significantly, probably due to the formation of annealing twins in addition to the growth twins, which are known to form in PRED, that compensate to the decrease in hardness due to grain-growth [219].

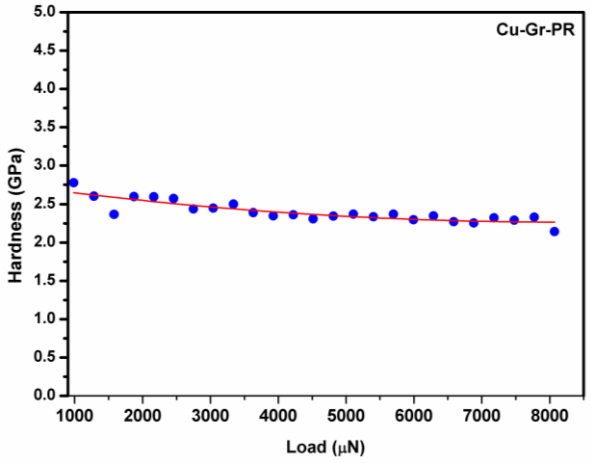

Figure 6.18 Variation of hardness with peak load, applied during nanoindentation, of Cu-Gr composite foils.

Nanoindentation was also carried out on PRED Cu-Gr (0.5 g/L) samples at different peak loads ranging from 1000 μN to 8000 μN and the obtained data is shown in Figure 6.18. From the Figure 6.18 it is clear that the hardness was constant throughout and was not influenced by the peak load (contact depth).

Although modulus is independent of the microstructure, in case of composites, the values depend on the reinforced material, its distribution and the volume fraction, in the matrix. It can be observed from Figure 6.17 that the modulus of the PRED Cu-Gr composite foils is higher, ranging between 127–137 GPa, compared to ~116 GPa for pure PRED Cu foils, attributed to the presence of Gr. Interestingly, only a slight decrease in the modulus values was observed after annealing at 300°C for both pure Cu and composite foils prepared by PRED while, a large decrease is observed for the samples deposited using DC. The large decrease in modulus for DC samples during annealing could be due to the annihilation of residual stresses induced during DC process [257].

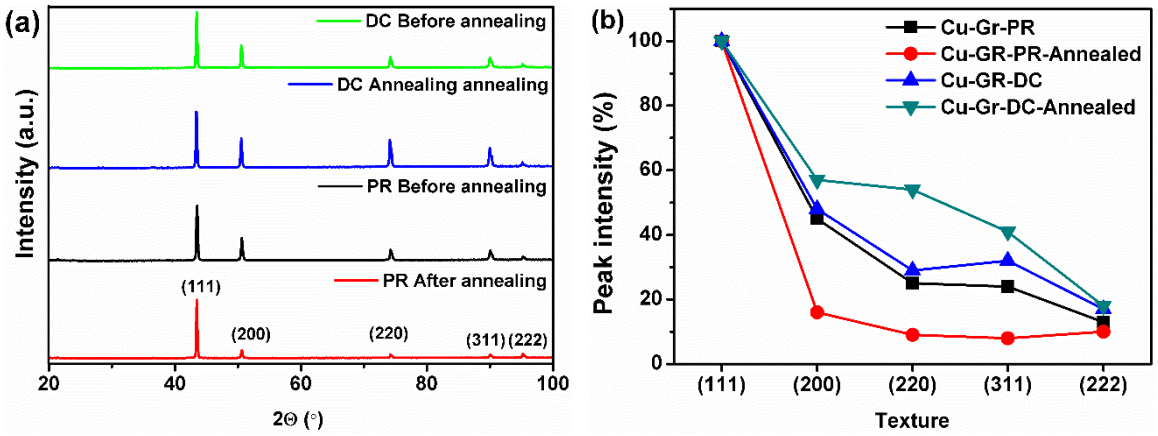

Figure 6.19 (a) X-ray diffractograms and (b) variation of intensities of crystallographic orientation calculated from X-ray diffractograms.

It has also been reported by Xiang et al., [258] that annealing can reduce the residual stresses resulting in decrease of the modulus [259]. Since PRED enables deposition of foils with very low residual stresses [260], only a slight decrease in the modulus is observed upon annealing (Fig.4d). In addition, they have shown an increase in the (111) orientation upon annealing, which is common in PRED films [261]. Many studies have shown that annealing can bring a preferential orientation of grains [262]. It favours high modulus[263, 264]. Recently we have also observed higher modulus for (111) textured pulse electrodeposited Cu foils compared to (100) and (101) oriented foils. Thus annealing induced (111) orientation in the present work compensates to some extent the decrease in modulus that arises from residual stress release , and lesser decrease in the value of modulus compared to that of the DC deposited foils is observed (Figure 6.19).

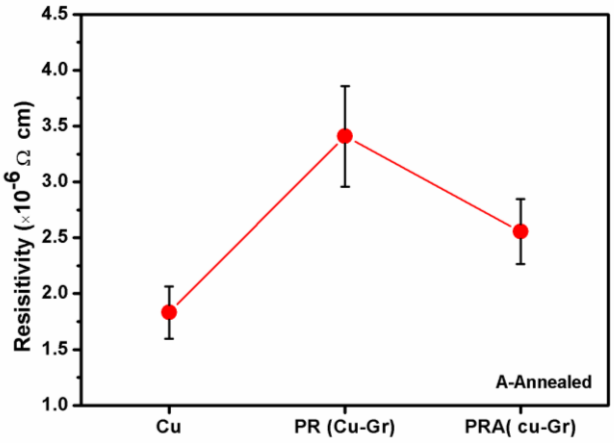

Figure 6.20 Electrical resistivity of Cu-Gr composite foils.

Electrical resistivity of Cu-Gr composite foils was measured by four-point probe method. The resistivity of as-deposited PRED Cu-Gr composite foils is observed to be ~ 3.4×10^{-6} Ω-cm and is decreased to ~ 2.3×10^{-6} Ω-cm upon annealing at 300°C under argon atmosphere, for 30min (Figure 6.20).The slight increment in the resistivity for as-deposited PRED Cu-Gr foils compared to that of pure Cu foils (1.7×10^{-6} Ω cm) might be either due to the presence of poorly conducting GO incorporated into the matrix or due to the formation of small amount of Cu oxide during anodic pulse. Generally, upon annealing in inert atmosphere, stress relaxation leading to grain growth and removal of residual oxygen leads to a decrease in the resistivity of a material. GO must be reacting with Cu to form Cu oxide and Gr, while Cu oxide being reduced to Cu during annealing [174]. The resistivity values obtained are well in the range of the values reported for Cu-Gr and Cu-CNT composites [174, 183].

From the observed outcomes and nanoindentation studies showed that the PRED electrodeposited Cu-Gr composite foils have exhibited a high hardness of 2.2-2.5 GPa (increased by ~96% of that of pure Cu). The uniformity throughout the foils in terms of hardness was high for the PRED films compared to those observed for the DC deposited foils. The elastic modulus of the foils prepared by PRED is ~137 GPa, which is ~30% higher than that for pure Cu foils. Annealing of PRED Cu-Gr foils have not shown considerable decrement in the hardness and modulus values indicating the promise of these foils, which can be used for several applications. The superior mechanical properties obtained are due to a) fine grain size of the Cu matrix, b) presence of twins in Cu matrix and c) presence of Gr as reinforcement

and its uniform distribution throughout the matrix. The uniformity in the microstructural features of these novel nanocomposites can be attributed to the feasibility to optimize several parameters including the applied current density, pulse 'on' and 'off' times both during the 'forward pulse' and the 'reverse pulse' unlike in DC deposition which allows variation of current density alone. Our present process is appropriate to prepare Cu-Gr composite foils with control over the mechanical and electrical properties, as it is a scalable low temperature process, economical and can be prepared on substrates with complex shapes with good reproducibility.

6.3 Summary

To conclude, Cu-Gr composite foils were synthesized for the first time, by varying the graphene content and by varying the pulse parameters (PRED/DC) in order to achieve superior mechanical properties, while exhibiting electrical conductivity in the same range as that of pure Cu. Application of pulse reverse current has resulted in uniform distribution of Gr in the metal matrix. In addition to the presence of optimum amount of graphene (0.5 g/L), application of PRED technique, sheet-like structure, available surface area which is in contact with copper matrix of finer grain size, uniform distribution and spread of graphene influenced the mechanical and electrical properties.

Chapter 7. Electrodeposition of copper-carbon nanotube (Cu-MWCNT) composite foils and their mechanical and electrical preoperties

The objective of the present chapter is to prepare the Cu-CNT composite foils prepared under similar conditions and to compare the mechanical and electrical properties with those of copper-graphene composite foils. The outcome of this work assesses the role of structure of the reinforced element in controlling the properties. The Cu-CNT composites in the present study are prepared by pulse reverse electrodeposition with the same pulse parameters used for Cu-Gr. Subsequently, in order to improve the strength, several novel approaches have been adopted to enhance the dispersion and to avoid the entanglement and agglomeration. A systematic study that reports the important and promising findings of the various approaches towards the synthesis to increase the properties are presented in the successive sections.

7.1 Copper foils reinforced with functionalized CNTs

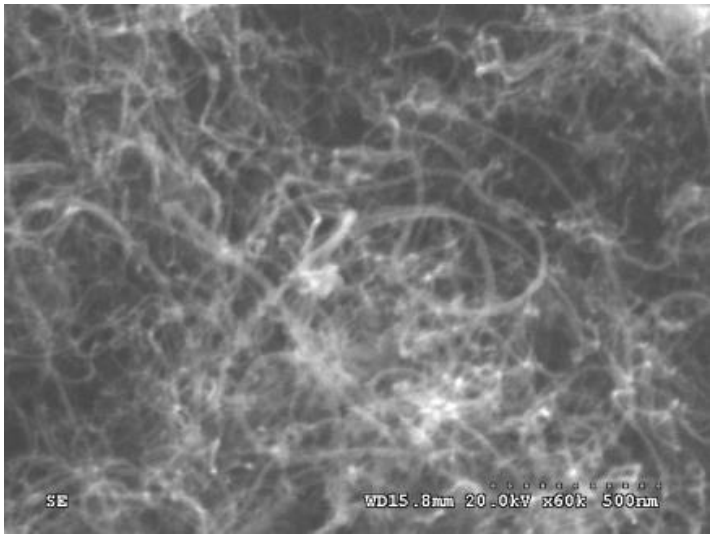

Figure 7.1 FESEM micrograph of as-received CNTs.

Effective utilization of CNTs as reinforcement in the metal matrix for improving the properties is limited due to their high aspect ratio. Added to it, structural defects, kinks and van der waal interactions are leading to the agglomeration of CNTs. This results in lack of interfacial

bonding and the load transfer from the matrix to CNTs is affected. Hence, this is a major issue for the commercial applications due to the inhomogeneous dispersion of CNTs along with poor interfacial bonding and hydrophobic nature with the matrix [265]. Therefore, it is necessary to modify the surface properties of MWCNTs in order to improve wettability and reduce the agglomeration [266, 267].

To address this, several approaches such as chemical and physical functionalization have been used [268, 269]. As a part of this, initially, as-received MWCNTs were chemically functionalized by acid treatment [270, 271] to make the surface of the CNTs hydrophilic. This step follows washing with de-ionised water until the pH reaches neutral. The functionalization introduces several functional groups including atomic oxygen (–O), hydroxyl (–OH) and carboxyl (–COOH) groups on the surface of CNTs [271]. These oxygen functional groups help to enhance the interaction between carbon and Cu. In addition, the oxygen present in the functional groups promote electron exchange between Cu and carbon atoms, or directly interact with Cu, thus, play a key role in the formation of Cu-CNT interfaces [272]. The functionalized CNTs were dispersed and utilized for deposition of Cu-CNT composites. The complete experimental details which includes dispersion of CNTs, addition of surfactant, co-deposition of Cu and CNTs follows the same procedure discussed for graphene reinforced composite foils [172]. For the deposition, ~0.5 g/L of functionalized CNTs were taken in order to compare the features with the graphene reinforced composite foils.

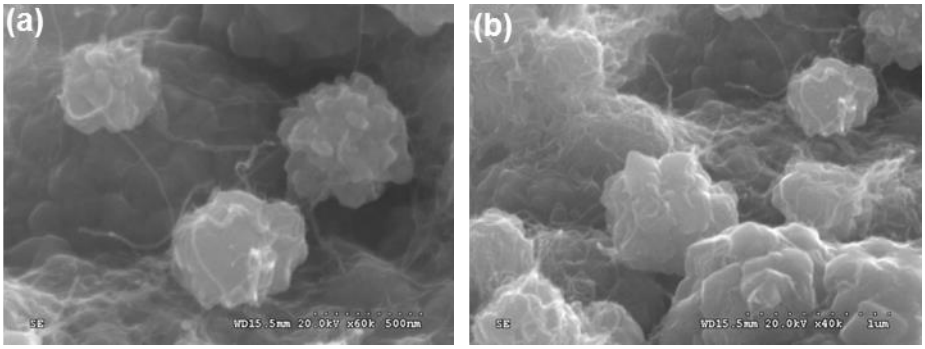

Figure 7.2 (a) &(b) FESEM micrographs of Cu-CNTs composite foils.

Figure 7.2 shows the composite "powder–like" microstructure with entangled CNTs and copper powder. This indicated that the composite powder was formed instead of compact film.

This powdery formation is probably due to the high aspect ratio of the CNTs (length of the CNTs ~5-20 µm).

Figure 7.3 Schematic representing the co-deposition of CNTs with high aspect ratio and copper particles.

Figure 7.3 shows the representation of co-deposition of long CNTs and copper leading to powdery deposition. It is expected that length reduction could reduce the entanglement to an extent and enables the CNTs to deposit along with copper, forming a compact film. Therefore, the entanglement of CNTs has to be avoided to overcome the powdery deposition. In order to avoid the powdery deposition falling into the electrolyte, and to reduce the agglomeration of the CNTs in the composites, the length of the CNTs was reduced prior to co-deposition.

To reduce the length of the CNTs, optimum method has to be chosen among the several approaches available [273-276]. The chemical and structural stability of the CNTs are very important in case of composites where the reinforcement will have a major role in deciding the properties. Therefore, CNTs were shortened by ultrasonication method without damaging the walls of CNTs. The subsequent sections give the detailed description of shortened CNTs and associated shortening mechanism.

7.2 Shortening of CNTs by ultrasonication in an organic solvent

Although chemical functionalization improves the wettability/ chemical compatibility with the matrix, entanglements in the CNTs caused by van der waal forces between neighbouring CNTs is still a major concern because of their high aspect ratio. Therefore, the length of the CNTs has to shortened. Many efforts have been made on enhancing the dispersion of CNTs by shortening/cutting the long CNTs mechanically or chemically [273, 274]. Several methods such as ball milling [277, 278], solid–state cutting [279] thermal oxidation [280] etc. have been used for this purpose. However the length of the CNTs treated by these methods was

not uniform. Wet methods such as ultrasonication [275, 276] and other polymer based methods, have been used to cut the CNTs due to their low impact on the CNT damage. This method is a room temperature method and reduction in length occurs in an organic solvent such as ethanol. Use of ethanol for shortening results in carbon nanotubes with high quality, shorter lengths and minimum defects with no material loss unlike the other processes. As the shortening during ultrasonication is caused by the intercollision of neighbouring CNTs, the defects and kink sites further increase the defects depending on the shortening media, ultrasonication time and power [281]. Therefore a low impact ultrasonication process in a solvent which aids in only shortening or cutting the CNTs with minimal structural defects is preferred. These issues can be resolved most likely by using eco-friendly organic solvents that reduce defects and act only as media during the process and cutting takes place only by intercollision. Hence, in the present study facile mild method for cutting SWCNTs and MWCNTs with high dispersion, short lengths has been adapted and reported here.

Transmission electron microscopy and Raman spectroscopy have been used for the microstructural studies to confirm the reduction in length and as well as to understand the crystallinity. An increment of only ~0.1 in I_D/I_G ratio (Figure 7.5) indicated minimal or negligible defects in CNTs after shortening. Therefore, the present process is a viable one to yield CNTs with uniform lengths and large enough quantities for a wide range of applications. In this process, shortening of CNTs was carried out under ultrasonication for a few minutes to hours depending on the type of CNTs. SWCNTs and MWCNTs before and after shortening process were observed in TEM and characterized by Raman spectroscopy for other microstructural studies.

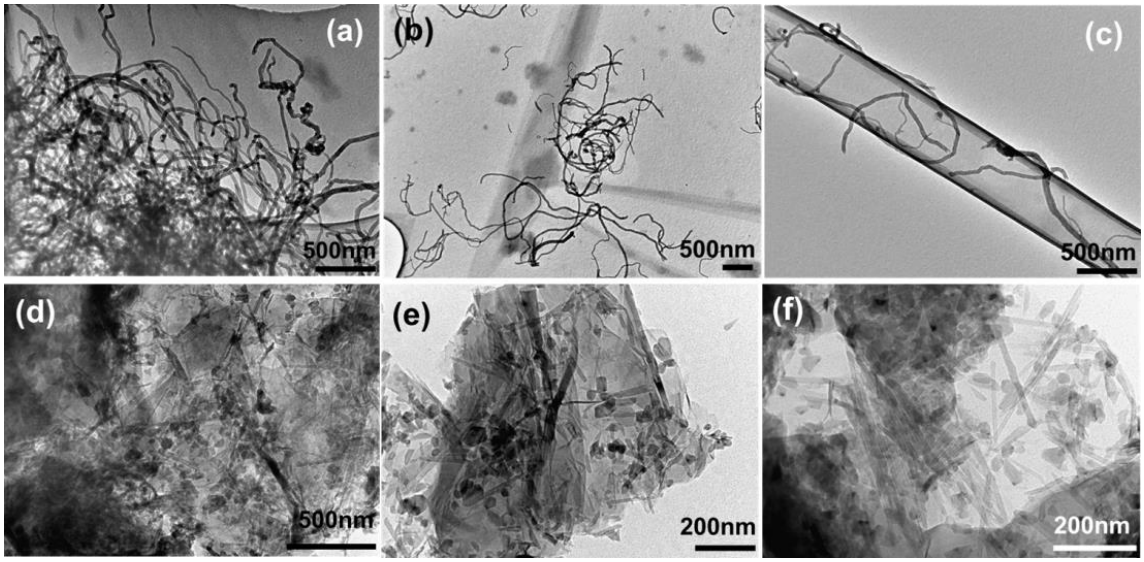

Figure 7.4 TEM micrographs of MWCNTs (a) & (d) as received MWCNTs and SWCNTs (0 min), (b) &(c) shortened MWCNTs after 60 and 120min and (e) & (f) shortened SWCNTs after 30 and 60min of ultrasonication.

Figure 7.4 (a-f) shows the TEM micrographs of the MWCNTs and SWCNTs before and after shortening respectively. It is clearly evident from these micrographs that, CNTs are shortened successfully from initial lengths of ~5-20 μm to submicron lengths of ~0.5- 2 μm within a short duration of 30–60 min for SWCNTs and 60-120 min for MWCNTs. Both SWCNTs and MWCNTs were shortened with minimal damage to the tubular structure (Figure 7.4). Use of ethyl alcohol, an organic solvent plays an important role in shortening, since it is neither acidic nor reacts with the CNT surface. It acts only as a medium during ultrasonication. It is anticipated that though the mechanism is similar to that of acidic media, in the present study, a simple solvent ethanol is used only to improve the wetting of the surface of the walls of the tube.

Initially, during ultrasonication, intercollision of CNTs occurs, which leads to the initiation of the scission of the side wall and then progressively cutting process takes place which is limited to the collision points locally [275]. Sonication induced scission has been reported earlier where nanotube scission arises from the fluid friction at the surface of the nanotubes in the radial elongational flow field that forms around a cavitation bubble [282]. An important point to note is that, in this study, the CNTs were neither functionalized nor oxidized unlike in prior methods/reports ([283, 284]). Functionalization of CNTs is generally required

prior to the shortening due to their hydrophobic nature. When these functionalized CNTs are further shortened in the acidic media, the process not only increases the defect sites, but also unzips the CNTs. The cutting process is faster at defect sites and continues from there, affecting the physical, chemical and mechanical properties of the shortened CNTs [285]. In the present study, in order to have defect-free CNTs, ethanol, which helps in wetting the surface of the walls of the CNTS that eases the dispersion of the CNTs is used as the solvent. Ethanol improves the wettability of the CNTs due to its lower contact angle compared to that of water and thus helps in the shortening process [286]. Therefore, during ultrasonication, bubbles nucleating at solid surfaces can push the tubes apart and nucleate the scission of the tube if they are wetted sufficiently by the fluid phase. The cutting process is well explained by power law, $L \sim t^{-m}$ [282] which is dependent on the power and time (t) used during ultrasonication. Exponent 'm' varies between 0.2-0.5 and L is the length of the CNTs.

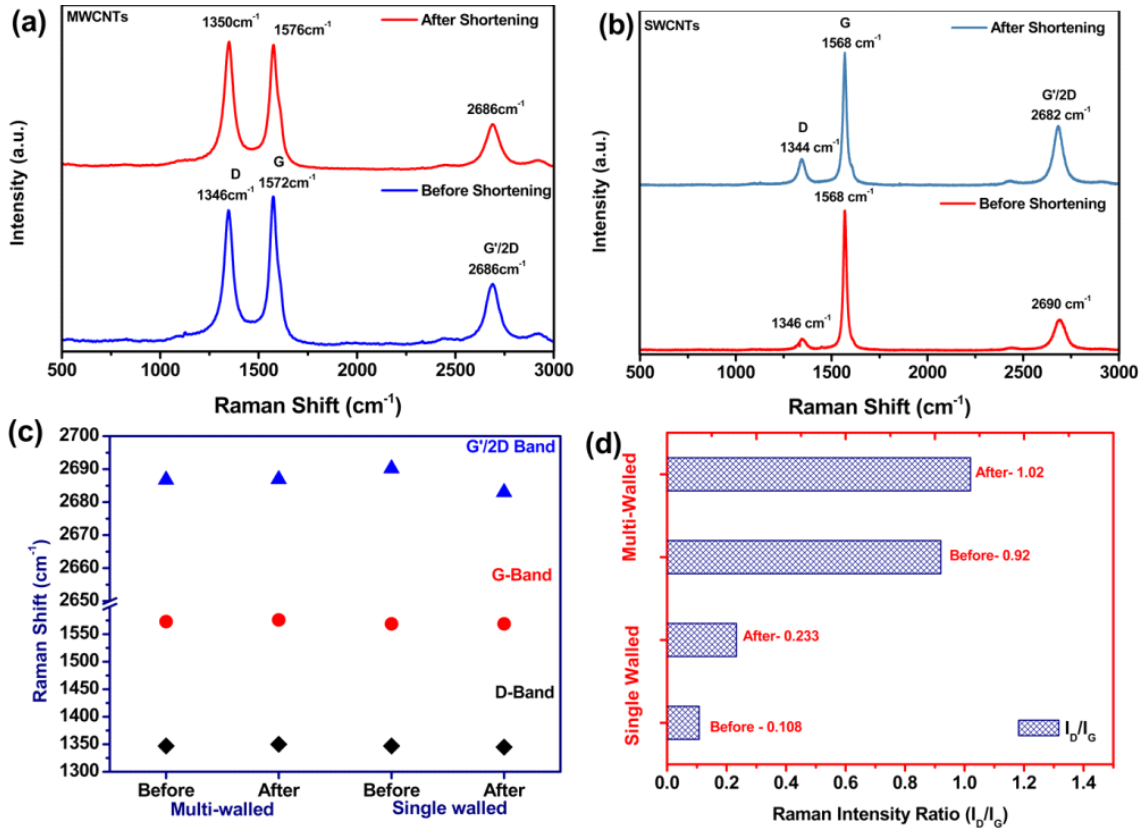

Figure 7.5 Raman spectra of (a) MWCNTs and (b) SWCNTs before and after shortening, (c) Raman peak shifts and (d) I_D/I_G ratios obtained from Raman spectra.

In order to study the presence of defects and the crystalline nature, the shortened CNTs were characterized by Raman spectroscopy (Figure 7.5 a-b). From Raman spectra, it has been observed that the D-band near 1350 cm^{-1} corresponds to the disordered, sp3-hybridized carbon present as defects, whereas the band at ~1575 cm^{-1} corresponds to the C–C stretching modes (G-band) representing the graphitic structure in carbon nanotubes. The 2D band can be used to observe specific changes that are sensitive than D-band. The D-band, G-band and 2D-bands observed for the MWCNTs and SWCNTs are shown in Figure 7.5(a-b). A small peak shift of ~6 cm^{-1} was observed in SWCNTs (Figure 7.5 c) after shortening. This shift is an indication of only negligible stresses/strains induced during the shortening process. Intensity ratio of D band to G band (D/G ratio) is generally used to evaluate the defects in the CNT walls. In the present study, a small increase of 0.92-1.02 and 0.10-0.23 of D/G ration (an increment of ~0.1 in the D/G ratio, compared to the as received CNTs) was observed for MWCNTs and SWCNTs respectively. Increment in the D/G ratio after the cutting process, often indicates a slight damage to the CNTs surface [188]. This damage could be on the sidewall or on the tubular structure of CNTs. From the Raman studies, it is confirmed that the shortening process did not induce noticeable defects in the graphitic structure. Further, the observed Raman spectra revealed that the shortening is limited to the collision points and resulted in holding the structure of CNTs. Ethanol might be helping in holding the graphitic structure, avoiding etching and formation of defects on the tube walls. Along with ultrasonication medium, duration of the process has a great influence on the cutting process. In the current study, SWCNTs required shorter (30-60 min) ultrasonic cation time as compared to that of MWCNTs (60-120 min). Although ultrasonication time and power decide the cutting efficiency according to a power law [282], ultrasonication in the organic solvent as a medium results in an efficient way of shortening the CNTs in large scale. Further, ethanol as a medium for shortening increases the efficiency of the process in terms of reduction in defects during shortening compared to several existing process [274, 276, 283, 284, 287]. These shortened CNTs are further used for co-deposition with copper.

7.3 Electrodeposition of shortened CNTs reinforced Cu composite foils

Once the shortening process is completed, the shortened CNTs were dried and functionalized as mentioned in the earlier section. Functionalized CNTs were dispersed in the electrolyte (experimental details in chapter 3) with a surfactant and Cu-CNT films were deposited by using PRED. In the present case as well, before depositing Cu-CNT composite, initially pure copper was deposited as a seed layer in order to peel off the composite foils from the substrate easily.

Figure 7.6 Scheme representing the co-deposition of short CNTs with copper.

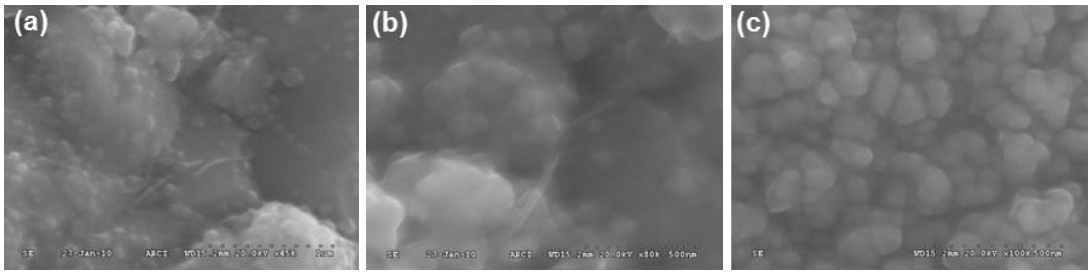

Figure 7.7 (a-c) FESEM micrographs of copper-CNT composite foils showing the presence of CNTs.

Figure 7.7 represents the scheme of co-deposited shortened CNTs and copper. After the deposition process, composite foils were characterized by FESEM for microstructural studies. From FESEM (Figure 7.7), it is evident that the compactness in Cu-CNT composite films is increased in comparison with those prepared using the long CNTs. In addition, less porosity and roughness was observed in these foils as the CNTs length has decreased.

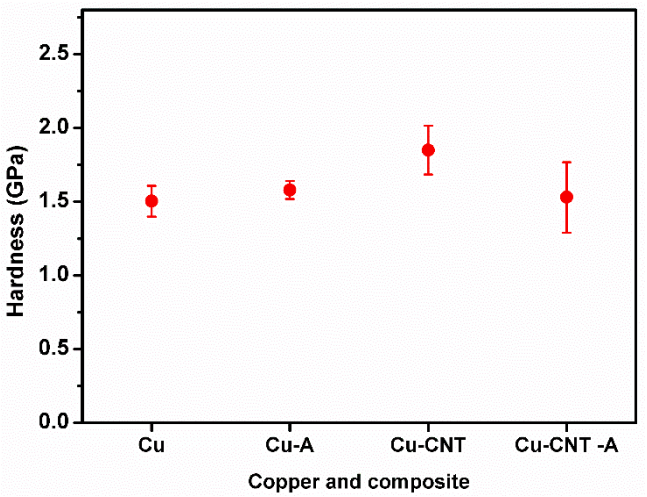

Figure 7.8 Hardness of Cu-CNT and pure copper foils prepared by PRED.

Hardness of Cu-CNT composite foils were determined by nanoindentation. From the Figure 7.8, it is clear that the hardness of Cu-CNT composites was improved slightly, exhibited a hardness of about ~1.8 GPa. This value is higher than that of the bulk copper (0.5-0.8 GPa). In contrast to that, hardness values were not uniform probably due to insufficient compactness and uniformity in the foils, although better than the composites prepared using longer CNTs. In addition, this behaviour was not noticed in the Cu-Gr composite foils. Therefore in order to improve the density and to reduce the porosity, the composite foils were annealed in argon atmosphere at 300°C for 30 min. The annealing of these composites have shown significant decrement in the hardness of to a value of ~1.4 GPa without any consistence. The reason could probably be the non-uniform dispersion and agglomeration of CNTs as bundles present in the matrix, which were observed in FESEM at few places of the composite.

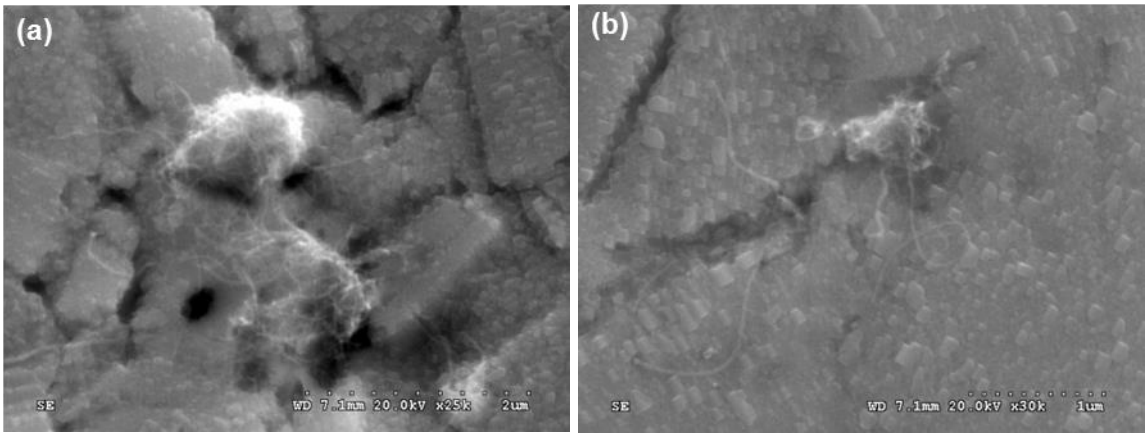

Figure 7.9 (a) & (b) FESEM micrograph showing CNT agglomerates in composite foil.

Figure 7.9 is a clear indication for the presence of agglomerated CNTs. Non-uniform distribution of CNTs was observed from TEM studies as well (Figure 7.10 c). Figures (Figure 7.10(a) and (b)) show TEM micrographs of the uniformly distributed CNTs and (c) the agglomerated CNTs in the composite foil.

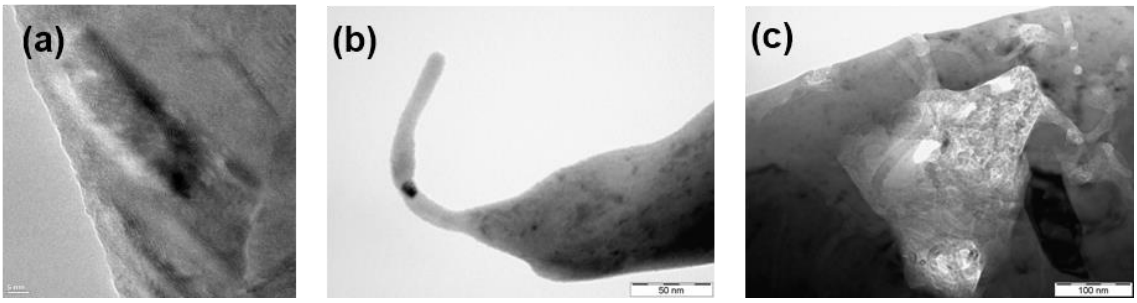

Figure 7.10 TEM micrographs of CNTs in composite indicates the (a,b) uniformly distributed CNTs and (c) agglomerates.

From Figure 7.10 it is observed that the CNTs were non-uniformly distributed at some places, although uniform dispersion is observed at majority of the areas in the composite foil. This might be due to the non-uniform dispersion of the CNTs throughout the matrix and agglomerates. Agglomeration could be due to the high surface energy of the CNTs, which tends CNTs to entangle and agglomerate which causes the poor density and roughness leading to poor mechanical properties. Therefore, as a final attempt, inorder to further improve the dispersion and interfacial bonding of CNTs with the matrix, copper was coated onto the CNTs

by electroless deposition and these copper coated CNTs were incorporated into copper matrix by PRED.

7.4 Electrodeposition of metal coated CNT reinforced copper composites

There are studies on electroless deposition of metal on CNTs such as Ni, Cu, Ag etc. because they possess better bonding between the CNTs and metal matrix. In this study as copper is the matrix and the application is focused towards the electronic industry, CNTs were coated by copper by electroless deposition prior to electrodeposition. In addition, copper exhibits high electrical conductivity and it may result in the enhanced conductivity of whole composite.

In this process, copper is coated on to the surface of CNTs by electroless deposition process (no usage of current) [288-290]. These coated CNTs could then be incorporated into metal matrices to produce new composites with novel properties. Here, deposited copper particles on CNTs are expected to avoid the agglomeration of CNTs in the plating bath and increase the interfacial bonding between Cu and CNTs during electrodeposition. In this process coating of copper on CNTs was attempted in two steps called sensitization-activation and metal deposition. Sensitization and activation provides the introduction of catalytic nuclei. These nuclei then initiates the redox reaction specifically on the activated surface. In this, Tin (Sn) sensitized layer enhances Palladium (Pd) adsorption as well as the binding strength of Pd to the surface and Pd acts as a catalyst for the metal to grow on CNT surface. The sensitized and activated CNTs were used for the electroless deposition of Cu. The complete experimental details for electroless deposition of Cu on CNTs surface were mentioned in the Chapter 3.

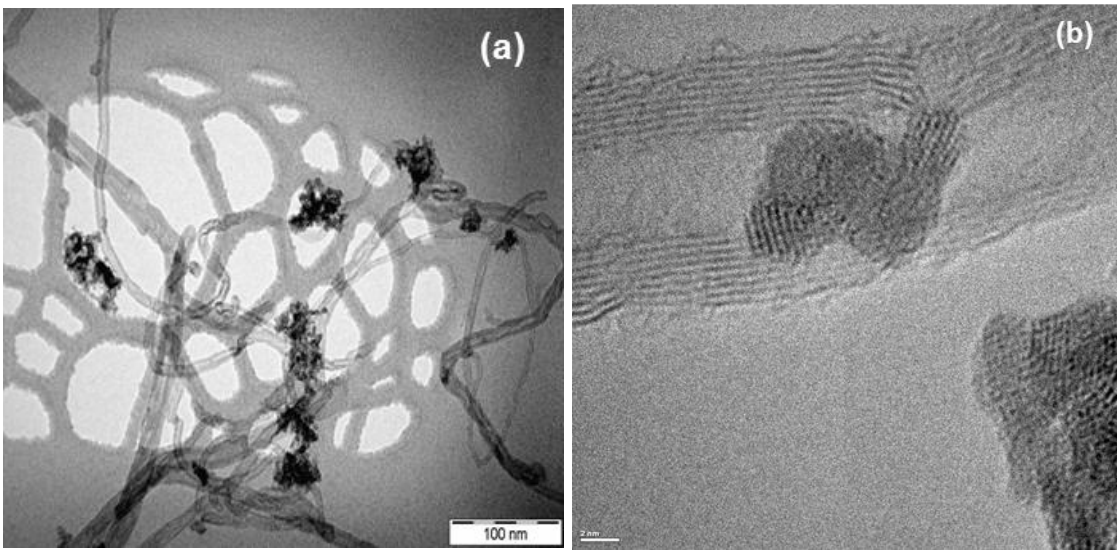

Figure 7.11 (a-b) Transmission electron micrographs of Cu coated on CNTs by electroless deposition.

Figure 7.11 shows the TEM micrograph of copper coated carbon nanotubes (Cu(CNT)) formed by electroless deposition

7.4.1 Electrodeposition of copper and copper coated carbon nanotubes (CNTs)

Although the copper has been coated by electroless deposition on CNT surface, the research on the metal coated CNTs reinforced composites has been reported only through powder metallurgy and other consolidation processes [289]. There are no reports on reinforcing metal coated CNTs into metal matrix by electrodeposition. Therefore, this work gives an idea to explore the metal coated CNTs incorporated by electrodeposition technique as well. In addition, electrodeposition is a wet method and the mechanical properties can be enhanced without application of heat treatments/melting of the metal and can be an appropriate method to employ for practical applications.

Pulse reverse electrodeposition (PRED) technique is employed to deposit the copper coated CNT reinforced copper composite films. Same pulse parameters which have been used to deposit the Cu-Gr composites has been applied in the present case as well.

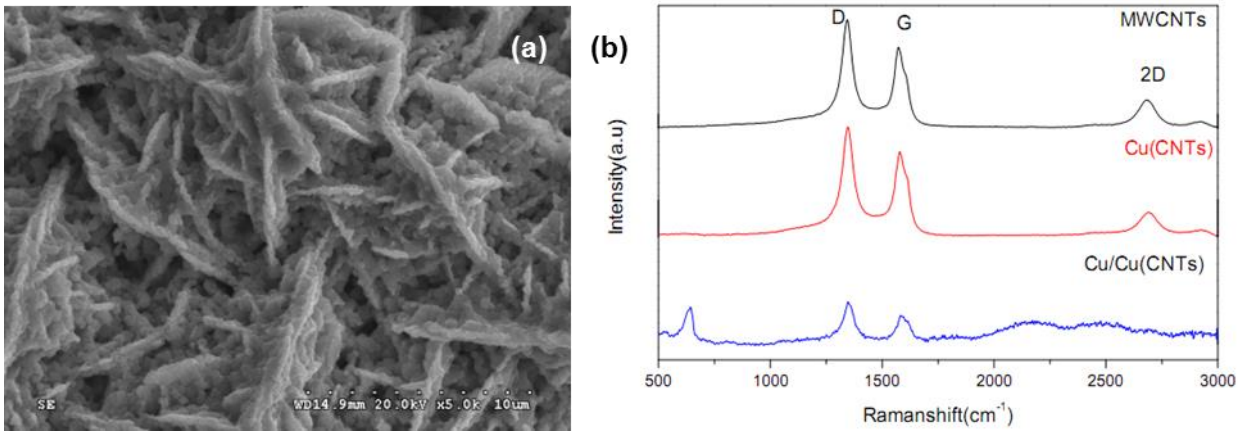

Figure 7.12 (a) Field emission scanning electron micrograph of Cu coated CNT- Cu composite and (b) Raman spectra for CNTs, Cu coated CNTs and Cu (CNTs)-Cu composite.

Figure 7.12 (a) shows the microstructure of composite foil, which is a different microstructure in comparison to that of Cu-CNTs composite and pure copper foils deposited with same pulse parameters. Further, the presence of CNTs in composite matrix was confirmed by Raman spectroscopy as shown in Figure 7.12 (b). From the above spectra, the presence of CNTs is evident in the composite. In Raman spectrum (Figure 7.12 (b)), bands near 1575 cm^{-1} called G-band (Graphitic band), a disordered band at 1350 cm^{-1} is called D-band confirmed the presence of CNTs. Additionally a band which has been appeared at 2691 cm^{-1} called second ordered D-band / G′-band. Strains and thermal stresses in the nanotubes can be measured from this band. In addition, for MWCNTs and Cu coated MWCNTs, notable difference in I_D/I_G ratio has not been observed. Hence, it appears that the electroless deposition of metal on CNTs and the process has not introduced any additional defects in CNTs. From Raman spectrum of composite, an additional peak was observed at 630 cm^{-1} due to the presence of very small amount of copper oxide on the surface of the composite foil. The hardness was determined for as-deposited and annealed copper coated CNTs reinforced Cu composite foils.

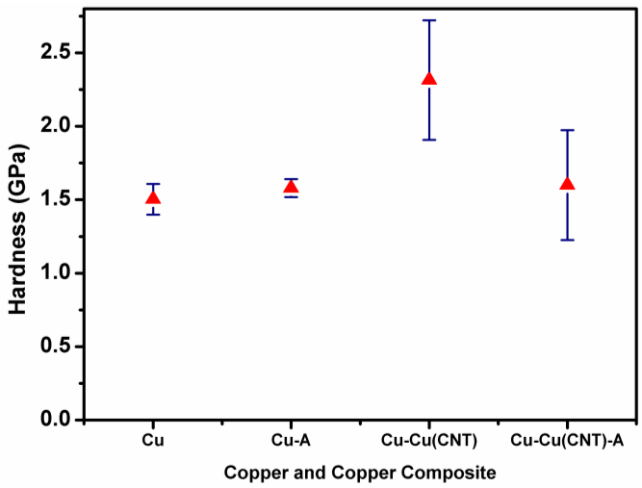

Figure 7.13 Hardness of copper coated CNTs reinforced composite foil.

Hardness of the composites was determined by nanoindentation. From Figure 7.13 metal coated CNT reinforced composites have shown a tremendous improvement in hardness in comparison to that of pure copper deposited with same pulse parameters. The enhancement in hardness is probably due to the better interface of copper which gives good interfacial bond between CNTs and copper matrix. In contrast, after annealing hardness is decreased similar to Cu-CNT composites.

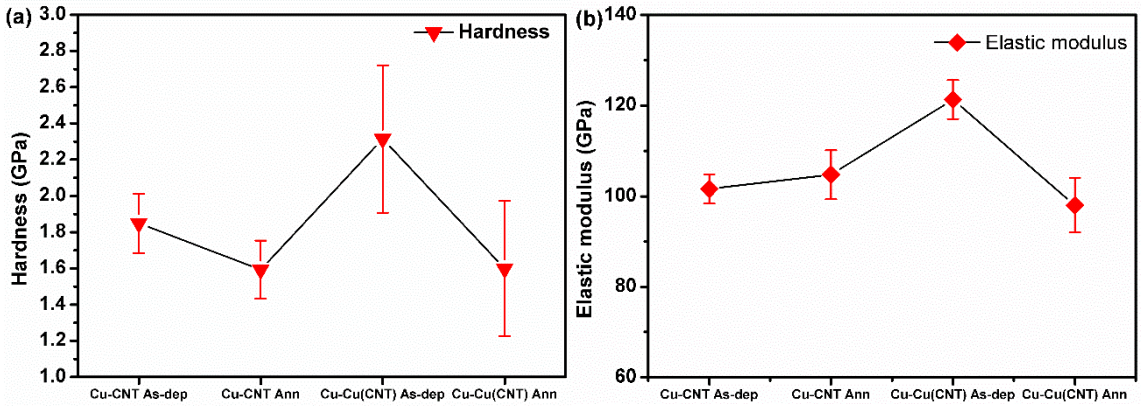

Figure 7.14 Mechanical properties of Cu-CNT and Cu coated CNT -Cu composites.

Mechanical properties of copper coated CNTs (Cu(Cu-CNT)) reinforced composites and Cu-CNT composites were compared in Figure 7.14. In comparison to that of Cu-CNT, Cu coated CNTs-Cu composites have shown better enhancement of the properties. However, reproducibility was not achieved in the Cu(Cu-CNT) composites and significant decrement in

properties was observed after annealing. These foils have shown the electrical resisitivty in the range of ~2.3-2.4 × 10^{-6} Ω-cm after annealing which could be due to the presence of oxygen functional groups attached to the CNTs.

7.5 Summary

The mechanical properties of Cu coated CNT reinforced copper composites have shown a significant enhancement of hardness (~2.4 GPa) compared to pure copper and Cu-CNT composites. However, the reproducibility in the mechanical properties was not observed in these foils. As a result, it can be concluded that the dispersion of CNTs is a major challenge, and it appears that non paractical for the industrial applications at this stage.

Chapter 8. Summary and conclusions

Preparation of highly textured free standing copper foils with control over the (111) (100) and (110) textures and twin density were prepared using PRED technique in an 'additive-free' electrolyte for the first time. The (111), (110) and (100) textures are confirmed by EBSD and XRD. The texture coefficient calculated for all the three textures was >2 suggesting that these copper foils are highly oriented in the respective directions. These copper foils have exhibited a high hardness in the range 2.0-2.7 GPa, while maintaining the electrical conductivity in the same range as that of bulk copper. Among the three textures and twinned foils, (111) textured foils exhibited higher hardness with an electrical resistivity in the range ~1.65-1.91×10^{-6} Ω-cm. The enhancement in the mechanical and electrical properties is probably due to a combined effect of grain size, texture and presence of coherent twin boundaries (CSLΣ3 boundaries). The room temperature stability of the copper foils was ascertained to ensure that these foils could be used in future practical electronic applications. These foils can easily be prepared in mass production by using this economical and environmental friendly PRED method.

Prior to the synthesis of Cu-Gr composite foils, an environmental friendly and upscalable electrochemical exfoliation process has been used to synthesize the graphene. For this exfoliation, an electrolyte containing HF and HNO_3, has been used for the first time to effectively exfoliated graphite to form a single to few layered graphene (1~6) sheets with lesser oxygen functional groups. The as prepared graphene has been characterized by TEM, Raman, XRD, FTIR and XPS to observe the number of layers, size of the graphene sheets, and to study the presence of functional groups on the surface of graphene respectively. Thereby these functional groups significantly improve the interfacial bonding with the matrix in the nanocomposites. Graphene sheets of controlled size and controlled number of layers could be prepared at large quantities, measuring up to several grams demonstrating the feasibility in industrial scale. The as prepared graphene has been used subsequently used as a reinforcement in Cu-Gr composites prepared by electrodeposition.

Graphene reinforced copper matrix composite foils are synthesized by using a complete electrochemical process, where graphene was prepared by electrochemical exfoliation and the

Summary and conclusions

Cu-Gr foils were made by a simple and economical PRED technique. By systematically varying the graphene concentration from 0-0.75 g/L in the electrolyte, a remarkable enhancement in the hardness from 1.5 GPa to ~2.7 GPa (~125% higher than bulk Copper) with increase in graphene content was achieved. Elastic modulus has increased from ~117 GPa to ~139 GPa (~30% higher than bulk copper) from P0-P5 with a slight decrement in modulus after annealing. A substantial decrement in the modulus to ~119 GPa, was observed for the as-deposited P75 foils. On further annealing these P75 foils the modulus has further decreased due to the possible annihilation of deposition-induced internal residual stresses, during annealing. From the hardness and modulus data, it can be concluded that the hardness increased continuously with increase in the amount of graphene in the matrix.The maximum modulus was achieved for 0.5 g/L (P5) graphene in the electrolyte and it was 139 GPa. On annelaing these samples at 573 K, the electrical resistivity has been reduced to ~2.3×10^{-6} Ω-cm, which is comparable to that of bulk copper. Most importantly the hardness and modulus of P5 are much higher and consistent, both for as-deposited and annealed foils when compared to the foils with other concentrations of graphene. These results clearly show the influence of graphene as a reinforcement material in tailoring the various properties of copper based composite foils.

To study the influence of pulse parameters, composite foils are also deposited using DC method with the optimized content of graphene (P5). Application of pulse reverse current has resulted in uniform distribution of Gr in the metal matrix compared to DC. Nanoindentation studies also showed that the PRED electrodeposited Cu-Gr composite foils have exhibited a high hardness of 2.2–2.5 GPa (increased by 96% of that of pure Cu) and good uniformity throughout the foils in terms of hardness compared to that observed for the DC deposited foils. The elastic modulus of the foils prepared by PRED have not shown considerable decrement in the hardness and modulus values after annealing indicating the promise of these foils for several applications. The superior mechanical properties obtained as already mentioned, are mainly due to fine grain size of the Cu matrix and presence of Gr as reinforcement and its uniform distribution throughout the matrix. The uniformity in the microstructural features of these novel nanocomposites can be attributed to the feasibility to optimize several pulse parameters unlike in DC deposition which allows variation of current density alone. Our present process is appropriate to prepare Cu-Gr composite foils with control over the

mechanical and electrical properties, as it is a scalable low temperature process, economical and can be prepared on substrates with complex shapes with good reproducibility.

For the comparative studies, several experiments have been performed, using the same set of pulse parameters which have been used for the preparation of copper-graphene composites, to synthesize Cu-CNT composites. Initially powder like deposition was obtained due to the presence of CNTs of several microns in length. Thereafter, the CNTs were shortened and deposited with copper in order to increase the dispersibility of the CNTs in the electrolyte. The mechanical properties including hardness and the modulus improved slightly. However, the hardness values were not uniform throughout the sample probably due to the non-uniform dispersion and agglomeration of CNTs in the matrix. This could be due to the high surface energy of the CNTs, which tends CNTs to entangle and agglomerate. Therefore, as a last attempt, inorder to further improve the dispersion of the CNTs, and also to improve the interfacial bonding between the CNTs, copper was coated onto the CNTs by electroless deposition and these copper coated CNTs were incorporated into copper matrix by PRED. However, reproducibility was not achieved with the Cu(Cu-CNT) composites and significant decrement in properties was observed after annealing. As a result, copper-CNT composites seem non paractical for the industrial applications at this stage based on our experimental investigations.

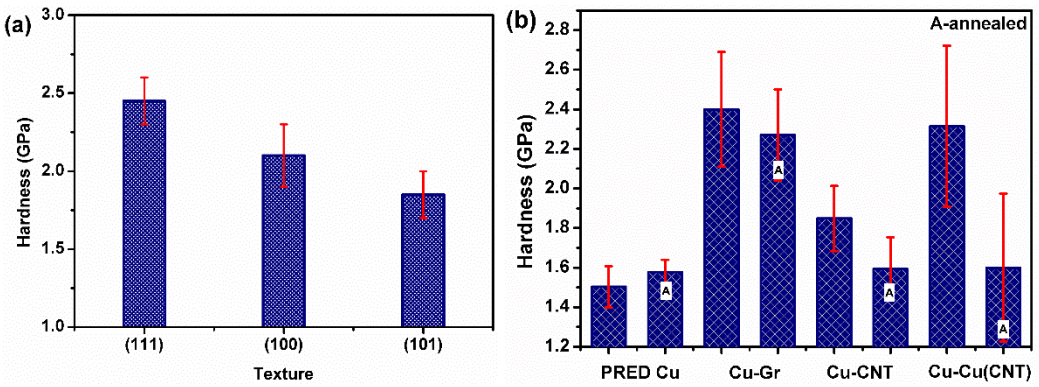

Figure 8.1 Variation of hardness in (a) highly textured copper foils and (b) copper nanocomposites prepared by PRED

From the strucutre-property correlations, it can be seen (Figure 8.1 a&b) that the required mechanical and electrical properties can be achieved in pure copper by simultaneously

controlling texture, introdcing CSL Σ3 coherent twin boundaries in addition to the grain refinement. For copper nanocomposites, graphene appears to be better reinforment material in terms of cost, reproducibility, industrial feasibility etc., compared to the CNTs. In addition, high aspect ratio and sheet like structure of 2D graphene is benificial in terms of better dispersion over 1D CNTs. Hence from Figure 8.1 depending on the requirement and operating conditions, textured pure copper and Cu-Gr composites could be used for industrial applications. Highly texured and twinned copper foils can be used for room temperature applications.Copper-graphene composite foils can be used even for slightly high temperature applications, where grain growth is inhibited by graphene and desired properties can be maintained.

Finally, the enhancement of mechanical properties could be probably possible by interfacial strengthening, where the load transfer depends on the interfacial bonding and shape of the reinforcement. In the current research, graphene has high aspect ratio with sheet like structure compared to CNTs. Therefore, two-dimensional structure of graphene crumpled, distributed and spread around grains is beneficial and is expected to enhance the mechanical properties by increasing the available interfacial contact area with the matrix compared to CNTs.

Chapter 9. Suggestions for future studies

- Microstructural details for the highly textured, twinned copper foils and copper nanocomposite foils.
- Micro-tensile testing of highly textured copper and copper nanocomposite foils to study the mechanical behavior.
- HRTEM studies on highly twinned copper foils prepared by PRED to study the twin boundary statistics.
- Identification of strengthening mechanism in copper nanocomposites and study the influence of 1D and 2D structure of CNTs and graphene.
- Strain rate sensitivity of pure copper and copper nanocomposite foils by nanoindentation to study the deformation mechanism.
- Modulus mapping for the Cu-Gr and Cu-CNT composite foils by nanoindentation to observe the dispersion and distribution of reinforcement in the copper matrix.
- Study on the enhancement of mechanical properties in Cu-CNT composites by increasing the dispersion and distribution of CNTs by coating Ni on CNTs.

The important outcomes of the work encouraged to further study where combination of CNTs and graphene reinforced copper composite foils prepared by PRED. The mechanical properties of PRED deposited pure copper, Cu-CNT, Cu-Cu (CNT), copper-graphene and Cu-Gr/CNT composites are discussed below. The initial results of Cu-CNT/graphene composites prepared by PRED have shown a significant increment in modulus up to ~150 GPa, which is higher than Cu-Gr composites are discussed in the following plot.

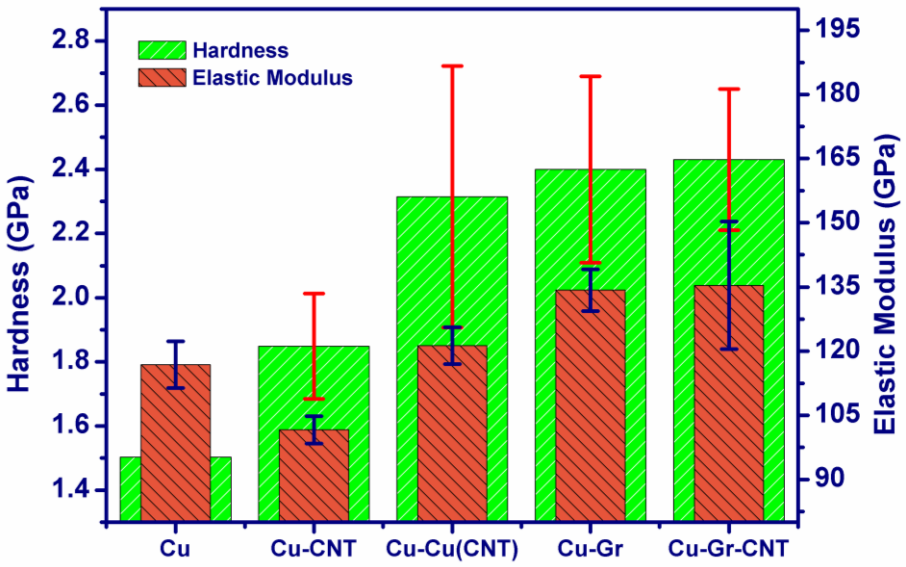

Figure 9.1 Hardness and modulus of copper nanocomposites

From the Figure 9.1 the outcomes of the present study suggested that the incorporation of CNTs alone may not probably enhance the properties, yet the combination of CNTs and graphene are expected to increase the modulus of composites along with the hardness compared to Cu-Gr. Therefore, it is suggested that the incorporation of graphene and CNTs can be an excellent alternative where CNTs are expected to form a network between graphene sheets where graphene is distributed through the grains and grain boundaries. The network of CNTs could increase the electrical conductivity and reinforcement of graphene takes care of mechanical properties. Hence, this can be a proposed work for the future in order to improve the electrical conductivity simultaneously with mechanical properties. In addition, the strain rate sensitivity of these composites can be an extended proposed work for advanced applications, where these composites are potential candidates for varied loading rate conditions.

9.1.1.1 Probable strengthening mechanism in Cu-Gr composites

The improved mechanical properties of the graphene reinforced nanocomposite foils in the current study could derive contributions from finer grain size of the matrix, twins in the matrix and probable operation of Orowan stengthening mechanism due to interaction between graphene sheets and lattice defects.

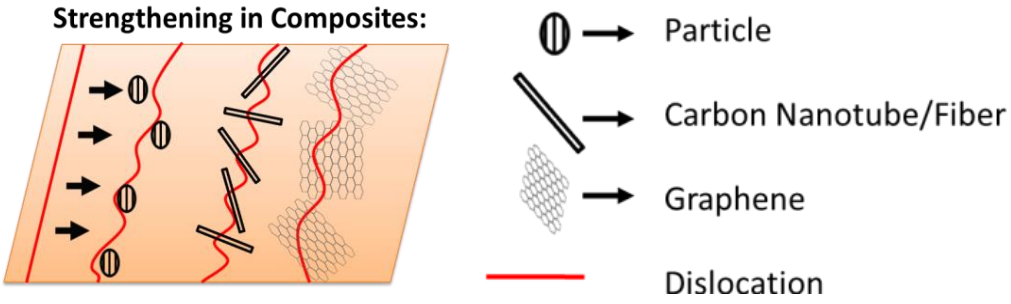

Figure 9.2 Possibility of Orowan looping in particles, tubes/fibers and graphene

The grain growth inhibition and maintaining the mechanical properties even after annealing could be due to the presence of graphene at the grain boundaries of composites which arrests the dislocation motion and grain growth. It is probable that a mechanism similar to Orowan mechanism might be operative in these novel composites. However, to fully understand this in greater detail, HRTEM and in-situ straining experiments in TEM have to be performed.

References

1. Lloyd, J. R. and J. J. Clement, Electromigration in copper conductors. Thin Solid Films, (1995), 262(1–2),135.

2. Basaran, Cemal and Minghui Lin, Damage mechanics of electromigration in microelectronics copper interconnects. International Journal of Materials and Structural Integrity, (2007), 1(1),16.

3. Council, International Copper Promotion. Copper users. http://www.copperindia.org/; Available from: http://www.copperindia.org/.

4. Copper and copper alloys, in Asm specialty handbook: Copper and copper alloys, ASM International, Editor. (2001), ASM International: USA.

5. Upadhyaya, Anish and G. S. Upadhyaya, Sintering of copper-alumina composites through blending and mechanical alloying powder metallurgy routes. Materials & Design, (1995), 16(1),41.

6. Chrysanthou, A. and G. Erbaccio, Production of copper-matrix composites by In-situ processing. Journal of Materials Science, (1995), 30,6339.

7. Ibrahim, I. A., F. A. Mohamed, and E. J. Lavernia, Particulate reinforced metal matrix composites - a review Journal of Materials Science, (1991), 26,1137.

8. Burroughes, Jeremy, Donal Bradley, and Richard Friend. Plastic electronics technology. Great British Innovation 2000; Available from: http://www.topbritishinnovations.org/ Future Innovations /Plastic Electronics.aspx.

9. Anderson, Timothy J. Copper diffusion barriers. Available from: http://www.che.ufl.edu /anderson/Diffusion_Barriers.htm.

10. Sakai, Y., K. Inoue, T. Asano, H. Wada, and H. Maeda, Development of highstrength, highconductivity Cu–Ag alloys for highfield pulsed magnet use. Applied Physics Letters, (1991), 59,2965.

11. Hu, Yanhong, Olge A Shenderova, Zushou Hu, Clifford W Padgett, and Donald W Brenner, Carbon nanostructures for advanced composites. Reports on Progress in Physics, (2006), 69,1847.

12. Hwang, Jaewon, Taeshik Yoon, Sung Hwan Jin, Jinsup Lee, Taek-Soo Kim, Soon Hyung Hong, and Seokwoo Jeon, Enhanced mechanical properties of graphene/copper nanocomposites using a molecular-level mixing process. Advanced Materials, (2013), DOI: 10.1002/adma.201302495.

13. Vidu, Ruxandra, Masoud Rahman, Morteza Mahmoudi, Marius Enachescu, Teodor Dan Poteca, and Ioan Opris, Nanostructures: A platform for brain repair and augmentation. Frontiers in Systems Neuroscience, (2014), 8.

14. Tan, C.M., Electromigration in ULSI interconnections. (2010): World Scientific.

15. Hara, Tohru, Kohji Sakata, and Yuji Yoshida Control of the (111) orientation in copper interconnection layer. Electrochemical and Solid-State Letters, (2002), 5(3),C41.

16. Ryu, Changsup, Alvin L. S. Loke, Takeshi Nogami, and S. Simon Wong. Effect of texture on the electromigration of cvd copper. in Proceedings of IEEE International Reliability Physics Symposium. 1997.

17. Lu, Lei, Yongfeng Shen, Xianhua Chen, Lihua Qian, and K. Lu, Ultrahigh strength and high electrical conductivity in copper. Science, (2004), 304,422.

18. Wei, H. L., Hanchen Huang, C. H. Woo, R. K. Zheng, G. H. Wen, and X. X. Zhang, Development of <110> texture in copper thin films. Applied Physic Letters, (2002), 80(13), 2290.

19. Liao, Chien-Neng, Yi-Cang Lu, and Di Xu, Modulation of crystallographic texture and twinning structure of cu nanowires by electrodeposition. Journal of the Electrochemical Society, (2013), 160(6),D207.

20. Lu, L., X. Chen, X. Huang, and K. Lu, Revealing the maximum strength in nanotwinned copper. Science, (2009), 323,607.

21. E.O, Hall, The deformation and ageing of mild steel: III discussion of results. Proceedings of Physical Society B, (1951), 64,747.

22. N.J, Petch, The cleavage strength of polycrystals. Journal of Iron and Steel Research, International (1953), 174,25.

23. Hansen, Niels, Hall–petch relation and boundary strengthening. Scripta Materialia, (2004), 51 801.

24. Baker, S. P., A. Kretschmann, and E. Arzt, Thermomechanical behavior of different texture components in cu thin films. Acta Materialia, (2001), 49,2145.

25. Toyoda, H., T. Kawanoue, S. Ito, M. Hasunuma, and H. Kaneko, Effects of aluminum texture on electromigration lifetime. Third international stress workshop on stress-induced phenomena in metallization.AIP Conference Proceedings, (1996), 373,169.

26. Randle, Valerie, Twinning-related grain boundary engineering. Acta Materialia, (2004), 52(14),4067.

27. Zhu, YT, XZ Liao, and XL Wu, Deformation twinning in nanocrystalline materials. Progress in Materials Science, (2012), 57(1),1.

28. Jang, Dongchan, Xiaoyan Li, Huajian Gao, and Julia R. Greer, Deformation mechanisms in nanotwinned metal nanopillars. Nature Nanotechnology, (2012), 7,594.

29. Lu, K., L. Lu, and S. Suresh, Strengthening materials by engineering coherent internal boundaries at the nanoscale. Science, (2009), 324,349.

30. Chen, Kuan-Chia, Wen-Wei Wu, Chien-Neng Liao, Lih-Juann Chen, and K. N. Tu, Observation of atomic diffusion at twin-modified grain boundaries in copper. Science, (2008), 321,1066.

31. Cui, B. Z., K. Han, Y. Xin, D. R. Waryoba, and A. L. Mbaruku, Highly textured and twinned cu films fabricated by pulsed electrodeposition. Acta Materialia, (2007), 55(13),4429.

32. Chan, Tsung-Cheng, Yu-Lun Chueh, and Chien-Neng Liao, Manipulating the crystallographic texture of nanotwinned Cu films by electrodeposition. Crystal Growth & Design, (2011), 11(11),4970.

33. Liu, Tao-Chi, Chien-Min Liu, Hsiang-Yao Hsiao, Jia-Ling Lu, Yi-Sa Huang, and Chih Chen, Fabrication and characterization of (111)-oriented and nanotwinned Cu by DC electrodeposition. Crystal Growth and Design, (2012), 12,5012.

34. Hsiao, Hsiang-Yao, Chien-Min Liu, Han-wen Lin, Tao-Chi Liu, Chia-Ling Lu, Yi-Sa Huang, Chih Chen, and K. N. Tu, Unidirectional growth of microbumps on (111)-oriented and nanotwinned copper. Science, (2012), 336,1007.

35. Sarada, Bulusu V., Ch. L. P. Pavithra, M. Ramakrishna, Tata N. Rao, and G. Sundararajan, Highly (111) textured copper foils with high hardness and high electrical conductivity by pulse reverse electrodeposition. Electrochemical and Solid-State Letters, (2010), 13(6),D40.

36. Xu, Luhua, Di Xu, K. N. Tu, Yuan Cai, Ning Wang, Pradeep Dixit, John H. L. Pang, and Jianmin Miao, Structure and migration of (112) step on (111) twin boundaries in nanocrystalline copper. Journal of Applied Physics, (2008), 104,113717.

37. Zhong, Sheng, Thomas Koch, Mu Wang, Torsten Scherer, Stefan Walheim, Horst Hahn, and Thomas Schimmel, Nanoscale twinned copper nanowire formation by direct electrodeposition. Small, (2009), 5(20),2265.

38. West, Alan C., Chin-Chang Cheng, and Brett C. Baker, Pulse reverse copper electrodeposition in high aspect ratio trenches and vias. Journal of the Electrochemical Society, (1998), 145(9),3070.

39. Quemper, Jean-Marie, Elisabeth Dufour-Gergam, Nad` ege Frantz-Rodriguez, Jean-Paul Gilles, Jean-Paul Grandchamp, and Alain Bosseboeuf, Effects of direct and pulse current on copper electrodeposition through photoresist molds. Journal of Micromechanics and Microengineering, (2000), 10,116.

40. Hu, Chi-Chang and Chi-Ming Wu, Effects of deposition modes on the microstructure of copper deposits from an acidic sulfate bath. Surface and Coatings Technology, (2003), 176,75.

41. Pearson, T. and J. K. Dennis, Effect of pulsed reverse current on the structure and hardness of copper deposits obtained from acidic electrolytes containing organic additives. Surface and Coatings Technology, (1990), 42,69.

42. Gu, Changdong, Hui Xu, and Tong-Yi Zhang, Fabrication of high aspect ratio through-wafer copper interconnects by reverse pulse electroplating. Journal of Micromechanics and Microengineering, (2009), 19(6),065011.

43. Oniciu, L. and L. Muresan, Some fundamental aspects of levelling and brightening in metal electrodeposition Journal of Applied Electrochemistry, (1991), 21,565.

44. Bakshi, S. R., D. Lahiri, and A.Agarwal, Carbon nantube reinforced metal matrix composites-a review. International Materials Reviews, (2010), 55(1),41.

45. Curtin, William A and Brian W Sheldon, Cnt-reinforced ceramics and metals. Materials Today, (2004), 7(11),44.

46. Khare, Rupesh and Suryasarathi Bose, Carbon nanotube based composites-a review. Journal of Minerals & Materials Characterization & Engineering, (2005), 4(1),31.

47. Huang, Xiao, Xiaoying Qi, Freddy Boey, and Hua Zhang, Graphene-based composites. Chemical Society Reviews, (2012), 41(2),666.

48. Kim, Y., J. Lee, M. S. Yeom, J. W. Shin, H. Kim, Y. Cui, J. W. Kysar, J. Hone, Y. Jung, S. Jeon, and S. M. Han, Strengthening effect of single-atomic-layer graphene in metal-graphene nanolayered composites. Nature Communications, (2013), 4,2114.

49. Geim, A. K. and K. S. Novoselov, The rise of graphene. Nature Materials, (2007), 6,183.

50. Su, Ching Yuan, Ang Yu Lu, Yanping Xu, Fu Rong Chen, Andrei N. Khlobystov, and Lain Jong Li, High-quality thin graphene films from fast electrochemical exfoliation. ACS Nano, (2011), 5(3),2332.

51. Park, Sungjin and Rodney S Ruoff, Chemical methods for the production of graphenes. Nature Nanotechnology, (2009), 4(4),217.

52. Lee, Dongju, Sung Ho Song, Jaewon Hwang, Sung Hwan Jin, Kwang Hyun Park, Bo Hyun Kim, Soon Hyung Hong, and Seokwoo Jeon, Enhanced mechanical properties of epoxy nanocomposites by mixing noncovalently functionalized boron nitride nanoflakes. Small, (2013), 9(15),2602.

53. Song, Sung Ho, Kwang Hyun Park, Bo Hyun Kim, Yong Won Choi, Gwang Hoon Jun, Dong Ju Lee, Byung-Seon Kong, Kyung-Wook Paik, and Seokwoo Jeon, Enhanced thermal conductivity of epoxy–graphene composites by using non-oxidized graphene flakes with non-covalent functionalization. Advanced Materials, (2013), 25 732.

54. Fan, Wei, Chao Zhang, Weng Weei Tjiu, and Tianxi Liu, Fabrication of electrically conductive graphene/polystyrene composites via a combination of latex and layer-by-layer assembly approaches. Journal of Materials Research, (2013), 28(4),611.

55. Low, C.T.J., R.G.A. Wills, and F.C. Walsh, Electrodeposition of composite coatings containing nanoparticles in a metal deposit. Surface Coatings Technology, (2006), 201,371.

56. Bicelli, Luisa Peraldo, Benedetto Bozzini, Claudio Mele, and Lucia D'Urzo, A review of nanostructural aspects of metal electrodeposition. International Journal of Electrochemical Science, (2008), 3(4),356.

57. Gurrappa, Injeti and Leo Binder, Electrodeposition of nanostructured coatings and their characterization—a review. Science and Technology of Advanced Materials, (2008), 9(4),043001.

58. Erb, U., Electrodeposited nanocrystals: Synthesis, properties and industrial applications. Nanostructured Materials, (1995), 6(5–8),533.

59. Landau, Uziel, Ernest Yeager, and Diane Kortan, "Plating-new prospects for an old art", electrochemistry in industry: New directions. (1982), New York: Plenum Press.

60. Centre, Naval Surface treatment. Electroplating. Available from: http://www.nstcenter.biz /writeup.aspx?title=Electroplating&page=TechResources Electroplating.html.

61. Schlesinger, Mordechay and Milan Paunovic, Modern electroplating. Vol. 55. (2011): John Wiley & Sons.

62. Avila, A. J. and M. J. Brown, Design factors in pulse plating. Plating, (1970), 57(11),1105.

63. Chandrasekar, M.S. and Malathy Pushpavanam, Pulse and pulse reverse plating — conceptual , advantages and applications. Electrochimica Acta, (2008), 53,3313.

64. Dynatronix. Pulse plating. Available from: http://www.dynatronix.com/learn/pulse-plating/.

65. Sharma, R.K., G. Shingh, and A.C. Rastogi, Solar Energy Materials and Solar Cells (2004), 82 201.

66. Mandich, NV, Pulse and pulse-reverse electroplating. Metal Finishing, (2000), 98(1),375.

67. Leisner, P., M. Fredenberg, and I. Belov, Transactions of the Institute of Metal Finishing, (2010), 88(5),243.

68. N.V.Mandich. HBM Engineering Co.: Lansing. p. 382.

69. E.J. Podlaha, D. Landolt, Pulse-reverse plating of nanocomposite thin-films. Journal of Electrochemical Society, (1997), 144, L200.

70. Vidrine, A.B. and E.J. Podlaha, Composite electrodeposition of ultrafine gamma-alumina particles in nickel matrices - Part I: Citrate and chloride electrolytes. Journal of Applied Electrochemistry, (2001), 31,461.

71. Podlaha, Elizabeth J., Selective electrodeposition of nanoparticulates into metal matrices. Nano Letters, (2001), 1(8),413.

72. Chaparro, Aperador, William Arnulfo, Lopez, and Enrique Vera, Electrodeposition of nickel plates on copper substrates using pc y prc. Revista Matéria, (2007), 12(4),583.

73. Kanani, Nasser, Chapter 4 - processes for the deposition of metallic coatings, in Electroplating, Nasser Kanani, Editor. (2004), Elsevier: Oxford. p. 87.

74. Gamburg, Y.D. and G. Zangari, Theory and practice of metal electrodeposition. (2011): Springer New York.

75. Ibl, N, Some theoretical aspects of pulse electrolysis. Surface Technology, (1980), 10(2),81.

76. Chang, L. M., Diffusion layer model for pulse reverse plating. Journal of Alloys and Compounds, (2008), 466(1–2),L19.

77. Guglielmi, N, Kinetics of the deposition of inert particles from electrolytic baths. Journal of the Electrochemical Society, (1972), 119(8),1009.

78. Celis, Jean-Pierre, JR Roos, and Christine Buelens, A mathematical model for the electrolytic codeposition of particles with a metallic matrix. Journal of the Electrochemical Society, (1987), 134(6),1402.

79. Hosford, W.F., Mechanical behavior of materials. (2005): Cambridge University Press.

80. Gleiter, H., Nanocrystalline materials. Progress in Materials Science, (1989), 33(4),223.

81. Nieh, T. G. and J. Wadsworth, Hall-petch relation in nanocrystalline solids. Scripta Metallurgica et Materialia, (1991), 25(4),955.

82. Siegel, Richard W. Mechanical properties of nanophase materials. in Materials Science Forum. 1996. Trans Tech Publ.

83. Carlton, C.E. and P.J. Ferreira, What is behind the inverse hall–petch effect in nanocrystalline materials? Acta Materialia, (2007), 55 3749.

84. Meyers, M.A. and K.K. Chawla, Mechanical behavior of materials. (2009): Cambridge University Press.

85. Field, David P., Textured structures, in Asm handbook: Metallography and microstructures, G.F. Vander Voort, Editor. (2004), ASM International. p. 215.

86. Jung, Anne, Stefan Diebels, Anjela Koblischka-Veneva, Jörg Schmauch, Afrooz Barnoush, and Michael R. Koblischka, Microstructural analysis of electrochemical coated open-cell metal foams by ebsd and nanoindentation. Advanced Engineering Materials, (2014), 16,15.

87. Föll, Prof. Dr. Helmut. Defects in crystals. Coincidence Lattice Sites; Available from: http://www.tf.uni-kiel.de/matwis/amat/def_en/kap_7/backbone/r7_1_2.html.

88. Randle, Valerie, The coincidence site lattice and the ‘sigma enigma'. Materials Characterization, (2001), 47,411.

89. Porter, D.A., K.E. Easterling, and M. Sherif, Phase transformations in metals and alloys, third edition (revised reprint). (2009), Taylor & Francis.

90. Chawla, N. and K.K. Chawla, Metal matrix composites. (2006): Springer US.

91. Thomson, C. B. and V. Randle, A study of twinning in nickel. Scripta Materialia, (1996), 35(3),385.

92. Wolf, U., F. Ernst, T. Muschik, M. W. Finnis, and H. F. Fischmeister, The influence of grain boundary inclination on the structure and energy of σ = 3 grain boundaries in copper. Philosophical Magazine A, (1992), 66(6),991.

93. Brandon, DG, The structure of high-angle grain boundaries. Acta Metallurgica, (1966), 14(11),1479.

94. Brandon, D. G., B. Ralph, S. Ranganathan, and M. S. Wald, A field ion microscope study of atomic configuration at grain boundaries. Acta Metallurgica, (1964), 12,813.

95. Randle, V., Grain boundary engineering: An overview after 25 years. Materials Science and Technology, (2010), 26(3),253.

96. Clyne, T.W. and P.J. Withers, An introduction to metal matrix composites. (1995): Cambridge University Press.

97. Reddy, A. K. N., Preferred orientations in nickel electro-deposits: I. The mechanism of development of textures in nickel electro-deposits. Journal of Electroanalytical Chemistry (1959), (1963), 6(2),141.

98. George, R., K. T. Kashyap, R. Rahul, and S. Yamdagni, Strengthening in carbon nanotube/aluminium (cnt/al) composites. Scripta Materialia, (2005), 53(10),1159.

99. Dieter, G.E. and D. Bacon, Mechanical metallurgy. (1988): McGraw-Hill.

100. Hull, D. and T.W. Clyne, An introduction to composite materials. (1996): Cambridge University Press.

101. Agarwal, Arvind, Srinivasa Rao Bakshi, and Debrupa Lahiri, Carbon nanotubes: Reinforced metal matrix composites. (2010): CRC press.

102. Hosseini, Sayed Abdollah and Habib Danesh Manesh, High-strength, high-conductivity ultra-fine grains commercial pure copper produced by ARB process. Materials & Design, (2009), 30(8),2911.

103. Habibi, Asiyeh, Mostafa Ketabchi, and Mohammad Eskandarzadeh, Nano-grained pure copper with high-strength and high-conductivity produced by equal channel angular rolling process. Journal of Materials Processing Technology, (2011), 211(6),1085.

104. Surekha, K. and A. Els-Botes, Development of high strength, high conductivity copper by friction stir processing. Materials & Design, (2011), 32(2),911.

105. Edalati, Kaveh, Kazutaka Imamura, Takanobu Kiss, and Zenji Horita, Equal-channel angular pressing and high-pressure torsion of pure copper: Evolution of electrical conductivity and hardness with strain. Materials Transactions, (2012), 53(1),123.

106. Efe, G Celebi, I Altinsoy, M Ipek, S Zeytin, and C Bindal, Effects of sic particle size on properties of Cu–SiC metal matrix composites. Acta Physica Polonica A, (2012), 121,251.

107. Yih, P and DD L Chung, Titanium diboride copper-matrix composites. Journal of Materials Science, (1997), 32(7),1703.

108. Safranek, W. H., The properties of electrodeposited metals and alloys. 2 ed. (1986), Orlando,FL: American Electroplaters and Surface Finishers Soc.

109. Seah, C. H., S. Mridha, and L. H. Chan, Dc/pulse plating of copper for trench/via filling. Journal of Materials Processing Technology, (2001), 114(3),233.

110. Han, K., R. P. Walsh, A. Ishmaku, V. Toplosky, L. Brandao, and J. D. Embury, High strength and high electrical conductivity bulk Cu. Philosophical Magazine, (2004), 84(34),3705.

111. Ma, E., Y. M. Wang, Q. H. Lu, M. L. Sui, L. Lu, and K. Lu, Strain hardening and large tensile elongation in ultrahigh-strength nano-twinned copper. Applied Physics Letters, (2004), 85(21),4932.

112. Lui, Guan-Tai, Delphic Chen, and Jui-Chao Kuo, EBSD characterization of twinned copper using pulsed electrodeposition. Journal of Physics D: Applied Physics, (2009), 42,215410.

113. Lu, Chia-Ling, Han-Wen Lin, Chien-Min Liu, Yi-Sa Huang, Tien-Lin Lu, Tao-Chi Liu, Hsiang-Yao Hsiao, Chih Chen, Jui-Chao Kuo, and King-Ning Tu, Extremely anisotropic single-crystal growth in nanotwinned copper. NPG Asia Mater, (2014), 6,e135.

114. Chen, Jian-hao, Chaun Jang, Shudong Xiao, Masa Ishigami, and Michael S. Fuhrer, Intrinsic and extrinsic performance limits of graphene devices on SiO_2. Nature Nanotechnology, (2008), 3,206.

115. Geim, Andre K. and Philip Kim, Carbon wonderland. Scientific American, (2008), 298,90.

116. Novoselov, K. S., A. K. Geim, S. V. Morozov, D. Jiang, Y. Zhang, S. V. Dubonos, I. V. Grigorieva, and A. A. Firsov, Electric field effect in atomically thin carbon films. Science, (2004), 306,666.

117. Katsnelson, Mikhail I., Graphene: Carbon in two dimensions. Materials Today, (2007), 10(1–2),20.

118. Dong, Liang-Xu and Qiang Chen, Properties, synthesis, and characterization of graphene. Frontiers of Materials Science in China, (2010), 4(1),45.

119. Tsoukleri, Georgia, John Parthenios, Konstantinos Papagelis, Rashid Jalil, Andrea C Ferrari, Andre K Geim, Kostya S Novoselov, and Costas Galiotis, Subjecting a graphene monolayer to tension and compression. Small, (2009), 5(21),2397.

120. Fujitsu develops technology for low-temperature full-service direct formation of graphene transistors on large-scale (2009), phys.org.

121. Zhao, Jinping, Songfeng Pei, Wencai Ren, Libo Gao, and Hui-Ming Cheng, Efficient preparation of large-area graphene oxide sheets for transparent conductive films. ACS Nano, (2010), 4(9),5245.

122. Torres, Jaime A. and Richard B. Kaner, Graphene synthesis: Graphene closer to fruition. Nature Materials, (2014), 13(4),328.

123. Choi, Wonbong, Indranil Lahiri, Raghunandan Seelaboyina, and Yong Soo Kang, Synthesis of graphene and its applications: A review. Critical Reviews in Solid State and Materials Sciences, (2010), 35(1),52.

124. Avouris, Phaedon and Christos Dimitrakopoulos, Graphene: Synthesis and applications. Materials Today, (2012), 15(3),86.

125. Lang, B, A LEED study of the deposition of carbon on platinum crystal surfaces. Surface Science, (1975), 53(1),317.

126. Rokuta, E, Y Hasegawa, A Itoh, K Yamashita, T Tanaka, S Otani, and C Oshima, Vibrational spectra of the monolayer films of hexagonal boron nitride and graphite on faceted Ni (755). Surface Science, (1999), 427,97.

127. Shioyama, H, Cleavage of graphite to graphene. Journal of Materials Science Letters, (2001), 20(6),499.

128. Novoselov, KS, D Jiang, F Schedin, TJ Booth, VV Khotkevich, SV Morozov, and AK Geim, Two-dimensional atomic crystals. Proceedings of the National Academy of Sciences of the United States of America, (2005), 102(30),10451.

129. Novoselov, K. S., V. I. Fal'ko, L. Colombo, P. R. Gellert, M. G. Schwab, and K. Kim, A roadmap for graphene. Nature, (2012), 490,192.

130. Zhu, Yanwu, Shanthi Murali, Weiwei Cai, Xuesong Li, Ji Won Suk, Jeffrey R. Potts, and Rodney S. Ruoff, Graphene and graphene oxide: Synthesis, properties, and applications. Advanced Materials, (2010), 22(35),3906.

131. Cai, Minzhen, Daniel Thorpe, Douglas H. Adamson, and Hannes C. Schniepp, Methods of graphite exfoliation. Journal of Materials Chemistry, (2012), 22(48),24992.

132. Chung, D. D. L., Exfoliation of graphite. Journal of Materials Science, (1987), 22(12),4190.

133. Parvez, Khaled, Zhong-Shuai Wu, Rongjin Li, Xianjie Liu, Robert Graf, Xinliang Feng, and Klaus Müllen, Exfoliation of graphite into graphene in aqueous solutions of inorganic salts. Journal of the American Chemical Society, (2014), 136(16),6083.

134. Ogino, Isao, Yuya Yokoyama, Shinichiro Iwamura, and Shin R. Mukai, Exfoliation of graphite oxide in water without sonication: Bridging length scales from nanosheets to macroscopic materials. Chemistry of Materials, (2014), 26(10),3334.

135. Lotya, Mustafa, Yenny Hernandez, Paul J. King, Ronan J. Smith, Valeria Nicolosi, Lisa S. Karlsson, Fiona M. Blighe, Sukanta De, Zhiming Wang, I. T. McGovern, Georg S. Duesberg, and Jonathan N. Coleman, Liquid phase production of graphene by exfoliation of graphite in surfactant/water solutions. Journal of the American Chemical Society, (2009), 131(10),3611.

136. Hernandez, Yenny, Valeria Nicolosi, Mustafa Lotya, Fiona M. Blighe, Zhenyu Sun, Sukanta De, I. T. McGovern, Brendan Holland, Michele Byrne, Yurii K. Gun'Ko, John J. Boland, Peter Niraj, Georg Duesberg, Satheesh Krishnamurthy, Robbie Goodhue, John Hutchison, Vittorio Scardaci, Andrea C. Ferrari, and Jonathan N. Coleman, High-yield production of graphene by liquid-phase exfoliation of graphite. Nature Nanotechnology, (2008), 3(9),563.

137. McAllister, Michael J, Je-Luen Li, Douglas H Adamson, Hannes C Schniepp, Ahmed A Abdala, Jun Liu, Margarita Herrera-Alonso, David L Milius, Roberto Car, and Robert K Prud'homme, Single sheet functionalized graphene by oxidation and thermal expansion of graphite. Chemistry of Materials, (2007), 19(18),4396.

138. Viculis, L. M., J. J. Mack, and R. B. Kaner, A chemical route to carbon nanoscrolls. Science, (2003), 299(5611),1361.

139. Berger, C., Z. M. Song, T. B. Li, X. B. Li, A. Y. Ogbazghi, R. Feng, Z. T. Dai, A. N. Marchenkov, E. H. Conrad, P. N. First, and W. A. de Heer, Ultrathin epitaxial graphite: 2d electron gas properties and a route toward graphene-based nanoelectronics. Journal of Physical Chemistry B, (2004), 108(52),19912.

140. Land, TA, Th Michely, RJ Behm, JC Hemminger, and G Comsa, Stm investigation of single layer graphite structures produced on pt (111) by hydrocarbon decomposition. Surface Science, (1992), 264(3),261.

141. Nagashima, Ayato, Kenji Nuka, Hiroshi Itoh, Takeo Ichinokawa, Chuhei Oshima, and Shigeki Otani, Electronic states of monolayer graphite formed on tic (111) surface. Surface Science, (1993), 291(1),93.

142. Datta, Sujit S, Douglas R Strachan, Samuel M Khamis, and AT Charlie Johnson, Crystallographic etching of few-layer graphene. Nano Letters, (2008), 8(7),1912.

143. Gass, Mhairi H, Ursel Bangert, Andrew L Bleloch, Peng Wang, Rahul R Nair, and AK Geim, Free-standing graphene at atomic resolution. Nature Nanotechnology, (2008), 3(11),676.

144. Meyer, Jannik C, CO Girit, MF Crommie, and A Zettl, Hydrocarbon lithography on graphene membranes. Applied Physics Letters, (2008), 92(12),123110.

145. Horiuchi, Shigeo, Takuya Gotou, Masahiro Fujiwara, Toru Asaka, Tadahiro Yokosawa, and Yoshio Matsui, Single graphene sheet detected in a carbon nanofilm. Applied Physics Letters, (2004), 84(13),2403.

146. Yu, Li, Satoshi Yasuda, and Kei Murakoshi, Synthesis of nanometer size single layer grapheneby moderate electrochemical exfoliation. Transactions of the Materials Research Society of Japan, (2012), 37(2),209.

147. Liu, Na, Fang Luo, Haoxi Wu, Yinghui Liu, Chao Zhang, and Ji Chen, One-step ionic-liquid-assisted electrochemical synthesis of ionic-liquid-functionalized graphene sheets directly from graphite. Advanced Functional Materials, (2008), 18(10),1518.

148. Ebbesen, Thomas W, Carbon nanotubes: Preparation and properties. (1996): CRC press.

149. Zhu, Yanwu, Shanthi Murali, Weiwei Cai, Xuesong Li, Ji Won Suk, Jeffrey R. Potts, and Rodney S. Ruoff, Graphene and graphene oxide: Synthesis, properties, and applications. Advanced Materials, (2010), 22,3906.

150. Pfautsch, Emily, Challenges in commercializing carbon nanotube composites. WISE Intern, (2007),1.

151. Kim, K. T., S. I. Cha, T. Gemming, J. Eckert, and S. H. Hong, The role of interfacial oxygen atoms in the enhanced mechanical properties of carbon-nanotube-reinforced metal matrix nanocomposites. Small, (2008), 4(11),1936.

152. Lee, Changgu, Xiaoding Wei, Jeffrey W. Kysar, and James Hone, Measurement of the elastic properties and intrinsic strength of monolayer graphene. Science, (2008), 321,385.

153. Balandin, Alexander A., Thermal properties of graphene and nanostructured carbon materials. Nature Materials, (2011), 10,569.

154. Rafiee, Mohammad A., Javad Rafiee, Zhou Wang, Huaihe Song, Zhong-Zhen Yu, and Nikhil Koratkar, Enhanced mechanical properties of nanocomposites at low graphene content. ACS Nano, (2009), 3(12),3884.

155. Stankovich, Sasha, Dmitriy A Dikin, Geoffrey HB Dommett, Kevin M Kohlhaas, Eric J Zimney, Eric A Stach, Richard D Piner, SonBinh T Nguyen, and Rodney S Ruoff, Graphene-based composite materials. Nature, (2006), 442(7100),282.

156. S.Walker, Luke, Victoria R. Marotto, Mohammad A. Rafiee, Nikhil Koratkar, and Erica L. Corra, Toughening in graphene ceramic composites. ACS Nano, (2011), 5(4),3182.

157. Wang, Jingyue, Zhiqiang Li, Genlian Fan, Huanhuan Pan, Zhixin Chen, and Di Zhang, Reinforcement with graphene nanosheets in aluminum matrix composites. Scripta Materialia, (2012), 66(8),594.

158. Bartolucci, Stephen F., Joseph Paras, Mohammad A. Rafiee, Javad Rafiee, Sabrina Lee, Deepak Kapoor, and Nikhil Koratkar, Graphene – aluminum nanocomposites. Materials Science and Engineering A, (2011), 528,7933.

159. Kuang, Da, Liye Xu, Lei Liu, and Wenbin Hu, Graphene-nickel composites. Applied Surface Science, (2013), 273,484.

160. Chen, Lian-Yi, Hiromi Konishi, Axel Fehrenbacher, Chao Ma, Jia-Quan Xu, Hongseok Choi, Hui-Fang Xu, Frank E. Pfefferkorna, and Xiao-Chun L, Novel nanoprocessing route for bulk graphene nanoplatelets reinforced metal matrix nanocomposites. Scripta Materialia, (2012), 67,29.

161. Rashad, M., F. Pan, M. Asif, and A. Ullah, Improved mechanical properties of magnesium–graphene composites with copper–graphene hybrids. Materials Science and Technology, 0(0),1743284714Y.0000000726.

162. Chu, Ke and Chengchang Jia, Enhanced strength in bulk graphene–copper composites. Physica Status Solidi A, (2014), 211(1),184.

163. Goli, Pradyumna, Hao Ning, Xuesong Li, Ching Yu Lu, Konstantin S Novoselov, and Alexander A Balandin, Thermal properties of graphene–copper–graphene heterogeneous films. Nano Letters, (2014), 14(3),1497.

164. Boden, André, Benji Boerner, Patryk Kusch, Izabela Firkowska, and Stephanie Reich, Nanoplatelet size to control the alignment and thermal conductivity in copper-graphite composites. Nano Letters, (2014).

165. Qu, Dong, Fangzhi Li, Haibin Zhang, Qian Wang, Tianliang Zhou, Chunfeng Hu, and Rongjun Xie, Preparation of graphene nanosheets/copper composite by spark plasma sintering. Advanced Materials Research, (2014), 833,276.

166. Cui, Ye, Lidong Wang, Bin Li, Guojian Cao, and Weidong Fei, Effect of ball milling on the defeat of few-layer graphene and properties of copper matrix composites. Acta Metallurgica Sinica (English Letters), (2014), 27(5),937.

167. Tang, Yanxia, Xiaomin Yang, Rongrong Wang, and Maoxin Li, Enhancement of the mechanical properties of graphene–copper composites with graphene–nickel hybrids. Materials Science and Engineering: A, (2014), 599(0),247.

168. Li, Meixia, Hongwei Che, Xiaoyan Liu, Shunxing Liang, and Hailong Xie, Highly enhanced mechanical properties in cu matrix composites reinforced with graphene decorated metallic nanoparticles. Journal of Materials Science, (2014), 49(10),3725.

169. Zhao, Chao and Jun Wang, Fabrication and tensile properties of graphene/copper composites prepared by electroless plating for structrual applications. physica status solidi (a), (2014), 211(12),2878.

170. Kim, W. J., T. J. Lee, and S. H. Han, Multi-layer graphene/copper composites: Preparation using high-ratio differential speed rolling, microstructure and mechanical properties. Carbon, (2014), 69(0),55.

171. Huang, Hai, Xiaobin Tang, Feida Chen, Yahui Yang, Jian Liu, Huan Li, and Da Chen, Radiation damage resistance and interface stability of copper–graphene nanolayered composite. Journal of Nuclear Materials, (2015), 460(0),16.

172. Arai, Susumu, Yoriyuki Suwa, and Morinobu Endo, Cu/multiwalled carbon nanotube composite films fabricated by pulse-reverse electrodeposition. Journal of Electrochemical Society, (2011), 158(2),D49.

173. Jagannadham, K., Thermal conductivity of copper-graphene composite films synthesized by electrochemical deposition with exfoliated graphene platelets. Metallurgical and Materials Transactions B: Process Metallurgy and Materials Processing Science, (2012), 43B,316.

174. Kasichainula, Jagannadham, Electrical conductivity of copper – graphene composite films synthesized by electrochemical deposition with exfoliated graphene platelets. Journal of Vacuum Science & Technology B, (2012), 30(3),03D109.

175. Xie, Guoxin, Mattias Forslund, and Jinshan Pan, Direct electrochemical synthesis of reduced graphene oxide (RGO)/copper composite films and their electrical/electroactive properties. ACS applied materials & interfaces, (2014), 6(10),7444.

176. Koltsova, Tatyana S., Larisa I. Nasibulina, Ilya V. Anoshkin, Vasily V. Mishin, Esko I. Kauppinen, Oleg V. Tolochko, and Albert G. Nasibulin, New hybrid copper composite materials based on carbon nanostructures. Journal of Materials Science and Engineering B, (2012), 2(4),240.

177. Pavithra, C.L.P., B.V. Sarada, K.V. Rajulapati, T.N. Rao, and G. Sundararajan, A new electrochemical approach for the synthesis of copper-graphene nanocomposite foils with high hardness. Scientific Reports, (2014), 4,4049.

178. Chen, Q., Carbon nanotube reinforced metal composites. (2010), Google Patents.

179. Chai, Guangyu, Ying Sun, Jianren 'Jenny' Sun, and Quanfang Chen, Mechanical properties of carbon nanotube – copper nanocomposites. Journal of Micromechanics and Microengineering, (2008), 035013(18),1.

180. Byrne, Michele T. and Yurii K. Gun'ko, Recent advances in research on carbon nanotube–polymer composites. Advanced Materials, (2010), 22, 1672.

181. Samal, Subhranshu Sekhar and Smrutisikha Bal, Carbon nanotube reinforced ceramic matrix composites- a review Journal of Minerals & Materials Characterization & Engineering, (2008), 7 (4),355.

182. Andrews, R and MC Weisenberger, Carbon nanotube polymer composites. Current Opinion in Solid State and Materials Science, (2004), 8(1),31.

183. Subramaniam, C., T. Yamada, K. Kobashi, A. Sekiguchi, D. N. Futaba, M. Yumura, and K. Hata, One hundred fold increase in current carrying capacity in a carbon nanotube-copper composite. Nature Communications, (2013), 4,2202.

184. Sun, Ying, Jianren Sun, Miao Liu, and Quanfang Chen, Mechanical strength of carbon nanotube–nickel nanocomposites. Nanotechnology, (2007), 18(50),505704.

185. Schwartz, A.J., M. Kumar, B.L. Adams, and D. Field, Electron backscatter diffraction in materials science. (2010): Springer US.

186. Cullity, B.D. and S.R. Stock, Elements of x-ray diffraction. (2001): Prentice Hall.

187. Lewis, I.R. and H. Edwards, Handbook of raman spectroscopy: From the research laboratory to the process line. (2001): CRC Press.

188. Kumar, C.S.S.R., Raman spectroscopy for nanomaterials characterization. (2012): Springer.

189. Larkin, P., Infrared and raman spectroscopy; principles and spectral interpretation. (2011): Elsevier Science.

190. Williams, D.B. and C.B. Carter, Transmission electron microscopy: A textbook for materials science. (2009): Springer.

191. van der Heide, P., X-ray photoelectron spectroscopy: An introduction to principles and practices. (2011): Wiley.

192. Varam, Sreedevi, P. V. S. L. Narayana, Muvva D. Prasad, D. Chakravarty, Koteswararao V. Rajulapati, and K. Bhanu Sankara Rao, Strain rate sensitivity of bulk multi-phase nanocrystalline al–w-based alloy. Philosophical Magazine Letters, (2014), 94(9),582.

193. Fischer-Cripps, A.C., Nanoindentation. (2013): Springer New York.

194. Oliver, W.C. and G.M. Pharr, An improved techniques for determining hardness and elastic modulus using load and displacement sensing indentation experiments. Journal of Materials Research, (1992), 7(6),1564.

195. Oliver, W.C. and G.M. Pharr, Measurement of hardness and elastic modulus by instrumented indentation: Advances in understanding and refinements to methodology. Journal of Materials Research, (2004), 19(1),3.

196. Chmiela, B and M Sozańska, Analysis of high angle boundaries in directionally solidified turbine blade made of cmsx-4® superalloy. IOP Conference Series: Materials Science and Engineering, (2011), 22(1),012008.

197. Huang, Hanchen, H. L. Wei, C. H. Woo, and X. X. Zhang, Copper thin film of alternating textures. Applied Physics Letters, (2003), 82(24),4265.

198. Muresan, Liana, Liviu Oniciu, Michel Froment, and Georges Maurin, Inhibition of lead electrocrystallization by organic additives. Electrochimica Acta, (1992), 37(12),2249.

199. Kim, S. H., H. J. Sohn, Y. C. Joo, Y. W. Kim, T. H. Yim, H. Y. Lee, and T. Kang, Effect of saccharin addition on the microstructure of electrodeposited fe–36 wt.% ni alloy. Surface and Coatings Technology, (2005), 199(1),43.

200. Hong, Bo, Chuan-hai Jiang, and Xin-jian Wang, Texture of electroplated copper film under biaxial stress. Materials Transactions, (2006), 47(9),2299.

201. Thompson, C. V., Coarsening of particles on a planar substrate: Interface energy anisotropy and application to grain growth in thin films Acta Metallurgica, (1988), 36(11),2929.

202. McLean, M. and B. Gale, Surface energy anisotropy by an improved thermal grooving technique. Philosophical Magazine, (1969), 20(167),1033.

203. Kozlov, V. M. and L. Peraldo Bicelli, Texture formation of electrodeposited fcc metals. Materials Chemistry and Physics, (2003), 77(1),289.

204. Nielsen, C Bergenstof, A Horsewell, and MJL Østergard, On texture formation of nickel electrodeposits. Journal of Applied Electrochemistry, (1997), 27(7),839.

205. Wang, S. G., E. K. Tian, and C. W. Lung, Surface energy of arbitrary crystal plane of bcc and fcc metals. Journal of Physics and Chemistry of Solids, (2000), 61(8),1295.

206. Stokes, Robert J and D Fennell Evans, Fundamentals of interfacial engineering. (1997): John Wiley & Sons.

207. Zielinski, E. M., R. P. Vinci, and J. C. Bravman, The influence of strain energy minimization on abnormal grain growth in copper thin films. MRS Proceedings, (1995), 391,103.

208. Thompson, C. V., Texture evolution during grain growth in polycrystalline films. Scripta Metallurgica et Materialia, (1993), 28(2),167.

209. Dubin, V. M., G. Morales, C. Ryu, and S. S. Wong. in Materials Research Society Symposium Proceedings. 1998.

210. Lee, Haebum and S. Simon Wong, Correlation of stress and texture evolution during self- and thermal annealing of electroplated cu films. Journal of Applied Physics, (2003), 93(7),3796.

211. Wei, H. L., Hanchen Huang, C. H. Woo, R. K. Zheng, G. H. Wen, and X. X. Zhang, Development of <110> texture in copper thin films. Applied Physic Letters, (2002), 80(13),2290.

212. Brongersma, S.H., E. Kerr, I. Vervoort, A. Saerens, and K. Maex, Grain growth, stress, and impurities in electroplated copper. Journal of Materials Research, (2002), 17(3),582.

213. Liu, Jun, Changqing Liu, and Paul P Conway, Crystallographic features of copper column growth by reversible pulse current electrodeposition, in Electronic Components and Technology Conference. (2007), IEEE.

214. Schu¨ler, Kerstin, Bastian Philippi, Martin Weinmann, Vera M. Marx, and Horst Vehoff, Effects of processing on texture, internal stresses and mechanical properties during the pulsed electrodeposition of nanocrystalline and ultrafine-grained nickel. Acta Materialia, (2013), 61,3945.

215. Lin, Ya-Wen, Jui-Chao Kuo, Kuan-Tai Lui, and Delphic Chen, Effect of plating current density and frequency on the crystallographic texture of electrodeposited copper. Materials Science Forum, (2010), 638-642,2841.

216. Maurer, Florian, Joachim Brotz, Shafqat Karim, Maria Eugenia Toimil Molares, Christina Trautmann, and Hartmut Fuess, Preferred growth orientation of metallic fcc nanowires under direct and alternating electrodeposition conditions. Nanotechnology, (2007), 18,135709.

217. Georgiadou, M and D Veyret, Modeling of transient electrochemical systems involving moving boundaries parametric study of pulse and pulse-reverse plating of copper in trenches. Journal of the Electrochemical Society, (2002), 149(6),C324.

218. Chung, Chia-Jeng, David P. Field, No-Jin Park, and Ross G. Johnson, Simulation of structure evolution in cu films. Thin Solid Films, (2009), 517(6),1977.

219. Xu, Di, Wei Lek Kwan, Kai Chen, Xi Zhang, Vidvuds Ozoliņš, and K. N. Tu, Nanotwin formation in copper thin films by stress/strain relaxation in pulse electrodeposition. Applied Physics Letters, (2007), 91,254105.

220. Xu, Di, Vinay Sriram, Vidvuds Ozolins, Jenn-Ming Yang, K. N. Tu, Gery R. Stafford, and Carlos Beauchamp, In situ measurements of stress evolution for nanotwin formation during pulse electrodeposition of copper. Journal of Applied Physics, (2009), 105(2),023521.

221. Kim, Myung Jun, Sung Ki Cho, Hyo-Chol Koo, Taeho Lim, Kyung Ju Park, and Jae Jeong Kim, Pulse electrodeposition for improving electrical properties of cu thin film. Journal of the Electrochemical Society, (2010), 157(11),D564.

222. Aroyo, M and N Tzonev, Pulse periodic reverse plating: Possibilities for electrodeposition of metal coatings with improved properties: Part 2. Plating and Surface Finishing, (2003), 90(2),50.

223. J.Koike, A.Sekiguchi, M.Wada, and K.Maruyama, A relationship between film texture and stress-voiding tendency in copper thin films, in Stress-Induced Phenomena in Metallization : Sixth Int'l. Workshop, S.P.Baker et.al, Editor. (2002), AIP.

224. Ebrahimi, F., A. J. Liscano, D. Kong, and V. Krishnamoorthy, Evolution of texture in electrodeposited ni/cu layered nanostructures. Philosophical Magazine, (2003), 83(4),457.

225. Liang, Haiyi, C.H. Woo, Hanchen Huang, A.H.W. Ngan, and T.X. Yu, Crystalline plasticity on copper (001), (110), and (111) surfaces during nanoindentation. Computer Modeling in Engineering & Sciences, (2004), 6(1),105.

226. Sirdeshmukh, D., L. Sirdeshmukh, and K.G. Subhadra, Micro- and macro-properties of solids: Thermal, mechanical and dielectric properties. (2006): Springer Berlin Heidelberg.

227. Tschopp, M A, D E Spearot, and D L McDowell, Atomistic simulations of homogeneous dislocation nucleation in single crystal copper. Modelling and Simulation in Materials Science and Engineering, (2007), 15(7),693.

228. Dub, S. N., Y. Y. Lim, and M. M. Chaudhri, Nanohardness of high purity cu (111) single crystals: The effect of indenter load and prior plastic sample strain. Journal of Applied Physics, (2010), 107(4),043510.

229. Shiraishi, M, T Takenobu, H Kataura, and M Ata, Hydrogen adsorption and desorption in carbon nanotube systems and its mechanisms. Applied Physics A, (2004), 78(7),947.

230. D.Y.Li, Q.Chen, and X.Y.Wang, Will crystallographic faces of a crystal keep their order in strength and friction coefficient when the contact force is reduced to nano/micro-newton level. Journal of Applied Physics, (2006), 99,044305.

231. Niyogi, Sandip, Elena Bekyarova, Mikhail E. Itkis, Jared L. McWilliams, Mark A. Hamon, and Robert C. Haddon, Solution properties of graphite and graphene. Journal of the American Chemical Society, (2006), 128(24),7720.

232. Wang, Xuan, Linjie Zhi, and Klaus Müllen, Transparent, conductive graphene electrodes for dye-sensitized solar cells. Nano Letters, (2008), 8(1),323.

233. Wang, Guoxiu, Bei Wang, Jinsoo Park, Ying Wang, Bing Sun, and Jane Yao, Highly efficient and large-scale synthesis of graphene by electrolytic exfoliation. Carbon, (2009), 47(14),3242.

234. Erickson, Kris, Rolf Erni, Zonghoon Lee, Nasim Alem, Will Gannett, and Alex Zettl, Determination of the local chemical structure of graphene oxide and reduced graphene oxide. Advanced Materials, (2010), 22(40),4467.

235. Greinke, Ronald Alfred and Robert Anderson Reyolds III, Expandable graphite and method. (2002), Google Patents.

236. Abdelkader, AM, AJ Cooper, RAW Dryfe, and IA Kinloch, How to get between the sheets: A review of recent works on the electrochemical exfoliation of graphene materials from bulk graphite. Nanoscale, (2015), 7(16),6944.

237. Alanyalıoğlu, Murat, Juan Josè Segura, Judith Oró-Solè, and Nieves Casañ-Pastor, The synthesis of graphene sheets with controlled thickness and order using surfactant-assisted electrochemical processes. Carbon, (2012), 50(1),142.

238. Lu, Jiong, Jia-xiang Yang, Junzhong Wang, Ailian Lim, Shuai Wang, and Kian Ping Loh, One-pot synthesis of fluorescent carbon nanoribbons, nanoparticles, and graphene by the exfoliation of graphite in ionic liquids. ACS Nano, (2009), 3(8),2367.

239. Xia, Zhen Yuan, Sergio Pezzini, Emanuele Treossi, Giuliano Giambastiani, Franco Corticelli, Vittorio Morandi, Alberto Zanelli, Vittorio Bellani, and Vincenzo Palermo, The exfoliation of graphene in liquids by electrochemical, chemical, and sonication-assisted techniques: A nanoscale study. Advanced Functional Materials, (2013), 23(37),4684.

240. Liu, Jilei, Chee Kok Poh, Da Zhan, Linfei Lai, San Hua Lim, Liang Wang, Xiaoxu Liu, Nanda Gopal Sahoo, Changming Li, and Zexiang Shen, Improved synthesis of graphene flakes from the multiple electrochemical exfoliation of graphite rod. Nano Energy, (2013), 2(3),377.

241. Mahanandia, Pitamber, Frank Simon, Gert Heinrich, and Karuna Kar Nanda, An electrochemical method for the synthesis of few layer graphene sheets for high temperature applications. Chemical Communications, (2014), 50(35),4613.

242. Khanra, Partha, Tapas Kuila, Seon Hyeong Bae, Nam Hoon Kim, and Joong Hee Lee, Electrochemically exfoliated graphene using 9-anthracene carboxylic acid for supercapacitor application. Journal of Materials Chemistry, (2012), 22(46),24403.

243. Zhou, Ming, Jie Tang, Qian Cheng, Gaojie Xu, Ping Cui, and Lu-Chang Qin, Few-layer graphene obtained by electrochemical exfoliation of graphite cathode. Chemical Physics Letters, (2013), 572,61.

244. Hong, Yanzhong, Zhiyong Wang, and Xianbo Jin, Sulfuric acid intercalated graphite oxide for graphene preparation. Scientific reports, (2013), 3.

245. Ferrari, A. C., J. C. Meyer, V. Scardaci, C. Casiraghi, M. Lazzeri, F. Mauri, S. Piscanec, D. Jiang, K. S. Novoselov, S. Roth, and A. K. Geim, Raman spectrum of graphene and graphene layers. Physical Review Letters, (2006), 97(18),187401.

246. Karlicky, Franti˘sek, Kasibhatta Kumara Ramanatha Datta, Michal Otyepka, and Radek Zbo˘ril, Halogenated graphenes: Rapidly growing family of graphene derivatives. ACS Nano, (2013), 7(8),6434.

247. Mathkar, Akshay, T. N. Narayanan, Lawrence B. Alemany, Paris Cox, Patrick Nguyen, Guanhui Gao, Patricia Chang, Rebeca Romero-Aburto, Sendurai A. Mani, and P. M. Ajayan, Synthesis of fluorinated graphene oxide and its amphiphobic properties. Particle & Particle Systems Characterization, (2013), 30(3),266.

248. Coopera, C.A., R.J. Younga, and M. Halsallb, Investigation into the deformation of carbon nanotubes and their composites through the use of raman spectroscopy. Composites A, (2001), 32,401.

249. Gleiter, H., The formation of annealing twins. Acta Metallurgica, (1969), 17(12),1421.

250. Esawi, AMK, K Morsi, A Sayed, M Taher, and S Lanka, Effect of carbon nanotube (cnt) content on the mechanical properties of cnt-reinforced aluminium composites. Composites Science and Technology, (2010), 70(16),2237.

251. Manchado, M. A. López, L. Valentini, J. Biagiotti, and J. M. Kenny, Thermal and mechanical properties of single-walled carbon nanotubes–polypropylene composites prepared by melt processing. Carbon, (2005), 43(7),1499.

252. Yang, Yingchao, William Rigdon, Xinyu Huang, and Xiaodong Li, Enhancing graphene reinforcing potential in composites by hydrogen passivation induced dispersion. Scientific Reports, (2013), 3,2086.

253. Niu, Yongan, Jiupeng Zhao, Xin Zhang, Xianjie Wang, Jie Wu, Yang Li, and Yao Li, Large area orientation films based on graphene oxide self-assembly and low-temperature thermal reduction. Applied Physics Letters, (2012), 101,181903.

254. Chang, Kunok, Weiming Feng, and Long-Qing Chen, Effect of second -phase particle morphology on grain growth kinetics. Acta Materialia, (2009), 57(17),5229.

255. Ohji, Guo-Jun Zhang and Tatsuki, Effect of bn content on elastic modulus and bending strength of sic-bn in situ composites. Journal of Materials Research, (2000), 15(9),1876.

256. Lavanya, Aryasomayajula and Wolter Klaus-Juergen, Carbon nanotube composites for electronic packaging applications: A review. Journal of Nanotechnology, (2013), 2013,6.

257. Alanazi, Nayef M., A.M. El-Sherik, Saleh H. Alamar, and Shouwen Shen, Influence of residual stresses on corrosion and wear behavior of electrodeposited nanocrystalline cobalt-phosphorus coatings. International Journal of Electrochemical Science, (2013), 8,10350.

258. Xiang, Y., T.Y. Tsui, and J.J. Vlassak, The mechanical properties of freestanding electroplatedcu thin films. Journal of Materials Research, (2006), 21(6),1607.

259. Okoro, Chukwudi, Kris Vanstreels, Riet Labie, OleL¨uhn, Bart Vandevelde, Bert Verlinden, and Dirk Vandepitte, Influence of annealing conditions on the mechanical and microstructural behavior of electroplated cu-tsv. Journal of Micromechanics and Microengineering, (2010), 20(045032),1.

260. Guan, Shan and Bradley J. Nelson, Pulse-reverse electrodeposited nanograinsized conip thin films and microarrays for mems actuators. Journal of the Electrochemical Society, (2005), 152(4),C190.

261. Kwon, Dukryel, Hyunah Park, S. Ghosh, Chongmu Lee, H. T. Jeon, and J. G. Lee, Recrystallization of the copper films deposited by pulsed electroplating on ecr plasma-cleaned copper seed layers. Journal of Korean Physical Society, (2004), 44(5),1108.

262. Fong, Dillon Dodd, Stresses in cu thin films and ag/ni multilayers.Thesis, in Engineering & Applied Sciences. (2001), Harvard University (Cambridge, Massachusetts).

263. Xiang, Yong, Xi Chen, and Joost J. Vlassak, The mechanical properties of electroplated cu thin films measured by means of the bulge test technique, in Materials Research Society Symposium Proceedings (2002), Warrendale, PA. p. L.4.9.1.

264. Srikanth, Narasimalu, J. Premkumar, M. Sivakumar, Y. M. Wong, and C. J. Vath III. Effect of wire purity on copper wire bonding. in 9th Electronics Packaging Technology Conference. 2007. Singapore. IEEE.

265. Esawi, Amal M. K. and Mahmoud M. Farag, Carbon nanotube reinforced composites: Potential and current challenges. Materials and Design, (2007), 28,2394.

266. Hilding, Jenny, Eric A Grulke, Z George Zhang, and Fran Lockwood, Dispersion of carbon nanotubes in liquids. Journal of Dispersion Science and Technology, (2003), 24(1),1.

267. Kuzmany, H, A Kukovecz, F Simon, M Holzweber, Ch Kramberger, and T Pichler, Functionalization of carbon nanotubes. Synthetic Metals, (2004), 141(1),113.

268. Chen, Lifei, Huaqing Xie, and Wei Yu, Functionalization methods of carbon nanotubes and its applications. (2011): INTECH Open Access Publisher.

269. Ding, Guifu, Yan Wang, Min Deng, Xuemei Cui, Huiqing Wu, and Lida Zhu, Research and application of cnt composite electroplating in Carbon nanotubes - from research to applications, Dr. Stefano Bianco, Editor. (2011), In Tech. p. 81.

270. Jeon, In-Yup, Dong Wook Chang, Jong-Beom Baek, and Nanjundan Ashok Kumar, Functionalization of carbon nanotubes. (2011): INTECH Open Access Publisher.

271. Gupta, Vinod and Tawfik Saleh, Syntheses of carbon nanotube-metal oxides composites; adsorption and photo-degradation. Carbon nanotubes - from research to applications. (2011).

272. Balasubramanian, Kannan and Marko Burghard, Chemically functionalized carbon nanotubes. Small, (2005), 1(2),180.

273. Chen, Li, Xiu-jiang Pang, Qing-tang Zhang, and Zuo-long Yu, Cutting of carbon nanotubes by a two-roller mill. Materials Letters, (2006), 60(2),241.

274. Chen, Li, Men-zhen Qu, Gu-min Zhou, Bai-lan Zhang, and Zuo-long Yu, Pc-mediated shortening of carbon nanotubes. Materials Letters, (2004), 58(29),3737.

275. Park, Ki Chul, Masatsugu Fujishige, Kenji Takeuchi, Susumu Arai, Shingo Morimoto, and Morinobu Endo, Inter-collisional cutting of multi-walled carbon nanotubes by high-speed agitation. Journal of Physics and Chemistry of Solids, (2008), 69(10),2481.

276. Xu, Hui, Hiroya Abe, Makio Naito, Yoshinobu Fukumori, Hideki Ichikawa, Shigehisa Endoh, and Kenji Hata, Efficient dispersing and shortening of super-growth carbon nanotubes by ultrasonic treatment with ceramic balls and surfactants. Advanced Powder Technology, (2010), 21(5),551.

277. Rubio, Noelia, Chiara Fabbro, M. Antonia Herrero, Antonio de la Hoz, Moreno Meneghetti, Jose L. G. Fierro, Maurizio Prato, and Ester Vázquez, Ball-milling modification of single-walled carbon nanotubes: Purification, cutting, and functionalization. Small, (2011), 7(5),665.

278. Kukovecz, Ákos, Tímea Kanyó, Zoltán Kónya, and Imre Kiricsi, Long-time low-impact ball milling of multi-wall carbon nanotubes. Carbon, (2005), 43(5),994.

279. Wang, Xiao Xia and Jian Nong Wang, Preparation of short and water-dispersible carbon nanotubes by solid-state cutting. Carbon, (2008), 46(1),117.

280. Tran, Michael Q., Charnwit Tridech, Alexander Alfrey, Alexander Bismarck, and Milo S. P. Shaffer, Thermal oxidative cutting of multi-walled carbon nanotubes. Carbon, (2007), 45(12),2341.

281. Datsyuk, V, M Kalyva, K Papagelis, J Parthenios, D Tasis, A Siokou, I Kallitsis, and C Galiotis, Chemical oxidation of multiwalled carbon nanotubes. Carbon, (2008), 46(6),833.

282. Pagani, Guido, Micah J Green, Philippe Poulin, and Matteo Pasquali, Competing mechanisms and scaling laws for carbon nanotube scission by ultrasonication. Proceedings of the National Academy of Sciences, (2012), 109(29),11599.

283. Sakka, Byung-Koog Jang and Yoshio, Dispersion and shortening of multi-walled carbon nanotubes by size modification. Materials Transactions, (2010), 51 (1), 192.

284. Sun, Yu Feng, Ai Min Zhang, Ying Yin, Yu Ming Dong, Yi Cheng Cui, Xu Zhang, and Jian Ming Hong, The investigation of adsorptive performance on modified multi-walled carbon nanotubes by mechanical ball milling. Materials Chemistry and Physics, (2007), 101(1),30.

285. Wu, Zheqiong and Somenath Mitra, Length reduction of multi-walled carbon nanotubes via high energy ultrasonication and its effect on their dispersibility. Journal of Nanoparticle Research, (2014), 16(8),1.

286. Lundgren, Mathias, Neil L. Allan, Terence Cosgrove, and Neil George, Wetting of water and water/ethanol droplets on a non-polar surface: A molecular dynamics study. Langmuir, (2002), 18(26),10462.

287. Kim, Dal-Hyun, Jinho Choi, Yung Ho Kahng, Sang Jung Ahn, Byong Chon Park, Joon Lyou, and Ki Young Jung, Shortening multiwalled carbon nanotube on atomic force microscope tip: Experiments and two possible mechanisms. Journal of Applied Physics, (2007), 101(6).

288. Wang, Feng, Susumu Arai, and Morinobu Endo, Metallization of multi-walled carbon nanotubes with copper by an electroless deposition process. Electrochemistry Communications, (2004), 6(10),1042.

289. Daoush, Walid M, Byung K Lim, Chan B Mo, Dong H Nam, and Soon H Hong, Electrical and mechanical properties of carbon nanotube reinforced copper nanocomposites fabricated by electroless deposition process. Materials Science and Engineering: A, (2009), 513,247.

290. Feng, Yi and Hailong Yuan, Electroless plating of carbon nanotubes with silver. Journal of Materials Science, (2004), 39(9),3241.

References